Seismic Performance and Design of Steel Multi-Tiered Buckling-Restrained Braced Frames

by

Moad Ahmed Bani

A thesis submitted in partial fulfillment of the requirements for the degree of

Master of Science
in
Structural Engineering

Department of Civil and Environmental Engineering
University of Alberta

ABSTRACT

Steel Multi-Tiered Buckling-Restrained Braced Frames (MT-BRBFs) are commonly used in moderate-to-high seismic regions of Canada and United States as the lateral-load resisting systems of tall single-storey buildings, such as sports facilities, airplane hangars, and warehouses, as well as in tall stories of multi-storey buildings. MT-BRBFs consist of two or more bracing panels stacked vertically between column out-of-plane support locations. A multi-tiered configuration is utilized when the use of a single bracing panel within a storey height is not practical nor economical. Although MT-BRBFs enjoy robust cyclic performance and large ductility capacity of their Buckling-Restrained Braces (BRBs), their seismic response differs from standard multi-storey BRBFs. Namely, lateral deformation under seismic loads may not evenly distribute along the frame height in MT-BRBFs as the tiers with tension-acting BRBs tend to deform more than those with compression-acting BRBs. This response may induce in-plane flexural demands on the braced frame columns, which may lead to plastic hinge formation or even column instability in the presence of a large axial force induced due to gravity loading and BRB capacity design forces. Furthermore, uneven distribution of frame lateral deformation can impose excessive strain demands on the BRBs yielding in tension, which can potentially cause fracture in the BRB core. In Canada, there are no design guidelines for MT-BRBFs in the 2019 Canadian steel design standard, CSA S16-19. Special design requirements were introduced for MT-BRBFs in the 2016 edition of AISC Seismic Provisions in the U.S. to improve column stability response and control tier drift demands. However, very limited supporting research data is available to verify these requirements. Given the extensive application of MT-BRBFs, often times in critical structures, there is an urgent need to develop a better understanding of their seismic response, estimate seismic force and deformation demands on their

members, evaluate the current U.S. seismic design provisions and propose potential improvements, and develop an enhanced design method in the framework of CSA S16.

This M.Sc. research project aims to evaluate the seismic response of steel MT-BRBFs designed to the Canadian and U.S. provisions and propose enhanced analysis and design methods to better represent MT-BRBF seismic response with the focus on column force and BRB strain demands. A combination of mechanics principles, structural analysis techniques, numerical simulation and experimental testing is used to achieve these objectives. A full-scale test program is conducted on a two-tiered BRBF to verify experimentally the behaviour of MT-BRBFs under seismic loading. The test frame is part of a prototype tall single-storey building located in Seattle, WA (AISC 341-10 design) or in Vancouver, BC (CSA S16 design). The results show that frame lateral deformation is unevenly distributed between the tiers and that the columns experienced significant in-plane bending due to this response. Moreover, large deformation demands develop in the BRBs, but no low-cycle fatigue fracture was observed under the applied loads. The results of the experiment also confirmed the need for an improved seismic design method for MT-BRBFs. A fibre-based numerical model of MT-BRBF is then developed and used to perform an extensive nonlinear response history analysis on a wider range of frames. The analysis results confirm that frame inelastic deformation tends to concentrate in the tier(s) undergoing tension yielding as they exhibited relatively lower post-yield stiffnesses and storey shear resistances than the tier(s) undergoing compression yielding. This lateral deformation pattern induces significant in-plane bending on the columns resulting in yielding or column buckling in some cases and causes excessive deformations in BRBs. A set of analysis and design methods is proposed in the framework of Canadian and U.S. seismic provisions. The proposed methods predict column moment demands and BRB strain with sufficient accuracy resulting in a safer and more economical design.

PREFACE

This thesis is an original work by Moad Bani.

DEDICATION

To my parents

ACKNOWLEDGEMENTS

My sincere gratitude is extended to my supervisor, Professor Ali Imanpour, for his invaluable guidance throughout my master's degree. Thanks to Professor Robert Tremblay and Brandt Saxey for their insights and contributions to the experimental portion of my research. I am grateful to the following students, staff, and technicians at the Structural Engineering Laboratory at Polytechnique Montréal for their assistance in preparation for and during my full-scale frame test, including Pablo Cano, Christophe Comeu, Simon Bourget, Yazid Cheklat, Dr. Armin Nassirini, Martin Leclerc, Marc-Antoine Bernier, Manar Benslama, Mathieu Robidas and Céleste Gaudreau. I would also like to thank the members of my thesis defence committee, Professors Yashar Pourrahimian, Charles-Philippe Lamarche, Hossein Daneshvar, and Larry Fahnestock for their valuable feedback that improved the quality of this thesis.

My research project was financially supported in part by the Natural Sciences and Engineering Research Council of Canada (NSERC) Alexander Graham Bell Canada Graduate Master's Scholarship, the Walter H Johns Graduate Fellowship, the Government of Alberta Graduate Excellence Scholarship, the DIALOG Gordan F. Anderson Scholarship, the Noman & Reid Family Graduate Scholarship, and the Brain Gerbrandt Memorial Graduate Scholarship. Additional support for the experimental phase of my research was provided by CoreBrace, the American Institute of Steel Construction (AISC), the Canadian Institute of Steel Construction (CISC), AtlasTube, Construction Proco, and DIALOG. This support is greatly appreciated.

TABLE OF CONTENTS

LIST OF TABLES

LIST OF FIGURES

LIST OF APPENDICES

LIST OF SYMBOLS AND ABBREVIATIONS

SYMBOLS:

A_{sc}	Cross-Sectional Area of The Yielding Segment of Steel Core
C_c	Column Axial Force Demand (CSA)
C_d	Deflection Amplification Factor as given in ASCE 7
C_n	Nominal Compression Resistance of the Column
C_{ny}	Nominal Column Weak-Axis Compressive Capacity
C_{prob}	Compression BRB Probable Tensile Resistance
C'_{prob}	Modified Compression BRB Probable Tensile Resistance
C_u	Upper Limit Period Coefficient
E	Young's Modulus
EI_y	Weak-Axis Flexural Stiffness of the Column
$\phi_\beta M_n$	Design Flexural Strength
$\phi_c P_n$	Design Axial Strength
F_y	Yield Stress
F_{ysc}	Yield Stress of The Steel Core
h	Total Height
h_i	Tier Height
I_E	Importance Factor (NBCC)
I_e	Importance Factor (ASCE 7)
K	Effective Length Factor
K_{axial}	Column Axial Stiffness
KF	Stiffness Modification Factor
K_θ	Column Torsional Stiffness

L_y	Length of the Yielding Segment of Steel Core
M_c	Column In-Plane Demand (CSA)
M_{py}	Weak-Axis Plastic Moment Capacity of The Column Section
M_u	Required Flexural Strength (AISC)
M_v	Higher Mode Effects Factor (NBCC)
M_w	Moment Magnitude
P_f	BRB Axial Force Demand
P_G	Column Gravity Load
P_{ny}	Nominal Column Weak-Axis Compressive Strength
P_u	Required Axial Strength (AISC)
P_{ysc}	Axial Yield Strength of Steel Core
R	Response Modification Coefficient as given in ASCE 7
R_d	Ductility-Related Force Modification Factor
R_o	Over-Strength-Related Force Modification Factor
RotD100	5% Damped Maximum Direction Response Spectrum
R_{rup}	Rupture Distance
R_{sh}	Strain Hardening Adjustment Factor
R_y	Material Overstrength Factor
S_1	Spectral Acceleration Parameter at 1.0s
S_{D1}	Design Spectral Acceleration Parameter at 1.0s
S_{DS}	Design Spectral Acceleration Parameter at Short Period
S_s	Spectral Acceleration Parameter at Short Period
T	Fundamental Period of the Structure
t	Time
T_a	Fundamental Empirical Period of the Structure

T_{prob}	Tension BRB Probable Tensile Resistance (CSA)
V	Design Base Shear
V_{bi}	Horizontal Component of BRB Resistances in Tier i
V_{ci}	Column Shear in Tier i
V_{s30}	Mean Shear Velocity
W	Seismic Weight
β	Compression Strength Adjustment Factor (AISC) / Friction Adjustment Factor (CSA)
β'	Modified Compression Strength Adjustment Factor (AISC) / Modified Friction Adjustment Factor (CSA)
Δ	Design Storey Drift
δ_{bi}	Deflection Due to Column In-Plane Bending as Obtained from the Simply Supported Column Assumption Under Unbalanced BRB Loads
$\Delta_{critical\ tier}$	Tier Drift in the Tier Undergoing the Largest Inelastic Deformation When the Frame is at the Maximum Storey Drift
Δ_e	Elastic Roof Drift Under Design Base Shear
δ_e	Elastic Roof Displacement Under Design Base Shear
Δ_i	Tier Drift in Tier I
δ_i	Total Inelastic Displacement in Tier i
δ_{ic}	The Lateral Deformation Produced Due to Column Bending in That Tier
δ_{if}	Deformation Due to the Roof Displacement at Design Storey Drift Assuming a Linear Variation Over the Frame Height
δ_{roof}	Inelastic Roof Displacement Under Design Base Shear
Δ_{st}	Inelastic Roof Drift (NLRHA)
δ_{st}	Inelastic Roof Displacement (NLRHA)
ε_{sc}	Core Strain
σ_p	Proportional Limit Stress

σ_y	Yield Stress
ω	Strain Hardening Adjustment Factor
ϕ	Strength Reduction Factor

ABBREVIATIONS:

ACI	American Concrete Institute
AISC	American Institute of Steel Construction
ASCE	American Society of Civil Engineering
ASTM	American Society for Testing and Materials
AWS	American Welding Society
BRB	Buckling-Restrained Brace
BRBF	Buckling-Restrained Braced Frame
CBF	Concentrically Braced Frame
CSA	Canada Standards Association
CSI	Computers And Structures, Inc.
DCF	Drift Concentration Factor
DIC	Digital Image Correlation
ELF	Equivalent Lateral Force Procedure
ESFP	Equivalent Static Force Procedure
FCAW-G	Gas-Shielded Flux-Cored Arc Welding
FEMA	Federal Emergency Management Agency
HSS	Hollow Structural Section
LHS	Left Hand Side
LVDT	Linear Variable Differential Transducer
MCE_R	Maximum Considered Earthquake

MDHTS	Multi-Directional Hybrid Testing System
MSE	Mean Squared Error
MT-BF	Multi-Tiered Braced Frame
MT-BRBF	Multi-Tiered Buckling-Restrained Braced Frame
MT-CBF	Multi-Tiered Concentrically Braced Frame
MT-OCBF	Multi-Tiered Ordinary Concentrically Braced Frame
MTS	Mts Systems Corporation
MT-SCBF	Multi-Tiered Special Concentrically Braced Frame
NBCC	National Building Code of Canada
NLRHA	Nonlinear Response History Analysis
NLYL	Notional Load Yield Line Method
OpenSees	Open System for Earthquake Engineering Simulation
PEER	Pacific Earthquake Engineering Research Center
PsDHSs	Pseudo Dynamic Hybrid Simulations
RHS	Right Hand Side
SAP2000	Structural Analysis Program
SDC	Seismic Design Category
SDOF	Single Degree-of-Freedom
SFRS	Seismic Force Resisting System
UHS	Uniform Hazard Spectra
UHS	Uniform Hazard Spectra
USGS	United States Geological Survey
WSDOT	Washington State Department of Transportation

CHAPTER 1 INTRODUCTION

1.1 Background

Buckling-Restrained Braced Frames (BRBFs) are commonly used as seismic force-resisting systems (SFRS) in buildings located in regions of in regions of moderate-to-high seismicity of Canada and United States. Unlike conventional Concentrically Braced Frames (CBFs), BRBFs utilize highly-ductile bracing members known as Buckling-Restrained Braces (BRBs) for which brace global buckling is prevented – allowing them to reach their full member cross-sectional strength in tension and compression without stiffness or strength degradation under seismic loading (Figure 1.1). This response is achieved by decoupling the BRB's force-resisting mechanism consisting of an internal steel plate (referred to as the core) and the buckling-restraining mechanism typically provided by a grout-filled steel tube. Since brace global buckling is precluded in BRBs, these braces offer robust cyclic performance and excellent ductility and energy dissipation capacities for braced frames by translating the inherent ductility of steel into system ductility and controlling the response of the structure under earthquake loading.

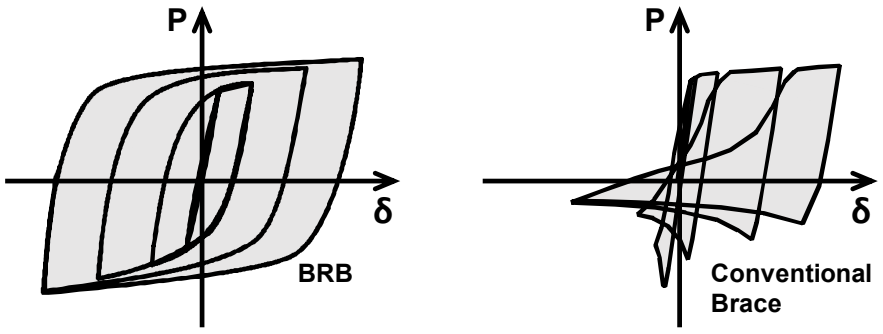

Figure 1.1: BRB and conventional brace hysteretic response.

In MT-BRBFs, multiple bracing panels consisting of BRBs are vertically stacked on top of each other along a storey height or between out-of-pane support locations to form a vertical truss to

resist lateral seismic loads. Intermediate horizontal struts are often used between the bracing panels to form a lateral load path after BRBs yield in tension and compression. A multi-tiered configuration is often used as opposed to a conventional (single-panel) bracing configuration in order to achieve a more efficient framing solution by avoiding very long braces and steep bracing angles. The use of a multi-tiered configuration can also help reduce the unbalanced length of the columns through the bracing provided by the horizontal struts at the tier levels leading to more economical column designs. Figure 1.2 shows the various applications of MT-BRBFs.

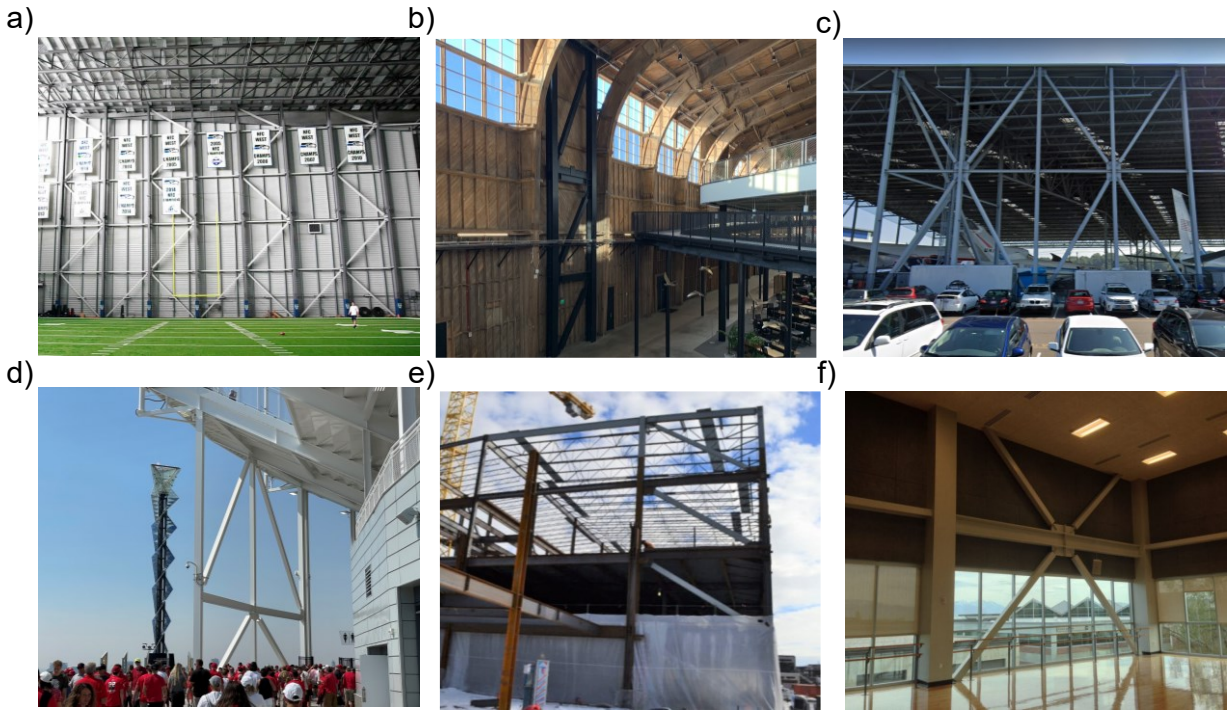

Figure 1.2: Multi-Tiered Buckling-Restrained Braced Frames: a) five-tiered BRBFs in a sports facility (courtesy of Michael Lawrie); b) three-tiered BRBF in a retrofit building (courtesy of Maren Dougherty); c) two-bay two-tiered BRBF in an airplane hangar (retrieved from Google Street View); d) two-bay two-tiered BRBFs in an stadium (courtesy of Brandt Saxey); e)-f) multi-storey BRBFs in a recreation centre (courtesy of CoreBrace).

Multi-tiered BRBFs are often used along the exterior of buildings and their columns are typically wide-flange members oriented such that out-of-plane loading induces strong axis bending in the cross-section over the frame height. Horizontal struts are typically wide-flange members or Hollow Structural Sections (HSSs) that form a lateral load path while bracing the columns in the plane of the frame. As shown in Figure 1.2, multiple bracing configurations can be employed in MT-BRBFs, including single-diagonal bracing, chevron, X-bracing, two-bay bracing. MT-BRBFs can also be used in tall stories of multi-storey buildings as shown in Figure 1.3. In all of these configurations, multi-tiered bracing panels act in series between out-of-plane support locations and resist lateral loads as a vertical truss system. Because tension and compression strengths in BRBs are nearly equal, single-diagonal configurations are very effective and are generally preferred in practice as it can reduce the number of bracing members and connections.

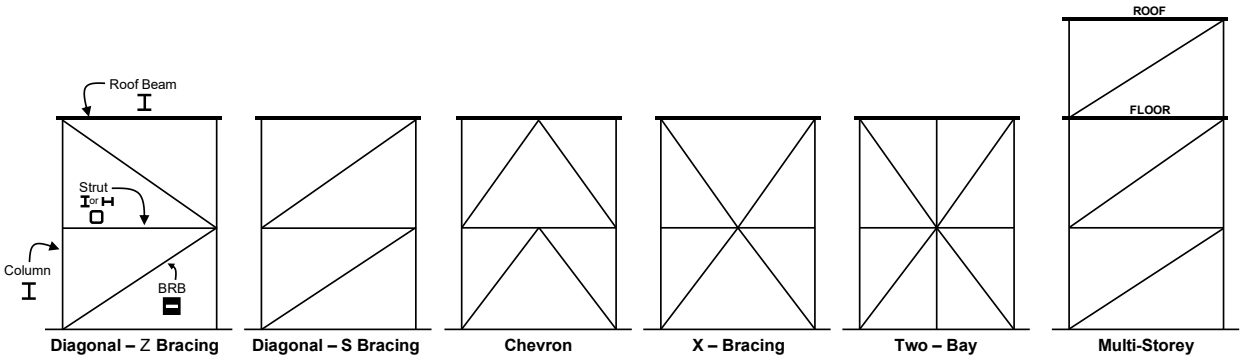

Figure 1.3: Typical multi-tiered BRBF configurations.

Since MT-BRBFs lack floor diaphragms along their height, which alters their seismic response from that of standard multi-storey BRBFs. MT-BRBFs behave as a single-degree-of-freedom (SDOF) systems under seismic loading as no horizontal inertia forces can develop at the tier levels to help maintain equilibrium between adjacent tiers when BRBs yield in tension and compression developing unequal tensile and compressive resistances and experiencing different post-yield stiffnesses – due to inherent asymmetric response of steel BRBs in tension and compression, which

exhibits higher strength and post-yield stiffness when yielding in compression (Merritt et al. 2003a; b; Tremblay et al. 2006; Fahnestock et al. 2007). As such, under lateral deformation, the tier(s) with BRBs yielding in tension tend to deform more than the ones with BRBs experiencing compressive yielding. This response is more pronounced in MT-BRBFs with single-diagonal bracing (Figure 1.3). To compensate for the difference in storey shear resistances between the tier with a tension-acting BRB and the adjacent tier with a compression-acting BRB, in-plane shear and flexure develop in braced frame columns as shown in Figure 1.4, which in the presence of a large axial compression force induced due to gravity and BRB axial resistances can lead to plastic hinge formation in the columns or column instability (Figure 1.4). Furthermore, uneven distribution of inelastic lateral deformation between tiers with tension and compression BRBs can impose excessive axial strain in the BRB core, potentially causing low-cycle fatigue fracture in the BRB core (Figure 1.4).

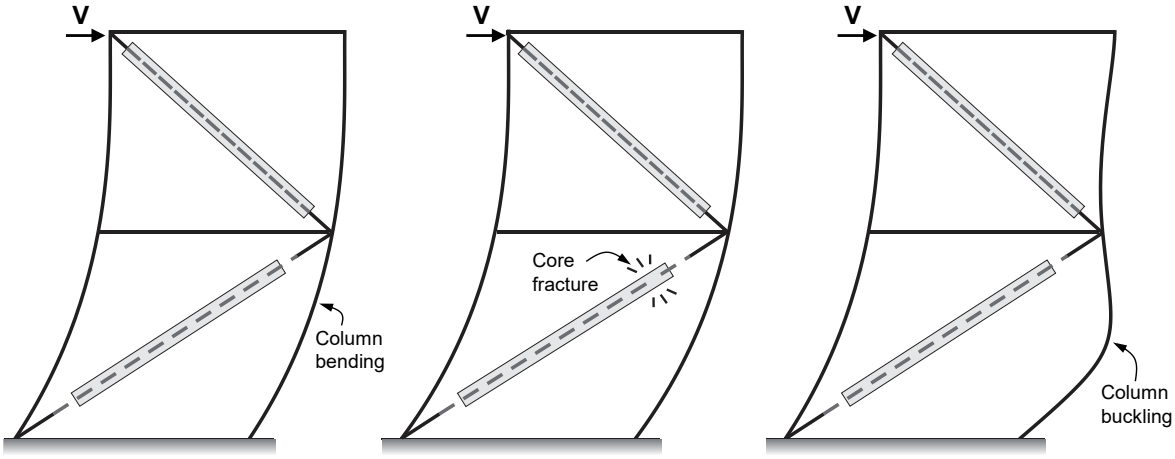

Figure 1.4: Two-Tiered BRBF lateral response and potential failure mechanism.

There has been limited research conducted to examine the behaviour of multi-tiered BRBFs as opposed to the seismic response of steel Multi-Tiered Concentrically Braced Frames (MT-CBFs), which has been the subject of an extensive research in the past decade (Imanpour et al. 2016a; b;

c, 2022; Imanpour and Tremblay 2016; 2017). The results of studies on MT-CBFs confirmed that inelastic lateral deformation tends to concentrate in the tier that possesses the smallest storey shear resistance, referred to as the critical tier, and yields first in tension. Uneven distribution of the frame lateral deformation induces in-plane bending on the columns, which in combination with a large axial compression force, can lead to column plastic hinging or even member instability. Similar but less pronounced performance concerns exist in MT-BRBFs (Imanpour et al. 2016b) as inelastic lateral deformation under seismic loading tend to non-uniformly distribute between tiers. The reason being a more stable seismic response of steel BRBs creating a lower unbalanced forces between BRBs in adjacent tiers and in turn lower shear demands on the braced frame columns compared to multi-tiered CBFs.

The current edition of the Canadian Steel Design Standard, CSA S16, (CSA 2019) does not prohibit the use of MT-BRBFs, however there are no special design requirements currently available to aid engineers in their design. Special seismic design provisions were introduced for the first time in 2016 for MT-BRBFs in the U.S. Seismic Provisions for Structural Steel Buildings, AISC 341-16. These provisions aim at preventing potential yielding in the columns and column instability while limiting deformation demands in the BRBs. The design requirements are summarized as follows:

1) Horizontal struts shall be provided at every BRB-to-column connection level.
2) The columns shall be designed for the combination of axial forces and in-plane moment demands. The column in-plane moment demands are to be calculated for a simply supported member with a length equal to the distance between points of column out-of-plane bracing under a set of in-plane point loads at the tier locations corresponding to the greater of:
    a. The summation of frame shears from the adjusted BRB strengths between adjacent tiers.

b. A notional load of 0.5% times the storey shear of the tier with the higher BRB capacity

3) The columns should be torsionally braced at every strut-to-column connection location.
4) The drift in any tier shall be limited to 2% when the anticipated storey drift is attained.
5) Member and connections design requirements are identical to those prescribed for standard BRBFs.

The same requirements are specified in the 2022 AISC Seismic Provisions (AISC 2022).

1.2 Problem Statement

When single-diagonal multi-tiered BRBFs are subjected to lateral seismic loads, frame inelastic deformation may distribute unevenly between tiers; tiers with tension-acting BRBs are expected to experience higher lateral deformation compared to the tiers whose BRBs yield in compression due to lower post-yield stiffness of BRBs when yielding in tension. This response can impose flexural bending in the columns, which in the presence of a large axial compression force may compromise the stability of the column. Furthermore, excessive inelastic deformation induced in tension-acting BRBs may cause strains in excess of cumulative plastic capacity of steel BRBs.

Limited numerical studies have been conducted to verify the performance concerns of MT-BRBFs and no experimental testing was done to examine the response of MT-BRBFs. The U.S., 2022 Seismic Provisions for Structural Steel Buildings, AISC 341-22, specifies design requirements for MT-BRBFs. However, very limited supporting research was available to verify the adequacy of these design requirements and propose improvements if needed. Furthermore, the 2019 edition of the Canadian steel design standard, CSA S16-19, does not address the design of MT-BRBFs, leaving engineers without unified design guidelines, which may lead to unsafe or uneconomical design solutions.

There is an urgent need to comprehend the seismic performance of steel multi-tiered BRBFs using numerical methods and full-scale experimental testing and propose design guidelines in the framework of the Canadian and U.S. standards to improve their seismic response.

1.3 Objectives

The main objective of this M.Sc. research project is to examine the seismic response of steel multi-tiered buckling-restrained braced frames and propose seismic design methods in the framework of the Canadian and U.S. provisions to improve their seismic performance.

The specific objectives of this research project are as follows (**O1 – O4**):

O.1 To evaluate the seismic response of MT-BRBFs designed in accordance with CSA S16-19 and AISC 341-10/22 seismic provisions using nonlinear response history analysis.

O.2 To experimentally evaluate the seismic response of a full-scale two-tiered BRBF designed per AISC 341-10 and CSA S16-19 seismic provisions, namely, the local and global behaviour of multi-tiered BRBFs, flexural bending induced in the columns taking into account the influence of base condition, and BRB strain demands under a loading protocol representing earthquake ground motions.

O.3 To develop seismic design requirements for MT-BRBFs in the framework of the Canadian steel design standard.

O.4 To improve the seismic design requirements prescribed by 2022 AISC 341 for MT-BRBFs.

1.4 Methodology

The following steps were taken to achieve the objectives of this research project (**M1 – M2**):

M.1 *Literature review*: a survey of past research on steel BRBs, BRBFs, multi-tiered braced frames, and the stability of wide flange columns under seismic loading was carried out **(O1 – 4)**.

M.2 *Braced frame design*: a set of archetypes BRBFs was selected by varying bracing configurations, frame heights, tier 1 to tier 2 height ratio, and number of tiers. The frames were then designed according to CSA S16 and AISC 341 seismic provisions (**O1**). MT-BRBFs studied in this research project involve single-diagonal BRBs (Figure 1.3) as this bracing configuration is expected to create the most critical deformation demands on BRBs and force demands on the braced frame columns. MT-BRBFs with two BRBs in each tier, e.g., chevron (Figure 1.3), are deemed to experience less pronounced multi-tier response and thus were not studied.

M.3 *Earthquake ground motions*: a set of ground motion records was selected and scaled for each of the Canadian and AISC designs according to the respective standards, 2015 NBC of Canada and the 2016 American Society of Civil Engineers, Minimum Design Loads for Buildings and Other Structures, ASCE 7-16 (ASCE 2016), respectively. (**O1**)

M.4 *Numerical model development*: a corroborated fibre-based numerical model of steel BRBFs was developed in the *OpenSees* environment with emphasis on the inelastic cyclic response of steel BRBs and steel wide-flange columns. (**O1**)

M.5 *Experimental testing*: a full-scale experimental program consisting of a two-tiered steel BRBF designed to meet the requirements of both Canadian and U.S. seismic provisions was

conducted on MT-BRBFs. The frame was tested using the quasi-static testing method under a three-phase loading protocol consisting of lateral displacement time histories corresponding to far-field and near-field ground motion records applied sequentially, and a final monotonic lateral displacement (pushover). (**O2**)

M.6 *Numerical simulation*: nonlinear response history analyses were performed on the selected prototype frames (in Canada and the U.S.) under hazard-specific sets of ground motion records for each of the two applications, Canadian and AISC designs. (**O1**, **O3-4**)

M.7 *Response evaluation*: the results of the nonlinear response history analyses were used to quantify key frame response parameters, including storey drift, tier drift, drift concentration ratio, BRB forces and displacements, and column flexural moment demands using statistical analyses. These results were then used to interrogate distribution of lateral frame deformation along the frame height, column force demands, tier lateral deformation and BRB strain demands. (**O1**, **O3-4**)

M.8 *Design guidelines*: a set of analysis and design guidelines were developed for steel multi-tiered BRBFs based on experimental test data and the results of nonlinear response history analyses. The design methods are aligned with the seismic provisions implicit in the 2019 Canadian steel design standard for steel BRBFs and special design provisions of 2022 AISC 341 for steel multi-tiered BRBFs. (**O3-4**)

1.5 Organization

This thesis consists of six chapters and six appendices. In Chapter 1, background information, research objectives, and methodology are presented. A literature review on the behaviour and design of steel buckling-restrained braces and buckling-restrained braced frames is presented in

Chapter 2 **(M1)**. Chapters 3, 4 and 5 focus on the findings of experimental testing, response evaluation and design methods presented in the following three articles (to be submitted to scientific journals), respectively:

1. Full-Scale Testing of Steel Two-Tiered Buckling-Restrained Braced Frames by Moad Bani, Ali Imanpour, Robert Tremblay, and Brandt Saxey **(M2-3**, **M5**, **M7-8)**
2. Seismic Response and Design of Steel Multi-Tiered Buckling-Restrained Braced Frames in Canada by Moad Bani and Ali Imanpour. (**M2-4**, **M6-8**)
3. Seismic Performance Assessment of Steel Multi-Tiered Buckling-Restrained Braced Frames in accordance with 2010 and 2022 AISC Seismic Provision by Moad Bani and Ali Imanpour. (**M2-3**, **M6-8**)

The conclusions of this research and recommendations for future studies are summarized in Chapter 6. Appendix A contains the conference paper published in the proceedings of the 10th International Conference on Behaviour of Steel Structures in Seismic Areas (STESSA) (Bani and Imanpour 2022); this paper presents the results of a pushover and dynamic analyses for a two-tiered BRBF designed in accordance with CSA S16-19 **(M4 & M6-M7)**. Appendix B contains the conference paper published in the proceedings of the Canadian Society of Civil Engineering (CSCE) Annual Conference 2022 (Bani and Imanpour 2023), which evaluates a two-tiered and a three-tiered BRBF designed in accordance with CSA S16-19 using dynamic analysis **(M4 & M6-M7)**. Appendix C and D presents the tensile coupon and the stub-column tests conducted as part of the experimental program, respectively **(M5)**. Appendix E contains the steel mill test reports of the provided structural steel **(M5)**. Appendix F includes the shop drawings of the experimental specimen, and instrumentation drawings for the test frame **(M5)**.

This thesis is organized based on research articles. Thus, some of the key assumptions of the project, e.g., literature review, and numerical model development, may be given more than once in Chapters 3 – 5 to keep each chapter standalone in terms of the technical content. The writing style employed throughout the thesis adheres to the conventions, spelling, and grammar of Canadian English.

CHAPTER 2 LITERATURE REVIEW

2.1 Introduction

In this chapter, a review of past studies on steel Buckling-Restrained Braces (BRBs), Buckling-Restrained Braced Frames (BRBFs), and Multi-Tiered Braced Frames (MT-BFs) is presented. First, the development and behaviour o f BRBs is briefly discussed. Then the seismic design requirements for BRBFs in Canada and the U.S. are summarized, followed by an overview of the seismic performance of BRBFs based on past numerical and experimental studies. Lastly, a review of past research performed on MT-BFs and the stability of wide-flange columns under seismic loading is presented.

2.2 Buckling-Restrained Braces

Buckling-Restrained Braces were first developed in Japan in the 1970s (Wada et al. 1992), and quickly gained acceptance as an alternative to conventional bracing in North America in the late 1990s (Clark et al. 1999, Tremblay et al. 1999, Black et al. 2004). As shown in Figure 2.1, a typical BRB consists of a mild steel plate (referred to as the core), encased in a grout- or mortar-filled steel tube. A proprietary un-bonding material or an airgap is used to de-couple the steel core and the grout such that the entire axial load is resisted by the steel core while the grout-filled tube prevents global buckling. Alternatively, the restraining mechanism can also be entirely made from steel sections and the core can be a variety of shapes. BRBs are designed to concentrate the inelastic action along the yielding length of the core while the end connection regions are stiffened to remain elastic. Under a major seismic event, the core is expected to yield in tension and compression, resulting in a stable and nearly symmetric hysteretic response. The hysteretic behaviour of BRBs makes them an attractive alternative to their conventional counter parts, which under cyclic loading

suffer from significant strength degradation due to global and local buckling or even low-cyclic fatigue fracture (Tremblay 2002).

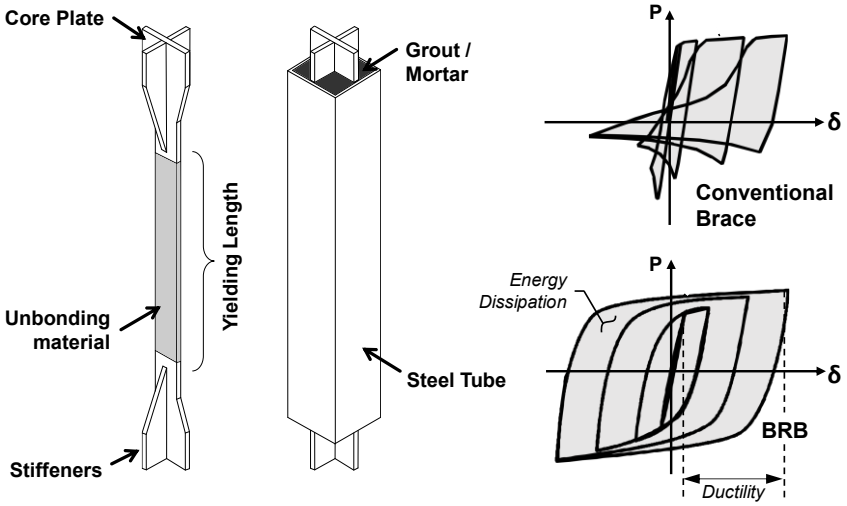

Figure 2.1: Typical BRB components and behaviour.

Due to their ability to yield in tension and compression, BRBs are highly ductile and offer significant energy dissipation. An example of the hysteretic response of a BRB obtained from experimental testing is shown in a Figure 2.2. The hysteretic response of BRBs is characterized by their combined isotropic and kinematic hardening resulting in positive post-yield stiffnesses in tension and compression with no strength degradation. The cyclic response of BRBs is asymmetric, that is, under cyclic loading they develop compressive forces higher than their respective tensile resistance due to the friction developed between the core and buckling-restraining mechanism as well as due to Poisson's effect. This asymmetric response is considered in the design of systems utilizing BRBs by using strength adjustment factors obtained through qualification testing to modify the BRB capacity. Considerable research and testing of BRBs has been undertaken in the past 30 years. Tests have shown that BRBs behave adequately at high strain demands (Merritt et al. 2003a; b; Black et al. 2004; Iwata and Murai 2006; Tremblay et al. 2006; Benzoni and

Innamorato 2007; Uriz and Mahin 2008). Fatigue test of BRBs have also shown that they are robust enough to withstand multiple earthquakes (Li eta al. 2022). Bruneau et al. (2011) and Takeuchi and Wada (2017) provide more information on the development and testing of BRBs.

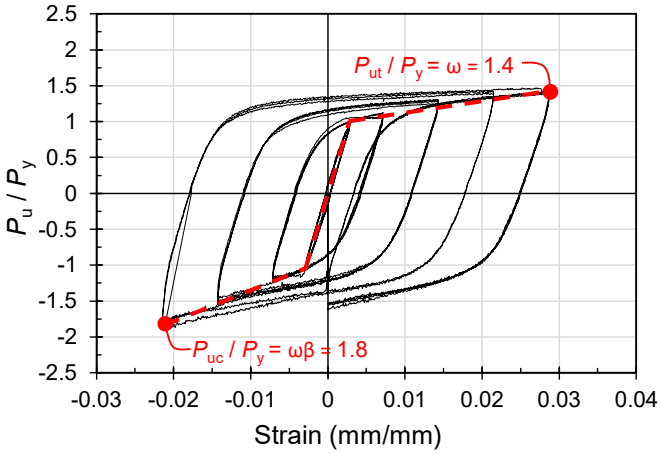

Figure 2.2: BRB Test Response (Tremblay 2007).

2.3 Buckling-Restrained Braced Frames

Design provisions for BRBFs were introduced in the U.S. in the 2005 edition of the Seismic Provisions for Structural Steel Buildings, AISC 341-05 (AISC 2005) and later in Canada in the 2009 edition of the CSA Steel Design Standard, CSA S16-09 (CSA 2009). In the U.S., the American Society of Civil Engineers, Minimum Design Loads for Buildings and Other Structures, ASCE 7-16 (ASCE 2016), assigns BRBFs a response modification factor, R, of 8. In Canada, the National Building Code of Canada, NBCC 2015 (NRC 2015), classifies BRBFs as ductile (Type D) lateral systems, that are assigned a ductility-related force modification factor, R_d, and an over-strength-related force modification factor, R_o, of 4 and 1.2, respectively. In both design standards, the BRB core areas are sized for the reduced design base shear and are expected to yield during an earthquake. A design engineer can use an area-based or a strength-based approach to design the BRBs. In the area-based approach, the designer specifies the required core area required using the

minimum yield strength assuming a typical yield strength range for the selected core material, e.g., F_y = 270 – 310 MPa for ASTM A36 steel (ASTM 2008). On the other hand, in the force-based approach the designer explicitly defines the required brace strength and the BRB manufactured sets the core area based on the required brace strength and confirmed material properties. Other frame members, such as the columns, beams, and connections are capacity-protected so that they remain elastic when subjected to the expected BRB capacities. The expected BRB capacities are based on a backbone curve of a tested BRB specimen (an example is shown in Figure 2.2). The BRB specimen should be tested according to testing protocol specified in Chapter K of AISC 341-16. From the backbone curve, the strain hardening adjustment factor, ω (R_{sh} is used instead in CSA S16), and compression strength adjustment factor, β, can be calculated. The strain hardening factor, ω, is calculated as the ratio of the maximum tension force and the compression strength adjustment factor, β, is calculated as the ratio of the maximum compression force to the maximum tension force. Both strength adjustment factors are measured at two times the BRB strain corresponding to the design storey drift in tension and compression. These adjustment values are typically provided by BRB manufacturers for design engineers to use. The expected BRB capacities used in design are $\omega A_{sc} R_y F_y$ in tension and $\beta\omega A_{sc} R_y F_y$ in compression. Where A_{sc} is the cross-sectional area of the core, and $R_y F_y$ is the expected yield strength of the steel core material. In the area-based approach the maximum value of the yield strength range for the selected core material would be used to calculate the expected BRB capacities whereas in the force-based approach, the cross-sectional strength of the core, i.e., $A_{sc} R_y F_y$, is replaced by the required BRB strength.

In the 2016 addition of AISC 341 (AISC 2016), the beams and columns in BRBFs shall satisfy the requirements of Section D1.1 for moderately ductile members whereas in the 2019 addition of CSA S16 (CSA 2019), the beams and columns must meet at least Class 2 section requirements

(seismically compact). Exclusive to CSA S16-19, columns are also designed for an additional bending moment equal to 20% of the plastic moment capacity. No such bending moment requirement exists in AISC 341-16.

CSA S16-19 does not prohibit the use of MT-BRBFs, however, there are no special seismic design requirements currently available, leaving engineers without comprehensive and unified design guidelines, which may lead to unsafe or uneconomical MT-BRBF designs. On the other hand, AISC 341-16 specifies design requirements for MT-BRBFs within the definition of BRBFs, which include provisions to design the columns under an axial compression force arising from BRB capacity forces plus an induced in-plane bending moment due to unbalanced forces between BRBs in adjacent tiers. Furthermore, the flexural stiffness of the columns must be sufficient to limit the drift in any tier to 2%. When computing the in-plane moment, the MT-BRBF column should be treated as a simply-supported member with a length equal to the distance between points of out-of-plane supports, then a set of transverse point loads are applied corresponding to the greater of 1) the summation of frame shears from the adjusted brace strengths between adjacent tiers, and 2) a minimum notional load equal to 0.5% times the frame shear coming from the higher strength adjacent tier. This approach is show in Figure 2.3, where “ABS” indicates the unbalanced loads due to variation in adjusted brace strengths between adjacent tiers applied to the columns and “NOT” indicates the required notional loads. Lastly, the columns must also be torsionally braced at every strut-to-column connection location. Very limited research studies were performed up to date to support the MT-BRBF design provisions prescribed in AISC 341-16.

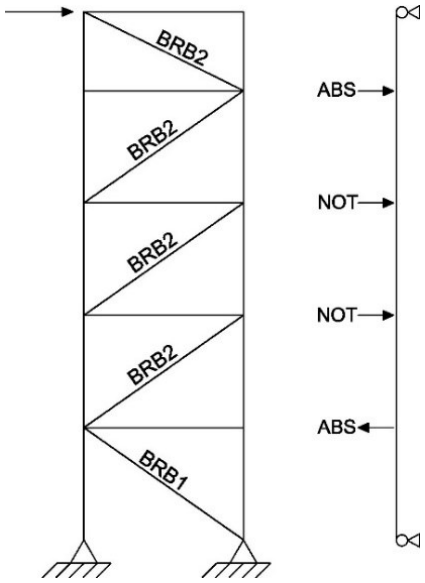

Figure 2.3: AISC 341-16 MT-BRBF Design Approach (AISC 2019).

2.4 Seismic Performance of BRBFs

There have been numerous numerical studies conducted on BRBFs in North America. (Tremblay et al. 2002; Sabelli et al. 2003, Kim et al. 2004; Tremblay et al. 2006; Fahnestock et al. 2007; Dehghani and Tremblay 2016). These studies have shown that BRBFs offer significantly better seismic performance compared to conventional braced frames. However, it was also showed that BRBFs have relatively less lateral stiffness than CBFs – which benefit from having stocky sections based on local buckling and slenderness requirements – resulting in situations where BRBFs can be governed by drift rather than strength for taller frames. Sabelli et al 2003 and Fahnestock et al. 2007, showed that the low lateral stiffness of BRBFs can also result in large residual deformations.

Several large-sale experimental studies on BRBFs have been conducted to confirm the performance of BRBFs under seismic loading (Fahnestock et al. 2007; Tsai and Hsiao 2008; Uriz and Mahin 2008; Palmer et al 2014). Fahnestock et al. 2007 experimentally tested a large-scale 4-storey BRBF (see Figure 2.4). It was found that the frame behaved well and satisfied performance objectives under MCE_R shaking, but the low post-yield stiffness of BRBs resulted in large residual

deformations. Other large-scaling testing of BRBFs also identified performance concerns related to connection behaviour (Uriz and Mahin 2008; Tsai and Hsiao 2008; Palmer et al. 2014). These studies have showed BRBFs can be susceptible to severe out-of-plane distortion at the gusset plates as a result of large flexural demands in the bracing connections. Figure 2.5a-c shows examples of such failures. To prevent undesirable connection performance various connection design methods have been suggested. One design solution proposed by Tsai and Hsiao (2008) is using an effective length factor of 0.65 for stiffened gusset plates and 2 for regular gusset plates when checking plate buckling according to the typical braced frame gusset plate design strategy shown in the AISC Seismic Design Manual (AISC 2018). Alternatively, detailed analytical models were developed to predict the global buckling of the BRB ends had been developed by Takeuchi et al. 2014 to determine the connection buckling strength. More recently a simplified method called the Notional Load Yield Line (NLYL) method has been proposed to check the out-of-plane stability of gusset plates (Zaboli et al. 2018).

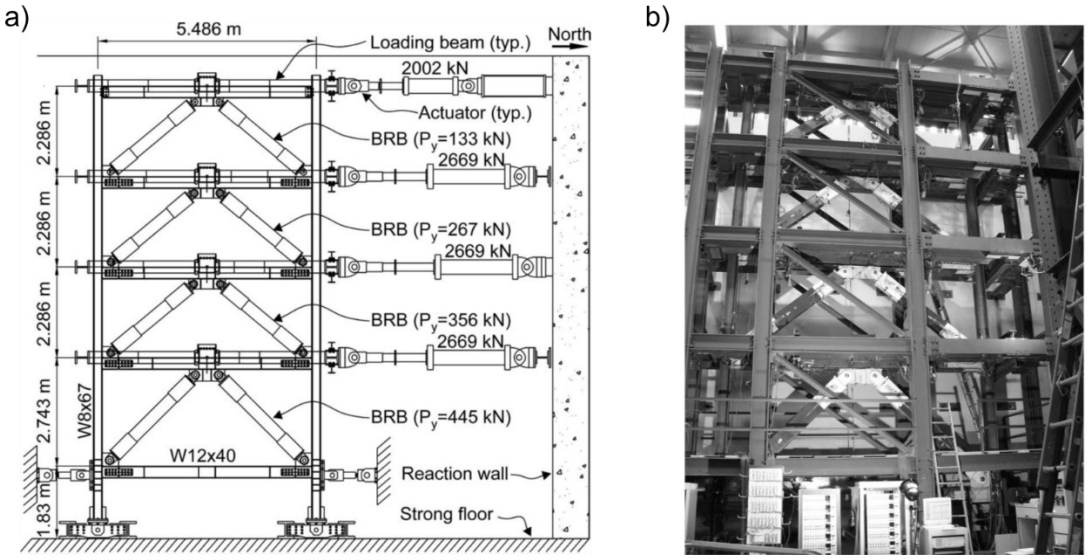

Figure 2.4: BRBF Test (Fahnestock et al. 2007).

Figure 2.5: BRBF connection failures: a) Uriz and Mahin 2005; b) Tsai et al. 2008; c) Palmer et al. 2014.

2.5 Multi-Tiered Braced Frames

Considerable analytical studies have been conducted in the past decade on Multi-Tiered Concentrically Braced Frames (MT-CBFs). These studies have shown that inelastic frame deformations in MT-CBFs are not uniformly distributed along the frame height, but rather concentrates in a single tier. This drift concentration induces significant in-plane bending moment demands on the columns. Column yielding was observed and, in several cases, column buckling occurred. To address these concerns, the 2016 Seismic Provisions for Structural Steel Buildings,

AISC 341 (AISC 2016) and the 2019 Canadian Steel Design Standard seismic provisions, CSA S16-19 (CSA 2019) include special seismic provisions for MT-CBFs. These requirements were mainly developed based on the findings from Imanpour et al. (2016b) and Imanpour and Tremblay (2017). The 2016 edition of AISC 341 also includes design requirements for MT-BRBFs which is based on Imanpour et al. (2016a).

Limited work has been done on MT-BRBFs. A nonlinear time history analysis of a four-tier BRBF was conducted by Imanpour et al. (2016a). Figure 2.6 shows the geometry and sections of the MT-BRBF studied. The frame was considered as an alternative to MT-CBFs for a tall single-storey building located in coastal California. The frame was subjected to a suite of 22 scaled ground motions from the far-field ground acceleration record set proposed in FEMA P695 (FEMA 2009). The frame was shown to undergo higher drifts than the SCBF option. Drift concentration in the first tier equal to 1.3 times the storey drift was observed on average resulting in an in-plane moment demand at the first-tier column of 16% of the plastic moment capacity of the column. This study did not consider additional frame archetypes and used a less robust BRB material numerical model. Also, no design strategy was provided by the author and the Canadian design standard was not addressed.

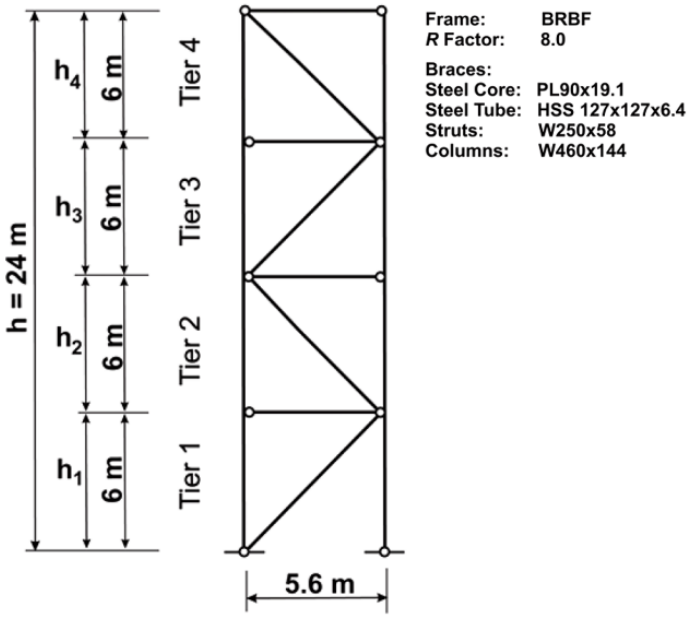

Figure 2.6: Four-Tier BRBF studied by Imanpour et al. 2016b.

2.6 Seismic Performance of Wide-Flange Columns

MT-BF columns are subjected to axial loads that vary along their height. This condition is common in columns part of frames used in industrial applications to support crane runway girders, conveyors, or mechanical equipment (see Figure 2.7). In these cases, the column cross section is typically varied along the height creating tapered or stepped columns. The column cross-section can be reduced at the top end to support the roof but increased at the crane level to carry additional loads. Similar to MT-BFs, these columns are usually unsupported about strong-axis bending and braced in the plane of the frame for weak-axis bending. There have been numerous studies looking into the behaviour of these kinds of columns under pure axial loading. Dalal (1969) solved the elastic buckling equation of several nonconventional cases of stepped columns in order to determine an effective buckling length under various axial load configurations. Design graphs were prepared as a function of axial loads, height ratio and the ratio of the moment of inertia between the different portions of the column. Figure 2.8 shows an example graph for the case the resembles

MT-BF columns the most: prismatic column with end and intermediate loads. Alternatively, an elastic Eigen buckling analysis can be performed to determine an estimate of the effective length factors for the columns with more than one intermediate loading point.

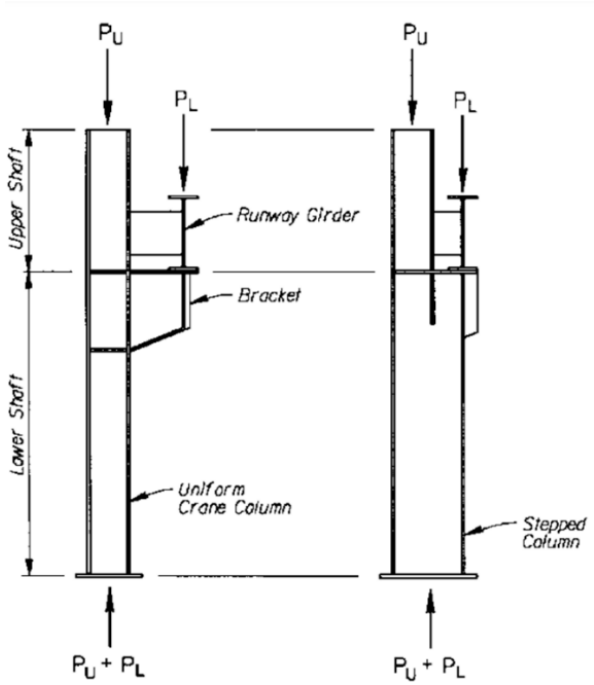

Figure 2.7: Crane/stepped columns.

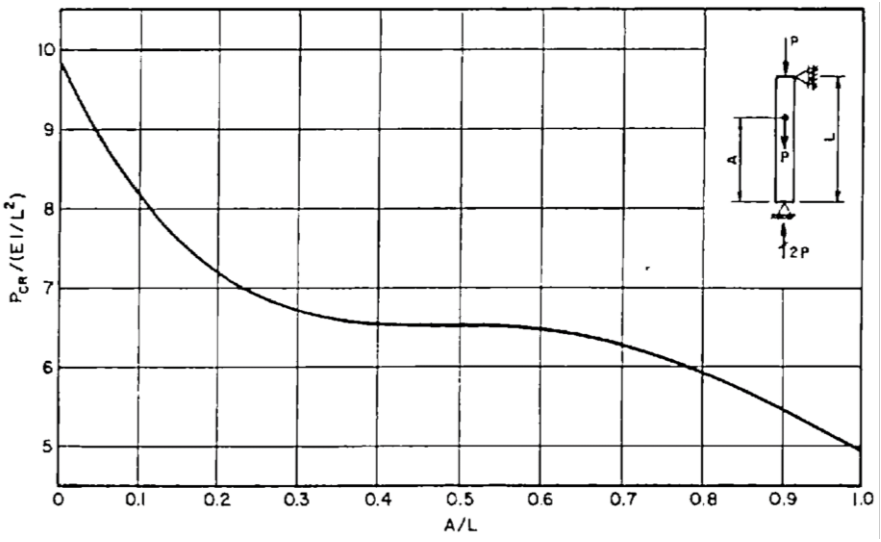

Figure 2.8: Uniform column with end and intermediate axial loads (Dalal 1969).

Sandhu (1972) also investigated determining the effective length factor, *K*, for columns subjected to an axial load at an intermediate point between two supports (see Figure 2.9). The study proposes a modified approach to calculate the effective length factor by considering the stability equation derived from solving the differential equations of the deflection curves for the upper and lower portions of the column separately, accounting for compatibility at the intermediate load point. The effective length factors were calculated by the author for various loading conditions and are summarized in Table 2.1. The author also suggested that this method can be extended to cases where there is more than one intermediate load. In such cases the modified *K* factor can be found for each intermediate load separately and the average of these values can be taken as the *K* factor for the design of the column.

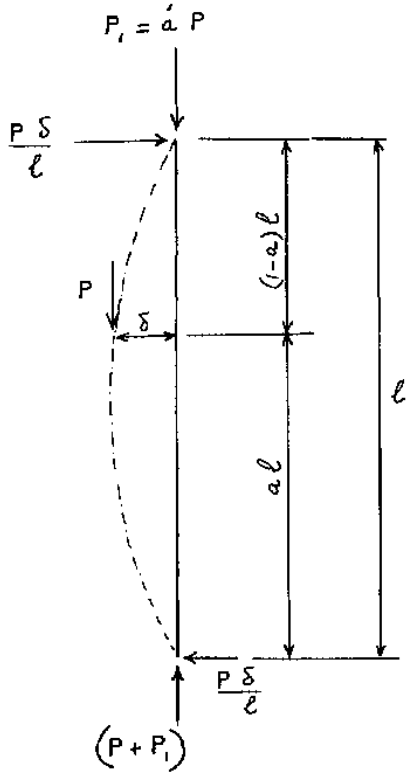

Figure 2.9: Pin-ended column loaded at ends and an axial load at intermediate point (Sandhu 1972).

Table 2.1: Effective Length Factors K for a pin-ended column with an intermediate axial load P at height aL and a load P_1 at the top (Sandhu 1972).

	$\frac{P_1}{P} = a' =$	0.10	0.25	0.50	0.75	1.0	2.0	3.0	4.0
a	Effective Length Factor K								
0.25		0.715	0.750	0.795	0.840	0.863	0.903	0.927	0.940
0.50		0.745	0.775	0.825	0.860	0.875	0.915	0.935	0.955
0.75		0.815	0.835	0.860	0.890	0.895	0.930	0.950	0.965
0.85		0.880	0.905	0.910	0.920	0.930	0.955	0.965	0.975
0.95		0.950	0.955	0.965	0.970	0.975	0.980	0.985	0.985
1.00		1.000	1.000	1.000	1.000	1.000	1.000	1.000	1.000

Several studies on the seismic behaviour and stability of wide-flange columns in braced frames have been conducted in the past decade. These studies looked at the response of wide-flange columns subjected to axial loads and inelastic rotation demands. Newell and Uang (2006) tested nine W360 columns part of a multi-storey BRBF under different axial load demands ranging from 0.35 to 0.75 of the column yield strength and a cyclic lateral displacement protocol applied in the strong axis direction. The displacement protocol consisted of variable displacement amplitude cycles ranging from 0 to 10% storey drift. Local flange buckling was the governing failure mode in all but one of the columns tested. No web local buckling or global buckling was observed in any of the columns. Figure 2.10 shows the deformed shape of the W360X197 loaded at 75% of its yield capacity at 4% and 10% storey drift and the axial force versus moment (P-M) interaction diagram. Given that the expected storey drift in braced frame buildings shouldn't exceed 2%, it was concluded that the columns exhibited excellent rotational ductility and their performance was deemed adequate.

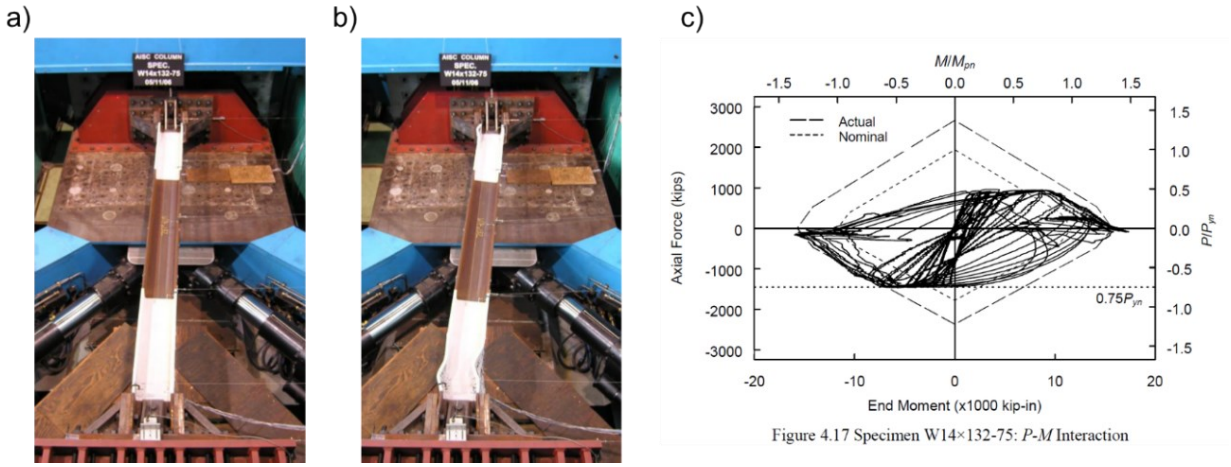

Figure 2.10: W360X196 specimen subject to 75% of its yield strength (Newell and Uang 2006): a) deformed shape at 4%; b) deformed shape at 10%; c) P-M interaction diagram.

Lamarche and Tremblay (2011) conducted full-scale testing on four W310X129 specimens to assess the buckling response of columns in multi-storey braced frames under seismic loading. An initial axial load of 60% of the column capacity was applied to all specimens. One specimen was then tested under monotonic loading and the rest under cyclic loading representing axial demands in braced frame columns. Axial load was applied concentrically to three specimens and eccentrically to one specimen. Weak axis buckling was observed in all the columns with plastic hinging of the column cross-section at mid-height of the specimens. Figure 2.11 shows the weak axis buckling of the column as well as the force versus axial displacement response. The results of this study suggest that wide-flange columns can undergo several cycles of inelastic bucking under seismic induced axial loading while maintaining sufficient compressive resistance to resist gravity loads.

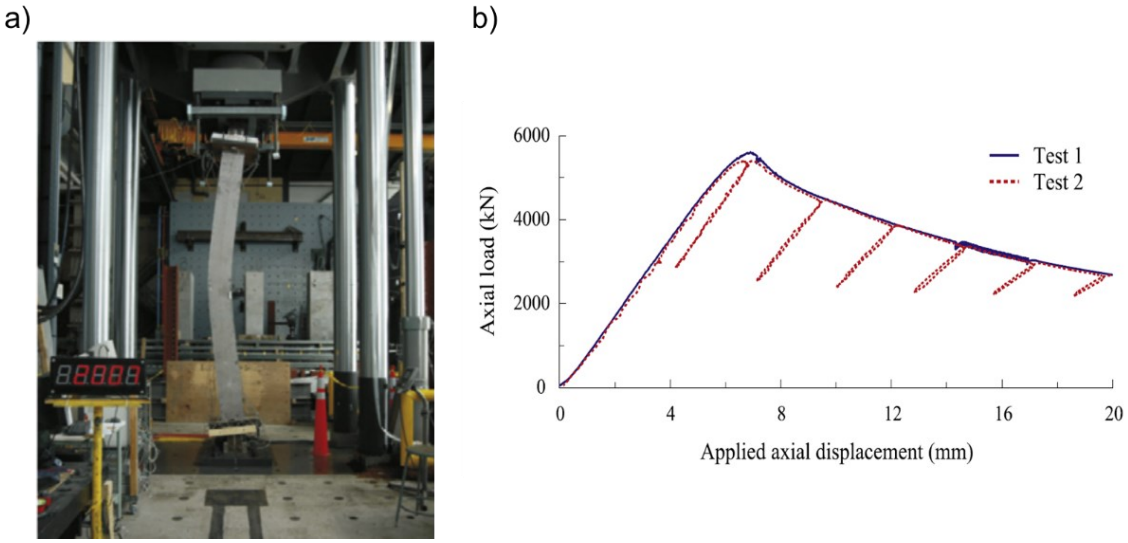

Figure 2.11: a) Weak axis buckling of column specimen; b) force versus axial displacement response (Lamarche and Tremblay 2011).

Auger et al. (2016) looked into the column response in multi-storey CBFs and moment resisting frames. Four full-scale W-shaped columns were tested using a Multi-Directional Hybrid Testing System (MDHTS). The tests aimed at investigating the plastic rotational capacity of the columns and their buckling response under cyclic and seismic loading. W250x101 column specimens were selected for this test program. One of the cyclic tests was performed about the weak axis of the wide-flange column specimen (a loading condition similar to MT-BFs) assuming fixed-fixed base connections. The column was subjected to 90% of its compressive yield strength which was maintained during the test as a cyclic lateral displacement and rotation protocol was applied at the top of the column. The normalized weak axis moment versus rotation at the top end of the column is shown in Figure 2.12a. Column buckling initiated at a rotation demand of 0.038 rad resulting in a in-plane moment demand on $0.5M_{py}$. The buckled shape at the end of the test is shown in Figure 2.12b. The tests showed that w-flange columns under cyclic and seismic loading can achieve considerable rotational ductility, even when carrying large compressive axial loads.

a) b)

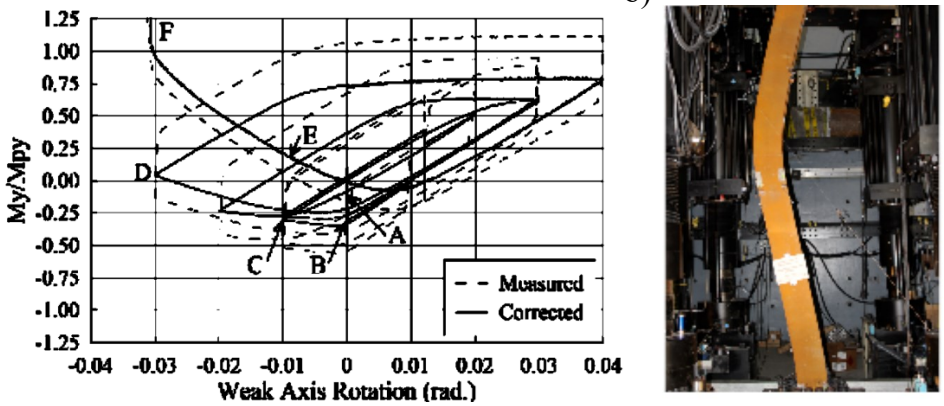

Figure 2.12: a) Normalized weak-axis moment demand versus weak-axis rotation; b) weak-axis buckling of column (Auger et al. 2016).

More recently Imanpour et al. 2022 performed two Pseudo Dynamic Hybrid Simulations (PsDHSs) on W250X101 columns part of a two-tiered CBF designed according to AISC 341-10 seismic provisions. In the hybrid simulations, the columns were assumed to be part of the first tier of the frame and were tested physically in a 6 degree-of-freedom testing machine while the rest of the frame components of the frame were modeled numerically in *OpenSees*. Nonlinear history analysis was performed under the 1992 Landers – Yermo Fire Station Record for the first PsDHSs and the 1989 Loma Prieta – Capitola record in the second PsDHSs. Gravity loads were applied as concentrated loads at the top of the columns. As shown in Figure 2.13a significant drift concentration in the first tier and consequently large induced in-plane bending moment on the columns during both ground motion records. In combination with axial compression forces, these moments caused buckling of the first-tier column under the 1992 Landers – Yermo Fire Station Record. Figure 2.13b shows the loss of axial stiffness of the columns as a result of global buckling and Figure 2.13c shows the column buckled shape at the end of the test.

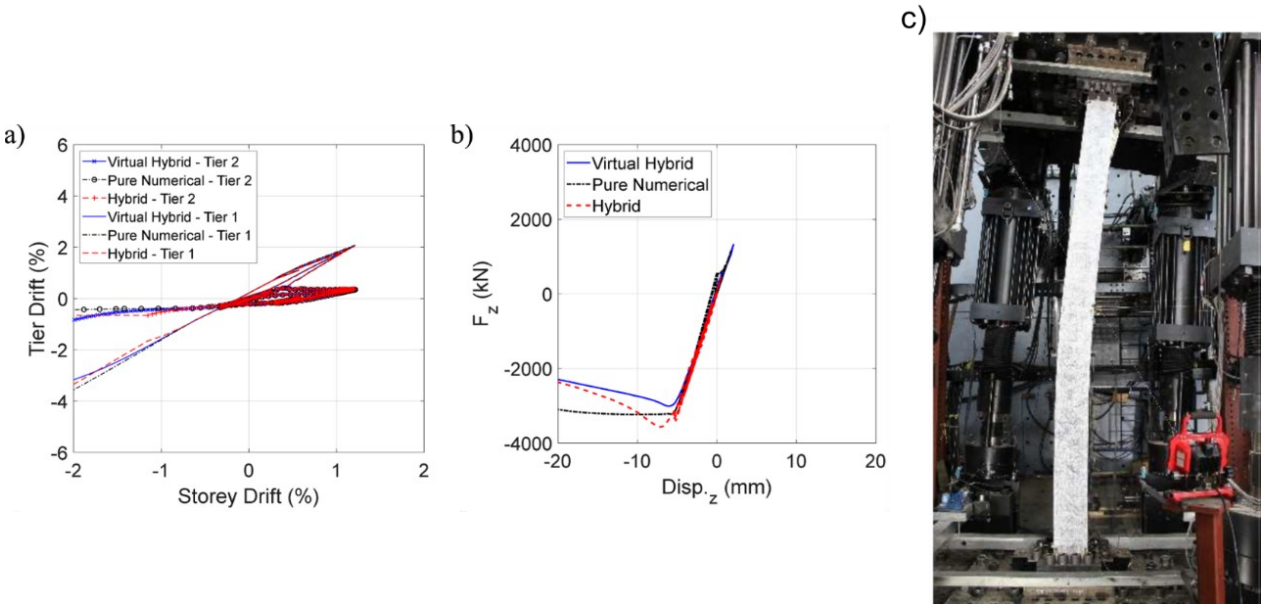

Figure 2.13: Hybrid test results (Imanpour et al. 2022): a) tier drift versus storey drift; b) axial force versus axial displacement response of column; c) column weak-axis buckling.

CHAPTER 3 FULL-SCALE TESTING OF STEEL MULTI-TIERED BUCKLING-RESTRAINED BRACED FRAMES

Abstract

A full-scale, two-tiered steel buckling-restrained braced frame (BRBF) was tested to evaluate experimentally the seismic behaviour of steel multi-tiered BRBFs, column stability response and seismic demands taking into account the influence of the base condition and tier deformations under a loading protocol representing earthquake ground motions. The test specimen consisted of diagonal braces oriented in opposing directions in the two adjacent tiers to create the most critical multi-tier response. The test frame was designed in accordance with the 2010 AISC Seismic Provisions as a lateral load-resisting system of a single-storey building. The frame was subjected to a three-phase loading protocol consisting of lateral displacement time histories corresponding to a far-field ground motion record and a near-field ground motion record applied sequentially achieving total frame drifts in excess of 3.5%, followed by a final monotonic lateral displacement corresponding to 4.5% storey drift. The test frame exhibited a stable response despite a non-uniform distribution of frame inelastic deformation between the tiers, which induced significant in-plane bending moments in the columns. Flexural bending, combined with a large axial compression force, led to partial yielding in the columns. Large deformation demands were also observed in the BRB, yielding in tension and attracting the majority of frame lateral deformation. On the basis of test results, a displacement-based analysis approach was proposed to relate column in-plane bending and flexural stiffness to relative inelastic tier deformations.

Keywords: Multi-tiered braced frames, Steel buckling-restrained braces, Full-scale testing, Seismic performance, Column stability, Base connection, Earthquake-resistant design, Metal and composite structures.

3.1 Introduction

Steel Multi-Tiered Braced Frames (MT-BFs) are commonly used as the lateral-load resisting system of tall single-storey buildings, such as sports facilities, airplane hangars, and warehouses, or tall multi-storey buildings, such as convention centers and auditoriums. MT-BFs consist of two or more bracing panels stacked vertically between column out-of-plane support locations, e.g., base and roof levels in single-storey structures, or diaphragms in multi-storey structures. A multi-tiered configuration is utilized when the use of a single bracing panel within a storey height is neither practical nor economical. As opposed to multi-storey braced frame structures, there are no diaphragms or out-of-plane supports to laterally brace MT-BF columns at the tier levels, and the bracing panels act in series to transfer lateral forces similar to a vertical truss spanning between lateral out-of-plane support points. In single-storey structures, MT-BFs are often used along the exterior of the building with wide-flange columns oriented such that they are subjected to strong axis bending due to out-of-plane wind loads. Intermediate horizontal struts are typically used between panels to brace the braced frame as well as between adjacent gravity columns in the plane of the frame to reduce their effective buckling length in-plane.

Originally developed in Japan in the 1970s (Watanabe et al. 1998; Wada and Takeuchi 2017), Buckling-Restrained Braces (BRBs) are used extensively for seismic applications in North America (Black et al. 2004; Tremblay et al. 1999, 2006; Uang et al. 2004; Xie 2005; Fahnestock et al. 2007) owing to their stable hysteretic response and large ductility capacity. Additionally, since they are restrained against buckling, their yielding core area is significantly smaller than the corresponding conventional brace area, which contributes to significantly reducing the capacity-induced forces on adjacent members, including beams, columns, connections, and footings. MT-BFs that utilize BRBs are referred to as Multi-Tiered Buckling-Restrained Braced Frames (MT-

BRBFs). Figures 3.1a and 3.1b show a three-tiered BRBF in a retrofitted airplane hangar and a five-tiered BRBF in a sports facility, respectively.

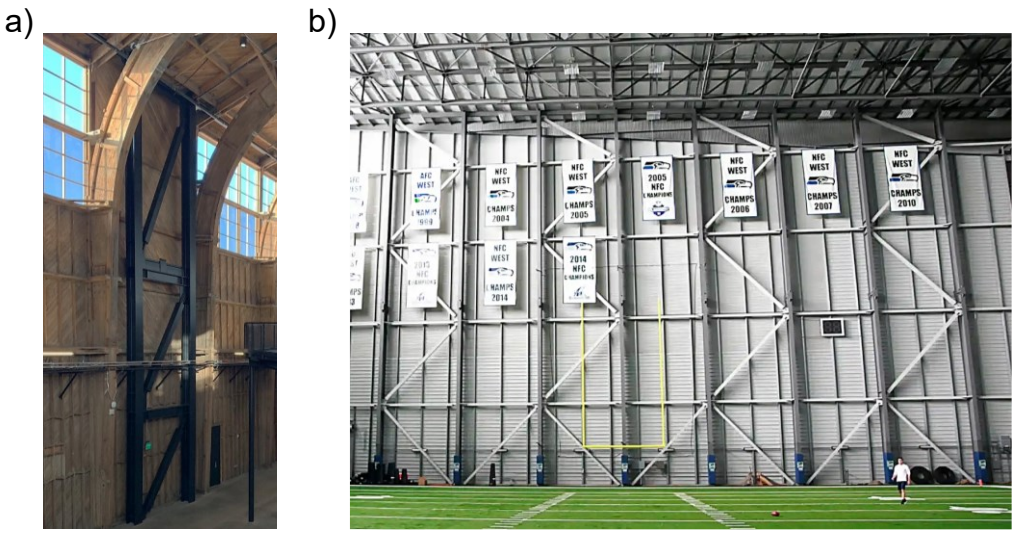

Figure 3.1: Multi-Tiered Buckling-Restrained Braced Frames: a) three-tiered BRBF (Courtesy of Maren Dougherty); b) five-tiered BRBFs (Courtesy of Michael Lawrie).

Over the past decade, a large body of knowledge has been accumulated in North America regarding the seismic response and design of steel Multi-Tiered Concentrically Braced Frames (MT-CBFs), which are often a preferred system with a multi-tiered configuration used, in particular, in low and moderate seismic regions. The results of the extensive numerical simulations performed in the past have confirmed that if MT-CBF columns are not designed for additional in-plane bending demands, inelastic lateral deformation tends to distribute unevenly between tiers because brace tensile yielding occurs only in one of the tiers (referred to as the critical tier) and the remaining tiers remain almost elastic, inducing relatively large in-plane bending in the columns and excessive lateral deformation in the tier where brace tensile yielding occurred (Imanpour et al. 2016b; Imanpour and Tremblay 2016). It has also been shown that the columns may experience instability due to large in-plane bending in the presence of a large axial compression force (Imanpour et al. 2022). Furthermore, appreciable axial deformation developed in the braces of the critical tier due to

damage concentration may result in brace fracture. To address these unsatisfactory limit states, special seismic design provisions have been developed in the United States and Canada for steel MT-CBFs based on the findings of past numerical studies (Imanpour et al. 2016c; Stoakes and Fahnestock 2016; Imanpour and Tremblay 2017). These provisions primarily target the design of the columns in MT-CBFs to ensure a more stable seismic response, which is achieved by verifying the columns' strength and stability in-plane and out-of-plane so that they can carry the combination of axial compression forces plus in-plane and out-of-plane bending demands. The provisions also dictate that tier drifts are to be limited to 2% to avoid excessive deformation in braces, and that intermediate horizontal struts are required between braced panels to form a vertical load path after brace yielding and buckling.

Similar to MT-CBFs, lateral frame deformation under seismic loading may not be uniformly distributed between tiers in multi-tiered BRBFs (Imanpour et al. 2016b; Bani and Imanpour 2022, 2023a); however, the utilization of BRBs in the multi-tiered configuration is expected to reduce nonuniformity of inelastic lateral deformation leading to a more stable seismic response when compared to their conventional counterparts. This is because BRBs are expected to yield both in compression and in tension with significant strain hardening, thus minimizing the difference between storey shear resistances of adjacent tiers and resulting in a potentially more uniform distribution of plastic deformation along the frame height. Despite the variation in expected BRB capacities, the compressive strength of BRBs is generally higher than their tensile strength because of the additional compressive forces developed due to the friction between the BRB core and the restraining material in combination with Poisson's effect; the post-yielding stiffness between adjacent tiers can still promote the non-uniform distribution of frame lateral deformation and produce in-plane bending in the columns, which may compromise column stability. This response

can also cause low-cycle fatigue fracture of the BRB core in the tier(s) that undergo excessive lateral deformation. Recent nonlinear response history analyses performed on two-tiered and three-tiered BRBFs (Bani and Imanpour 2022, 2023), designed in accordance with the 2019 Canadian steel design standard CSA S16 (CSA 2019), and a four-tiered BRBF (Imanpour et al. 2016b), designed in accordance with the 2010 AISC Seismic Provisions for Structural Steel Buildings, AISC 341 (AISC 2010a), showed that these moments can reach on average 17% of the column plastic moment capacity. Moreover, the peak tier drift developed in the tier in which BRB undergoes tension is on average 25 – 60% higher than that induced in the tier with a compression BRB. Based on the results from past dynamic analyses, the critical tier or tiers in MT-BRBFs are defined as the tier or tiers in which BRBs are in tension and the frame inelastic deformation tends to concentrate. The location of the critical tiers changes under cyclic loading as it depends on the direction of the frame lateral displacement. However, no experimental evidence is yet available to verify these findings and confirm the stability of MT-BRBF columns.

The 2022 edition of the AISC 341 (AISC 2022) specifies special design requirements for steel multi-tiered BRBFs. As per these provisions, 1) an intermediate horizontal strut is needed between braced tiers; 2) columns shall be designed under the combination of axial compression forces arising from adjusted brace strengths and gravity-induced axial forces plus an in-plane bending under unbalanced brace loads produced due to unequal storey shears contributed by adjusted brace strengths between adjacent tiers; 3) columns at every strut-to-column connection location shall be torsionally braced; and 4) relative tier deformation shall not exceed 2% of the tier height when design storey drift is reached. Note that a notional load equal to 0.5% of the greater of the frame shear strengths of adjacent tiers computed using adjusted BRB strengths should be used in lieu of an unbalanced brace load when the storey shear strengths in any adjacent tiers are identical. When

computing in-plane bending, MT-BRBF columns are treated as a simply-supported member spanning the points of out-of-plane bracing that is subjected to an in-plane point load at each tier level. Despite comprehensive seismic design provisions prescribed by the 2022 AISC 341, very limited supporting research studies are available in the literature and no experimental testing has yet been conducted to validate these design requirements. Full-scale laboratory testing is therefore urgently needed to examine experimentally the seismic response of multi-tiered BRBFs and verify the design requirements currently used by design engineers in North America.

This paper aims to produce the much-needed experimental data on multi-tiered steel BRBFs, evaluate the seismic response of these frames — namely, column stability response and column in-plane flexural demands, taking into account the influence of the base connection and tier deformations — and verify the AISC 341 special seismic design provisions for such frames. This paper also aims to enhance the state of knowledge on the behaviour of BRBs in general when subjected to the demands of earthquake ground motion. The experimental test program, including the design of the test specimen, test setup, and loading scheme, is first presented. The experimental results, including the frame base shear, storey, and tier drift demands, the hysteric response of BRBs, and the in-plane and out-of-plane column demands, are then discussed followed by a displacement-based analysis method to analyze the frame under lateral seismic loads.

3.2 Experimental Program

3.2.1 Test Specimen

A tall, single-storey warehouse building located in Seattle, WA was selected for this study. The building has a rectangular plan that measures 112 m ×140 m. The height of the building is h = 9 m. The columns are spaced at 7 m along the building perimeter. In addition to exterior columns, the

building has three interior column lines with the same spacing (7 m) dividing the width of the building into four identical 28-m interior bays. The building's roof consists of a corrugated steel deck supported by 28-m long steel trusses that span the columns in the short direction of the building and steel joists in the perpendicular direction. The building is assumed to be of Risk Category II and is located on site Class C (dense soil) with a mean shear velocity, V_{s30}, between 360 and 760 m/s. The seismic force-resisting system of the building consists of multi-tiered steel buckling-restrained braced frames. A pair of two-tiered BRBFs with equal tier heights of 4.5 m were used along each exterior wall in each principal direction of the building. One of the braced frames in the long direction of the building was tested in this study. The selected frame shown in Figure 3.2a consists of single diagonal BRBs in alternating orientation in each tier, i.e., BRBs in both tiers intersect at a common bracing connection on the right column. This configuration is often preferred in practice, as shown in Figure 3.1b, to reduce the number of bracing connections and strut sizes. Additionally, it is expected that MT-BRBFs with alternating BRB orientations in each tier create a more critical loading condition on the braced frame columns compared to the configuration where BRBs are oriented in the same direction. The roof dead load *D*, live load *L*, and snow load *S* are equal to 1.0, 0.96, and 0.67 kPa, respectively. The unit weight of the exterior cladding, which consists of insulated metal wall panels, is 0.5 kPa.

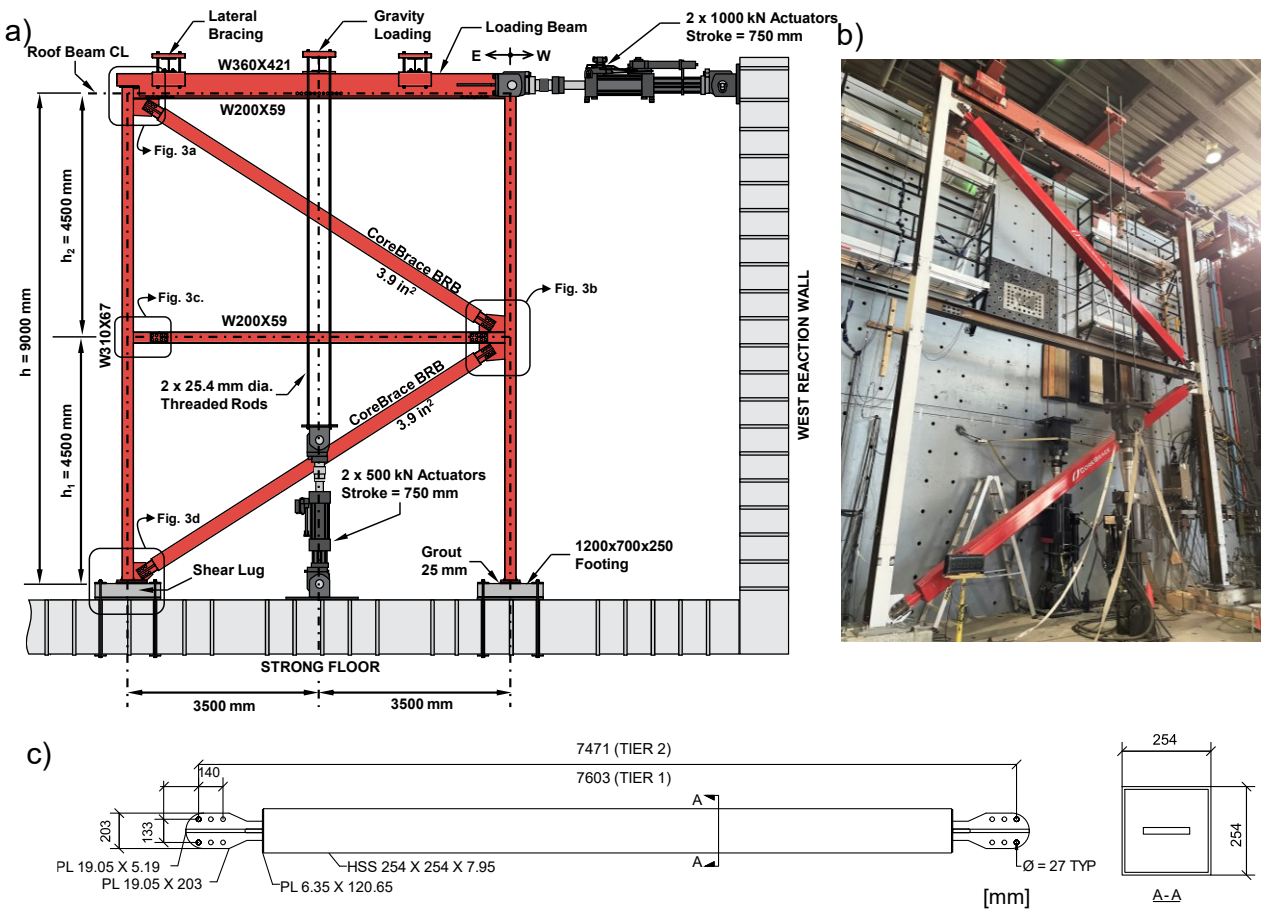

Figure 3.2: a) Test frame and setup; b) Photograph of test frame before the test; c) BRB dimensions.

The ASCE 7-10 (ASCE 2010) seismic load combination $1.2D + E_v + E_h + L + 0.2S$ was considered for the design of the braced frame members. The building was assumed to be of normal importance with an importance factor of $I_e = 1.0$ and assigned to the Seismic Design Category (SDC) D. Design spectral response acceleration parameters in the short period and at 1 second are $S_{DS} = 0.93$g and $S_{D1} = 0.46$g, respectively. The BRBF system, with a response modification coefficient $R = 8$ and deflection amplification factor $C_d = 5$, was used per ASCE 7-10. The seismic design base shear was determined using the equivalent lateral force procedure. The design fundamental period of the building was computed as $C_u T_a = 0.53$ s, where $T_a = 0.0731 h^{0.75}$ is the approximate fundamental period, and $C_u = 1.4$ is the coefficient for the upper limit on the calculated period. The resulting

design spectral response acceleration $S(C_uT_a)$, seismic weight per braced frame, seismic response coefficient C_s, and design base shear per braced frame including 5% accidental torsion effects, V, are equal to 0.93g, 4204 kN, 0.12, and 540 kN, respectively.

Frame members were designed in accordance with AISC 341-10 and AISC Specifications for Structural Steel Buildings, AISC 360-10 (AISC 2010b). BRBs were designed to resist the design base shear in tension and compression using a force-based approach as opposed to an area-based approach (AISC 2018). The brace force capacity was therefore used as the specified BRB design strength $\varphi P_u = 640$ kN to fabricate BRBs in an effort to reduce the effect of material variability and produce identical BRBs in adjacent tiers. The BRB core size was then determined by the BRB manufacturer (CoreBrace) based on the yield strength of the ASTM A36 (ASTM 2008) plate used to fabricate the core ($F_y = 282$ MPa) to satisfy the specified BRB strength. The cross-sectional area of the BRB provided by the manufacturer was therefore 2516 mm^2 (3.9 in^2). A set of three standard tension coupons cut from the BRB core material was tested as per ASTM E8 (ASTM 2022) to determine the actual yield strength of the BRB core. The average measured yield and tensile strength were found as $F_y = 269$ MPa and $F_u = 417$ MPa, respectively. The tension and compression overstrength factors were assumed as $\omega = 1.36$ and $\beta = 1.24$, respectively, at an expected specified design storey drift of 1.5%. Similarly, the length of the yielding core and a stiffness modification factor were taken to be 70% of the length between BRB workpoints and 1.24, respectively. The stiffness modification factor was used to account for the added stiffness provided by the BRB elastic regions and connections. Figure 3.2c shows the details of the BRB selected and designed with bolted lug-plate connections. Note that the two BRBs used in the frame test had identical capacities but slightly different lengths due to the variation in the size of their connections, which will be discussed later.

In the absence of special seismic design guidelines for MT-BRBFs in AISC 341-10, the columns were designed to resist in compression their tributary gravity loads applied as a point load at the roof level plus the axial load produced by BRB axial capacities, resulting in the required compressive strength equal to 1363 kN. A W310×67 (W12×45) profile conforming to ASTM A992 (ASTM 2015) with a specified yield strength of $R_y F_y$ = 345 MPa was selected for the columns. The available axial strength of the selected column was computed assuming an effective length equal to the tier height for in-plane buckling and the full frame height for out-of-plane buckling is $\phi_c P_n$ = 1450 kN. The selected wide-flange section satisfies the highly ductile member requirement in AISC 341-10. The yield strength of the column material, which was determined using a stub-column test conducted following the recommendation per Technical Memoranda B.3 by the Structural Stability Research Council Technical Memorandum B.3 (Ziemian 2010), is F_y = 370 MPa.

A W200×59 (W8×40) section conforming to ASTM A992 was selected for the strut and the roof beam. The strut was designed to carry the axial tension force corresponding to the horizontal component of the difference between BRB adjusted strength in tension in Tier 1 and the BRB adjusted strength in compression in Tier 2. The roof beam was only designed to resist the axial force arising from the horizontal component of the BRB adjusted strength in tension in Tier 2. The gravity load of the frame was applied through a W360×421 (W14×283) loading beam directly to the top of the columns as described in the next section. The selected BRB core areas and member sizes are given in Figure 3.2a.

The design storey drift computed as $\Delta = C_d \delta_e / h I_e$ is equal to 1.4%, where h is the total height of the frame and δ_e is the frame roof displacement under the base shear calculated using the fundamental period of 0.89 s from modal analysis, which is longer than the period corresponding to the upper

limit $C_u T_a$ = 0.53 s used in the design. The design storey drift is lower than the drift limit of 2% prescribed by ASCE 7-10.

A nearly identical frame was also designed per the Canadian steel design standard, CSA S16-19 (CSA 2019) for a prototype building located in Victoria, British Columbia, Canada. The prototype building was assumed to be in Victoria as it has the most comparable seismic hazard to Seattle. Furthermore, the prototype building dimensions and number of braced frames along each orthogonal direction were changed respectively to achieve design loading similar to the test frame.

The details of the frame connections are shown in Figure 3.3. The connection plates conform to ASTM A572 Gr. 50 steel (ASTM 2017a), and, for convenience, all bolts are 25.4-mm (1 inch) in diameter, conforming to ASTM A490 (ASTM 2017b). All welds were designed and performed in accordance with AWS D1.8 (AWS 2016) using gas-shielded flux-core arc welding (FCAW-G) with E70XX electrodes. Full-height gusset plates extending through the beam depth were shop-welded to the web of the columns (Sabelli and Saxey 2021) to mimic BRBF design practice while facilitating the fabrication of the specimen (Figures 3.3a and 3.3b). Within the width of gusset plates at the tier and roof levels, out-of-plane stiffeners were fillet-welded to the gusset plates to mimic the flanges of a W200×59 section, as shown in Figures 3.3a and 3.3b. At the beam/strut-to-column connections where no BRB connection is present, a beam-stub consisting of W200×59 was shop-welded to the columns (Figure 3.4c) to eliminate the need for field welding. Bolted splice connections were used to connect the roof beam and strut to the beam stubs and full-height gusset plates. The splice connections were designed to resist the required axial and shear forces while transmitting negligible moments, effectively behaving as a pin (Fahnestock et al. 2007). The rotational ductility of the strut and beam splices were finally verified as extended shear plate connections to accommodate a rotation of 0.025 rad., as per AISC 360-10. Due to the large forces

arising from the BRB resistance, splice plates in double shear were used at the roof level where the BRB connects to the column (Figure 3.3a), whereas splice plates in single shear were used elsewhere. A web doubler plate was groove-welded to the roof beam at the splice connection to increase the available strength to block shear rupture. The gusset plates were designed to resist the adjusted brace strength in tension and compression. Past experimental studies confirmed the potential out-of-plane deformation and instability of BRBF gusset plates designed following conventional gusset plate design similar to SCBFs (Palmer et al. 2014; Tsai and Hsiao 2008). To avoid potential excessive out-of-plane deformation and out-of-plane instability of the gusset plates under large strain-hardened BRB forces, the design method proposed by Zaboli et al. (2018) for BRB gusset plates was used to ensure a stable response of the gusset plates at anticipated roof drifts during the test, which resulted in 25.4-mm thick gusset plates.

The frame base connections were intended to simulate the base condition typically used for BRBFs. Details of the base connection of the east column are shown in Figure 3.3d. The base plates were designed to resist adjusted BRB strength, creating axial tension and shear forces at the column base of 971 and 1011 kN, respectively. A 38.1 mm-thick plate was finally selected for the base plates. A 12.5-mm thick stiffener was also added to the web of the east column above the gusset plate (Figure 3.3d) to increase the column web resistance against shear forces produced as a result of the brace workpoint being below the base plate. Four 38.1-mm (1-1/2 inch) ASTM A193 B7 (ASTM 2017c) anchor rods positioned inside the column profile were used to resist the required axial strength of the footing, 971 kN, due to brace adjusted strength. A shear lug was designed for the base plate to transfer BRB forces to the footing (east column base plate) using the recommendations by Aguirre and Palma (2009). The steel fiber reinforced concrete footing was designed per ACI 318-19 (ACI 2019) assuming a compressive strength of 25 MPa for concrete, and two layers of

15M and 30M steel reinforcement with a minimum yield strength of f_y = 400 MPa was added to increase the pull-out and punching capacities of the footing. The column base plates were placed on a 1200×700×250 mm reinforced concrete footing with 25.4-mm thick grout with a compressive strength of 35 MPa. Six standard compression cylinder tests were carried out on the samples taken from fiber-reinforced concrete and four cubes were tested for the grout. The measured compressive strengths of the fiber-reinforced concrete and grout were determined as 26 MPa and 36 MPa, respectively.

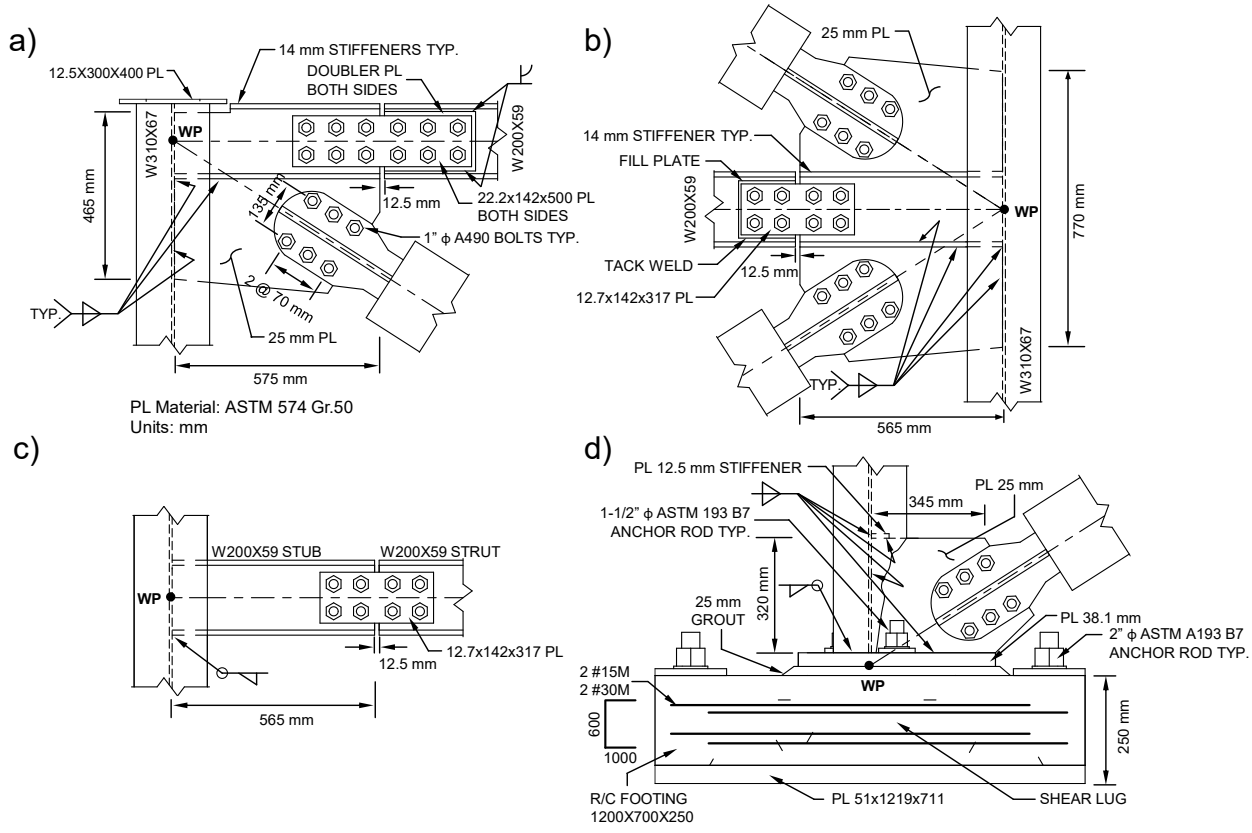

Figure 3.3: Test specimen connection details: a) BRB-to-beam/column connection at the roof level; b) BRB-to- strut/column connection at the tier level; c) strut-to-column splice connection; d) column base connection.

3.2.2 Test Setup

The test program was conducted at the Structural Engineering Laboratory of Polytechnic Montréal. Figure 3.2a shows the elevation of the two-tiered BRBF test setup, including gravity and lateral loading systems, base supports, lateral support apparatus, and the loading beam. A W360×421 loading beam was designed to transfer vertical and lateral forces from the actuators to the frame while providing out-of-plane support at the roof level. The loading beam was oriented such that the web is in the horizontal plane and is directly seated on top of the column end plates where the vertical gravity load is transferred directly to the columns. The loading beam was connected using a channel section on each side of the specimen's roof beam to transfer the lateral load to the test frame. Two horizontal 1000 kN hydraulic actuators installed parallel to the loading beam (as shown in Figure 3.2a) were used to apply the lateral load to the frame. The actuators were fixed to the west reaction wall and attached to both sides of the loading beam using heavy welded transfer brackets. The horizontal actuators were positioned such that they had 450 mm of stroke to the west and 250 mm to the east to allow imposing the displacement time history as described in the following section. To apply the gravity load to the test frame, two 500 kN hydraulic actuators installed parallel to the vertical direction of the frame (Figure 3.2a) were used. Two 25.4-mm threaded rods were installed on each vertical actuator to pull a spreader-beam welded to the top of the loading beam at its mid-length (Figure 3.2a), creating an axial compression load in the columns through flexure in the loading beam. Out-of-plane support was provided to the frame using two sliding guides that are fixed to the south reaction wall at each end of the loading beam (Figure 3.2a). These guides were prepared to minimize friction on the loading beam while the frame is laterally moving by the placement of a Teflon sheet between greased contact surfaces to allow the loading beam to slide freely in the horizontal direction. Frame reaction forces were transferred to

the strong floor using the footing anchorage system shown in Figure 3.3d. The column base plates were anchored to a 50.8-mm steel plate placed with threaded holes located below the concrete footing (not shown in Figure 3.2d), which was fixed to the strong floor using six 50.8-mm rods, two in the middle of the plate anchoring the plate directly to the strong floor and four at each corner anchoring the plate through the footing (two of them are shown in Figure 3.3d). Figure 3.2b shows a photograph of the test specimen prior to testing.

A multi-axis MTS control system was used to apply the lateral displacement and vertical load. The lateral displacement was applied in the displacement-controlled mode by controlling the displacement of the north horizontal actuator with the south horizontal actuator slaved to it. The force-controlled mode was used to apply the vertical gravity load to the frame using two vertical actuators. For this purpose, the load in the north actuator was controlled with the south vertical actuator slaved to it. The swivel heads of the vertical actuators rotate as the frame moves in a horizontal direction, allowing the gravity load to stay vertical and nearly constant throughout the test.

A combination of load cells, strain gauges, string potentiometers, linear variable differential transducer (LVDTs), inclinometers, and a Digital Image Correlation (DIC) system were used to measure the local and global responses of the test specimen. Actuator load cells were used to measure the forces applied to the frame. A total of 36 strain gauges were placed on the column flange tips above and below the tier level, at the base, and on the flanges of the roof beam and strut at their ends, to record strains; these were then used to calculate internal forces and moments. The locations of strain gauge placement were selected along the member length sufficiently far away from regions of expected yielding. String potentiometers were mounted to the west reaction wall and used to monitor the movements of the west column along its height using three-dimensional

triangulation. The potentiometer data was finally transformed into relative in-plane and out-of-plane displacements of the column. One string potentiometer was used to measure axial deformation along the height of the west column, i.e., the critical column, because of the higher axial compression force. Two inclinometers were used near the base of the west column, one on each side, to record the average relative rotation of the column base with respect to the footing. Two sets of DIC cameras were set up to record the strain distributions in the west column along the first-tier height. Two string potentiometers were used along each BRB, one on each side, to measure the average axial deformation of the core. The string potentiometers were placed outside the connection region to eliminate connection slip from the readings. Two LVDTs were placed on the connection region of Tier 1 BRB along the BRB longitudinal axis to measure the average connection slip and monitor out-of-plane gusset plate movement. Whitewash was applied to the columns and connections to detect potential plastic deformations during the test.

3.2.3 Loading Scheme

The quasi-static testing method was used to perform the experiment. The loading scheme involved gravity loading, lateral displacement time histories (Phases I&II) corresponding to two ground motion records applied sequentially, and a final monotonic lateral displacement (Phase III). A vertical load equal to the design gravity load of 392 kN was first applied to the specimen using the vertical actuators and was kept constant throughout the test. Figure 3.4 shows the lateral displacement time histories applied at the roof level along with the ground motion records used to produce the displacement histories, which are the 1994 Northridge Beverly Hills earthquake record (east-west component) and the 1989 Loma Prieta Saratoga-Aloha earthquake record (fault-perpendicular component). The first earthquake is representative of a far-field record while the second one is a near-field record. The application of the two earthquake records sequentially

represents a demand under an earthquake record component free of any rupture directivity effects as well as from a pulse-type aftershock earthquake using the fault-perpendicular component that exhibits the highest velocity pulse (Dehghani and Tremblay 2017). The roof displacement time histories were obtained from nonlinear response history analysis of the BRBF model performed in the *OpenSees* program (Mckenna et al. 2010) under the selected ground motion records scaled to the MCE_R response spectrum, representing a 2% in 50-years probability of exceedance using Method 2 described in ASCE 7-16 Chapter 16 (ASCE 2016). Both positive and negative scaling factors were considered for the selected ground motion records in order to achieve the most critical frame response: the largest non-uniform deformation in one tier and column bending moment demand. The numerical model of the BRBF was constructed using the recommendations described in Bani (2023). The measured material strengths, cross-sectional properties, and average initial geometric out-of-straightness (1/2250 and 1/1000 times the test column's unsupported length in-plane and out-of-plane, respectively, measured using a three-dimensional scanner) were assigned to the numerical model. The displacements associated with both records were truncated by removing low-amplitude signals at the end of each earthquake to achieve a reasonable testing time in the laboratory. As shown in Figure 3.4, the truncated regions of the induced roof displacement (solid line) do not produce large deformation relative to the rest of the record. Once the displacement time histories were applied, the third phase of the loading protocol, which consists of a monotonic lateral displacement inducing a storey drift of 4.5% in the west direction, was applied to examine the potential failure mode of the specimen under a large storey drift. The rate of the application of the lateral displacements was adjusted to avoid strain rate effects on BRBs (Bruneau 2011).

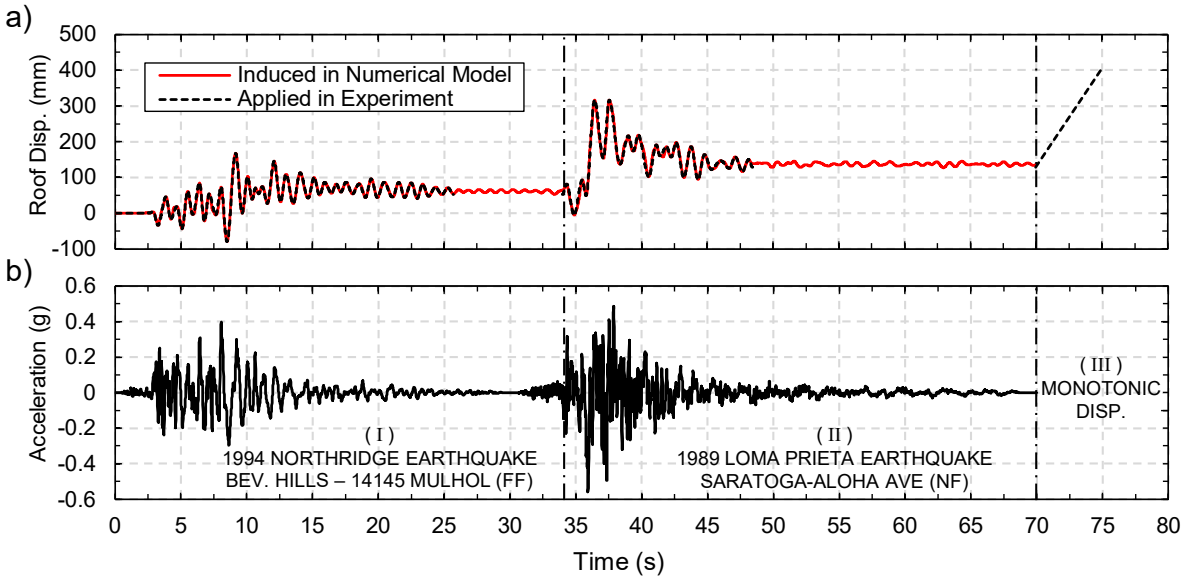

Figure 3.4: Loading scheme: a) applied lateral displacement history; b) ground motion records associated with Phases I and II.

3.3 Experimental Results

3.3.1 General Observations

Overall, the frame remained stable throughout the test. Limited inelastic deformation developed during the first phase of loading (Figure 3.4). However, the majority of inelasticity observed in the test specimen emerged during the second displacement time history (Phase II), which was created by the near-field pulse-type ground motion.

The BRBs responded well to the applied loading demands, without fracturing or noticeable out-of-plane deformation. The elongation of the BRB core observed is shown in Figure 3.5a. Minor yielding initiated at the base of the east column at 0.92% storey drift under the first displacement history (Phase I) at t_1 = 6.4s, and continued to grow and propagate towards the west direction as the test progressed under the second displacement history and the final push. Figure 3.5a shows the base of the east column with the yield lines observed at the end of the test. A similar response was

observed in the west column through the DIC strain measurement results as no whitewash was applied to that column. Cracks in the grout under the west column started to develop at 1.1% storey drift at t_I = 8.9s under the first displacement history and continued as the column experienced additional tension and compression cycles during the second displacement history. Figure 3.5b shows the cracks in the grout under the west column at the end of the test. No sign of cracking was recorded in the east column grout as it was subjected to lower axial force demands throughout the test. At 3% storey drift at t_{II} = 36.3s under the second displacement history, yielding began to develop in both columns at the tier level near the strut connections, which propagated above and below the strut level during the test, as shown in Figure 3.5c for the east column at the end of the test.

The splice connections accommodated the in-plane rotational demands expected in design as the frame experienced significant lateral displacements in both directions (Figure 3.5d). Very limited out-of-plane displacement was observed in the splice plates when the frame reached the maximum storey drift of 3.5% at t_{II} = 36.5s under the second displacement history before the final monotonic loading. This observation is likely attributed to the *P*-δ effect on the column, creating out-of-plane deformation.

Under the final monotonic displacement applied during Phase III (400 mm), the yielding areas observed under the ground motion records propagated but no new yielding or damage was developed. The applied lateral displacement in this phase (Figure 3.6) created an appreciable elongation in the tension-acting BRB (Tier 1) and minimal shortening in compression-acting BRB (Tier 2). Non-uniform distribution of the inelastic response between BRBs of adjacent tiers resulted in significant in-plane flexural deformation in the columns, as shown in Figures 3.6b and 3.6c for east and west columns, respectively.

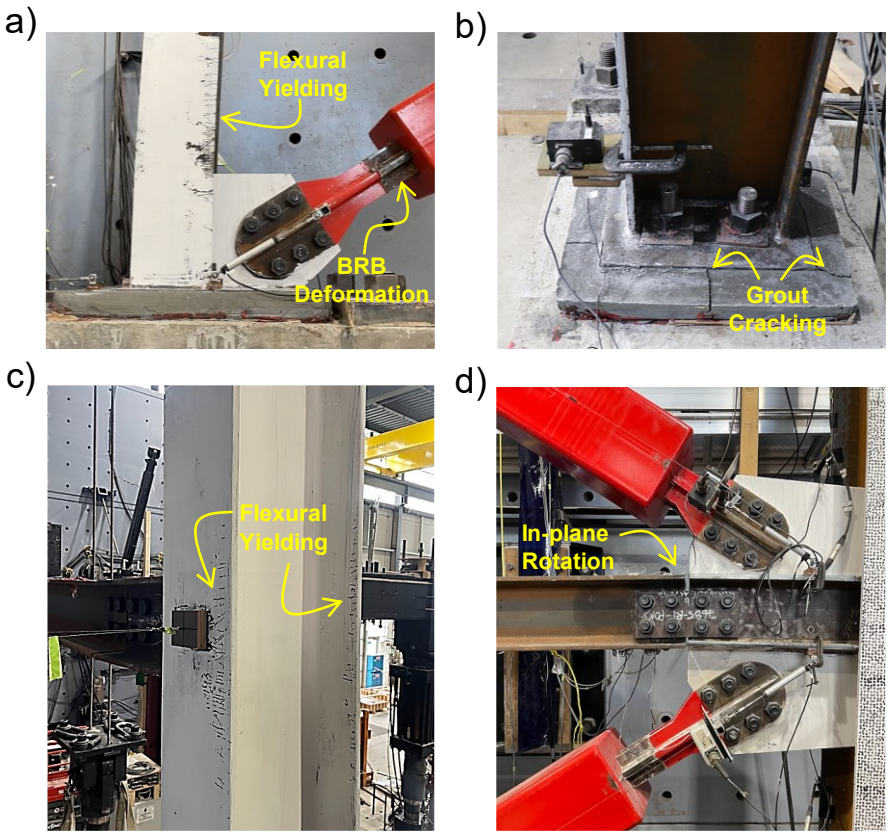

Figure 3.5: Connection response: a) yielding of the east column base; b) grout cracking at the base of the west column; c) yielding of the east column at the strut level; d) in-plane rotation of the strut splice connection to west column.

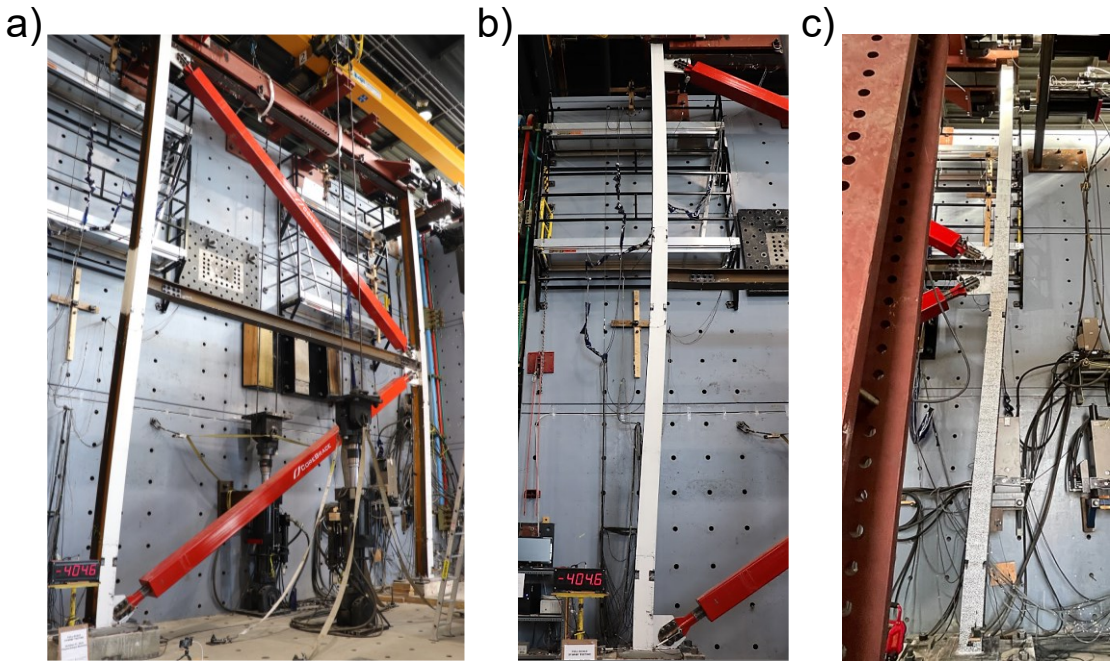

Figure 3.6: Deformed shape of the specimen at the end of the test: a) frame; b) east column; c) west column.

3.3.2 Global Response

The storey shear - storey drift response of the specimen, is shown in Figure 3.7a. The storey shear is normalized by the design base shear. The storey drift is computed as the ratio of the roof's lateral displacement to the frame height, *h*. As shown in Figure 3.7a, the frame remained elastic until both BRBs yielded under the first displacement history at 0.5% storey drift, which corresponds to a storey shear of 1.12 times the design base shear. The storey shear increased significantly after BRB yielding due to the cyclic hardening of the BRBs in tension and compression. The storey shear in the compression tier increased at a faster rate than the tension tier due to the higher post-yield stiffness of the BRB in compression, which is attributed to Poisson's effect and friction between the core and the restraining material. The maximum storey shear achieved at the end of the test was 1.45 times the design base shear. Figure 3.7b shows the tier drifts against the storey drift. The tier drift is computed by dividing the relative lateral displacement of each tier by the respective tier

height h_i (where i = 1 and 2, for Tier 1 and Tier 2 respectively). As shown, the frame lateral inelastic deformation tends to concentrate in the tier with BRB undergoing tensile yielding (critical tier), e.g., Tier 1 when the roof displacement is positive and Tier 2 when the roof displacement is negative. Referring to Figure 3.7b, the first tier acts as the critical tier of the frame for the majority of loading cycles because the frame is pushed to the west for most of the duration of both displacement histories (see Figure 3.4a), thus creating tension-acting Tier 1 BRB and compression-acting Tier 2 BRB. Therefore, lower storey shear resistance was provided by Tier 1 BRB compared to that offered by Tier 2 BRB in compression. For instance, as the frame is pushed to –0.87%h at t_1 = 8.5s, approximately 0.73%h of the applied roof displacement takes place in Tier 2, creating a tier drift of 1.47% in Tier 2, and the remaining lateral displacement of 0.14%h is induced in Tier 1, which corresponds to 0.27% tier drift in Tier 1. A similar yet more pronounced response was observed throughout the test. To quantify drift concentration, the drift concentration factor (DCF) — defined as the ratio of the critical tier drift to the storey drift — is used where a DCF greater than 1.0 indicates non-uniformity of lateral displacements between braced tiers. For instance, DCF is equal to 1.68 when the roof displacement reaches –0.87%h. At the peak storey drifts under the first and second displacement histories, +1.85% and +3.5%, respectively, the majority of the frame lateral deformation takes place in Tier 1, resulting in a DCF of 1.45 and 1.36, respectively. An appreciable residual storey drift equal to 4% was observed at the end of the test after unloading the frame (Fahnestock et al. 2007; Palmer et al. 2014), which was mainly due to the pulse-type near-fault ground motion and the final monotonic push.

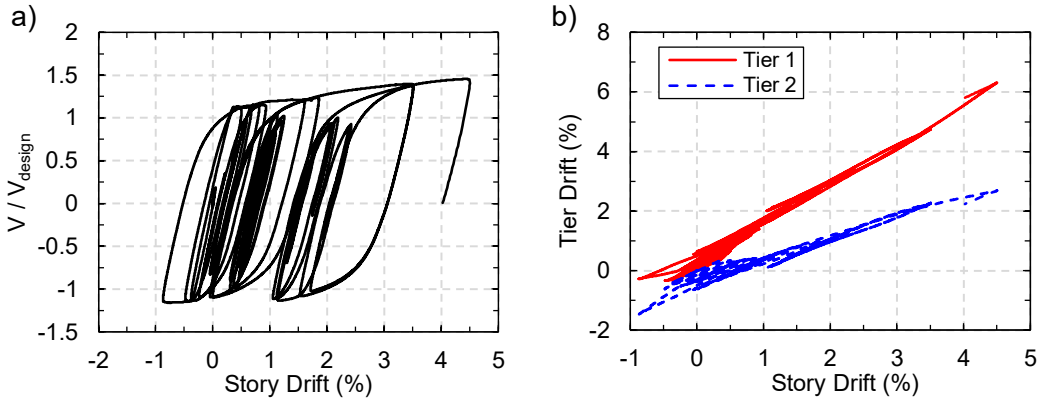

Figure 3.7: a) Base shear versus storey drift; b) tier drifts versus storey drift.

3.3.3 BRB Response

The axial force versus axial strain of the BRB core, ε_{sc}, in Tier 1 and Tier 2 are shown in Figures 3.8a and 3.8b, respectively. The BRB axial force is normalized by the yield strength of the core, P_{ysc}. As shown, Tier 1 BRB was in tension under the majority of the loading cycles, while the applied displacement often created compression in Tier 2 BRB. The tensile strain of the core in Tier 1 BRB at the peak roof displacement of the second displacement history was more than two times the compressive strain of the core in Tier 2 BRB (2.8% vs. -1.25%), suggesting a higher amount of damage in the first tier BRB (Tremblay et al. 2006; Fahnestock et al. 2007; Li et al. 2022). Figure 3.8c shows the normalized BRB axial forces against their respective tier drifts. As shown, Tier 1 BRB, which is often in tension under the applied displacement histories, experienced significantly higher displacement in comparison with Tier 2 BRB in compression (6.3%h_1 vs. 2.7%h_2). Referring to Figure 3.8c, an interesting observation was made: the overstrength of Tier 2 BRB in compression (1.42) was lower than that of the first tier BRB in tension (1.63) at the end of the test, which runs counter to the design assumption where the adjusted brace strength in compression was higher than that in tension with a multiplier equal to the compression strength adjustment factor, e.g., β = 1.24 in the specimen tested here. This finding suggests that the BRB

forces in the tiers acting in compression may be lower than the code-specified adjusted brace strength in compression because of lower deformation demands developed in the compression-acting tiers of an MT-BRBF compared to the higher deformation demands induced in tension tiers, which itself stems from the fact that the post-yielding stiffness of the compression BRB is relatively higher than that of the tension BRB, imposing higher lateral deformation in tension tiers. It is significant to note that the BRBs tested as part of this frame satisfied the 2022 AISC 341 prequalification requirements achieving a strain greater than would be expected from a prequalification test and a cumulative ductility demand exceeding 200 times the core yield strain, ε_{scy} = 0.2% (AISC 2016).

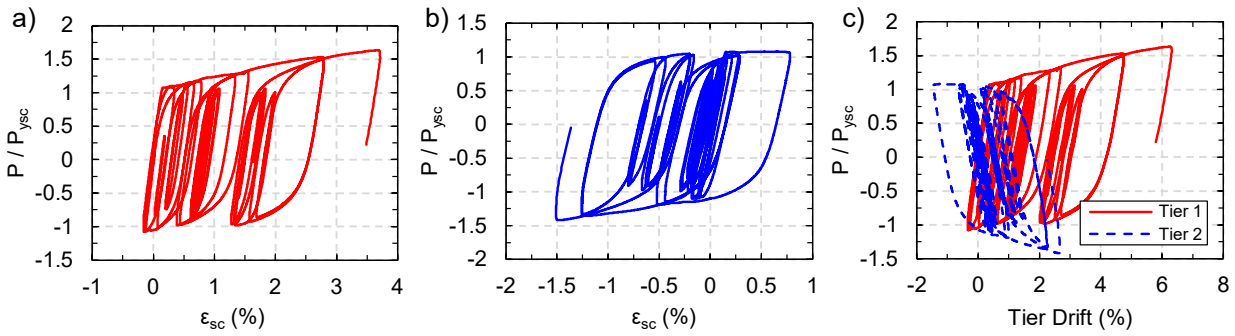

Figure 3.8: a) Hysteretic response of Tier 1 BRB; b) hysteretic response of Tier 2 BRB; c) BRB forces versus tier drift.

3.3.4 Column Response

The asymmetric post-yielding behaviour of the BRBs in tension and in compression in adjacent tiers at a given roof displacement resulted in unequal horizontal shears contributed by the BRBs in each tier. Given that the storey shear in all the tiers is identical in a multi-tiered braced frame, the unbalanced storey shear produced by braces in any adjacent tiers should be compensated by the columns through their flexural deformations, which induces the in-plane bending demands in the MT-BRBF columns. Figures 3.9a-e show the histories of storey drift, tier drifts, BRB forces, and

west column in-plane (weak axis) and out-of-plane (strong axis) bending moments, respectively. The column moment, M_y, was measured 800 mm below the strut level and was normalized by the weak axis plastic moment capacity of the section M_{py}. Referring to Figure 3.9d, the in-plane moment demands induced in the column were directly correlated with the difference between the tier drifts (Figure 3.9b) rather than with the BRB forces (Figure 3.9c), which were nearly equal in both tiers. At t_I = 9s, when the maximum storey drift of 1.9% was attained under the first displacement history, the in-plane moment demand in the west column reached $0.3M_{py}$. The west column experienced its maximum in-plane moment demand $0.4M_{py}$ under the ground motion records at t_{II}= 35s, at the early stages of the second displacement history. At this point, significant yielding was observed and recorded in the columns at the strut level where the largest in-plane moment was induced along the column height. A similar response but with a more pronounced moment demand, $0.5M_{py}$, was observed when the final monotonic loading displacement corresponding to 4.5% storey drift was applied. It is worth noting that the rotational stiffness of the strut-to-column connection can also affect column in-plane bending, which was minimal in the test frame due to the use of a close to pinned splice connection (AISC 2017) as shown in Figure 3.5d.

The columns experienced limited out-of-plane moment demands. As shown in Figure 3.9e, the maximum out-of-plane moment demand was $0.02M_{px}$. This minimal out-of-plane moment was likely attributed to the enhanced gusset plate design method that resulted in stiff gusset plates, which in turn limited out-of-plane deformation of the BRBs. Figure 3.9f shows the 2D strain contours from the DIC results on the north flange of the west column near the strut level as well as the estimates of the in-plane bending moment at key points using the north flange DIC strains at highlighted key points. As can be seen, the moment estimate using the DIC agrees well with the strain gauge results. The accuracy of the moment estimated using the north flange DIC results

further confirms the limited out-of-plane demands induced on the columns. Although not observed in the test frame here, there could be scenarios where noticeable out-of-plane demand is generated in MT-BRBF columns, e.g., due to out-of-plane deformation of BRB gusset plates or appreciable P-δ effects, and thus it is recommended that the columns be torsionally braced at the strut-to-column connections as prescribed by AISC 341-22.

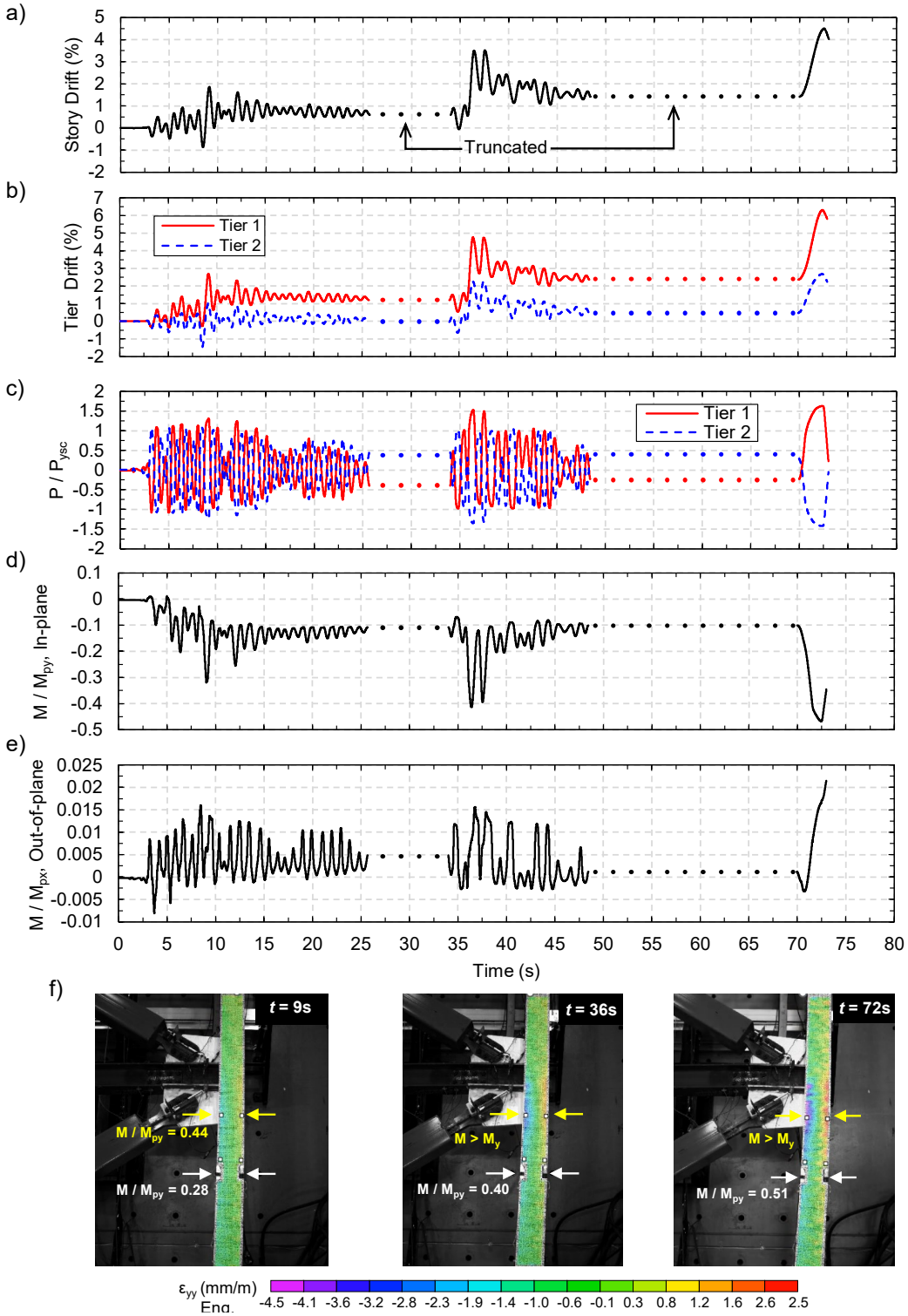

Figure 3.9: Frame response history: a) storey drift; b) tier drifts; c) BRB axial forces; d) column in-plane bending moment at the tier level; e) column out-of-plane bending moment at the tier level; f) strain contours at mid-height of the west column.

The histories of storey drift, column in-plane rotation at the base, and in-plane bending at the base of the west column are given in Figures 3.10a-c, respectively. The column rotation at the base was computed using the average of the readings from two inclinometers located at the north and south flange of the column, respectively. Overall, column in-plane bending near the base was negative and its amplitude was always higher than that at the strut level, as reported in Figure 3.10d, which resulted in reverse curvature bending in the columns (Figures 3.6b and 3.6c), and improved the stability of the column under large in-plane bending in the presence of a high axial compression force (Imanpour et al. 2016b). In other words, the flexural stiffness provided by the base connection and footing increased significantly the flexural stiffness of the column, thus distributing the in-plane moment demand induced due to the non-uniform distribution of frame inelastic response and reducing P-Δ effects on the column. Owing to the large negative moment at the base, significant yielding was observed in the column at the base as shown in Figure 3.5a. The highest base rotation under the first displacement history was recorded as –0.012 rad., resulting in an in-plane moment of $0.5M_{\text{py}}$ at t_I = 9s, which corresponds to the time when the largest in-plane moment at the strut level was observed under the first displacement history. At t_{II} = 35s, i.e., the time corresponding to the peak base rotation of -0.02 rad. under the second displacement history, the base in-plane moment reached $0.6M_{\text{py}}$.

The normalized in-plane bending of the west column near the base against its rotation at the base is shown in Figure 3.11a. Using this plot, an average rotational stiffness was calculated for the column at its base as K_θ = 2008 kN-m/rad, which is approximately 64% of the elastic rotational stiffness of a fixed-base column (3159 kN-m/rad). This suggests that the column base condition, although designed under axial tension and compression loads only, offers an appreciable flexural stiffness, which significantly enhanced the column stability response in the test frame. However,

the resulting moment at the column base raises a question regarding the design demands of the column base in steel braced frames, which requires further testing and investigation.

The axial force, the axial shortening response, of the west column is shown in Figure 3.11b. In this figure, P_{ny} is the nominal weak-axis compressive strength of the column section and axial shortening was computed using a string potentiometer measuring displacement along the height of the column. The average axial stiffness of the column was measured as K_{axial} = 420 kN/mm. As shown, the axial stiffness of the column was almost linear until the end of the test when the monotonic loading was applied during which the axial stiffness started to degrade, indicating the possibility of column buckling had the frame lateral displacement been further increased. The response of the east column at its base was almost identical to the west column, except that the east column was under a lower axial load due to the orientation of the BRBs.

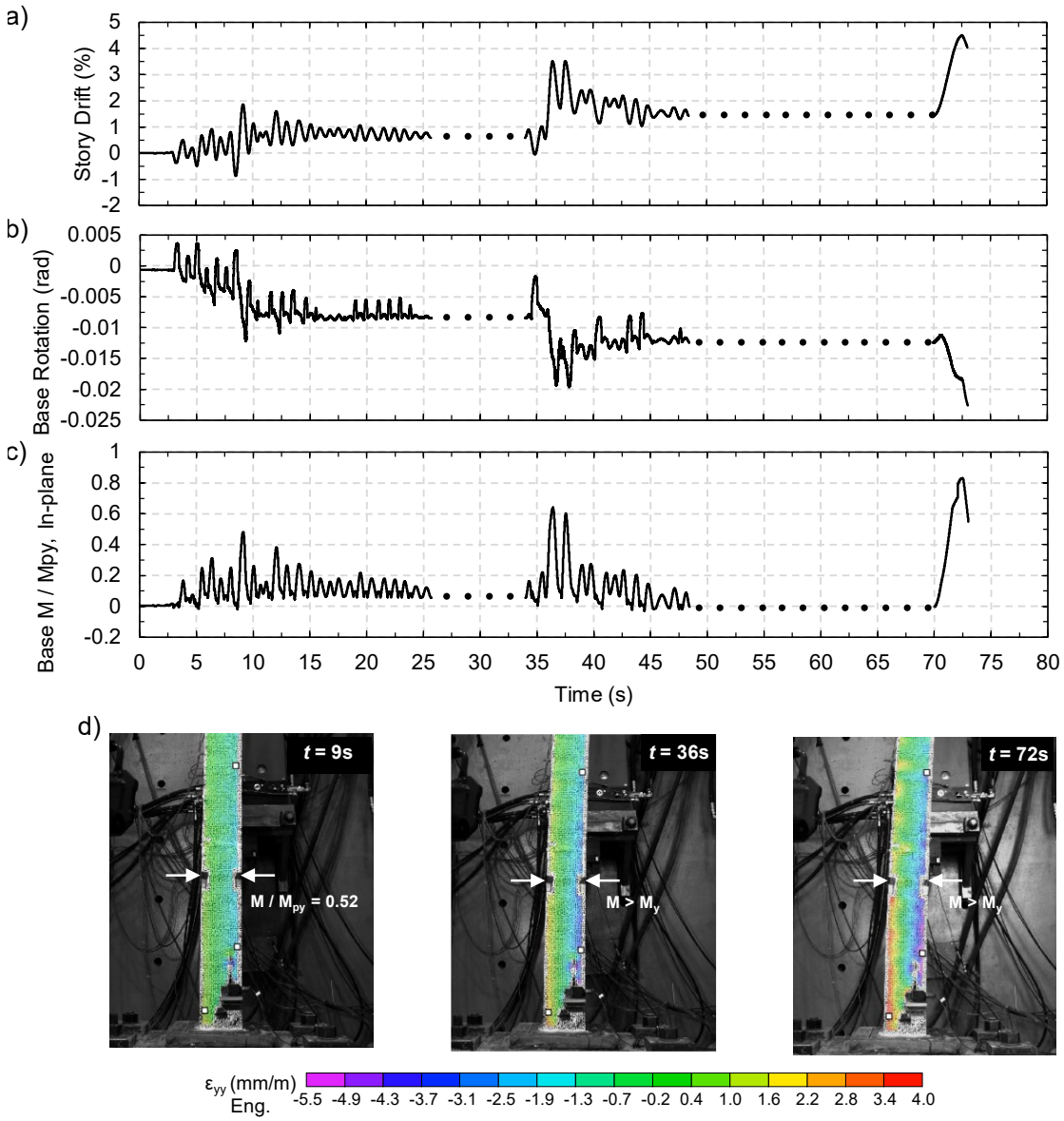

Figure 3.10: a) Storey drift history; b) west column base rotation; c) in-plane moment demand history at the base of west column; d) strain contour at the base of the west column.

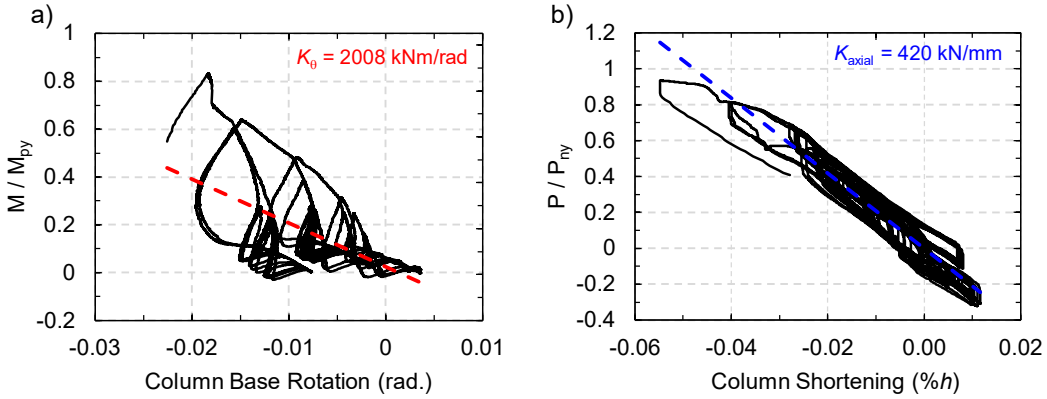

Figure 3.11: West column hysteresis response: a) normalized in-plane moment versus base rotation; b) normalized axial force versus shortening.

The axial force and in-plane bending interaction at the tier level and base of the west and east columns are shown in Figures 3.12a and 3.12b, respectively. In the interaction plots, P/P_{ny} is the ratio of the column axial load to its nominal weak-axis compressive strength with positive values indicating compression. The AISC 360 beam-column interaction curve was also plotted in these figures to identify the potential column failure. When calculating the nominal buckling resistance of the column, the base was assumed to be pinned with an effective length factor equal to unity. Referring to Figure 3.12, both east and west columns had similar moment demands at the tier and base level. The west column, however, had larger axial loads due to the orientation of the BRBs and the direction of loading. The difference between the axial forces between Tier 1 and the base in the west column is attributed to *P*-Δ effects and possible errors in the strain gauge readings in the nonlinear range of the material. For the west column (Figure 3.12a), the *P*-*M* interaction of the west column exceeded the AISC 360 limit but no instability was observed, which likely stems from the increased rotational capacity of the columns contributed by the flexural stiffness of the base connection and footing. As shown in Figure 3.12b, the east-column *P*-*M* interaction approached the AISC 360 limit but remained below the limit duo to its lower axial force.

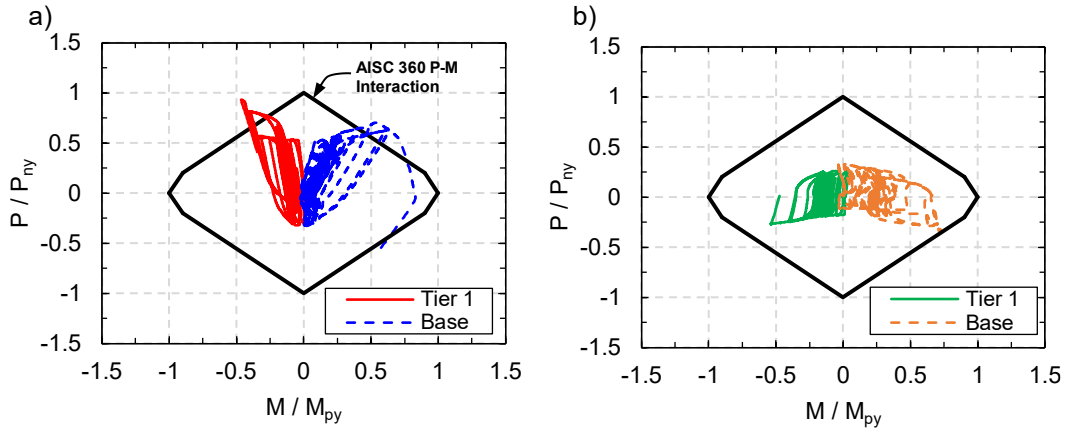

Figure 3.12: Axial force – In-plane bending interaction: a) west column; b) east column.

3.4 Proposed Analysis Technique

The results obtained from the full-scale testing of the two-tiered BRBF confirmed that frame inelastic deformation is not uniformly distributed between tiers in frames with BRBs undergoing tensile yielding in one of the tiers and compressive yielding in the adjacent tier at a given roof displacement. Moreover, it was found that the columns in the two-tiered BRBF specimen experienced significant flexural deformation due to the uneven distribution of the frame inelastic deformation between tiers, which produced flexural bending in the columns. This should be considered in design to ensure the columns have sufficient flexural strength to resist the combination of an axial force and in-plane bending. Finally, the experimental test results indicated that excessive axial deformation may be induced in the BRBs acting in tension under the ground motion record, which may cause a low-cycle fatigue fracture of the steel core under major seismic events. This necessitates additional stiffness requirements to prevent excessive drift demands in braced tiers, such as potentially adjusting the flexural stiffness of the columns. A displacement-based seismic analysis technique is proposed here to analyze multi-tiered BRBFs based on the observed specimen response. The technique is only applicable to single-diagonal MT-BRBFs, which is generally the preferred configuration in practice. The proposed procedure differs from the

isolated column analysis method implemented in 2022 AISC 341 for multi-tiered BRBFs. In particular, it relates the column bending moment and flexural stiffness to relative tier deformations, which was found to directly influence the MT-BRBF seismic response.

The column in-plane flexural demand is obtained when the frame reaches the roof deformation corresponding to the expected storey drift, $C_d\delta_e$, assuming that the inelastic frame deformation, $\delta_{in} = C_d\delta_e - \delta_e$, occurs only in the tier or tiers where BRBs undergo tensile yielding in each horizontal loading direction. This implicitly means that in each loading direction, the tier or tiers whose BRBs are in compression do not contribute to the inelastic frame response. This strategy is expected to result in a conservative prediction of the column moment while simplifying the distribution of the frame lateral deformation. Two loading scenarios (one for positive roof displacement and one for negative roof displacement) should be considered and the largest moment obtained from both loading directions should be used in design (Figures 3.13a and 3.13b). The proposed deformation profile is shown in Figure 3.13a for the two-tiered BRBF specimen when the frame is pushed to the right inducing tension in Tier 1 BRB and compression in Tier 2 BRB. At this point, the frame reaches its expected roof displacement of $C_d\delta_e$ = 125 mm and the respective inelastic deformation of $\delta_{in} = C_d\delta_e - \delta_e$ = 104 mm. The frame is then analyzed under the proposed deformation profile to calculate column shear and in-plane flexural bending assuming that the bases of the columns are pinned in flexure, which is often used in the design of steel braced frames. Although the results of the experimental study showed that the column base can attract flexural bending due to the partial fixity provided by the anchor rods and base plate, a pinned base condition was adopted here to achieve a simple analysis technique and conservative estimations of column moment. The proposed analysis technique can be easily conducted using a computer-aided structural analysis program. As shown in Figure 3.13c, using a linear numerical model of the frame developed in SAP2000 (CSI

2018), the moment induced in the columns of the test specimen at the tier level under δ_{in} = 104 mm is equal to 32 kN-m. The columns are designed to resist the combination of required axial strength and in-plane flexural moment. For the frame example, a W200×100 was found to satisfy the strength requirements when considering the in-plane moment, calculated using the proposed method. A similar analysis should be performed when the frame is subjected to the expected storey drift in the opposite direction as shown in Figure 3.13b. This deformation profile represents tensile yielding in Tier 2 BRB and compression yielding in Tier 1 BRB. In this case, since the compression tier is located in Tier 1, it is assumed that no drift occurs in this tier and thus Tier 1 is restrained horizontally when imposing the total inelastic deformation in Tier 2. The moment induced in the columns at the tier level of the frame example is identical in both loading scenarios, as shown in Figure 3.13c.

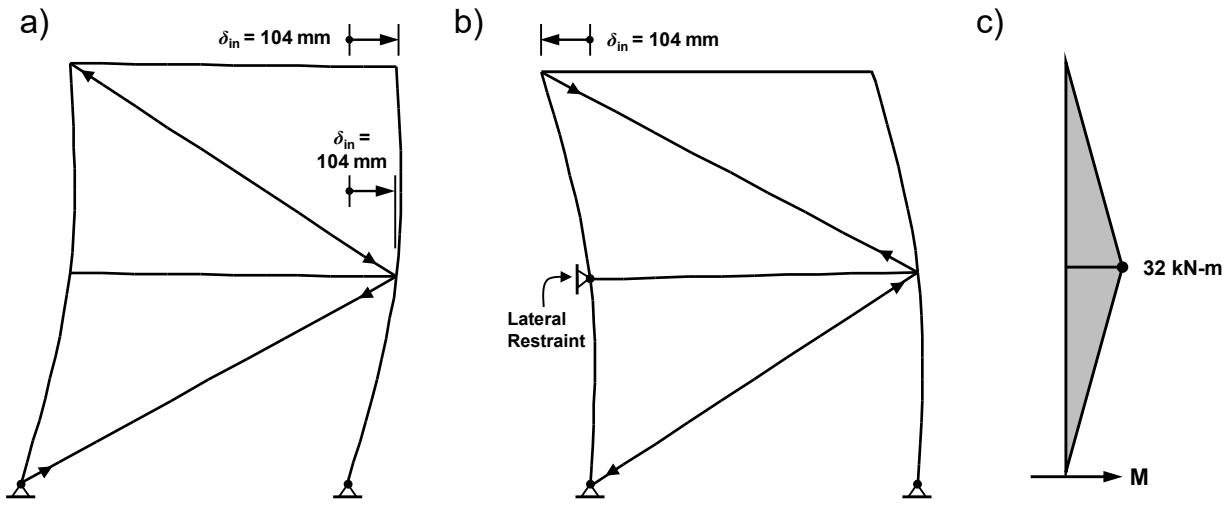

Figure 3.13: Proposed analysis technique: a) analysis scenario 1 (Tier 1 in tension); b) analysis scenario 2 (Tier 2 in tension); and c) column in-plane bending moment for both scenarios.

To further evaluate the prediction of flexural bending demands in multi-tiered BRBF columns using the proposed technique, the in-plane bending moment is computed for the columns of the

test specimen at the tier level when the peak roof displacement is attained in each of the three phases of the displacement histories (Figure 3.4a). The moment demand under the peak roof displacement of +171 mm under the first displacement history is obtained as 46 kN-m, which is slightly larger than the moment observed in the test, 36 kN-m (Figure 3.14b). Upon increasing the roof displacement to +315 mm, which represents the peak roof displacement under the second displacement history, the resulting in-plane moment is found as 90 kN-m, which is again higher than the moment recorded in the test — 47 kN-m (Figure 3.14c). Using the peak frame displacement of +405 mm achieved at the end of the monotonic push, the in-plane moment is calculated as 118 kN-m, which is significantly higher than the observed in-plane moment of 59 kN-m. As shown in Figures 3.14b-c, the proposed method always yields a conservative estimation of column in-plane bending moment, with a higher level of conservatism as the storey drift increases. This overestimation is mainly attributed to the fact that the contribution of the tier(s) with a BRB yielding in compression to the overall frame inelastic deformation is completely neglected in the analysis.

While this method is conservative when compared to the experimental results, it still provides a required in-plane flexural strength that is seven times lower than that computed using the 2022 AISC 341 analysis method (32 vs. 221 kN-m), leading to a potentially more efficient and economical design.

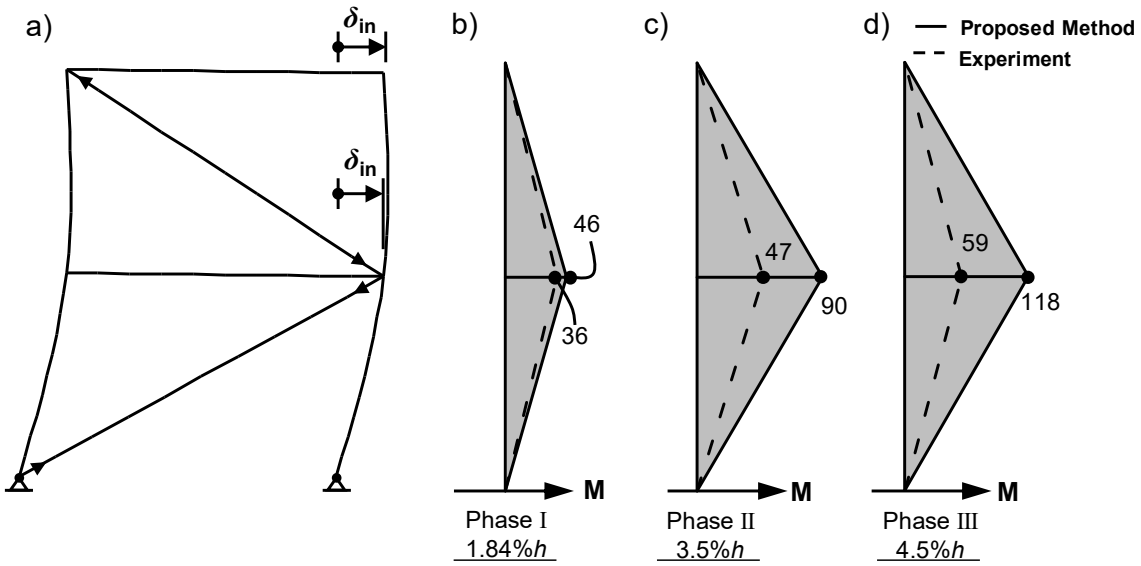

Figure 3.14: Comparison of proposed analysis technique and test results: a) analysis scenario considered; b-d) column in-plane moments at the peak storey displacements corresponding to each loading phase (h = 9 m; units = kN-m).

The proposed analysis technique can also be used to verify tier drifts. As per 2022 AISC 341, tier drift should be limited to 2% when the anticipated design storey drift is attained. Column flexural stiffness in the plane of the frame can be used to achieve this goal in multi-tiered BRBFs. For the frame specimen under the positive roof displacement, columns with a weak-axis moment of inertia of at least 2.89×10^7 mm^4 are required to limit the tier drift in Tier 1 to 2% when the anticipated design storey drift is attained. W200×100 columns previously selected to satisfy the column strength requirement are sufficient to limit the tier drift in both tiers to the code-specified limit of 2%.

3.5 Conclusions

A full-scale, two-tiered steel Buckling-Restrained Braced Frame (BRBF) part of a single-storey building designed in accordance with 2010 AISC 341 was experimentally tested. This test constituted the first full-scale experimental investigation into the column stability response and

distribution of frame lateral deformation under a loading protocol representing earthquake ground motions. The loading protocol consisted of the roof displacement histories obtained from nonlinear response history analyses under two ground motion records (far-field and near-field records) plus a monotonic push. The test results provide valuable insight into the seismic behaviour of multi-tiered BRBFs, namely column in-plane flexural bending, taking into account the influence of the base condition and the non-uniform deformation of the frame lateral deformation between tiers. The primary findings of this study are summarized as follows:

- Frame inelastic deformation tends to concentrate in the tier with the lowest storey shear resistance and post-yield stiffness; this is the tier where the BRB yields in tension. Tension-acting BRB (Tier 1 for the most part of the test) experienced an appreciably higher axial strain compared to compression-acting BRB in Tier 2 (2.65% vs. -1.17% at the maximum drift under the far-field record).
- Non-uniform distribution of frame lateral deformation between adjacent tiers with BRBs yielding in tension and compression induces significant in-plane flexural bending on the columns. The flexural moment reached 0.3 of weak axis plastic moment capacity of the column (M_{py}) at a maximum storey drift of 1.85% during the far-field 1994 Northridge Beverly Hills earthquake record, $0.4M_{py}$, at a maximum storey drift of 3.5% during the near-field 1989 Loma Prieta Saratoga-Aloha earthquake, and $0.5M_{py}$ when the frame lateral displacement was monotonically increased to create a 4.5% storey drift.
- Significant flexural yielding was observed in the column carrying a higher axial compression load (the west column when the frame moved west) at its base, mid-height and tier level under the far-field displacement history when the frame reached its maximum

storey drift, but no column instability occurred during the test and the frame achieved an over-strength of 1.32 times the design base shear at the end of the far-field loading protocol.

- The base of the frame behaved more like a fixed-base as it was subjected to significant flexural bending due to rotational restraints provided by the column base connection, anchor rods and concrete footing. This forced the column to deform in a double-curvature. The elastic rotational stiffness of the column base was estimated as 64% of the rotational stiffness of a fixed-base column (K_θ = 3159 kN-m/rad).
- The BRBs exhibited acceptable seismic performance, achieving a cumulative ductility demand in excess of 200 times the core yield strain as required by AISC 341 prequalification testing.
- A computer-aided analysis technique was proposed to analyze multi-tiered BRBFs based on the observed specimen response. This technique distributed inelastic frame deformation only between tier(s) with tension BRBs to approximately reproduce column curvature, producing flexural bending in the columns, and relative tier deformation was anticipated under lateral seismic loads. This technique can be used in the design of steel multi-tiered BRBFs.

CHAPTER 4 SEISMIC RESPONSE AND DESIGN OF STEEL MULTI-TIERED BUCKLING-RESTRAINED BRACED FRAMES IN CANADA

Abstract

This paper examines the seismic behaviour of steel Multi-Tiered Buckling-Restrained Braced Frames (MT-BRBFs) and proposes analysis and design methods within the framework of the Canadian steel design standard. A set of 16 prototype frames, part of a single-storey building, are selected and designed. The fibre-based numerical model of the frames is then developed in the *OpenSees* environment and is used to analyze the frames under earthquake accelerations. The seismic response of the prototype frames is interrogated using local and global response parameters including storey and tier drifts, BRB force-deformation response, column axial force and flexural bending demands. The results of the dynamic analyses show that frame lateral deformation tends to concentrate in the tier(s) undergoing tensile yielding, creating larger inelastic deformation in tension-acting BRBs compared to those yielding in compression and imposing in-plane flexural bending on the columns. Two analysis and design methods, including a detailed method and a computer-aided (alternative) technique are proposed and demonstrated for a four-tiered BRBF. The proposed methods can predict with sufficient accuracy column in-plane flexural bending and tier drift demands, while leading to an improved seismic response.

Keywords: Steel multi-tiered braced frames, Buckling-restrained braces, Seismic response, Nonlinear analysis, design method.

4.1 Introduction

Tall single-storey buildings are widely used in North America to serve as warehouses, airplane hangars, industrial buildings, sports facilities and shopping centres. A steel multi-tier bracing

configuration, which consist of multiple bracing tiers stacked vertically between the foundation and roof levels, is often employed in such buildings to resist lateral seismic and wind loads. The reason for this is that the application of a single bracing panel along the full building height is not feasible, e.g., due to significantly long braces or steep bracing connections. Multi-Tiered Braced Frames (MT-BFs) are also used in multi-storey buildings with tall storey heights or in non-building structures such as stadiums. Intermediate horizontal struts are typically used between bracing panels to provide a load path for the lateral seismic load and brace the columns in the plane of the frame. However, the columns are typically unbraced along the frame height for out-of-plane buckling. To achieve a more economical design, the MT-BF columns located on the exterior walls typically consist of wide-flange profiles oriented such that out-of-plane wind loads create strong axis bending.

Although Multi-Tiered Concentrically Braced Frames (MT-CBFs) are more prevalent in low-to-moderate seismic regions in particular, Buckling-Restrained Braces (BRBs) can be used in MT-BFs in regions of high seismicity as an alternative to conventional steel braces. This framing configuration is referred to as Buckling-Restrained Braced Frames (MT-BRBFs). Figure 4.1a shows an application of five-tiered BRBFs in a sports facility. Various bracing configurations, including single-diagonal, V-, inverted V-, X-, or two-bay X-bracing, can be utilized in MT-BRBFs, as shown in Figure 4.1b. Single-diagonal bracing configurations consisting of a single-diagonal brace in each tier can be achieved with BRBs having an opposing orientation in adjacent tiers that meet at a common bracing connection at the column, i.e., a zigzag pattern (designated as Z-bracing here), as shown in Figure 4.1b, with BRBs having the same orientation along the frame height (designated as S-bracing here) as shown in Figure 4.1b, or a combination of both (designated as ZS-bracing here). The zigzag pattern is preferred in practice to reduce construction costs due to a reduced number of BRB connections and smaller strut sizes. Reduced seismic force is induced in the intermediate struts of MT-BRBFs

with a zigzag pattern (Z-bracing) in comparison to MT-BRBFs which utilize S-bracing whereby the entire base shear is transmitted through the intermediate struts. MT-BRBFs with ZS-bracing may be used to reduce the net tension force in the columns and the resulting uplift force on the braced frame footing, while lessening unbalanced forces in the columns.

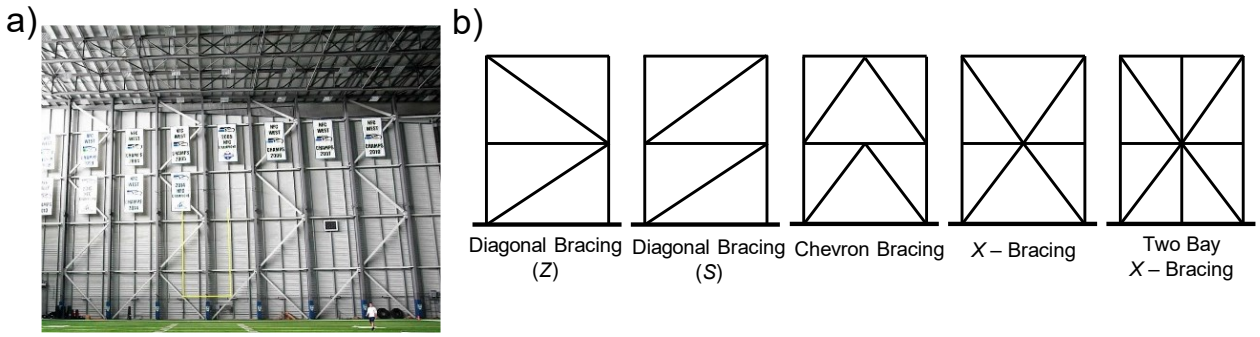

Figure 4.1: a) Five-tiered BRBF used in a sports facility (Courtesy of Michael Lawrie); b) multi-tiered BRBF configurations.

Multi-tiered concentrically braced frames have been given significant attention over the past decade. The past numerical and experimental studies performed on MT-CBFs have shown that if the columns are designed under an axial load only, inelastic deformation of the frame under seismic loading tends to distribute unevenly along the height of the frame, concentrating in the tier that yields first (referred to as the critical tier). Brace tensile yielding in the critical tier, along with the loss of the axial strength of the compression brace of the same tier in the post-buckling range, prevents yielding of the braces in other tiers. This results in excessive demands in the critical tier, which in turn, induces significant in-plane flexural bending on the columns (Imanpour et al. 2016a; b; c, 2022; Imanpour and Tremblay 2016; 2017; Cano and Imanpour 2020). In-plane flexural demand in the presence of a large axial compression force in the columns can cause column plastic hinging or even column instability. Nonuniform distribution of frame inelastic lateral deformation may also cause low-cycle fatigue failure of the bracing members in the critical tiers due to excessive deformation demands induced in

the braces of the critical tier. A preliminary study conducted recently to assess the seismic behaviour of MT-BRBFs confirmed that similar but less pronounced performance concerns exist in MT-BRBFs (Bani and Imanpour 2022, 2023). It was shown that although BRBs, due to their similar tensile and compressive resistances, promote a more uniform distribution of inelastic lateral deformation along the frame height in comparison to their conventional counterparts, variations in BRB's probable capacities and post-yield stiffnesses between adjacent tiers can still create a relatively lower lateral deformation in the tier with a BRB acting in compression compared to the one with a tension-acting BRB, producing in-plane flexural bending demands on the columns. When combined with a large axial compression force induced in the column due to gravity loads plus BRB axial capacities, such flexural demands may compromise column stability. To address these concerns in the United States, the 2016 Seismic Provisions for Structural Steel Buildings, AISC 341 (AISC 2016), introduced special seismic provisions for MT-BRBFs, which require that the columns be designed for the combination of an axial force arising from gravity loads plus BRB probable strengths and in-plane flexural bending due to the difference between BRB probable strengths in any adjacent tier. To obtain the column bending demands, the MT-BRBF column can be isolated from the frame with a pin support at its ends and be subjected to a transverse in-plane point load at each tier level with an amplitude of the greater of 1) the summation of frame shears from the probable brace strengths between adjacent tiers, and 2) a minimum notional load equal to 0.5% times the probable frame shear due to the brace's probable strength in the tier with a higher shear strength in any adjacent tier. Furthermore, intermediate horizontal struts are required between tiers and the columns must be torsionally braced at every strut-to-column connection. Although not prohibited, there are no design guidelines for MT-BRBFs in the 2019 Canadian steel design standard, CSA S16 (CSA 2019). In view of the extensive application of MT-BRBFs in practice, often in critical structures, a design

method in the framework of the Canadian steel design standard is urgently needed to address the concerns raised regarding the seismic performance of such frames.

This paper examines the seismic response of steel multi-tiered BRBFs designed to the Canadian seismic provisions and proposes analysis and design methods to improve the seismic performance of such frames. A set of 16 prototype frames, with different bracing configurations, frame heights, number of tiers, relative tier heights, and material yield strengths are selected and designed in accordance with the 2019 Canadian steel design standard. The seismic behaviour of the frames is then numerically evaluated under seismic ground motion records using the nonlinear response history analysis. Lastly, a detailed procedure and an alternative design procedure are proposed to determine the column minimum in-plane flexural strength and stiffness.

4.2 Prototype Multi-Tiered BRBFs

A single-storey sports facility located in Victoria, British Columbia, Canada was selected in this study. The building plan dimensions are 70 m × 126 m. The building is of normal importance and is located on a Class C site. The roof system consists of corrugated steel deck supported by steel joists sitting on steel trusses that span the full building width. The columns are located on the exterior walls of the building and are spaced at 7.0 m. The lateral-load resisting system of the building consists of six multi-tiered BRBFs in each principal direction. One of the BRBFs in the long direction of the building was studied in this paper.

A set of 16 frames having different configurations (Z, S, ZS), total heights (h = 8, 12, 18, 24, 30 m), number of tiers (i = 2, 3, 4, 6), and relative tier heights (h_1/h_2 = 1.0, 1.5) were considered to generate a virtual test matrix, as shown in Figure 4.2. Chevron or X-bracing configurations were not considered in this study as their response has been deemed not as critical as a diagonal bracing configuration when used with multi-tiered framing systems. The reason for this is that almost

identical storey shear resistances develop between tiers when each tier possesses two BRBs, one acting in tension and the other acting in compression under lateral seismic loads. The labeling scheme for each frame is number of tiers, i – frame total height, h – tier height ratio, and h_1/h_2 – bracing configuration. For example, 6T-30-1.5-Z represents a six-tiered BRBF with a total height of 30 m, a height ratio of $h_1/h_2 = 1.5$, and BRBs oriented in a Z-pattern.

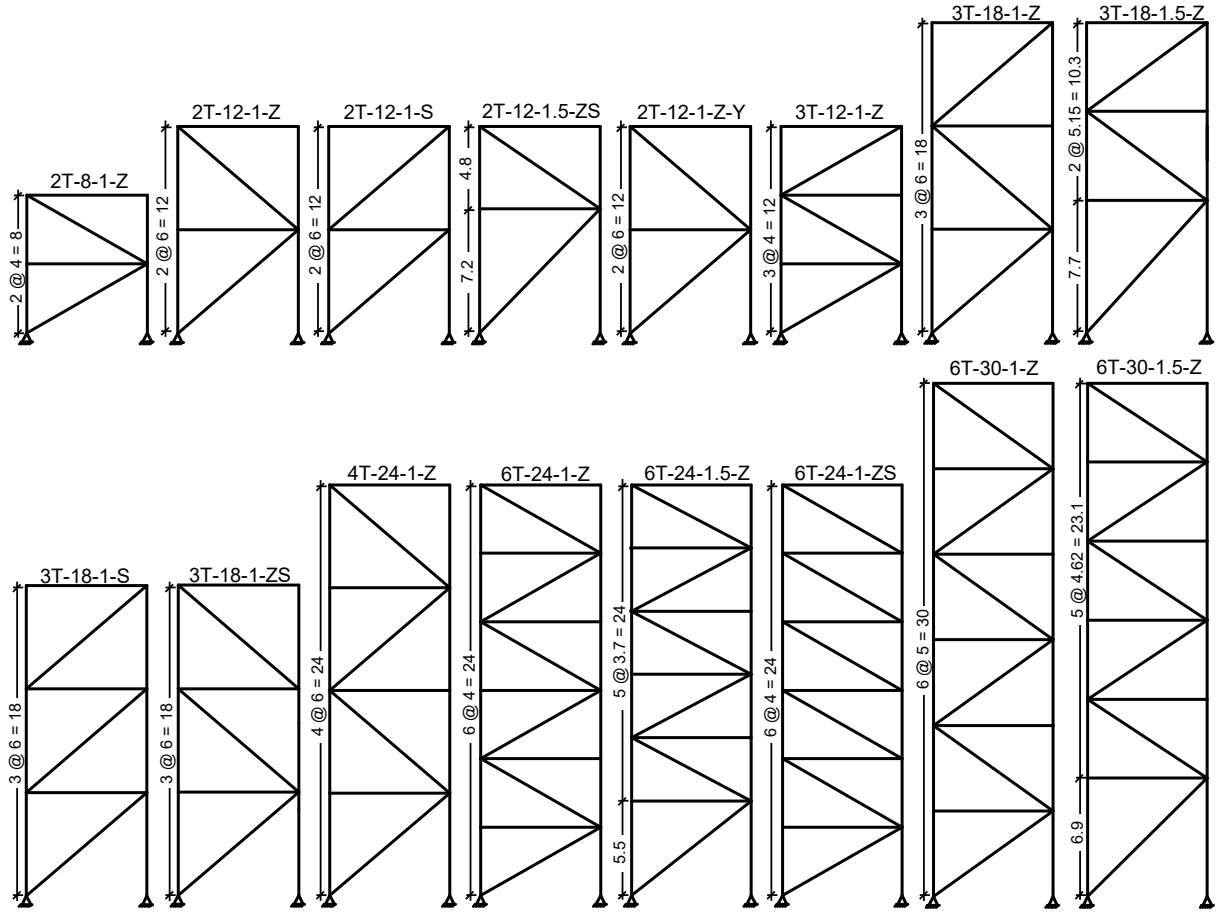

Figure 4.2: Prototype multi-tiered BRBFs (Bay width = 7 m; all Dimensions in m).

The gravity and seismic loading was determined in accordance with the 2015 National Building Code (NBC) of Canada (NRC 2015a). The gravity loads included the roof dead load (D) of 1.2 kPa, live load (L) of 1.0 kPa, and snow load (S) of 1.14 kPa. The unit weight of the exterior cladding was taken

to be 1.0 kPa. The factored column gravity load under the NBC load combination $D + E + 0.5L + 0.25S$ was equal to $P_G = 243$ kN for all the frames.

The design base shear, V, was calculated using the Equivalent Static Force Procedure (ESFP). The importance factor, I_E, and factor accounting for higher mode effects, M_v, were both taken as 1.0. The tributary seismic weight of each frame, W, was calculated using the roof dead load and tributary wall dead load plus 25% of the roof snow load. Multi-tiered BRBFs were designed as a ductile (Type D) BRBF with the ductility- and overstrength-related modification factors of $R_d = 4.0$ and $R_o = 1.2$, respectively. The design period to obtain the design spectral acceleration was taken as two times the fundamental period computed using the NBC empirical method ($T_a = 0.025h$, where h is the height of the frame). The design base shear was obtained taking into account accidental torsion, P-Δ effects and notional loads. The design base shear, along with the key seismic design parameters, are summarized in Table 4.1 for prototype frames. For all the frames studied here, the base shear under the lateral wind load obtained, assuming a 50-year return period, was lower than the respective seismic base shear.

Table 4.1: Prototype frames: seismic design parameters and selected members.

Frame Names	Design Parameters				Frame Properties						
	$2T_a$ (s)	$S(2T_a)$ (g)	W (kN)	V (kN)	A_{sc1} (in^2)	A_{sci} (in^2)	Column	Roof Beam	Strut	T (s)	$R_dR_o\Delta_e$ (%)
2T-8-1-Z	0.40	1.21	2706	712	4.9	4.9	W310X67	W200X59	W200X59	0.58	1.33
2T-12-1-Z	0.60	1.07	2846	688	5.4	5.4	W310X107	W200X59	W200X59	0.72	1.26
2T-12-1-S					5.4	5.4	W360X101	W200X59	W250X89	0.73	1.28
2T-12-1.5-Z					5.9	5.0	W310X107	W200X59	W200X59	0.74	1.31
2T-12-1-Z-Y*					5.4	5.4	W310X107	W200X59	W200X59	0.72	1.26
3T-12-1-Z	0.60	1.07	2846	688	4.7	4.7	W360X91	W200X59	W200X59	0.77	1.44
3T-18-1-S	0.90	0.78	3056	543	4.3	4.3	W460X128	W250X73	W250X73	1.08	1.37
3T-18-1-Z					4.3	4.3	W460X128	W200X59	W200X59	1.08	1.37
3T-18-1-ZS					4.3	4.3	W460X128	W250X73	W250X73	1.08	1.37
3T-18-1.5-Z					4.8	4.0	W460X144	W200X59	W200X59	1.11	1.44
4T-24-1-Z	1.20	0.63	3266	470	3.7	3.7	W530X150	W200X59	W200X59	1.44	1.44
6T-24-1-Z	1.20	0.63	3266	470	3.2	3.2	W530X150	W200X59	W200X59	1.51	1.62
6T-24-1-ZS					3.2	3.2	W530X150	W250X73	W250X73	1.51	1.62
6T-24-1.5-Z					3.6	3.2	W530X150	W200X59	W200X59	1.52	1.65
6T-30-1-Z	1.50	0.54	3476	434	3.2	3.2	W610X174	W200X59	W200X59	1.82	1.64
6T-30-1.5-Z					3.6	3.1	W610X174	W200X59	W200X59	1.84	1.68

* Yield strength of Tier 1 BRB reduced by 10%.

The prototype frames were designed in accordance with CSA S16-19. BRBs were designed using a mild steel plate conforming to ASTM A36 (ASTM 2008) with a yield stress of F_y = 290 MPa, which is taken as the average of the typical lower and upper bound yield strength of ASTM A36, i.e., Fy = 0.5 (262 MPa + 317 MPa). In each tier, the BRB core area, A_{sc}, was determined to resist the design base shear. The BRB core sizes are given in Table 4.1 for prototype frames. In the table, A_{sc1} is the selected BRB core area in Tier 1 and A_{sci} is the BRB core area in the remaining tiers. The strain hardening and the friction adjustment factors were assumed as R_{sh} = 1.36 and β =1.24, respectively (Saxey, personal communication 2022). The BRB probable resistances, calculated as $R_{sh}A_{sc}R_yF_y$ in tension and $\beta R_{sh}A_{sc}R_yF_y$ in compression, were used to compute seismic demands on columns, beams and struts. These demands, in addition to the forces induced due to gravity loads, were used to design the columns, beams and struts from wide-flange sections conforming to ASTM A992 (ASTM 2015) with a yield stress of F_y = 345 MPa. The columns were pinned at the base and the roof levels. Effective length factors lower than unity were used to obtain column buckling capacities in-plane

and out-of-plane taking into account distributed axial loads along the frame height and continuity of the column (Dalal 1969). Struts were sized under an axial force induced due to the unbalanced force between adjacent tiers plus the nodal bracing force required by CSA S16 to brace the columns in-plane. The roof beams were designed as a beam-column resisting an axial compression force due to BRB probable resistances, plus strong-axis bending under roof gravity loads. The roof beams were assumed to be laterally supported by the steel deck and joists. The wide-flange members selected comply with the CSA S16 width-to-thickness ratio limits for Class 2 sections. The selected columns, struts and beams are given in Table 4.1.

The frame lateral roof displacements, including inelastic effects, were calculated as $R_d R_o \Delta_e / I_E$ where Δ_e is the elastic roof displacement calculated under the design base shear. Roof drifts for all the frames (see Table 4.1) meet the NBC storey drift limit of 2.5%. The frames also satisfy the storey drift limit of 0.2% under the lateral wind load with a 10-year return period as per the 2015 NBC User's Guide - Commentary I (NRC 2015b).

4.3 Numerical Model and Ground Motions

A three-dimensional, fibre-based numerical model of MT-BRBFs was developed in the *OpenSees* program (McKenna et al. 2010) to perform nonlinear time history analyses. The model is shown in Figure 4.3a for a two-tiered BRBF with a Z-bracing arrangement. The model was pin-supported at its base and braced in the out-of-plan direction at the top to account for the lateral support provided by the roof system. The columns were modeled using nonlinear, force-based beam column elements in each tier with fiber discretization of the cross section. The Giuffre-Menegotto-Pinto (*Steel02*) material model (Filippou et al. 1983) with kinematic and isotropic hardening was selected for the columns. *Steel02* material parameters (b = 0.0067, R_0 = 23.43, cR_1 = 0.89, cR_2 = 0.07, a_1 = 0.35, a_2 = 12.12, a_3 = 0.33, and a_4 = 12.09) were adapted from the calibration performed against the CSA

G40.21-350WT steel cyclic coupon tests (Ashrafi and Imanpour 2021). Residual stresses based on the pattern proposed by Galambos and Ketter (1958) were assigned to the column section. To capture global buckling, the columns in each tier were divided into ten elements and an initial bi-directional, sinusoidal out-of-straightness corresponding to the column in-plane and out-of-plane buckling modes was assigned to the columns with a maximum amplitude of 1/1000 times the length between in-plane and out-of-plane supports, respectively. The roof beam and struts were modeled using elastic force-based beam-column elements.

The BRBs were modeled using corotational truss elements with an equivalent stiffness modification factor of 1.32, which was approximated based on the design tables provided by the BRB manufacturer (Saxey, personal communication 2022). The nonlinear cyclic response of BRBs was reproduced using the *Steel4* material model, which is capable of simulating the asymmetric, kinematic and isotropic hardening exhibited by steel BRBs (Zsarnóczay 2013). *Steel4* parameters, including $b_k = 0.01$, $R_0 = R_{0c} = 25$, $r_1 = r_{1c} = 0.9$, $r_2 = r_{2c} = 0.15$, $b_i = 0.0014$. $\rho_i = 1$, $b_1 = b_{1c} = 0.0001$, $R_i = R_{ic} = 1$, $l_{yp} = 1$, $b_{kc} = 0.028$, $b_{ic} = 0.05$, $p_{ic} = 0.601$, $R_u = 1.45$, $f_u = 1.65F_y$, $R_{uc} = 2.95$, and $f_{uc} = 2F_y$, were set to achieve the best match between the predicted response by the numerical model of this study and the test data obtained from the experimental testing of BRBs under quasi-static cyclic and seismic loading protocols (Dehghani and Tremblay 2017), as shown in Figures 4.3b and 4.3c, respectively. As shown, the *steel4* material can properly simulate the asymmetric, inelastic cyclic response of the BRBs under both loading histories. Young's modulus, $E = 200$ GPa, was assigned to all the materials and the yield strength, $F_y = 345$ MPa, was assigned to the wide-flange members while $F_y = 290$ MPa was assigned to the BRB cores. For one of the two-tiered BRBFs with Z-bracing (2T-12-1-Z), the BRB yield strength was reduced by 10% in the analysis to indirectly evaluate the effect of uncertainties that may originate from variations in the core material strength and cross-

sectional area (Schmidt and Bartlett 2002), the increase in material strength due to strain rate effects (Bruneau et al. 2011; Lamarche and Tremblay 2011; Dehghani 2016) and the brace connection details. This frame is labeled 2T-12-1-Z-Y.

A corotational formulation that accounts for *P*-Δ effects and large deformations was selected to simulate geometric nonlinearities. A leaning column was modeled using an elastic element with a relatively high axial and flexural stiffness to create large *P*-Δ effects due to the gravity load leaning on the selected braced frame. The lateral horizontal displacement of the leaning column at the roof level was constrained to that of the frame. Two lumped masses representing the mass tributary to the selected brace frame were assigned to the top end of the braced frame columns. The Rayleigh damping approach with mass proportional damping corresponding to 2% of critical in the first mode of vibration was assumed. To perform the analysis, gravity loads were applied first, and then a nonlinear time history analysis was performed using scaled ground motion accelerations.

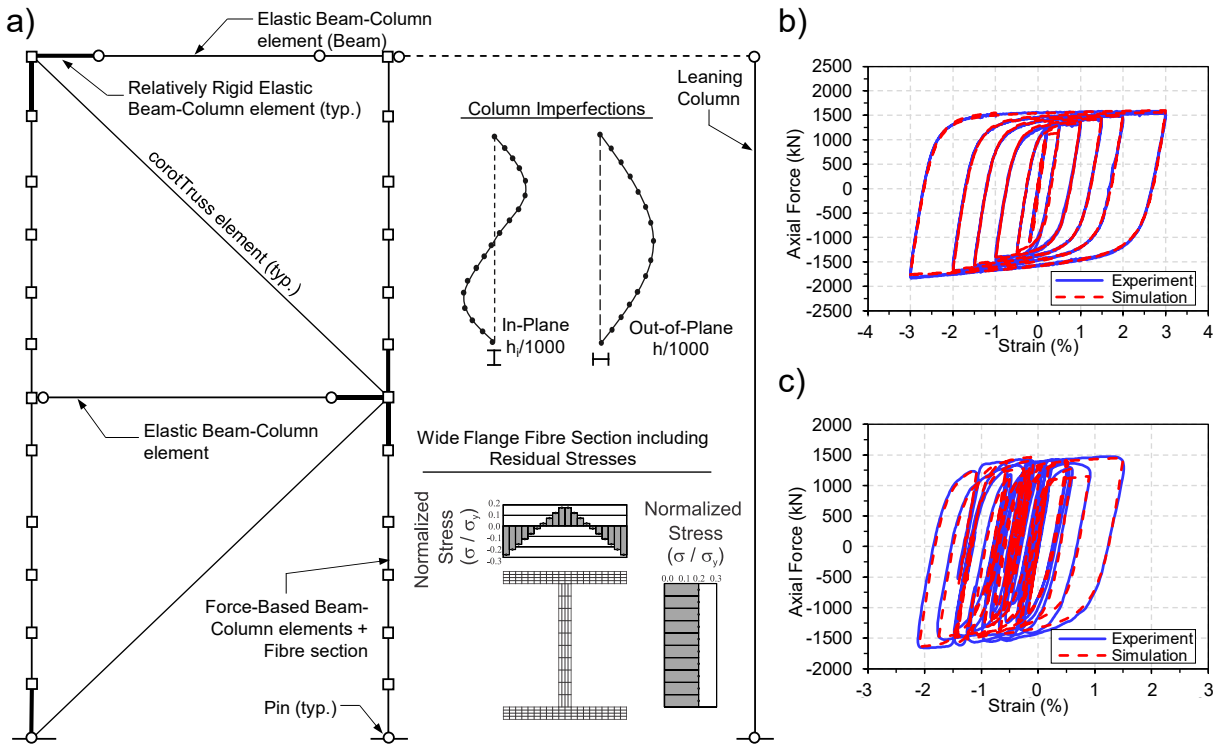

Figure 4.3: a) MT-BRBF fibre-based numerical model; b-c) Steel4 calibration under cyclic and seismic displacement histories.

Ground motion records were selected and scaled in accordance with the method prescribed in the 2015 NBC User's Guide - Commentary J (NRC 2015b). The records were selected considering the magnitude-distance scenarios that have the largest contribution to the seismic hazard at the building location, including magnitude M6–7 shallow crustal (far-field) earthquakes with a rupture distance, R_{rup}, ranging between 5–20 km, M6–7 deep in-slab earthquakes having a rupture distance ranging between 30–90 km, and M8+ subduction interface earthquakes with a rupture distance within the 10–70 km range. The selected records were then evaluated against the 2015 NBC Uniform Hazard Spectrum (UHS) for Victoria, BC, within three hazard scenario-specific period ranges over a period range of $0.15T_{min}$ to $2T_{max}$, where T_{min} and T_{max} are the minimum and maximum analytical fundamental periods of prototype frames, respectively. Each hazard scenario-specific period range was defined based on the dominant periods of the records associated with the magnitude-distance

scenarios obtained from the 2015 NBC seismic deaggregation data for a seismic hazard with a 2% probability of exceedance in 50 years. A set of 34 ground motions were finally selected, including 11 crustal, 12 in-slab, and 11 interface records. Table 4.2 provides the details of the selected records including event name, date, moment magnitude, M_w, rupture distance, R_{rup}, and recording station. The PEER NGA-West2 ground motion database was used to collect the crustal records (Ancheta et al. 2013) and subduction interface ground motions were obtained from the PEER NGA-Sub flatfiles (Mazzoni et al. 2021). The scaling of the records was performed in two steps: 1) individual records in each scenario-specific hazard set were scaled using a factor that minimizes the Mean Squared Error (MSE) between their 5% damped response spectra and the UHS over the scenario-specific period range, and 2) all ground motions in a scenario-specific hazard set were then collectively scaled using a second scaling factor such that their mean response spectra did not fall more than 10% below the UHS over the scenario-specific period range. Figures 4.4a-c show the 5% damped response spectra of the scaled ground motion records for crustal, in-slab and interface events, respectively.

Table 4.2: Selected ground motion records for Victoria, BC

Seismic Source (Database)	Event (Component)	Year	M_w	R_{rup} (km)	Station
Crustal (NGA-West2)	Imperial Valley-06 (237)	1979	6.5	15.2	Cerro Prieto
	Victoria (045)	1980	6.3	14.4	Cerro Prieto
	Loma Prieta (000)	1989	6.9	15.2	Capitola
	Landers (LN)	1992	7.3	19.7	Coolwater
	Northridge-01 (090)	1994	6.7	8.7	Arleta - Nordhoff Fire Sta
	Northridge-01 (090)	1994	6.7	10.1	Sun Valley - Roscoe Blvd
	Hector Mine (000)	1999	7.1	11.7	Hector
	Parkfield-02 (090)	2004	6.0	5.2	VINEYARD CANYON
	Niigata (EW)	2004	6.6	9.5	NIGH01
	Chuetsu-oki (NS)	2007	6.8	16.1	Yoitamachi Yoita Nagaoka
	L'Aquila (TE)	2009	6.3	6.8	V. Aterno -Colle Grilli
In-Slab (NGA-Sub)	Olympia (086)	1949	6.7	47.6	OLY0
	CA - 69 (NS)	1982	7.3	60.0	2747
	CA - 38 (NS)	1992	6.5	93.1	2894
	Nisqually (180)	2001	6.8	64.6	WEK
	Nisqually (N)	2001	6.8	65.2	TKCO
	Geiyo (NS)	2001	6.8	43.6	KURE
	Pingtung-Doublet-01 (E)	2006	7.0	40.7	KAU082
	Pingtung-Doublet-02 (E)	2006	6.9	31.9	KAU082
	SA - 2575090 (EW)	2007	6.7	46.4	MEJILLONE
	Ferndale (360)	2010	6.6	41.2	89509
	Ferndale (360)	2010	6.6	36.2	Loleta
	Ferndale (090)	2010	6.6	32.9	1725
Interface (NGA-Sub)	Michoacan (E)	1985	8.0	18.4	Aeropuerto Zihuatanejo
	Tokachi-oki (EW2)	2003	8.3	85.5	ASYORO-E
	Tokachi-oki (NS)	2003	8.3	92.2	SHIHORO
	Tokachi-oki (EW)	2003	8.3	61.2	47418
	SA - 2844986 (097)	2010	8.8	30.4	Concepción
	SA - 2844986 (T)	2010	8.8	36.5	CONT
	SA - 2844986 (T)	2010	8.8	49.8	HUAL
	Tohoku (NS)	2011	9.1	90.1	41207
	Tohoku (NS)	2011	9.1	86.3	Taiwa
	Tohoku (NS)	2011	9.1	52.6	GN5
	Iquique (E)	2014	8.2	71.4	MNMCX

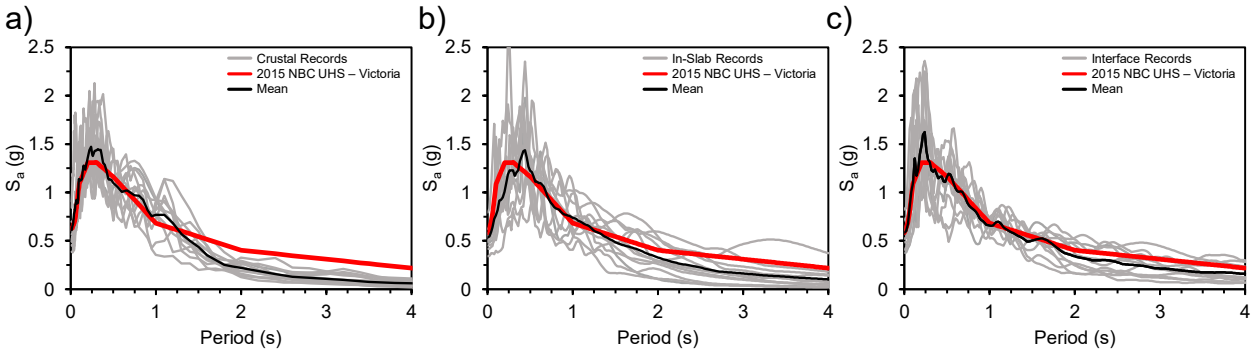

Figure 4.4: Response spectra of selected ground motion records: a) crustal; b) in-slab; and c) subduction interface.

4.4 Seismic Response of Multi-Tiered BRBFS

4.4.1 Four-Tiered BRBF Case Study

The seismic response of the four-tiered BRBF (4T-24-1-Z) is evaluated in this section. The key response parameters, including tier drifts, BRB forces, and column flexural bending demands are first presented under the 2007 Chile-Mejillone EW earthquake record. The statistics of these response parameters under the full suite of ground motions are then discussed.

Figure 4.5a shows tier drifts versus storey drift for 4T-24-1-Z under the selected ground motion record. In this figure, tier drift is measured as the relative lateral displacement of each tier divided by the respective tier height, h_i, and storey drift is defined as the roof displacement divided by the total frame height, h. Under this ground motion, the frame was subjected to predominately positive storey drift throughout the duration of the ground motion with the maximum storey drift reaching 2.5%h at t = 26s. Under positive roof displacement exceeding 0.4%h, Tiers 1 and 3 BRBs underwent tensile yielding, while Tiers 2 and 4 BRBs experienced yielding in compression. Referring to Figure 4.5a, the majority of the frame inelastic lateral deformation was concentrated in Tiers 1 and 3 (the weakest tiers under positive roof displacement), reaching 4.1% and 2.7% in Tiers 1 and 3, respectively, at

2.5% storey drift. At this storey drift, tier drifts in Tiers 1 and 3 were approximately 2.2 and 1.7 times those observed in Tiers 2 and 4, where BRBs were subjected to compression. Under each loading direction (positive or negative roof displacement), the tier or tiers where the frame inelastic lateral deformation tended to concentrate were referred to as the critical tier(s). These tiers can be identified by comparing the tier shear resistance obtained from the BRB probable resistance under each loading direction. BRB forces normalized by their respective yield strength ($A_{sc}F_y$) were plotted in Figure 4.5b versus the BRB core strain, assuming a yielding core length of 60% of the length of the brace between workpoints. As shown, tension BRB cores (in Tiers 1 and 3 under positive roof displacement) exhibited significantly larger axial strain demands compared to the compression BRB cores (in Tiers 2 and 4 under positive roof displacement) due to the lower post-yield stiffness of the BRBs in tension versus compression (Tremblay et al. 2006). The non-uniform distribution of inelastic lateral deformation along the frame height produced unequal BRB forces in tension and compression in adjacent tiers. To maintain storey shear equilibrium between tiers, the shear was induced in the braced frame columns, which resulted in in-plane flexural bending in the columns. Figure 4.5c shows the axial force – the in-plane flexural bending interaction of the left-hand-side (LHS) and right-hand side (RHS) columns at the strut level of Tier 1. Under the maximum positive roof displacement of 2.5%h, the RHS column was subjected to an axial compression force of $0.7C_n$, where C_n is the nominal compression resistance of the column, and a flexural moment of $0.4M_{py}$, where M_{py} is the weak-axis plastic moment capacity of the column section. No column buckling was observed under this ground motion, but partial plastic hinging of the column at mid-height of Tier 1 was confirmed due to the yielding observed at the flange tips.

The profiles of tier drifts under the full ground motion suite, including individual record and peak responses, are given in Figure 4.5d for the four-tiered BRBF. To obtain the peak response parameters,

the ground motion records were first categorized into two groups: those creating maximum absolute roof displacement in the positive direction and those with the maximum absolute roof displacement in the negative direction. Under each loading direction, i.e., positive or negative roof displacement, the peak response was computed by taking the 84th percentile results over the entire ground motion suite. The 84th percentile results were used to achieve consistent demand parameters for the positive and negative ground motions separately in comparison with the maximum of means of the ground motion ensembles using the absolute values of the demand parameters as recommended by the 2015 NBC User's Guide - Commentary J. Referring to Figure 4.5d, lateral frame deformation tends to concentrate in Tiers 1 and 3 (with peak tier drifts of 1.9% and 1.4%, respectively) when the frame is displaced in the positive roof displacement direction, whereas higher drift develops in Tiers 2 and 4 (with peak tier drifts of -1.4% and 1.8%, respectively) under the negative roof displacement. In both loading directions, a large proportion of frame inelastic lateral deformation takes place in the tiers undergoing tensile yielding. Figure 4.5e shows the profiles of BRB strains. As shown, the peak BRB strain demands in tension are nearly double those in compression in all the tiers (1.6% vs. 0.8%). Despite uneven distribution of BRB strain demands, they are not expected to cause low-cycle fatigue fracture in the BRB core (Li et al. 2022).

The profiles of column in-plane flexural bending demands are shown in Figure 4.5f for the RHS column. Column moments involve sign reversals occurring between adjacent tiers with opposing BRB orientations due to uneven distribution of frame lateral deformation in tension and compression BRBs, creating a kink at every tier level. The 84th percentile of the peak absolute flexural bending reached $0.18M_{py}$, $0.12M_{py}$ and $0.17M_{py}$, in the strut levels of Tiers 1-3, respectively.

The dynamic analysis of 4T-24-1-Z under the 2007 Chile-Mejillone EW earthquake record was repeated by reversing the sign of the column's in-plane initial out-of-straightness to examine the

influence of P-δ effects on the column moment demands. This analysis confirmed that column initial imperfection has negligible effects on the column in-plane bending demands and the overall frame response.

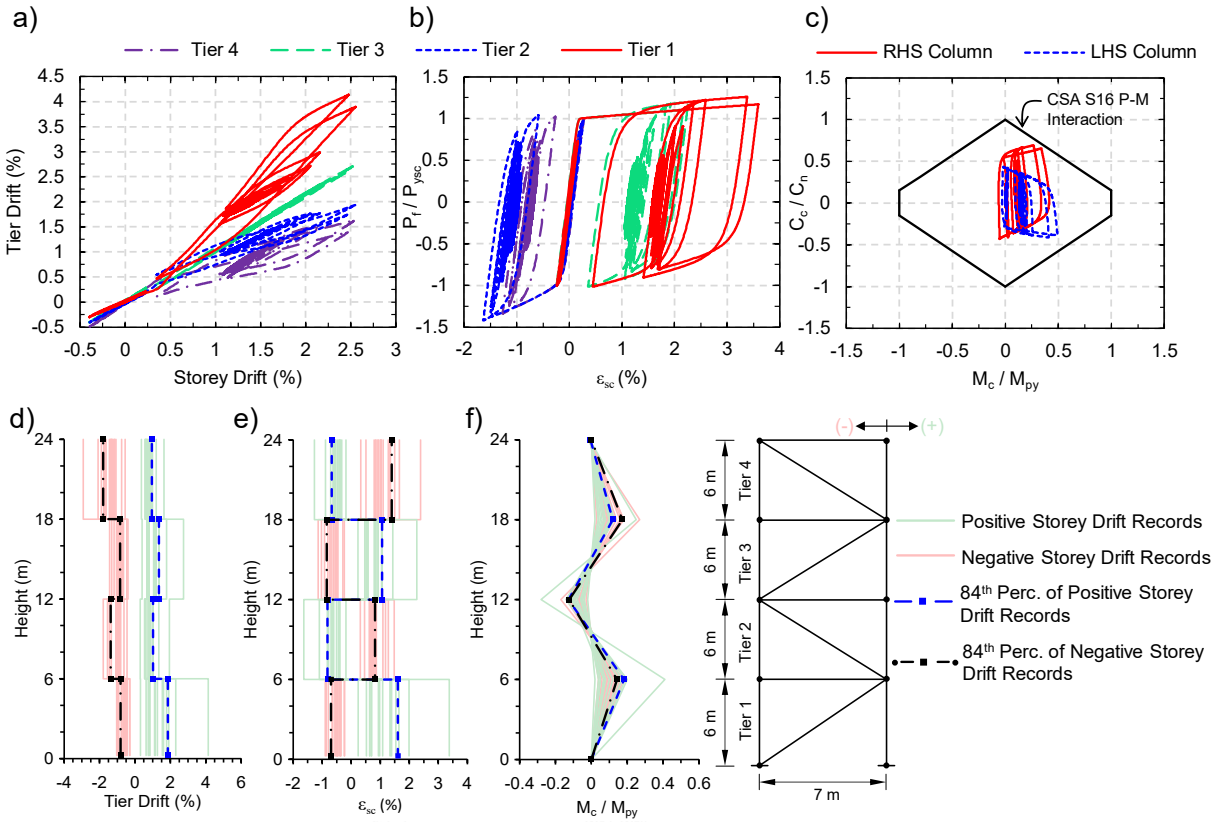

Figure 4.5: a-c) Seismic response of four-tiered BRBF, 4T-24-1-Z, under the 2007 Chile-Mejillone EW earthquake record: a) tier drift versus storey drift; b) BRB axial force – axial strain; c) column axial force – weak-axis moment; d-f) response profiles under ground motion suites: d) tier drift profile; e) BRB strain demand profile; f) right-hand-side column in-plane bending profile.

4.4.2 Prototype Multi-Tiered BRBFs

Peak response parameters, including storey drift, tier drifts, and column in-plane bending, obtained from the multi-tiered BRBF test matrix (see Figure 4.2) are interrogated here. The statistics of the

response parameters of the frames are given in Table 4.3. As shown, peak storey drifts are very close to the design storey drift ($R_dR_o\delta_e/h$) for the two- and three-tiered BRBFs. However, the taller four- and six-tiered frames experienced lower storey drifts compared to their anticipated storey drift (on average 30% lower). A similar observation was made by Imanpour and Tremblay (2016) and Imanpour et al. (2016b) for multi-tiered CBFs. This could be attributed to the nature of the deflection amplification factor (R_dR_o/I_e) used by NBC, which is independent of the frame height and framing configuration. However, further studies are required to verify this argument. The analysis results confirm that the variation of BRBF configurations has a negligible impact on the frame storey drift demand. The critical tier drift, $\Delta_{\text{critical tier}}$, was computed as the drift angle in the tier undergoing the largest inelastic deformation when the frame reaches the maximum storey drift under any given ground motion. The peak tier drifts developed in the tiers with BRBs acting in tension in the respective loading direction are always larger than the storey drifts recorded in the same loading direction for all BRBFs, indicating an uneven distribution of inelastic lateral deformation along the frame height. The extent of drift concentration can be quantified using the drift concentration ratio (DCF), defined as the ratio of the critical tier drift with respect to the peak storey drift. Larger DCFs were observed for BRBFs with a *Z*-bracing pattern compared to other configurations: on average, a DCF of 1.4 was recorded for MT-BRBFs with *Z*-bracing versus a DCF of 1.05 for MT-BRBFs with S-bracing. Frames with non-uniform tier heights exhibited slightly higher DCF compared to their uniform counterparts because of larger column unbraced lengths and steeper BRB angles in Tier 1 resulting in larger variations in storey shears and BRB post-yield stiffnesses between tiers. The variability in the material yield strength of the BRB core between tiers for 2T-12-1-Z-Y resulted in a storey drift ratio and DCF of 1.32% and 1.45, respectively, that were nearly the same as the frame with identical BRB yield strengths between tiers (2T-12-1-Z) of 1.30% and 1.43, respectively.

Overall, limited variations between peak tier drifts were observed among the tiers in each frame due to the tendency of the critical tier(s) to alternate between adjacent tiers throughout the duration of the ground motion as the frame was pushed in both positive and negative directions.

Table 4.3: Statistics of multi-tiered BRBF response parameters.

Parameter	2T-8-1-Z	2T-12-1-Z	2T-12-1-S	2T-12-1.5-Z	2T-12-1-Z-Y	3T-12-1-Z	3T-18-1-S	3T-18-1-Z	3T-18-1-ZS	3T-18-1.5-Z	4T-24-1-Z	6T-24-1-Z	6T-24-1-ZS	6T-24-1.5-Z	6T-30-1-Z	6T-30-1.5-Z
Δ_{st} (%)	1.63	1.30	1.30	1.30	1.32	1.33	1.49	1.42	1.44	1.41	1.15	1.18	1.22	1.18	1.13	1.13
δ_{st} / $R_o R_d \delta_e$	1.22	1.03	1.02	0.99	1.05	0.93	1.08	1.04	1.04	0.98	0.80	0.73	0.75	0.72	0.69	0.68
$\Delta_{critical\ tier}$ (%)	2.48	1.90	1.35	1.89	1.95	1.77	1.55	1.83	2.14	1.82	1.75	1.65	1.70	1.70	1.51	1.57
DCF	1.48	1.43	1.05	1.47	1.45	1.35	1.06	1.37	1.60	1.38	1.49	1.39	1.40	1.48	1.44	1.48
Δ_6 (%)	-	-	-	-	-	-	-	-	-	-	-	1.32	1.35	1.53	1.37	1.37
Δ_5 (%)	-	-	-	-	-	-	-	-	-	-	-	1.20	1.33	1.43	1.14	1.15
Δ_4 (%)	-	-	-	-	-	-	-	-	-	-	1.30	1.15	1.27	1.35	1.12	1.15
Δ_3 (%)	-	-	-	-	-	1.40	1.55	1.51	1.49	1.45	1.16	1.13	1.15	1.35	1.07	1.09
Δ_2 (%)	1.95	1.43	1.35	1.54	1.20	1.40	1.50	1.45	1.36	1.48	1.05	1.11	1.10	1.17	1.07	1.09
Δ_1 (%)	1.61	1.41	1.25	1.34	1.61	1.35	1.40	1.39	1.67	1.40	1.34	1.28	1.34	0.60	1.07	1.10
C_c / C_n	0.72	0.59	0.80	0.66	0.57	0.67	0.66	0.64	0.66	0.69	0.63	0.61	0.60	0.63	0.68	0.69
M_{c5} / M_{py}	-	-	-	-	-	-	-	-	-	-	-	0.12	0.01	0.12	0.11	0.11
M_{c4} / M_{py}	-	-	-	-	-	-	-	-	-	-	0.01	0.08	0.03	0.08	0.07	0.07
M_{c3} / M_{py}	-	-	-	-	-	0.01	0.00	0.01	0.00	0.01	0.13	0.09	0.03	0.09	0.08	0.08
M_{c2} / M_{py}	0.02	0.01	0.01	0.01	0.01	0.23	0.01	0.17	0.04	0.15	0.11	0.08	0.05	0.09	0.08	0.07
M_{c1} / M_{py}	0.27	0.20	0.02	0.21	0.20	0.25	0.02	0.19	0.19	0.18	0.15	0.13	0.14	0.11	0.11	0.12
No. of column instability	0	0	0	0	0	0	0	0	0	0	0	0	1	0	0	0

Peak column axial force and in-plane flexural bending demands are given in Table 4.3 for the RHS column of prototype frames. Force demands on the RHS columns are more critical than those induced in the LHS columns because of the selected bracing configuration and ground motion records. The axial force, C_c, measured in Tier 1 was normalized by the nominal axial compressive resistance of each column, C_n. As shown in Table 3.3, the normalized column axial forces, C_c/C_n, vary between 0.60 to 0.80. These demands are less than unity due to the fact that BRBs, in particular those in compression, do not achieve their probable resistances assumed in design. No significant variation was observed between the amplitude of column axial force and the geometrical parameters of the

studied frames. Column peak in-plane bending demands, M_c, measured at the strut levels were normalized by their weak-axis plastic moment capacity, M_{py}. For all frames studied, the largest in-plane moment demand occurred in the first tier, which can be explained by 1) the lower stiffness provided by the pinned base condition creating a greater curvature in Tier 1, and 2) the critical tier being the first tier under most of the ground motion records. Peak in-plane bending varied between $0.1 – 0.30M_{py}$ for all frames, except for those with BRBs in an S-bracing configuration for which insignificant bending (in the order of $0.01M_{py}$) was observed. Overall, column bending demands in the frames with Z-bracing or ZS-bracing configuration decreased as the frame height increased, which can be attributed to a larger number of tiers with tension-acting BRBs (critical tier) that helped lessen concertation of inelastic lateral deformation between tiers. Column partial flexural yielding was observed due to the combined effect of in-plane flexural bending and an axial compression force at the mid height of Tier 1 under multiple ground motions for all the frames studied, except for those with the S-bracing arrangement. Column instability occurred in the Tier 1 segment of the RHS column of 6T-24-1-ZS under the 2007 Chile-Mejillone EW earthquake record. This instability was triggered by a large axial compression force ($0.7C_n$) and an appreciable in-plane moment ($0.4M_{py}$) under this record.

4.4.3 Selected Frames Response Profiles

The seismic response of single-diagonal multi-tiered BRBFs is a function of the direction of the loading imposed by the earthquake base excitation and thus it is particularly important to assess separately the behaviour of the frames under positive and negative storey drift ratios. In this section, the profile of peak tier drifts, BRB forces and strains, and column in-plane bending demands as obtained from dynamic analyses are evaluated for seven frames selected among the total 18 frames studied. The frames presented in Figure 4.6 serve as examples covering the varied parameters

explored in the parametric study matrix, including number of tiers, tier heights, total frame height, and bracing configuration. Each response profile presents the results obtained from individual ground motions and the two 84^{th} percentile results, one associated with the records causing a larger storey drift in the positive loading direction and the second representing the records creating a larger storey drift in the negative loading direction. The profiles of the tier drifts shown in Figure 4.6a confirm a non-uniform distribution of the frame lateral displacement for BRBFs that have BRBs with opposing diagonals, i.e., Z- and ZS-bracing configurations. The tendency for the lateral displacement to concentrate in the tiers whose BRBs are undergoing tensile yielding can be observed under both positive and negative roof lateral displacement. This results in a unique behaviour where the critical tier varies during the duration of the ground motion depending on the direction of the roof displacement at any given time of the motion. For all the frames in Figure 4.6a, the peak tier drift was lower than 3% for both loading directions. The profiles of BRB forces are given in Figure 4.6b. As shown, the BRB tension and compression forces were nearly identical in all the tiers under positive and negative lateral displacements, thus raising the question regarding the applicability of multi-storey BRBFs' provisions with respect to the friction adjustment factor, which is intended to account for the additional strength developed in steel BRBs in compression compared to their tensile capacity.

Figure 4.6c shows the profile of the BRB strain demands which were calculated assuming a core yielding length equal to 60% of the length between workpoints. The evaluation of the BRB strain demands confirms that BRB strains under tension loading are nearly two times those under compression due to excessive deformation demands induced in tension-acting BRBs in each loading direction, which strengthened the argument regarding the reassessment of the BRB friction adjustment factor for the design of multi-tiered BRBFs due to the fact that their seismic behaviour is

heavily dominated by relative tier lateral deformation. Figure 4.6d gives the profiles of column in-plane bending. Referring to BRBFs with Z-bracing configuration profiles, the 84th percentile values of column absolute in-plane bending at tier levels vary between 0.16– 0.4M_{py} with the largest moment recorded at the Tier 1 level. Furthermore, moment reversals were observed along the column height with the inflection points occurring at almost mid-height of the adjacent intermediate tiers. Nearly no in-plane bending was induced in the columns of BRBFs with S-bracing. For the frame utilizing ZS-bracing (3T-18-1-ZS), the 84th percentile values of column in-plane bending reached 0.3M_{py} within the portion of the frame with BRBs oriented in opposing directions resulting in significant bending demands on the column in Tier 1.

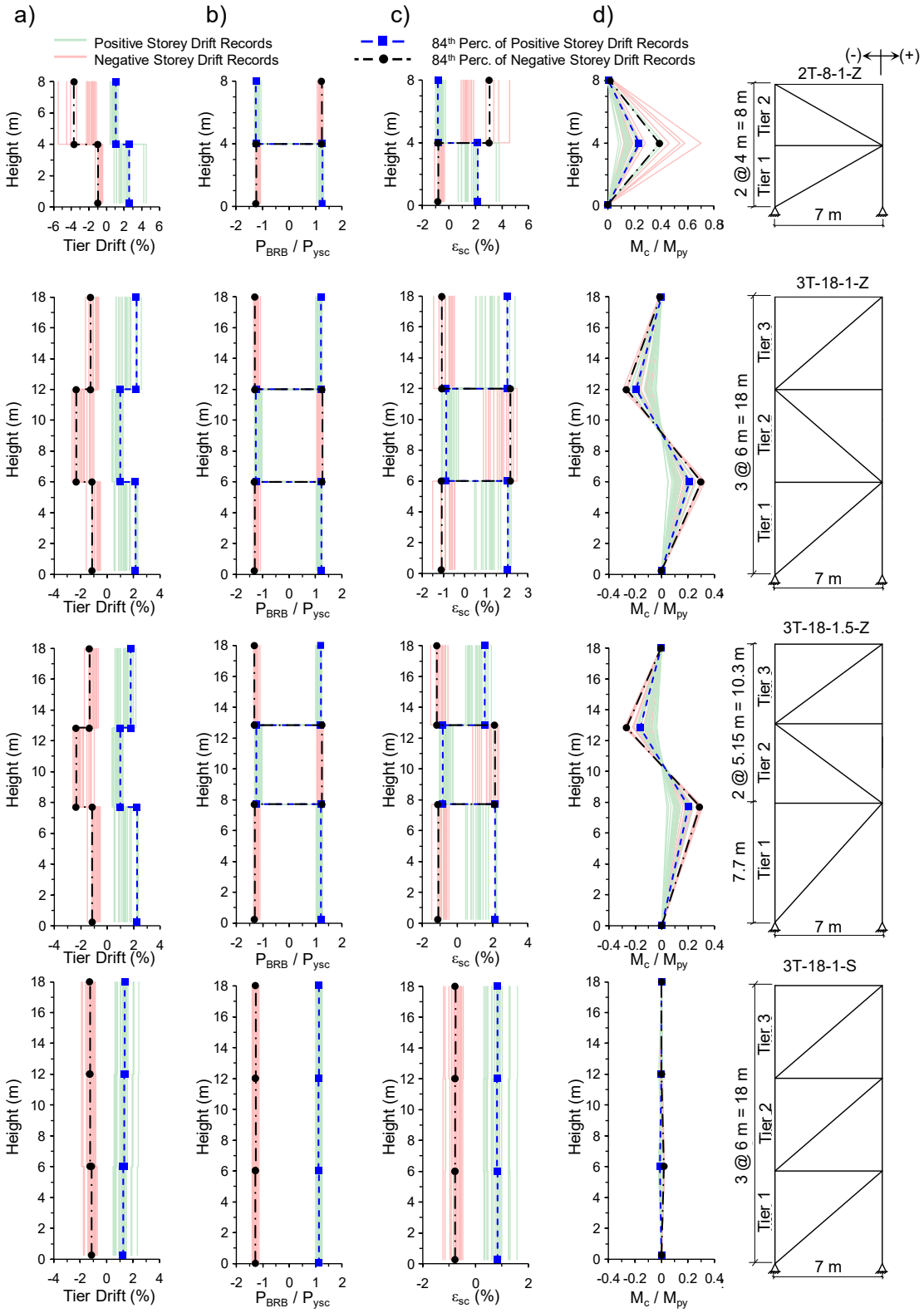

Figure 4.6: Profiles of response parameters: a) tier drifts; b) column in-plane moments; c) BRB forces; d) BRB strains (continued on next page).

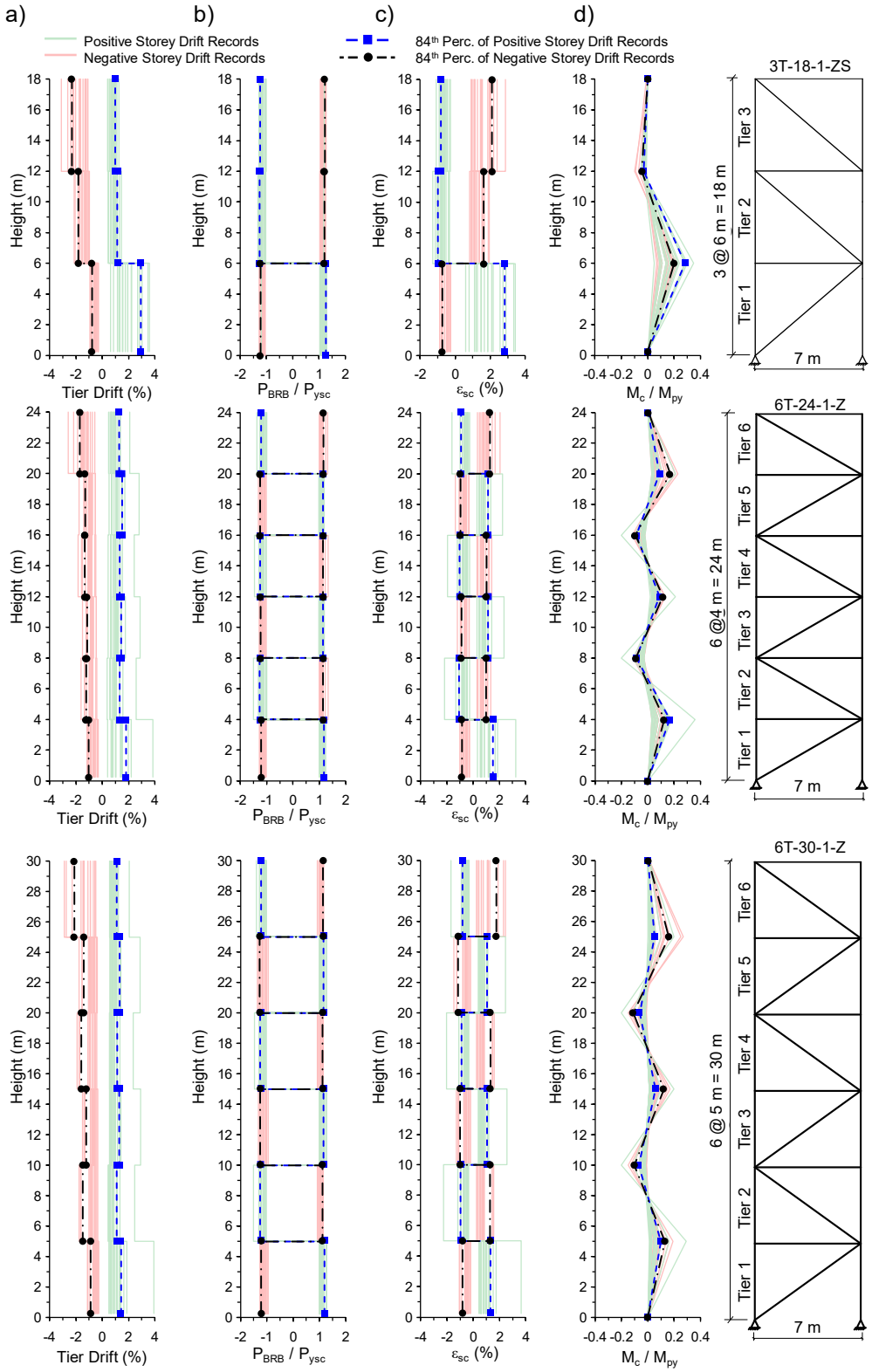

Figure 4.6: Profiles of BRBF response parameters: a) tier drifts; b) column in-plane moments; c) BRB forces; d) BRB strains.

4.5 Proposed Analysis and Design Methods

On the basis of the observed multi-tiered BRBF seismic response, two analysis and design methods are proposed in this section to 1) quantify the force demands induced in the columns and deformation demands in the braces of multi-tiered BRBFs due to the development of a large proportion of inelastic lateral deformation in tension-acting tiers, and 2) address those demands in design, namely by selecting columns with sufficient in-plane flexural strength and stiffness to achieve an enhanced seismic stability response for multi-tiered BRBFs.

A detailed analysis and design method that is based on mechanics principles is first presented, followed by an alternative displacement-based analysis and design method that can be easily realized by a computer program. Both methods are proposed within the framework of the Canadian steel design standard. The four-tiered case study BRBF, which was presented earlier, is used here to demonstrate the proposed methods.

4.5.1 Detailed Approach

Step 1 (identify critical tiers): For each loading direction, the displacement corresponding to the design storey drift is attained at the roof in the positive and negative directions, and a deformation pattern is set assuming 1) a full plastic mechanism is formed, i.e., BRBs in all tiers reach their respective probable resistances, and 2) tiers with tension-acting BRBs (critical tiers) in the loading direction of interest deform more than those with compression-acting BRBs, leading to column curvature with one or more inflection points along the frame height for frames with more than two tiers. For the four-tiered BRBF example of Figure 4.7, the positive loading direction (displacement to the right) is considered under the design roof displacement of 345 mm (1.43%h), which leads to

two tension-acting tiers, Tiers 1 and 3. This loading direction is examined here because it results in the most critical loading condition for the column design.

Step 2 (create substructures for moment calculation): The frame is broken down in multiple substructures bounded by the location of column inflection points once the full plastic mechanism is developed. Each substructure consists of two adjacent tiers with BRBs oriented in opposing orientations. The column inflection points can be assumed to occur at mid-height of the adjacent intermediate tiers for frames with more than two tiers (note that two-tiered BRBFs would only need one substructure). The respective substructures are shown for the four-tiered BRBF example in Figure 4.7a. As shown, Tiers 1 and 2 form Substructure 1, Tiers 2 and 3 form Substructure 2, and Tiers 3 and 4 form Substructure 3.

Step 3 (determine column shear and bending moment for each substructure): Column in-plane shear and bending in each substructure is determined from the horizontal equilibrium of shear forces contributed by columns and BRBs acting in the respective substructure. For example, for Substructure 1 (Tiers 1 and 2 in Figure 4.7a), we can set up the force equilibrium relationship as:

$$-2V_{c2}+V_{b2} = 2V_{c1}+V_{b1} \quad [1]$$

where V_{c2} and V_{c1} are the column shears in Tiers 1 and 2, respectively, and $V_{b1} = T_{prob}\cos\theta_1$ and $V_{b2} = C'_{prob}\cos\theta_2$ are the horizontal components of BRB resistances in Tiers 1 and 2, respectively. $T_{prob} = R_{sh}A_{sc}R_yF_y$ is the BRB probable tensile resistance and $C'_{prob} = \beta' R_{sh}A_{sc}R_yF_y$ is the BRB modified probable compressive resistance computed using a modified friction adjustment factor of β'. θ_1 and θ_2 are the BRB angles in Tiers 1 and 2, respectively, with respect to the horizontal plane. The modified friction adjustment factor is calculated as $\beta' = 0.5(\beta + 1)$, based on the results of full-scale experimental testing of a two-tiered BRBF (Bani 2023) and those obtained from the dynamic

analyses performed here. These results confirm that BRB tensile yielding prevents compression BRBs in other tiers (having an identical probable tensile resistance) from attaining their full probable compressive resistance $C_{prob} = \beta R_{sh} A_{sc} R_y F_y$ because compression-acting BRBs reach approximately half of their anticipated design strain demands due to their higher post-yield stiffness. It should be noted that the BRB-modified probable compressive resistance is only proposed for calculating in-plane flexural demands; column axial forces must be calculated using BRB probable resistances, as per CSA S16.

Knowing the location of column inflection points in each substructure and the fact that the maximum moment occurs at the strut levels (Figure 4.7b), column shears at each substructure can be related. For the frame of Figure 3.7a, column shears in Substructure 1 (Tiers 1 and 2) are related as:

$$V_{c1} h_1 = V_{c2} h_2 / 2 \qquad [2]$$

For the frame example, horizontal shears due to the BRB probable tensile resistance in Tier 1 and due to the BRB modified probable compressive resistance in Tier 2 are V_{b1} = 710 kN and V_{b2} = 794 kN, respectively. Substituting these values into Eq. 1 and knowing Eq. 2, the column shear in Tier 1 is determined as V_{c1} = 14 kN, and therefore the moment at the Tier 1 level is equal to $M_{c1} = V_{c1} h_1$ = 86 kN-m (= $0.25 M_{py}$). This in-plane moment is slightly higher than the moment $0.18 M_{py}$ determined from the dynamic analysis of this frame at the Tier 1 level, as shown in Figure 4.7e, suggesting that the proposed method predicts column seismic demands with sufficient accuracy. The column shear in Tier 2 is then determined as V_{c2} = 28 kN and the moment at the Tier 2 level is equal to $M_{c2} = M_{c1} - V_{c2} h_2$ = – 86 kN-m (= $0.25 M_{py}$).

For the frame example, the second substructure involves the braces and columns bounded by the first and second column inflection point in Tiers 2 and 3, respectively, as shown in Figure 4.7a. Knowing

the column shear in Tier 2, V_{c2}, the column shear in Tier 3, $V_{c3,}$ can be determined by equating the horizontal shear forces in Tiers 2 and 3:

$$2V_{c3}+V_{b3} = -2V_{c2}+V_{b2} \quad [3]$$

The column shear in Tier 3 is determined as V_{c3} = 28 kN and the moment at the Tier 3 strut level is therefore equal to $M_{c3} = M_{c2} + V_{c3}h_3$ = 86 kN-m (= $0.25M_{py}$).

Lastly, for Substructure 3, knowing that a column inflection point occurs at the mid-height of Tier 3 (Figure 4.7b) and that the moment is zero at the roof level, the column shear for the substructure (Tiers 3 and 4) can be related as:

$$V_{c4}h_4 = V_{c3}\, h_3/2 \quad [4]$$

Using V_{c3} = 28 kN, the shear in Tier 4 can be determined as 14 kN and the moment at Tier 4 is confirmed to remain zero, $M_{c4} = M_{c3} - V_{c4}h_4 = 0$. Alternatively, ignoring Substructure 2, Substructure 3 can be analyzed in a similar manner to Substructure 1, i.e., by using Eq. 4 and considering the horizontal equilibrium of shear forces in the columns and BRBs acting in Tiers 3 and 4. Note that both approaches yield identical results.

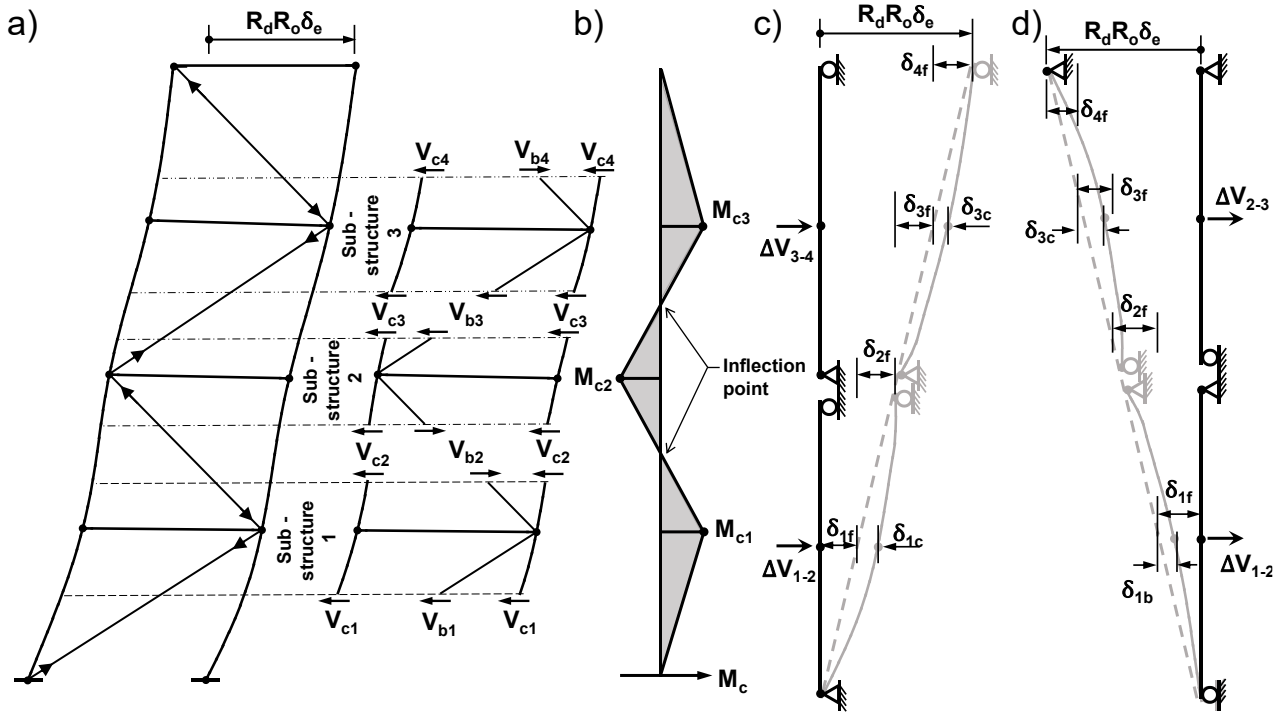

Figure 4.7: Detailed analysis method: a) Frame deformed-shape and substructures for moment calculation; b) column in-plane moment diagram; c) simply-supported column substructures for BRB strain calculation under positive roof displacement; d) simply-supported column substructures for BRB strain calculation under negative roof displacement.

Step 4 (size columns): The columns are designed to resist the combined effects of the axial force induced due to gravity loads plus the vertical components of BRB probable resistances, and in-plane bending as obtained in *Step* 3. The strength and stability of the columns should be verified using the CSA S16 axial force – the bending moment interaction equation in each column segment. For the frame example, the most critical column segment is the Tier 1 segment under an axial compression force induced due to gravity loads plus BRB probable resistances, C_f = 2968 kN, and the weak-axis flexural moment computed in Step 3 from the substructure associated with Tiers 1 and 2 when the frame is displaced to the right (Figure 4.7a), M_{fy} = 86 kN-m. A W610×195 column was selected to resist these demands, with an interaction ratio of 0.88.

Step 5 (check BRB strain): The BRB strains in the tiers that experience tensile yielding in each loading direction should be verified to ensure they remain below the strain demand corresponding to two times the design storey drift, as obtained from the BRB qualification testing requirements per AISC 341-16 Chapter K3. In this study, the in-plane flexural stiffness of multi-tiered BRBF columns is used to limit the lateral deformation developed in the critical tension tiers which, in turn, controls the BRB axial strain in these tiers. To obtain lateral deformation of the tension tier, δ_i, in multi-tiered BRBFs with opposing bracing orientations, a set of simply-supported columns — each spanning the tension tier under consideration and the adjacent compression tier — is proposed based on the observed profile of lateral deformations in the MT-BRBFs studied here. The designer should verify the tier lateral deformation and BRB strains under both loading directions. Figures 4.7c-d show the proposed simply-supported columns for the four-tiered BRBF example under positive and negative storey drift, respectively. When the roof displacement reaches the displacement corresponding to the design storey drift, the lateral deformation of the tension tier, δ_i, is therefore equal to the deformation due to the roof displacement at the design storey drift $\delta_e R_d R_o / I_E$, assuming a linear variation over the frame height δ_{if} plus the lateral deformation produced due to column bending in that tier δ_{ic} under BRB unbalanced forces, ΔV ($= C'_{prob2} \cos\theta_2 - T_{prob1} \cos\theta_1$ for the simply-supported column associated with Tiers 1 and 2 in the frame example) acting on the simply-supported column at the location of the intermediate strut. When calculating BRB unbalanced forces, the modified probable compressive resistance should be used. For the frame example, the BRB core strain in the first tier when the design storey drift is attained in the positive direction (Figure 4.7c) is calculated as:

$$\varepsilon_{sc1} = \left[\frac{\delta_e R_d R_o}{I_e} \frac{h_1}{h} + \frac{\left(C'_{prob2} \cos\theta_2 - T_{prob1} \cos\theta_1 \right)(h_1 + h_2)^3}{48 E I_y} \right] \frac{\cos\theta_1}{L_y} \qquad [4]$$

in which h_1+h_2 is the length of the assumed simply-supported column for Tiers 1 and 2, EI_y is the weak-axis flexural stiffness of the column, and L_y is the length of the BRB yielding region. A similar equation as Eq. 4 can be set up to determine the axial strain in the BRB core of the next tension tier (Tier 3 in the frame example) ε_{b3} when the design storey drift is reached in the positive direction (Figure 4.7c):

$$\varepsilon_{sc3}=\left[\frac{\delta_e R_d R_o}{I_e}\frac{h_3}{h}+\frac{\left(C'_{prob4}\cos\theta_4 - T_{prob3}\cos\theta_3\right)(h_3+h_4)^3}{48EI_y}\right]\frac{\cos\theta_3}{L_y} \qquad [5]$$

For the frame example, assuming the column designed in *Step* 4 and L_y = 5500 mm, the total BRB strain in Tier 1 is equal to ε_{sc1} = 1.20% + 1.50% = 2.70%, which is higher than the proposed BRB strain limit of 2.40%, i.e., two times the strain demand corresponding to the design storey drift. A stiffer W360×216 column was therefore selected to satisfy the BRB strain limit in Tier 1. The BRB strain in Tier 1 was then reduced to ε_{sc1} = 1.17% + 0.75% = 1.92% using the stiffer column section. The strength and stability of the new column cross-section was verified following *Step 3*. The selected column had a factored axial resistance of 6749 kN and a factored weak-axis moment resistance of 677 kN-m, resulting in an axial force – or flexural moment interaction ratio — of 0.6. A similar check should be performed to verify the BRB strain in Tier 3; however, since in this example all the tiers have identical tier heights and BRB core sizes, the strain in Tiers 1 and 3 would be identical, ε_{sc1} = ε_{sc3}. When the roof displacement reaches the displacement corresponding to the design storey drift in the positive direction, the BRB strains in Tiers 2 and 4 are found as ε_{sc2} = 1.2% and ε_{sc4} = 1.2% using the proposed simply supported approach (Figure 4.7c), confirming that the selected column section is sufficient to limit BRB deformation in these tiers as well. Although not critical in this example, similar steps should be taken to check BRB strains in all the tiers under negative design storey drift using the simply supported approach, as shown in Figure 4.7d.

4.5.2 ZS-Bracing Configuration

To demonstrate the application of the proposed design method to other BRBF configurations, an example of an MT-BRBF with opposing bracing used only at the first and second tiers creating a ZS-bracing configuration is demonstrated in this section. The frame was first designed according to CSA S16-19 provisions, resulting in identical BRB core areas and column section sizes to the four-tiered BRBF discussed earlier (A_{sc} = 2313 mm^2 = 3.7 in^2 BRBs and W530×150 columns). This frame was first analyzed using the same set of ground motion accelerations described earlier to characterize deformation and force demands induced under seismic loading. The tier drift profile, BRB strain demands, and column in-plane flexural moments are shown in Figures 4.8a-c, respectively. Referring to this figure, the frame lateral response is dominated by Tiers 1 and 2 in which opposing bracing is used resembling the zigzag orientation described earlier. Tier drift in Tier 1 and respective BRB strains are both more critical when the frame is moved in the positive direction because that favours a single tension-acting BRB in Tier 1, whereas the roof displacement in the negative direction induces tension in Tiers 2-4, promoting a less critical deformation and force demands for the BRBs and columns, respectively. These results suggest that the frame demands can be estimated by investigating the substructure involving zigzag BRBs, namely, Tiers 1 and 2 in this example.

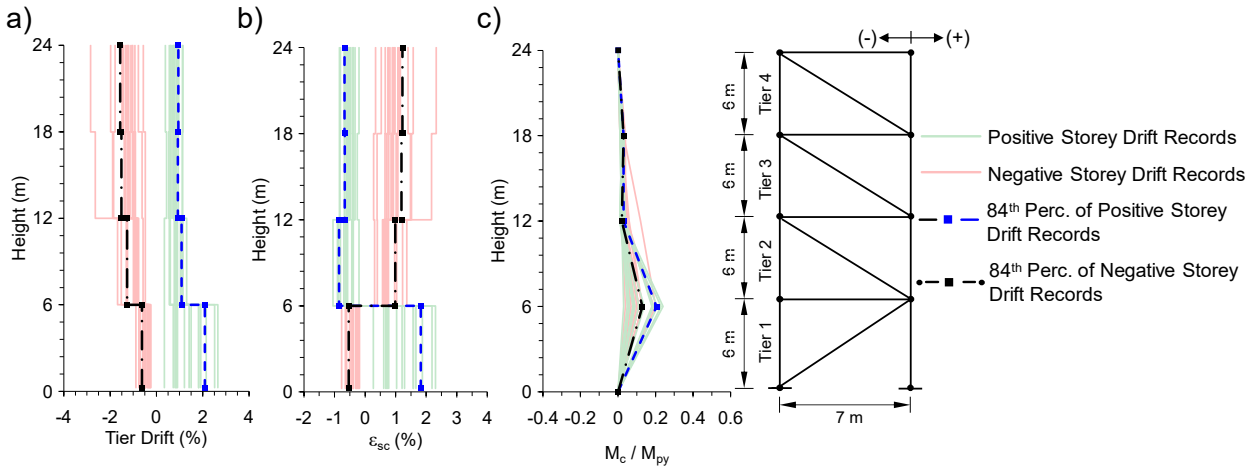

Figure 4.8: Profiles of the response parameters for the four-tiered BRBF with ZS-bracing: a) tier drift profile; b) BRB strain profile; c) column in-plane bending profile.

The proposed design method was applied to the four-tiered BRBF with the ZS-bracing shown in Figure 4.9a when the roof displacement was positive. The substructure involving adjacent tiers with BRBs oriented in opposing orientations, including Tier 1 (the tier with a tension-acing BRB) and Tier 2 (the tier with a compression-acting BRB), was then created as shown in Figure 4.9a. The column flexural moment at the strut level of Tier 1 was calculated for the selected substructure by setting up an equilibrium of forces relationship within the substructure as given in Eq. 1, where $V_{b1} = T_{prob} \cos\theta_1 = 710$ kN and $V_{b2} = C'_{prob} \cos\theta_2 = 794$ kN, and assuming that the moment at the top end of the Tier 2 column segment was equal to zero (Figure 4.8c), which indicates that the column moment at the top of Tier 1 and the bottom of Tier 2 were equal, $V_{c1}h_1 = V_{c2}h_2$. The resulting moment in Tier 1 was therefore $M_{c1} = V_{c1}h_1 = 21\text{kN} \times 6.0\text{m} = 126$ kN-m ($= 0.36M_{py}$). Since there were no unbalanced forces developed between Tiers 2 and 3 and between Tiers 3 and 4, no moment was induced in the columns at these tiers, which agreed with the results obtained from dynamic analyses (Figure 4.8c). A W360×216 column was chosen to carry an axial compression force induced by gravity loads plus BRB probable resistances, and in-plane bending obtained from the substructuring

technique. The strain demand in the BRB of the first tier, which undergoes tension when the roof is displaced in the positive direction, was computed as $\varepsilon_{sc1} = 1.2\% + 0.75\% = 1.94\%$ when the design storey drift was attained by creating a simply-supported column spanning Tiers 1 and 2 and was subjected to the BRB unbalanced force equal to $\Delta V_{1\text{-}2} = C'_{prob}\cos\theta_2 - T_{prob}\cos\theta_1 = 84$ kN (Figure 4.9c). The strain demand in the BRB of Tier 1, $\varepsilon_{b1} = 2.2\%$, was less than the BRB strain limit of 2.4% and thus the selected section for the columns was adequate. Since no unbalanced forces were generated between other tiers, the BRB strain demands at these tiers were set equal to the strain corresponding to tier drift, assuming a linear variation of the storey drift over the frame height. Although not critical here, identical steps should be followed to obtain BRB strains under negative roof displacement.

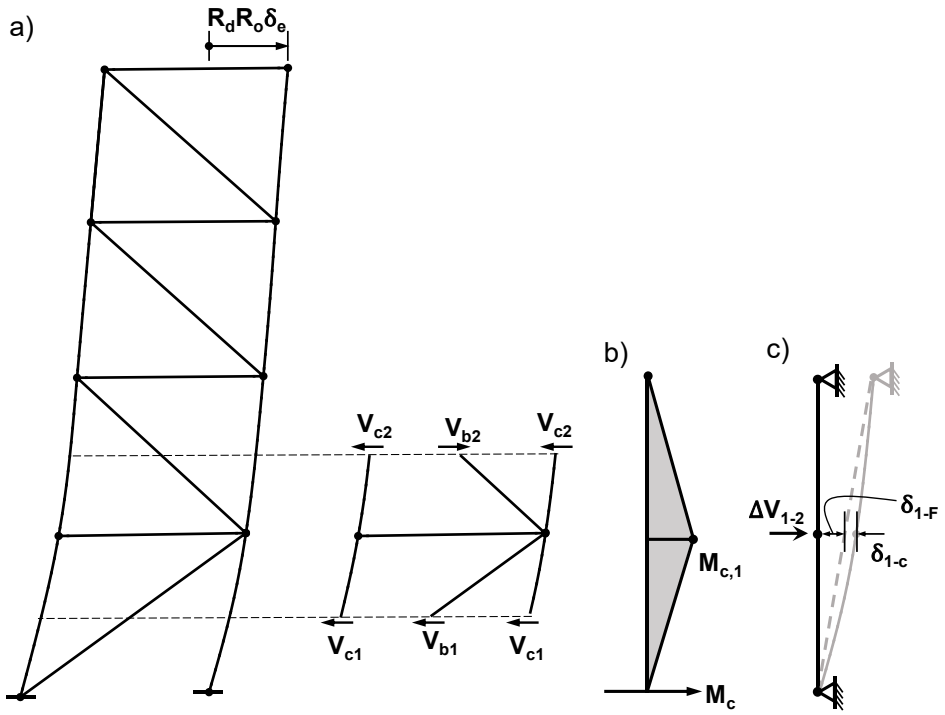

Figure 4.9: a) Deformed-shape of the four-tiered BRBF with KS-bracing and storey shears resisted by braces and columns in Tiers 1-2 substructure for moment calculation; b) in-plane bending moment diagram; c) simply-supported column substructures for BRB strain calculation under positive roof displacement.

4.5.3 Alternative (Displacement-Based) Approach

An alternative, computer-aided, analysis method that is based on imposed lateral displacements is proposed for multi-tiered BRBFs based on the observations from the numerical parametric study presented earlier. Column in-plane bending moments in each loading direction (positive and negative) were determined by imposing the inelastic lateral deformation anticipated in design to only the tiers expected to act in tension in that loading direction. This analysis is schematically shown in Figure 4.10 for the four-tiered BRBF of Figure 4.7 when the roof displacement reached the displacement corresponding to the design storey drift in the positive direction. The motivation behind this method is the limited lateral deformation developed in the tiers with compression-acting BRBs

(see Figure 4.5e), which can be conservatively set equal to zero for the purpose of calculating column flexural demands. Lateral displacements imposed externally to the tiers with tension BRBs will result in the deformation profile expected under lateral seismic loads, creating the respective curvature and moments in the columns. For the four-tiered BRBF of Figure 4.7, the design roof displacement was 345 mm (1.44%*h*), of which 75 mm was the share of frame elastic deformation. Using the linear numerical model of the frame constructed in SAP2000 (CSI 2018), the remaining lateral displacement — 270 mm as frame inelastic deformation — was distributed between the tiers with tension-acting tiers (Tiers 1 and 3 under positive roof displacement) in proportion to their heights, resulting in 270 mm applied to Tier 3 and 135 mm applied to Tier 1, while the relative lateral displacement of Tiers 2 and 4 were kept as zero, as shown in Figure 4.10a. These imposed lateral displacements displaced the frame laterally, as shown in Figure 4.10b. The column flexural bending resulting from this imposed displacement profile, as obtained from the computer model of the frame, is given in Figure 4.10c, was approximately double that computed using the detailed method in Figure 4.7. Overall, the alternative method yields higher moments in the columns because it is assumed in this method that the total inelastic lateral deformation of the frame is developed in the tiers undergoing tension yielding which, although simple to apply, is expected to create more severe column kinks and thus conservative moment estimates. Once column bending demands are obtained, the columns should be designed under an axial compression force and in-plane bending, as described in *Step* 3 of the detailed method. For the four-tiered frame example of Figure 4.7a, the same column profile, W360×216, selected using the detailed method is required when the alternative method is used. BRB strains in the tiers with tension-acting BRBs were verified using the frame inelastic deformation profile shown in Figure 4.10b. BRB strains in Tiers 1 and 3 (critical under positive displacement) are equal to 2.12% assuming a yielding core length of 5500 mm. Although strains are

below the strain limit of 2.40%, they are 10% higher than those computed using the detailed method due to more severe tier deformations imposed on the tiers with tension-acting BRBs. This analysis should be repeated when the roof displacement reaches the displacement corresponding to design storey drift in the negative direction.

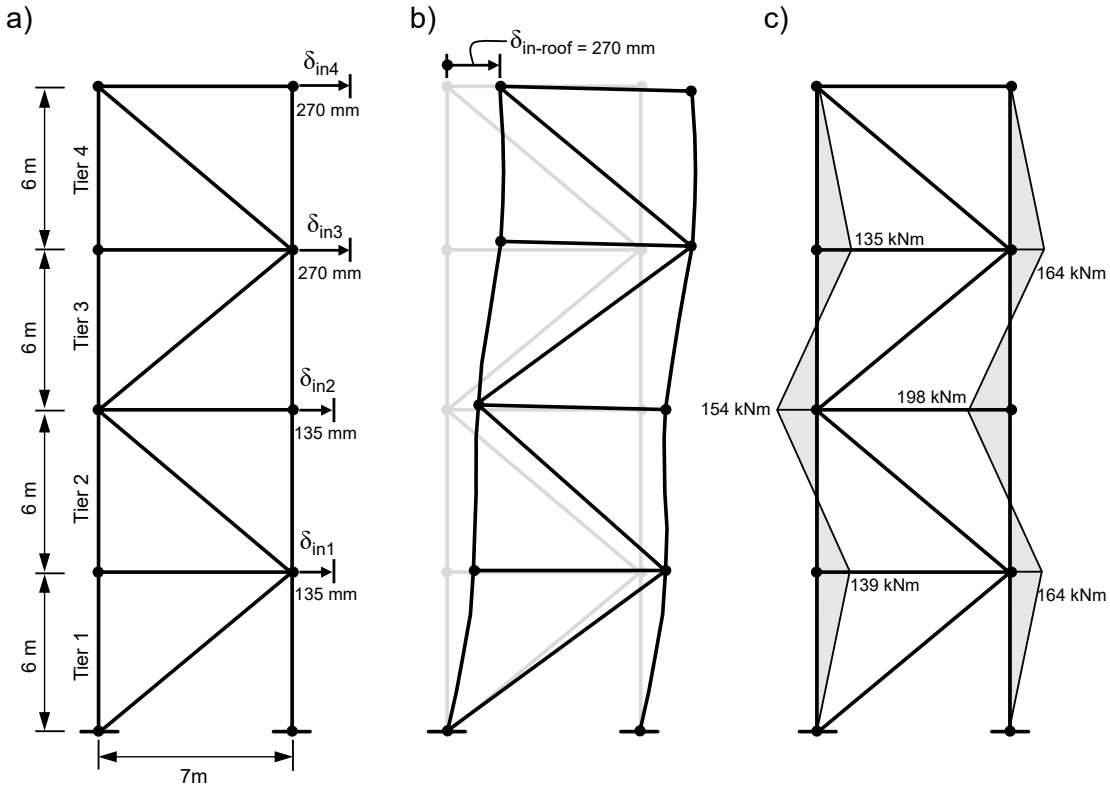

Figure 4.10: Alternative (displacement-based) analysis method: a) imposed inelastic lateral displacements; b) frame deformed-shape under imposed displacements of (a); c) column in-plane bending moment diagrams from SAP2000.

4.6 Verification of the Proposed Method

Nonlinear response history analyses were performed in the frame example of Figure 4.7a, 4T-24-1-Z BRBF, under the same suite of ground motion records described previously to evaluate the proposed analysis and design method, specifically the column and BRB demands predicted here. The frame was designed using the detailed method, once with W610×195 columns selected to resist

column force demands only, and then with W360×216 columns selected to meet both column force demands and the BRB strain limit. The profiles of tier drifts, BRB strains, and column in-plane moment demands obtained from the dynamic analyses and those predicted using the detailed method are given in Figures 4.11a-c, respectively, for the 4T-24-1-Z BRBF with W360×216 columns. Referring to Figure 4.11a, lateral deformation tends to concentrate – although to a lesser extent compared to the frame designed according to CSA S16 – in the tiers undergoing tensile yielding (Tiers 1 and 3 for positive displacement and Tiers 2 and 4 for negative displacement). For example, under positive roof displacement, Tiers 1 and 3 underwent the highest peak storey drifts of 1.5% and 1.3% respectively, whereas under negative roof displacement, the highest peak tier drifts recorded in Tiers 2 and 4 were –1.3% and –1.8% respectively. As shown in Figure 4.11b, the peak BRB strain demands in tension are nearly 1.5 times those in compression in all the tiers which is lower than that observed under the frame designed according to CSA S16-19 for which the peak strain demands observed in tension-acting BRBs were double those in compression-acting BRBs. Referring to Figures 4.11a and 4.11b, tier drifts and BRB strains estimated using the detailed method appear to sufficiently envelope, with an acceptable level of conservatism, the peak tier drifts and BRB strains obtained from the dynamic analysis. The design predictions were estimated using the peak storey drift obtained from the dynamic analysis, i.e., 1.21%h. For instance, in Tier 1 under the positive storey drift, the tier drift and BRB strain demands are 1.5% and 1.23% versus the predicted tier drift and BRB strain of 2.1% and 1.75%. The conservatism in the demand prediction, particularly in the tiers undergoing tension yielding, stems from the additional flexibility introduced through the simply supported column that was assumed when calculating the tier deformations. Figure 4.11c. shows the profiles of column in-plane flexural bending compared to the demand predicted by the proposed detailed method. As expected, the column moment reached its local maximum at the tier levels and

changed signs between adjacent tiers. The proposed method resulted in a moment profile that enveloped that obtained from the dynamic analysis. The moment demands calculated using the proposed method are approximately twice those observed in the dynamic analysis, i.e., $0.25M_{py}$ versus $0.13M_{py}$ in Tier 1. The conservative estimation of column flexural demands is attributed to the variability in the ground motion and key assumptions of the moment calculations in the proposed method: 1) BRB probable resistance in tension; 2) BRB modified probable compressive resistance; and 3) column inflection points being located at tier mid-heights. The latter is likely more influential in deviating moment predictions because column inflection points are not exactly located at tier mid-height (Figures 4.5f, 4.6, 4.7) contrary to the assumptions made in design. The accuracy of the moment estimation can be improved in future studies, for example by considering more realistic column inflection point locations.

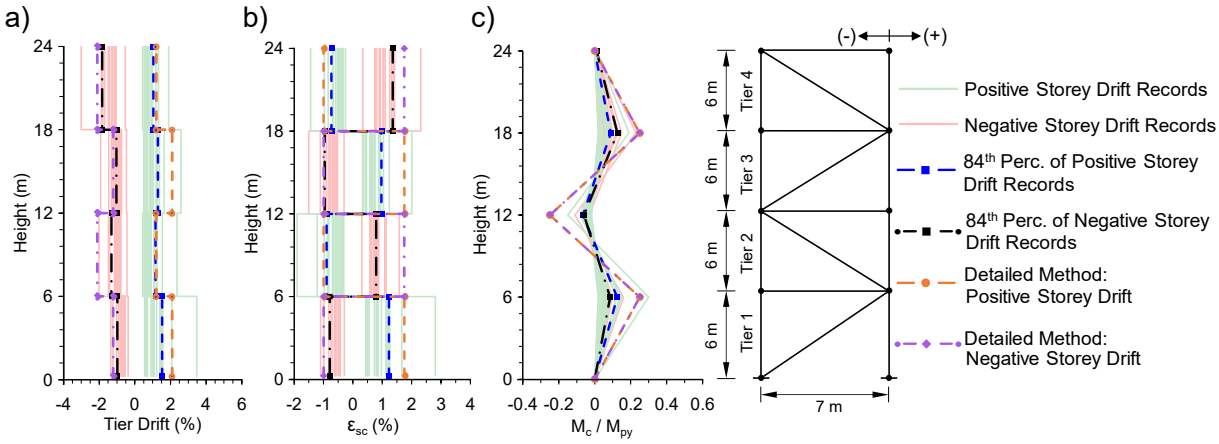

Figure 4.11: Profiles of the response parameters for improved 4T-12-1-Z with W360×216 columns: a) tier drift profile; b) BRB strain profile; and c) column in-plane bending profile.

Table 3.4 shows statistics of the peak response parameters for the improved 4T-12-1-Z BRBF with W610×195 columns meeting the minimum strength requirements only and W360×216 columns meeting the minimum strength and stiffness requirements. These response parameters were computed by taking the maximum of means over the earthquake ensembles of the peak response

parameter obtained under each ground motion record. The statistics for the original 4T-12-1-Z BRBF design with W530×150 columns are given again in Table 4.4 for comparison purposes. Referring to this table, all BRBFs experienced a lower storey drift than that anticipated in design where the improved frames underwent slightly larger overall storey drifts (1.19% and 1.21% versus 1.15%). Moreover, the improved frame meeting both strength and stiffness requirements (with W360×216 columns) resulted in a reduced peak critical tier drift and a lower DCF compared to the original CSA S16 design (1.64% and 1.33% versus 1.75% and 1.49%). Overall, the improved frames exhibited a more uniform distribution of inelastic deformation over the frame height. For the improved frame with W610×195 columns, the average peak tier drifts predicted using the detailed design method are 1.06 – 2.82 times higher than the tier drifts obtained using the dynamic analysis. For the frame with W360×216 columns, the predicted tier drifts are 1.05 – 1.94 times higher than the dynamic analysis results. This suggests the conservatism implicit in the proposed method when predicting tier drift and resulting BRB strains. Since the tier drift in the roof level (Tier 4) was only a function of the design storey drift, the predicted tier drift was nearly identical to the numerical results. The column in-plane bending demands at each tier level for the three designs are presented in Table 3.4. As shown, column moments are nearly equal to $0.1M_{py}$ in all the designs. Comparing the predicted column in-plane moment to the peak moment demands from the dynamic analysis shows that the moments are overestimated in the range of 1.7 – 3.7 for the design utilizing W610×195 columns and 1.14 – 1.90 for the design considering the strength and stiffness requirement with W360×216. The overestimation is likely due to the assumed location of column inflection points, as described earlier.

Comparing the predictions by the detailed and alternative methods for the 4T-12-1-Z BRBF with W360×216 in Table 3.4 confirmed that the alternative design method predicts on average 1.2 times higher tier drifts and about 2 times higher in-plane moments than the predictions by the detailed

method. The tier drift predictions using the alternative design method varied between 1.08 – 2.17 times the tier drifts obtained from the dynamic analyses. The overestimation of column in-plane moments in the tier levels using the alternative compared to the analytical results varied between 2.17 and 4.33, which was mainly attributed to the conservative assumption of inelastic frame deformation occurring in tiers with tension-acting BRBs only. These results suggest that although simpler to apply than the detailed method, the alternative design method yields appreciably more conservative results. The accuracy of the alternative design method can increase by relaxing the assumption that 100% of the inelastic frame deformation develops in the tension-acting BRBs when further numerical analyses are performed in future studies.

Table 4.4: Statistics of peak frame response parameters for standard and improved 4T-24-1-Z BRBFs.

Parameter	4T-24-1-Z Design Column Sections		
	W530×150	W610×195	W360×216
Δ_{st} (%)	1.15	1.19	1.21
$\delta_{st} / R_o R_d \delta_e$	0.80	0.89	0.93
$\Delta_{critical\ tier}$ (%)	1.75	1.74	1.64
DCF	1.49	1.41	1.33
Δ_4 (%)	1.30	1.33	1.34
$\Delta_{4\text{-Predicted}} / \Delta_{4\text{-NLRHA}}$	-	1.06	1.05 (1.08)*
Δ_3 (%)	1.16	1.14	1.18
$\Delta_{3\text{-Predicted}} / \Delta_{3\text{-NLRHA}}$	-	2.82	1.94 (2.17)
Δ_2 (%)	1.05	1.11	1.14
$\Delta_{2\text{-Predicted}} / \Delta_{2\text{-NLRHA}}$	-	1.28	1.02 (1.26)
Δ_1 (%)	1.34	1.20	1.22
$\Delta_{1\text{-Predicted}} / \Delta_{1\text{-NLRHA}}$	-	2.67	1.87 (2.09)
C_c / C_n	0.63	0.41	0.70
$M_{cy\text{-}3} / M_{py}$	0.13	0.11	0.10
$M_{cy\text{-}3\text{-Predicted}} / M_{cy\text{-}3\text{-NLRHA}}$	-	1.69	1.14 (2.17)
$M_{cy\text{-}2} / M_{py}$	0.11	0.05	0.06
$M_{cy\text{-}2\text{-Predicted}} / M_{cy\text{-}2\text{-NLRHA}}$	-	3.72	1.90 (4.33)
$M_{c\text{-}1} / M_{py}$	0.15	0.11	0.10
$M_{cy\text{-}1\text{-Predicted}} / M_{cy\text{-}1\text{-NLRHA}}$	-	1.69	1.14 (2.17)

*Alternative design method prediction to peak response from dynamic analyses in the parentheses.

4.7 Conclusions

This paper evaluated the seismic response of steel Multi-Tiered Buckling-Restrained Braced Frames (MT-BRBFs), designed as per Canadian standards, and proposed new seismic analysis and design methods in the framework of the Canadian steel design standard. Two methods, including a detailed approach, which is based on mechanics principles, and a displacement-based alternative approach with the aid of a structural analysis program, were introduced. The methods aim to determine column design forces, BRB strain demands, and tier drift; size columns to carry the combined axial force and flexural bending; and make use of the column's flexural stiffness to limit BRB strain demands. A four-tiered BRBF was selected to demonstrate the methods. Nonlinear response history analysis was finally performed to examine the behaviour of the improved frame and evaluate column in-plane flexural moment and tier drift. The key findings of this study can be summarized as follows:

- In MT-BRBFs with opposing BRB orientations (Z- and ZS-bracing), inelastic deformation tends to concentrate in the tiers in which the BRBs undergo tensile yielding. This is due to the variations in BRB probable capacities and post-yield stiffnesses between adjacent tiers. A more uniform lateral deformation response was observed in frames where BRBs are oriented in the same direction (S-bracing).
- The design storey drift computed in accordance with 2015 NBC exceeds the storey drift demand obtained from the nonlinear response history analyses for frames with heights exceeding 18 m while accurately estimating the storey drift demand for other BRBFs.
- Under a large roof displacement, since tension-acting BRBs posses a lower capacity and post-yield stiffness they attract higher inelastic deformation and create relatively larger lateral displacements in tiers with BRBs yielding in tension compared to those with BRBs

yielding in compression. To compensate for the difference between BRB capacities in any adjacent tiers, in-plane shear and flexure are induced on the columns.

- In-plane flexural bending on the columns was more pronounced in shorter frames and decreased when the frame height was increased. Frames with BRBs oriented in opposing directions in the first two adjacent tiers and in the same direction in other tiers (ZS-bracing) experienced the most severe concertation of frame lateral deformation and therefore the largest moment demands in their columns. For example, for a three-tiered BRBF with ZS-bracing (3T-18-1-ZS), the average recorded in-plane bending reached 19% of the plastic moment capacity of the column. The variation of 10% in the yield strength between adjacent BRBs has a negligible effect on the frame response.
- MT-BRBF columns should be designed to resist the combined effects of axial compression and flexural bending while having adequate flexural stiffness to limit BRB strain in any tier to the BRB strain corresponding to two times the design storey drift as obtained from the BRB qualification testing requirements per AISC 341-16 Chapter K3. Two analysis and design techniques, a detailed (mechanics-based) approach and an alternative (displacement-based) method that is best suited to using a computer program, were proposed to improve the seismic response of steel MT-BRBFs.
- In the mechanics-based method, column flexural bending is determined as a function of the modified unbalanced BRB shear resistances in adjacent tiers. The probable BRB resistance in compression is modified to account for lower deformation demands induced in compression-acting BRBs. Tier drift in the tiers with BRBs yielding in tension is computed by adding the drift due to the design storey drift assuming a linear variation over the frame height to the contribution from column bending. This column bending is obtained by

isolating a simply-supported column spanning adjacent tiers and subjecting it to an in-plane transverse load at any strut level within the isolated column with an amplitude of the modified unbalanced BRB storey shears in any adjacent tiers.

- In the displacement-based method, column flexural bending is obtained by applying the inelastic tier drift obtained by distributing the inelastic frame deformation between the tension tiers in proportion to the height of the frame. This method is best suited for design with the aid of a structural analysis program. Both loading directions should be examined.
- In the displacement-based method, the tier drift in the tension tiers is obtained by adding the tier drift due to the elastic storey drift, and assuming a linear variation over the frame height to the inelastic tier drift obtained by distributing the inelastic frame deformation between tension tiers in proportion to height.
- Both the mechanics-based and displacement-based methods proposed here can sufficiently predict the column seismic demands and tier drift with varying levels of conservatism. For instance, the predicted column in-plane moments using the detailed method are on average 1.7 – 3.7 higher than the respective peak moments observed in the dynamic analyses.

Future studies should examine other bracing configurations possible in multi-tiered BRBFs, including two-bay X, V-, and inverted V-bracing. The results of such studies should be used to refine the proposed methods to estimate column moments and tier drifts. Furthermore, the effect of out-of-plane demands arising from BRB connections (Takeuchi et al. 2014; Zaboli et al. 2018) on the stability of MT-BRBF columns should be estimated and accounted for in design.

CHAPTER 5 SEISMIC PERFORMANCE ASSESSMENT OF MULTI-TIERED STEEL BUCKLING RESTRAINED BRACED FRAMES DESIGNED TO 2010 AND 2022 AISC SEISMIC PROVISIONS

Abstract

This paper aims to evaluate the seismic response of Multi-Tiered Buckling-Restrained Braced Frames (MT-BRBFs), assess the design provisions specified by the 2022 AISC Seismic Provisions for multi-tiered BRBFs and propose improvements to these provisions. A set of 16 frames are first selected by varying the bracing configuration, frame height, number of tiers, and tier height ratio. The frames are then designed in accordance with the 2010 and 2022 AISC Seismic Provisions. A numerical parameter study is performed under a set of 21 ground motion accelerations. The results of the parametric study show that when the frames are designed to the 2010 provisions, the frame inelastic deformation tends to concentrate in the tier(s) undergoing tensile yielding due to their lower post-yield stiffness, compared to BRBs yielding in compression which creates unequal storey shear in adjacent tiers with BRBs in tension and compression and engages column flexure to compensate for unbalanced brace storey shear between tiers. Columns experience yielding and even buckling in several cases due to combined flexural and axial load demands. MT-BRBFs designed to the 2022 AISC Seismic Provisions exhibit a more uniform deformation response between tiers and relatively lower flexural demands in the columns. However, these provisions may overestimate column in-plane flexural demands (on the order of 3), resulting in potentially uneconomical design solutions. On the basis of the numerical simulations, modifications are proposed to compression BRBs' adjusted strength to better estimate column in-plane flexural demands and tier deformation while achieving an economical column design. The proposed improvements are validated using dynamic analyses.

Keywords: Steel multi-tiered braced frames, buckling-restrained braces, seismic design, nonlinear analysis.

5.1 Introduction

Steel Multi-Tiered Buckling-Restrained Braced Frames (MT-BRBFs) consist of multiple Buckling-Restrained Brace (BRB) panels stacked vertically along the storey height. Such frames are commonly used in regions of moderate to high seismicity in tall, single-storey buildings such as warehouses, airplane hangars, and sports facilities, and in tall stories of multi-storey buildings. Figs. 1a and 1b show a three-tiered BRBF and a two-tiered BRBF, respectively, both in a single-storey building. The multi-tiered bracing configuration is often preferred over the single-panel bracing configuration to avoid overly long braces and steep bracing angles, while achieving an economical design. Intermediate horizontal struts are often used between bracing panels to form a lateral load path when BRBs yield in tension and compression. These struts can also be used to brace the columns in the plane of the frame, reducing their effective length factor for in-plane buckling. However, the columns are considered unbraced out-of-plane over the full frame height. In single-storey buildings, multi-tiered BRBFs are often located on the exterior walls of the building (Figure 5.1) where their columns are subjected to the lateral wind load and are typically selected from wide-flange profiles oriented such that the lateral wind load produces strong cross-sectional axis bending.

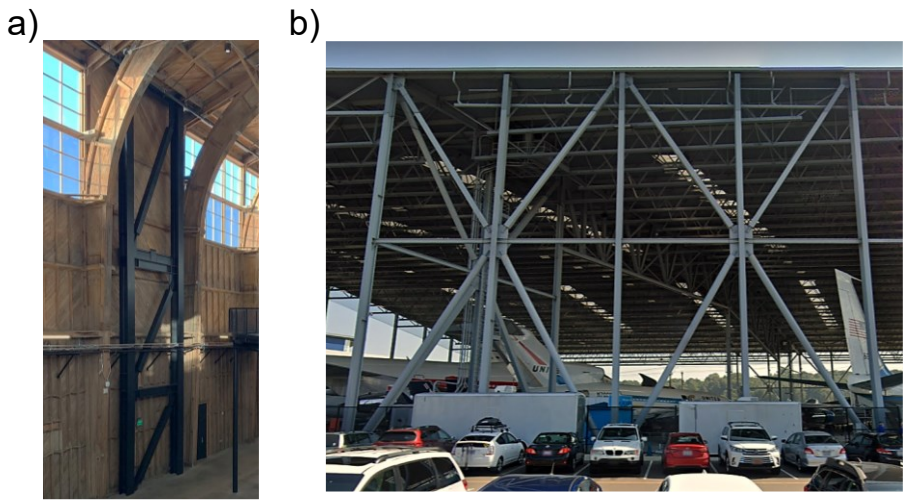

Figure 5.1: Multi-tiered buckling-restrained braced frames: a) three-tiered BRBF with single diagonal bracing (Courtesy of Maren Dougherty); b) two-tiered BRBF with two-bay bracing (retrieved from Google Street View).

Under lateral loads, multi-tiered BRBFs behave as a single-degree-of-freedom (SDOF) system as there are no horizontal inertial forces that develop between the roof and foundation levels, e.g., in a single-storey structure, to help maintain equilibrium between adjacent tiers when BRBs yield in tension and compression. This contributes to the development of unequal tensile and compressive resistances and different post-yield stiffnesses, due to the inherent asymmetric response of steel BRBs in tension and compression, which exhibits higher strength and post-yield stiffness when yielding in compression (Merritt et al. 2003a; b; Tremblay et al. 2006; Fahnestock et al. 2007). As such, under lateral deformation, the tier(s) with BRBs yielding in tension tend to deform more than the ones with BRBs experiencing compressive yielding. To compensate for the difference in storey shear resistances between the tier with a tension-acting BRB and the adjacent tier with a compression-acting BRB, in-plane shear and flexure develop in braced frame columns, as shown in Figure 5.2. In the presence of a large axial compression force induced due to gravity and BRB axial resistances, this can lead to plastic hinge formation in the columns or column instability

(Figure 5.2). Furthermore, uneven distribution of inelastic lateral deformation between tiers with tension and compression BRBs can impose excessive axial strain in the BRB core, potentially causing a low-cycle fatigue fracture in the BRB core (Figure 5.2).

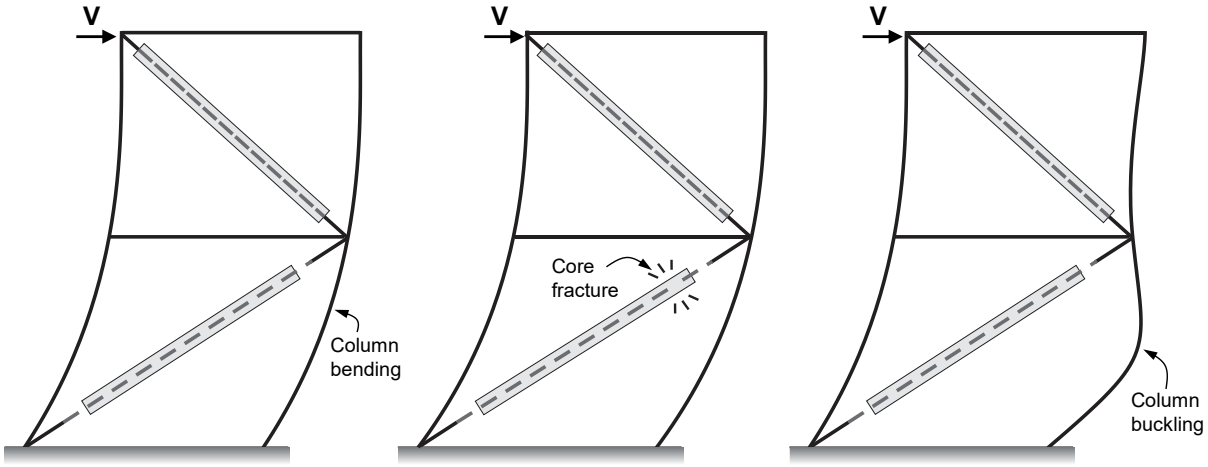

Figure 5.2: Lateral response of two-tiered BRBF and potential failure mechanisms.

Although a large number of research studies have been performed to evaluate the seismic behaviour of steel Multi-Tiered Concentrically Braced Frames (MT-CBFs) and develop design guidelines for such frames, very little information is available regarding the seismic behaviour of multi-tiered BRBFs and whether or not the current seismic design provisions are sufficient to address their potential limit states. Past studies investigating MT-CBFs confirmed that inelastic brace response tends to concentrate in one tier, referred to as the critical tier, over the frame height due to the tensile yielding of the tension-acting brace and the post-buckling response of the compression-acting brace in that tier, which reduces storey shear resistance and precludes brace tensile yielding in other non-critical tiers. The non-uniform distribution of frame lateral deformation induces in-plane bending on the columns which, in combination with a high axial compression force produced by gravity loads plus brace axial resistances, can lead to column instability (Imanpour et al. 2016a; b, 2022; Imanpour and Tremblay 2016; Cano and Imanpour 2020). Past studies also investigated

the means of addressing the observed limit states in MT-CBFs, which led to the development of new design guidelines in the framework of the U.S. design standards (Stoakes and Fahnestock 2016; Imanpour et al. 2016c; Imanpour and Tremblay 2017). These special design requirements were then included in the 2016 AISC Seismic Provisions for Structural Steel Buildings, AISC 341 (AISC 2016) for Multi-Tiered Special Concentrically Braced Frames (MT-SCBFs) and Multi-Tiered Ordinary Concentrically Braced Frames (MT-OCBFs). The same provisions are included in the recent 2022 AISC Seismic Provisions for Structural Steel Buildings, AISC 341 (AISC 2022).

The 2016 and the more recent 2022 AISC Seismic Provisions include requirements for multi-tiered BRBFs, which require designers to select columns with enough strength to resist the combined axial load and in-plane flexural bending and torsionally brace the columns at every strut-to-column location. Furthermore, they require that the lateral deformation of the frame in each tier must not exceed 2% of the tier height. These requirements were developed primarily based on the findings from multi-tiered CBF studies (Imanpour et al. 2016c; Imanpour and Tremblay 2017b), and only limited information is available on the seismic performance of steel multi-tiered BRBFs (Imanpour et al. 2016b). Thus, there is an urgent need to comprehend the seismic performance of steel multi-tiered BRBFs designed to both consider and neglect 2022 AISC 341, to assess these provisions and to propose potential improvements to the multi-tiered BRBF design.

This paper aims to evaluate the seismic response of steel multi-tiered BRBFs designed in accordance with the 2010 and 2022 AISC Seismic Provisions (AISC 2010a, AISC 2022), assess the 2022 AISC 341 design requirements for multi-tiered BRBFs and propose improvements to these provisions. The rest of the paper is organized as follows. First, the multi-tiered BRBF design provisions in 2022 AISC 341 are reviewed. The seismic design of 16 prototype multi-tiered BRBFs, involving various single-diagonal configurations, frame heights, number of tiers, and tier

height ratios, is then presented. Of the 16 prototype frames, a set of 14 frames are designed in accordance with the 2010 AISC 341 (i.e., no special design requirements), while 2022 AISC 341 provisions are followed for the design of the other two frame to evaluate the 2022 design requirements. The numerical model of prototype BRBFs is developed and used to perform nonlinear response history analyses (NLRHA). Several geometric parameters and two design methodologies are interrogated through parametric simulations by evaluating storey and tier drifts, BRB forces and strains, and column flexural bending demands. The results of the NLRHA are also used to make recommendations to improve the 2022 AISC 341 provisions for multi-tiered BRBFs. The proposed improvements are finally validated using dynamic analyses.

5.2 2022 AISC 341 Seismic Provisions for Multi-tiered BRBFs

The 2022 edition of AISC 341 prescribes special design requirements for multi-tiered BRBFs. As per these requirements, 1) the effects of out-of-plane forces due to the mass of the structure shall be taken into account in the analysis of the frame; 2) intermediate horizontal struts shall be placed between braced tiers at every brace-to-column connection location; 3) columns shall be designed as beam-columns under an axial compression force induced by gravity loads plus vertical components of adjusted brace strengths acting on the column, and in-plane flexural bending induced by the difference between storey shear resistances of adjacent tiers when a full plastic mechanism is achieved; 4) columns shall be braced torsinally at every strut-to-column connection location (Helwig and Yura, 1999); and 5) lateral deformation of the frame in each tier shall not exceed 2% of the tier height. When computing column flexural bending, MT-BRBF columns are treated as simply supported members spanning points of out-of-plane bracing subjected to a point load at every brace-to-column location equal to the greater of the summation of frame shears from the adjusted brace strengths between adjacent tiers and a minimum notional load equal to 0.5% of

the frame shear obtained from the higher strength adjacent tier. This approach is deemed acceptable given that multi-tiered BRBFs behave as an SDOF system under lateral seismic loads and that a full plastic mechanism is expected under in-plane seismic demands. To meet the specified tier drift limit, column in-plane flexural stiffness can be used; alternatively, the cross-sectional area of BRB cores can be adjusted to better distribute frame lateral deformation between tiers and reduce the concentration of lateral deformation in one or a limited number of tiers. In the latter approach, the engineer should consider the trade-off between column axial force and bending moment when adjusting BRB cores.

5.3 Seismic Design of MT-BRBFs

5.3.1 Prototype Building and Frames

A single-storey building representing a sports facility located near Seattle, Washington (Latitude: 47°32'09"N; Longitude: 122°11'53"W) was selected in this study. The building plan dimensions are 70 m × 126 m as shown in Figure 5.3a. The building is of normal importance and located on site Class C. The roof system consists of a corrugated steel deck supported by steel trusses that span the full width of the building in the north-south direction (Figure 5.3a). The lateral load-resisting system consists of four multi-tiered BRBFs in each orthogonal direction of the building. A set of 16 MT-BRBFs were selected by varying the frame total height h, number of tiers n, bracing configuration, and tier height ratio, defined as the ratio of the height of the first tier to the height of the other tiers, h_1/h_2. The geometrical properties of the prototype frames are given in Table 5.1. As shown in Figure 5.3b, three different single-diagonal bracing configurations were considered: BRBs oriented in opposing directions (zigzag-bracing or Z-bracing), BRBs oriented in the same direction (S-bracing), and a combination of both (ZS-bracing). MT-BRBFs with Z-bracing are often preferred in practice to reduce the number of BRB-to-beam/column connections and to

achieve a balanced footing design by reducing the uplift force at the base of the frame. The S-bracing configuration is used to eliminate unbalanced forces on the columns by directly engaging the struts in the lateral load path. MT-BRBFs utilizing ZS-bracing combine the benefits of both Z- and S-bracing configurations. In this study, the ZS-bracing configuration, where the first tier is opposite to the upper tiers (Figure 5.3b), was chosen as it is deemed to lead to the most critical multi-tier response while representing a common bracing configuration.

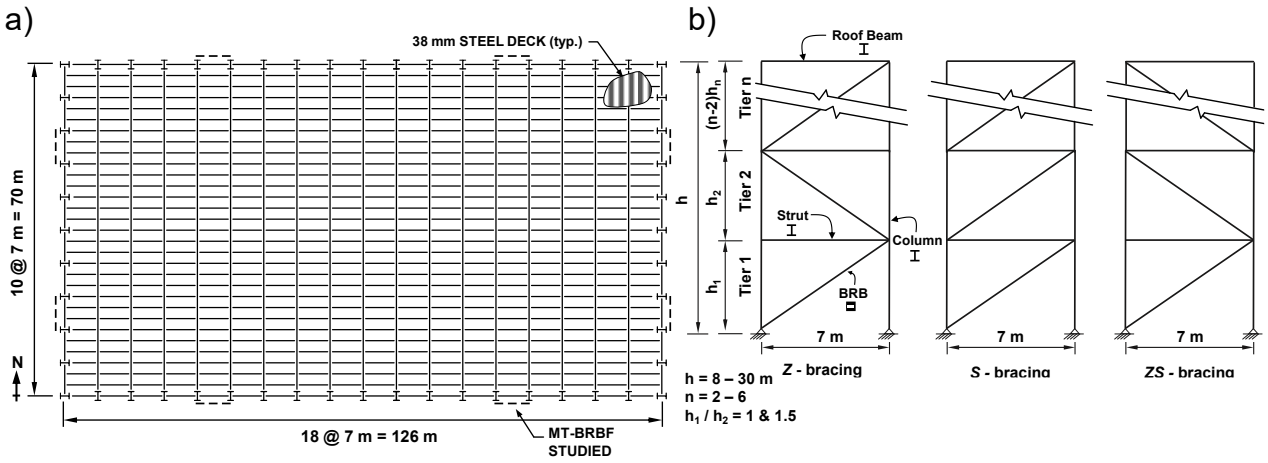

Figure 5.3: Prototype building and frame configurations.

Table 5.1: Geometrical properties and design details of prototype multi-tiered BRBFs.

Frame	Total Height (h) m	No. of Tiers (n)	Bracing Config.	h_1 / h_2	Tier 1 BRB Core Area A_{sc1} (in^2)	Tier i BRB Core Area A_{sci} (in^2)	Design Storey Drift ($C_d\delta_e$/H) %	Column Section	Roof Beam Section	Strut Section
2T-8-1-Z	8	2	Z	1.0	3.2	3.2	1.35	W360X58	W310X52	W200X59
2T-12-1-Z	12	2	Z	1.0	2.9	2.9	1.25	W360X79	W310X45	W200X59
2T-12-1-S	12	2	S	1.0	2.9	2.9	1.32	W360X79	W310X45	W250X73
2T-12-1.5-Z	12	2	Z	1.5	3.2	2.7	1.35	W200X86	W310X45	W200X59
2T-12-1-Z-22[†]	12	2	Z	1.0	2.9	2.9	1.13	W360X147	W310X45	W200X59
3T-12-1-Z	12	3	Z	1.0	2.5	2.5	1.43	W410X67	W310X45	W200X59
3T-18-1-S	18	3	S	1.0	2.3	2.3	1.40	W530X101	W310X45	W250X67
3T-18-1-Z	18	3	Z	1.0	2.3	2.3	1.40	W530X101	W310X45	W200X59
3T-18-1-ZS	18	3	ZS	1.0	2.3	2.3	1.40	W360X101	W310X45	W250X67
3T-18-1.5-Z	18	3	Z	1.5	2.6	2.2	1.37	W360X101	W310X45	W200X59
3T-18-1-Z-22[†]	18	3	Z	1.0	2.3	2.3	1.33	W460X128	W310X45	W200X59
4T-24-1-Z	24	4	Z	1.0	2.0	2.0	1.43	W410X114	W310X45	W200X59
6T-24-1-Z	24	6	Z	1.0	1.8	1.8	1.65	W460X97	W310X45	W200X59
6T-24-1.5-Z	24	6	Z	1.5	2.5	2.2	1.65	W530X123	W310X45	W200X59
6T-30-1-Z	30	6	Z	1.0	2.3	2.3	1.66	W610X140	W310X45	W200X59
6T-30-1.5-Z	30	6	Z	1.5	2.6	2.2	1.60	W530X165	W310X45	W200X59

[†] Frame is designed in accordance with 2022 AISC Seismic Provisions.

5.3.2 Gravity and Seismic Loading

Gravity and seismic loads were determined in accordance with 2010 ASCE 7 (ASCE 2010). Dead (D), live (L), and snow (S) loads of the roof were 1.2, 1.0, and 0.96 kPa, respectively. The unit weight of the exterior cladding was 1.0 kPa.

The seismic base shear was determined using the Equivalent Lateral Force (ELF) procedure. The building was assumed to be of normal importance, I_e = 1.0, and assigned to Risk Category II and Seismic Design Category (SDC) *D*. The mapped maximum considered earthquake (MCE_R) spectral response acceleration parameters are S_s = 1.44g at the short period and S_1 = 0.55g at the 1.0s period, which result in the design spectral response acceleration parameters S_{DS} = 0.96g and S_{D1} = 0.475g, where *g* is the gravitational acceleration. BRBFs were designed as the special BRBF system, with a

response modification coefficient R = 8 and a deflection amplification factor C_d = 5. The design period was taken as C_uT_a for all the frame, where C_u is the upper limit period coefficient equal to 1.4, and T_a is the fundamental period of the structure defined as $T_a = 0.0731h^{0.75}$, where h is the total height of the frame as shown in Figure 5.2b. Table 5.2 gives the design fundamental period, design spectral response acceleration, seismic weight per frame and design storey shear per frame, including a 5% amplification for accidental torsion, for the prototype frames based on their total height.

The lateral wind load was computed as per ASCE 7 assuming a wind speed corresponding to a 7% probability of exceedance in 50 years (mean recurrence interval = 700 years). For the BRBFs selected in this study, the lateral seismic load governs the design of the lateral load-resisting system.

Table 5.2: Seismic design parameters of prototype multi-tiered BRBFs.

Frame Total Height (H) m	Design Fundamental Period (C_uT_a) s	$S(C_uT_a)$	Seismic Weight/Frame (W) kN	Design Storey Shear/Frame (V) kN
8	0.40	1.21g	2706	712
12	0.60	1.07g	2846	688
18	0.90	0.78g	3056	543
24	1.20	0.63g	3266	470
30	1.50	0.54g	3476	434

5.3.3 Frame Design

Multi-tiered BRBFs were designed as per AISC 341 and 2010 AISC Specification for Structural Steel Buildings, AISC 360 (AISC 2010b), under the ASCE 7 load combination $1.2D + E + L + 0.2S$, where E is the seismic load effect. Both horizontal and vertical seismic load effects were considered in design. The seismic design of the 18-m tall, three-tiered BRBF with Z-bracing and equal tier heights, 3T-12-1-Z, is presented here. The geometry of this frame is shown in Figure 5.4a. The frame was first designed following 2010 AISC 341 (3T-12-1-Z in Table 4.2) and then

was redesigned in accordance with 2022 AISC 341 (3T-18-1-Z-22 in Table 5.2). The special provisions implicit in 2022 AISC 341 only affected the column design, while the BRB, strut and roof beam sizes remained identical between the two designs. Note that the seismic load was kept the same for both the 2010 and 2022 designs to allow for comparison.

5.3.4 BRB Design

BRBs are designed to resist the lateral seismic base shear in tension and compression. For 3T-12-1-Z, BRB cores were chosen from mild steel plates conforming to ASTM A36 (ASTM 2008) with a yield strength of F_y = 290 MPa, which is taken as the average of the typical lower and upper bound yield strength of ASTM A36, i.e., F_y = 0.5 (262 MPa + 317 MPa) (AISC 2018), to resist a required compressive strength of 392 kN, which resulted in steel core area of A_{sc} = 1506 mm^2 (= 2.3 in^2) with the axial yield strength equal to 436 kN. The material overstrength factor, R_y, was not considered in design due to the fact that the BRB design force would directly be used to select the BRB core cross sectional areas (AISC 2018). The strain hardening adjustment and compression strength adjustment factors were ω = 1.36 and β = 1.24, respectively, as obtained from communication with the BRB fabricator (Saxey, personal communication, 2022). The adjusted strengths in tension and compression were therefore equal to $\omega A_{sc} F_y$ = 740 kN and $\omega\beta A_{sc} F_y$ = 916 kN, respectively. The stiffness modification factor KF = 1.32 was used based on design tables provided by a BRB manufacturer (Saxey, personal communication, 2022) to adjust brace axial stiffness accounting for the added stiffness provided by the BRB transition length and connections.

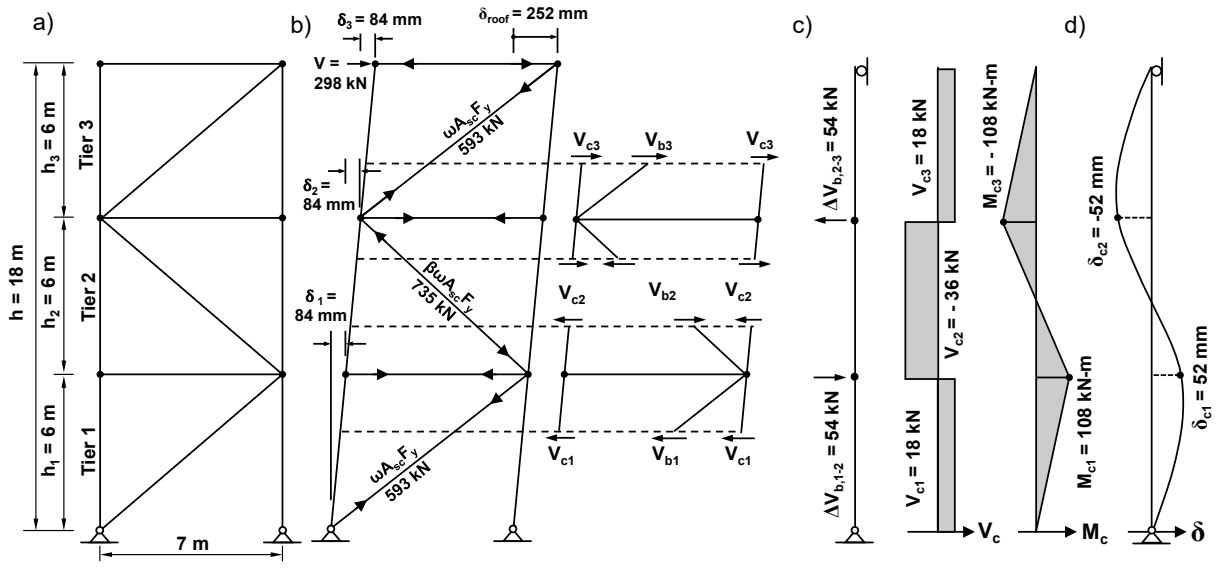

Figure 5.4: Seismic analysis of three-tiered BRBF: a) fame geometry; b) member forces under adjusted brace strengths at positive expected storey drift; c) brace unbalanced loads, column in-plane shear and flexural bending; and d) tier deformation due to column bending based on 2022 AISC 341 simply-supported column approach.

5.3.5 Design of Struts and Roof Beam

The intermediate horizontal struts and the roof beam were designed using wide-flange sections conforming to ASTM A992 (ASTM 2015) steel with a yield strength of F_y = 345 MPa to resist adjusted BRB strengths in tension and compression. The required strut compressive strength $P_{u,s}$ = 108 kN was obtained as the unbalanced brace storey shear between tiers. A W200×59 section was selected to carry this load. Note that although required by AISC 341-16, the strut-to-column connection was assumed to be pinned in the numerical model due to the limitations of the analysis program used. Additionally, it was confirmed in the recent testing programs on steel multi-tiered braced frames that torsional bracing of the column has minimal influence on the frame response (Cano et al. 2023). The roof beam was oriented such that its web is in the plane of the frame and was assumed to be laterally supported on both its flanges by the roofing system. A W310×44.5 was

selected to resist the required axial strength $P_{u,b}$ = 450 kN developed due to the BRB's adjusted strengths plus the required flexural strength $M_{ux,b}$ = 46 kN induced by the roof gravity load. The selected beam had a design axial strength of $\phi_c P_{n,b}$ = 880 kN and a design flexural strength of $\phi_b M_{nx,b}$ = 49 kN-m. Both strut and beam sections selected met the requirements associated with moderately ductile members per AISC 341.

5.3.6 Column Design per 2010 AISC 341

The columns were sized to resist the maximum seismic-induced axial compression load equal to 1250 kN due to BRB strengths, which occured in the first-tier segment of the right column (Figure 5.4b), the axial load induced due to vertical acceleration effects (= $0.2S_{DS}$D) that were 28 kN, and a factored gravity-induced (1.2D) axial load of P_G = 259 kN. The required column axial strength in Tier 1 was therefore $P_{u,c}$ = 1537 kN (Figure 5.4b). The columns were assumed to be pinned at the base and the roof level in both planes. The columns were laterally braced by intermediate struts in the plane of the frame; however, they can buckle out-of-plane along the frame's full height. Reduced column buckling lengths were obtained for in-plane (0.86 h_1) and out-of-plane (0.79h) flexural buckling resistances due to distributed axial loads along the column height and the continuity of the columns (Dalal 1969). A W530×101 profile made of ASTM A992 steel was selected. This section satisfied highly ductile member requirements and had a design axial strength of $\phi_c P_{n,c}$ = 1587 kN. The selected column section was also verified under an axial compression force due to gravity plus out-of-plane flexural bending under wind.

5.3.7 Column Design per 2022 AISC 341

The columns of 3T-12-1-Z-22 were redesigned following 2022 AISC 341 to resist the combination of an axial compression force as described earlier ($P_{u,c}$ = 1537 kN) and in-plane bending when a

full plastic mechanism is achieved through yielding of BRBs in all tiers. The design moment was computed by isolating the column as a simply supported member under in-plane transverse point loads applied at the strut-to-column locations, as shown in Figure 5.4c. Each point load was obtained as the summation of frame storey shears from the BRB's adjusted strengths between adjacent tiers, i.e., unbalanced brace loads, distributed between two braced frame columns, which are equal to 54 kN per each MT-BRBF column of the frame example, resulting in required in-plane flexural strength $M_{uy,c}$ = 108 kN-m. A W460×113 column was selected to resist the combined effects of the axial force and flexural bending using the AISC 360 axial force and flexure interaction equation, resulting in an interaction ratio of 0.98. The selected column met the provisions for moderately ductile members, and had a design axial strength of $\phi_c P_{n,c}$ = 2880 kN and a design weak axis flexural strength of $\phi_b M_{ny,c}$ = 215 kN-m. In-plane flexural stiffness of the braced frame columns (EI_y) is used here to limit tier drifts to the code-specified limit of 2% when the roof displacement reached the lateral displacement corresponding to the design storey drift $\Delta = C_d\delta_e/hI_e$, where δ_e is the elastic roof displacement calculated under the design base shear. The drift in each tier was calculated by summing up the drift created due the overall frame drift when the frame reached the design storey drift including inelastic effects, i.e., $\Delta h_i/H$, and the distortion due to column in-plane bending as obtained from the simply supported column of Figure 5.4d under unbalanced BRB loads, δ_{bi}/h_i. For the frame example, when the frame was displaced to the right (positive displacement), the lateral deformation in Tiers 1 and 3 were the same and equal to 84 mm due to an overall frame drift of 1.4% plus 52 mm due to column bending, resulting in a total lateral displacement of 136 mm, which corresponds to a tier drift of 2.3% (= 136 mm/6000 mm). The tier drift in Tier 2 was computed as 0.53% due to lateral deflection equal to 82 mm as a result of the overall frame drift and -52 mm due to column bending. A stiffer W460×128 column which still

met the strength requirements was finally selected to limit the tier drifts in Tiers 1 and 3 to the code-specified limit of 2%. A similar drift check was performed when the frame was laterally moved to the left, which resulted in the same tier drifts. However, tier drifts under each positive and negative roof displacement would be different if the tier heights or the BRB resistances between tiers were not the same, suggesting that both roof displacements (positive and negative) must be checked in design. For the frame example, the column size selected when using 2022 AISC 341 provisions was 26% heavier than that required when the special seismic design requirements were excluded (2010 AISC 341 design). A primary contributor to the increased steel tonnage in this example was the tier drift check. The designer may use other methods to satisfy the tier drift limit, for instance, using wide flange columns in strong axis, cruciform columns, or latticed columns to increase in-plane stiffness. Similar design steps were followed for other prototype frames. Table 5.1 summarizes the selected members for the multi-tiered BRBFs studied.

5.3.8 Frame Storey Drift

Once members were sized, the design storey drift — including inelastic effects calculated as Δ = 1.40% for the 2010 design and = 1.33% for the 2022 design — was checked against the ASCE 7 limit of 2%. Table 4.1 gives the design storey drift for all multi-tiered BRBFs studied. A similar check was finally completed under the lateral wind load, where the elastic roof displacement under the wind load computed with a wind speed corresponding 10-year mean recurrence interval was compared to the h/400 limit as per the ASCE 7 Commentary.

5.4 BRBF Nonlinear Numerical Model

A fiber-based numerical model of multi-tiered BRBFs was constructed in the *OpenSees* program (McKenna et al. 2010) to evaluate the seismic performance of MT-BRBFs and assess their respective

design guidelines in both 2010 and 2016 AISC 341. The model is shown in Figure 5.5a for a two-tiered BRBF example with Z-bracing. Braced frame columns were pin-supported at their base and braced in the out-of-plan direction at their top ends to account for the lateral support provided by the roof system. The columns were modeled using nonlinear force-based beam column elements with fiber discretization of the cross-section. The Giuffre-Menegotto-Pinto (*Steel02*) material model (Fillippou et al. 1983) that features steel kinematic and isotropic hardening was used to model the columns. *Steel02* hardening parameters (b = 0.0067, R_0 = 23.43, cR_1 = 0.89, cR_2 = 0.07, a_1 = 0.35, a_2 = 12.12, a_3 = 0.33, and a_4 = 12.09) were adapted from the calibration performed by Ashrafi and Imanpour (2021) on a CSA G40.21-350WT steel coupon (Dehghani et al. 2017). Residual stress distribution, based on the pattern proposed by Galambos and Ketter (1958), was assigned to the column sections. To capture global flexural buckling, the columns in each tier were divided into ten elements and an initial bi-directional sinusoidal out-of-straightness corresponding to column in-plane and out-of-plane buckling modes (Figure 5.5a) was assigned to the columns with a maximum amplitude of 1/1000 times the length between in-plane and out-of-plane supports, respectively. The roof beam and struts were modeled using elastic frame elements.

To simulate BRBs, corotational truss elements were employed with the same stiffness modification factor of 1.32 as described earlier. The *Steel4* uniaxial material model was used to reproduce the asymmetric kinematic and isotropic hardening response of BRBs (Zsarnoczay 2013). *Steel4* material parameters (b_k = 0.01, R_0 = R_{0c} = 25, r_1 = r_{1c} = 0.9, r_2 = r_{2c} = 0.15, b_i = 0.0014, ρ_i = 1, b_1 = b_{1c} = 0.0001, R_i = R_{ic} = 1, l_{yp} = 1, b_{kc} = 0.028, b_{ic} = 0.05, p_{ic} = 0.601, R_u = 1.45, f_u = 1.65F_y, R_{uc} = 2.95, and f_{uc} = 2F_y) were calibrated using the data obtained from experimental testing of steel BRBs under cyclic and seismic displacement histories (Dehghani and Tremblay 2017). Figures 5.5b and 5.5c show the axial force – axial strain responses of the selected BRBs obtained from the test data as compared to the

numerical prediction, confirming that the selected material model can properly simulate the inelastic response of steel BRBs. Young's modulus E = 200 GPa was assigned to the steel materials in the model. The specified yield strength F_y = 345 MPa was used for wide flange members while F_y = 290 MPa, the average of the upper- and lower-bound yield strengths for ASTM A36 steel, was assigned to BRB cores.

A corotational formulation that is well suited to capture P-Δ effects and large deformations in a nonlinear analysis was selected to account for geometric nonlinearities. A leaning column was modeled using an elastic truss element with relatively large axial and flexural stiffness to simulate P-Δ effects due to the gravity load-carrying system whose tributary seismic weight was resisted by the BRBF selected (see Figure 5.5a). The rotational degrees-of-freedom (DOFs) at the two ends of the leaning column were released to create a lean-on condition. The horizontal displacement of the top of the leaning column was coupled to the top end of the BRBF columns. Lumped masses representing the seismic weight tributary to the selected BRBF were applied at the top of the BRBF columns. The Rayleigh damping method was used to reproduce classical damping, with mass and stiffness proportional damping corresponding to 2% of critical. The gravity analysis was first performed using a static analysis procedure, followed by a nonlinear response history analysis (NLRHA) under a ground motion acceleration imposed in the horizontal direction in the plane of the frame.

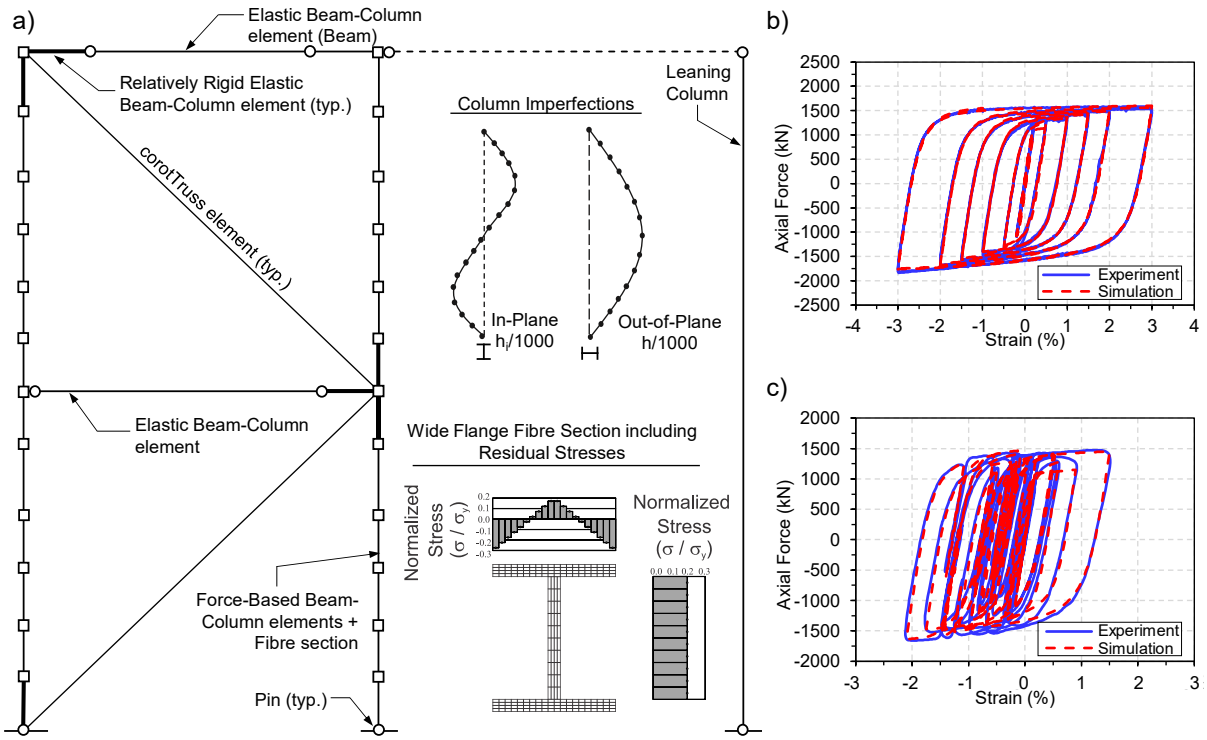

Figure 5.5: a) MT-BRBF numerical model; b) BRB axial force – axial strain under cyclic displacement protocol; c) BRB axial force – axial strain under seismic displacement history.

5.5 Ground Motion Accelerations

Ground motions accelerations were selected and scaled following ASCE 7-16 recommendations using the ASCE 7-10 uniform hazard spectra (UHS). An initial set of 95 ground motion records were first selected with the magnitude, fault distance, and source mechanism that matched the seismic hazard deaggregation data based on the 2014 National Seismic Hazard Model for the Conterminous U.S. of the building site (USGS 2023), Seattle, WA. Two major events contributing to the seismic hazard in Seattle are shallow crustal and subduction interface earthquakes. Due to the proximity of the prototype building to the Seattle Fault, near-fault crustal earthquakes inducing pulse-type ground motions were also considered (Baker 2007). These ground motions are strongly influenced by rupture directivity effects, such that the maximum direction of response tends to occur normal to the fault, which has been shown to cause critical seismic demands on structures

(Sun et al. 2016). The crustal records were obtained from the PEER NGA-West2 database (Ancheta et al. 2013) and the PEER NGA-Sub flatfiles (Mazzoni et al. 2021) were used to select the subduction interface ground motions. The records consisted of pairs of orthogonal ground motion components, except for pulse-like records, and the ground motion components that rotated to the fault-normal direction were used. Out of the 95 records initially selected, 50 were far-field crustal records, 20 belonged to near-field crustal events and 25 were subduction interface records. The initial selection of ground motion records was narrowed to 21 (8 non-pulse crustal, 6 pulse-like crustal, and 7 subduction interface) by ranking the records in each hazard set based on their Mean Squared Error (MSE) with respect to UHS, while avoiding excessively high, i.e., greater than 5, or excessively low, i.e., less than 0.5, scaling factors. Moreover, records with excessive spectral acceleration peaks greater than 4g were excluded from the final sets. Priority was given to records also included in the Washington State Department of Transportation (WSDOT) WA-RD 791.1 ground motion record sets (Steven et al. 2012) and the FEMA P695 far-field and near-field record sets (FEMA 2009), as long as the MSE was not more than two times that of the other ground motions selected and the scaling factors met the criteria described here. Table 4.3 summarizes the event name, event year, moment magnitude M_w, rupture distance R_{rup}, and recording station for the selected records.

The ground accelerations were scaled to match the ASCE 7-10 5% damped code-prescribed response spectra at the MCE_R hazard level over the period range $0.2T_{min}$ to $1.5T_{max}$, where T_{min} and T_{max} are the minimum and maximum fundamental periods of the prototype frames. The target spectrum was split into two scenario-specific period ranges where each period range was based on the dominant periods of the events having the highest contribution to the seismic hazard. The crustal earthquakes dominated the hazard for shorter periods, whereas longer periods were heavily

influenced by the interface earthquakes. Ground motion scaling factors were applied in two steps: 1) the individual records in each ground motion set were scaled using a factor that minimized the MSE between their 5% damped maximum direction response spectrum (RotD100) constructed from the two horizontal ground motion components and the target spectra along the scenario-specific period range, 2) all the records in each set were collectively scaled using a second scaling factor such that their mean RotD100 spectra does not fall more than 10% below the target spectra along the scenario-specific period range. An amplitude scaling method, as opposed to spectrum-matching, was chosen since it does not affect the frequency content of the ground motion records. Figures 5.6a and 5.6b show the response spectra of the scaled ground motions together with the mean spectra of scaled records and target MCE_R response spectra for the crustal and subduction interface earthquakes, respectively.

Table 5.3: Selected ground motion records for Seattle, WA.

Seismic Source (Database)	Event	Year	M_w	R_{rup} (km)	Recording Station
Far-Field Crustal (NGA-West2)	Imperial Valley-06	1979	6.53	15.19	Cerro Prieto
	Superstition Hills-02	1987	6.54	11.16	Poe Road (temp)
	Loma Prieta	1989	6.93	18.33	Gilroy Array #6
	Cape Mendocino	1992	7.01	6.96	Cape Mendocino
	Northridge-01	1994	6.69	8.66	Arleta – Nordhoff Fire Sta
	Duzce Turkey	1999	7.14	6.58	Duzce
	Chuetsu-oki Japan	2007	6.8	11.75	Kawanishi Izumozaki
	Iwate Japan	2008	6.9	12.85	Kurihara City
Near-Field Crustal (NGA-West2)	Irpinia Italy-01	1980	6.9	10.84	Sturno (STN)
	Loma Prieta	1989	6.93	12.82	Gilroy Array #3
	Loma Prieta	1989	6.93	8.5	Saratoga – Aloha Ave
	Cape Mendocino	1992	7.01	8.18	Petrolia
	Northridge-01	1994	6.69	5.3	Sylmar – Olive View Med FF
	Niigata Japan	2004	6.63	8.93	NIGH11
Subduction Interface (NGA-Sub)	South Peru	2001	8.41	89.67	MOQ1
	Tokachi-oki	2003	8.29	85.06	ASHORO
	Tokachi-oki	2003	8.29	107.35	HIDAKA
	Chile – 2844986	2010	8.81	133.66	LCON
	Tohoku	2011	9.12	159.56	42221
	Tohoku	2011	9.12	101.43	FUKUSHIMA
	Tohoku	2011	9.12	86.33	TAIWA

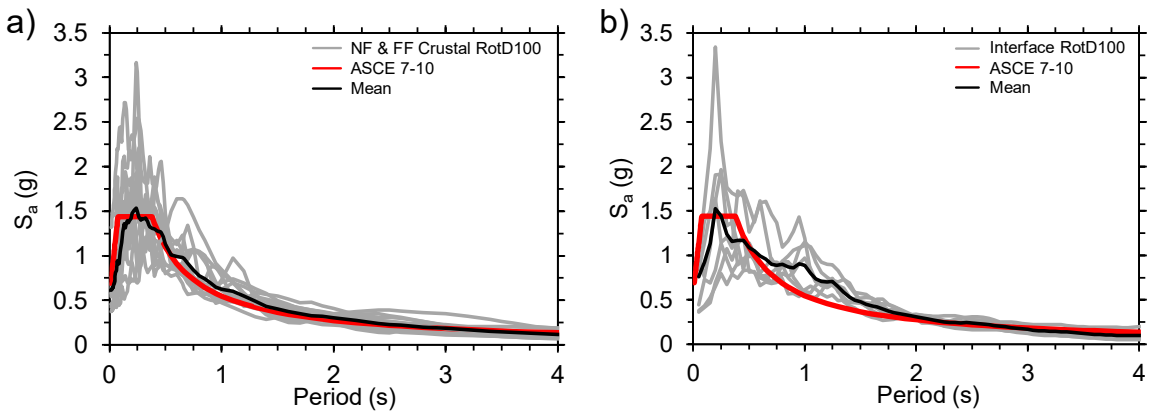

Figure 5.6: Response spectra of the scaled ground motion records: a) Near-Field (NF) and Far-Field (FF) crustal records; b) Subduction interface records.

5.6 Seismic Response of Multi-Tiered BRBFs

5.6.1 Single-Record Case Study of Three-Tiered BRBF

The results obtained from the NLRHA of 3T-12-1-Z (Figure 5.4a) under the E-W component of the 2011 Tohoku, TAIWA earthquake are presented here to study the seismic response of MT-BRBFs designed to 2010 AISC 341. Figures 5.7a and 5.7b show the time histories of the storey drift and tier drifts, respectively. The storey drift is computed as the ratio of the roof lateral displacement to the building height, h, and the tier drift is defined as the ratio of the relative lateral displacement of each tier to the tier height, h_n (where n is the tier number). Under this record, the peak storey drift is 2.5% observed at t = 105 s shortly before column buckling occurs in the right column, which causes significant lateral displacement, as shown in Figure 5.7b. As shown in the tier drift histories of Figure 5.7b, frame inelastic lateral deformation tends to occur mainly in the tier or tiers with BRBs undergoing tensile yielding, which are referred to as critical tiers here, e.g., Tiers 1 and 3 when the frame is displaced to the right (positive displacement) and Tier 2 when the frame moves to the left (negative displacement). Under this particular ground motion, frame lateral deformation is predominantly positive before column buckling t = 0 – 105 s, creating tensile

yielding in the BRBs of Tiers 1 and 3. The uneven distribution of frame inelastic lateral deformation is also confirmed by Figure 5.7c, which shows the variation of tier drifts versus storey drift. Figure 5.7d shows the BRB axial force normalized by the core yield strength, P/P_{ysc}, versus the BRB core axial strain. Due to asymmetric isotropic and kinematic hardening of BRBs in tension and compression (Merritt et al. 2003a; b; Uang et al. 2004; Tremblay et al. 2006; Benzoni and Innamorato 2007, Fahnestock et al. 2007), which translates to a slightly higher post-yield stiffness when the BRB undergoes compression. Tiers 1 and 3 (critical tiers when the lateral displacement is positive) experience significantly larger deformation compared to Tier 2 (a non-critical tier when the lateral displacement is positive) during the majority of ground motion time. This response creates unequal BRB forces at any given time of the ground motion between the tension and compression tiers because of the highly nonlinear response of the BRBs after yielding and the fact that the MT-BRBF columns contribute to storey shear resistance when the BRBs respond in the inelastic region, mainly because their share of lateral stiffness increases as the BRBs unevenly lose their initial elastic stiffness. Given that no inertia forces develop at the strut levels in multi-tiered braced frames, storey shear must remain the same between adjacent tiers, and the MT-BRBF columns therefore compensate for the difference of the storey shear resistances provided by the BRBs between any adjacent tiers, attracting in-plane flexural bending as shown in the deformed shape of Figure 4.6a, given at t = 105 s. The histories of column in-plane bending recorded at the tier levels are shown in Figure 5.7e for the right-hand side (RHS) column (the critical column, as it is subjected to a higher axial compression load when the roof displacement is positive). In this figure, the column in-plane bending moment, M_{ny}, is normalized by the weak-axis plastic moment capacity of the column, M_{py}. As shown, at t = 100 s, the moment in Tiers 1 and 2 reached approximately $0.2M_{py}$ after which a flexural plastic hinge formed at the column's mid-height in

Tier 1 due to the induced flexural bending demand amplified by the presence of an axial compression force (due to P-Δ effects) plus a large axial compression force produced by gravity loads and BRB resistances. After the first plastic hinging in the RHS column, the bending moment started to redistribute within the first-tier segment of the RHS column (as column flexural stiffness started to diminish). Upon increasing the lateral displacement of the frame, the bending moment in the strut level changed sign as a complete column curvature reversal occurred in the column. Bending continued to increase in the strut level until a second flexural plastic hinge formed at that location at t = 105 s, resulting in flexural buckling of the RHS column in the plane of the frame. Plastic hinge formation in the column was confirmed by monitoring axial stresses at column flanges in the fibers of the cross-section and the change of column axial stiffness. The axial force – in-plane bending (P-M) interaction of the column is shown in Figure 5.7f against the AISC 360 interaction curve. As shown, the column axial compression force appreciably dropped after plastic hinging in the first tier; furthermore, column instability was well predicted by the AISC 360 interaction equation. Limited overstrength observed in the column force response featured by the P-M interaction is believed to be due to the material strain hardening while force demands redistribute in the columns.

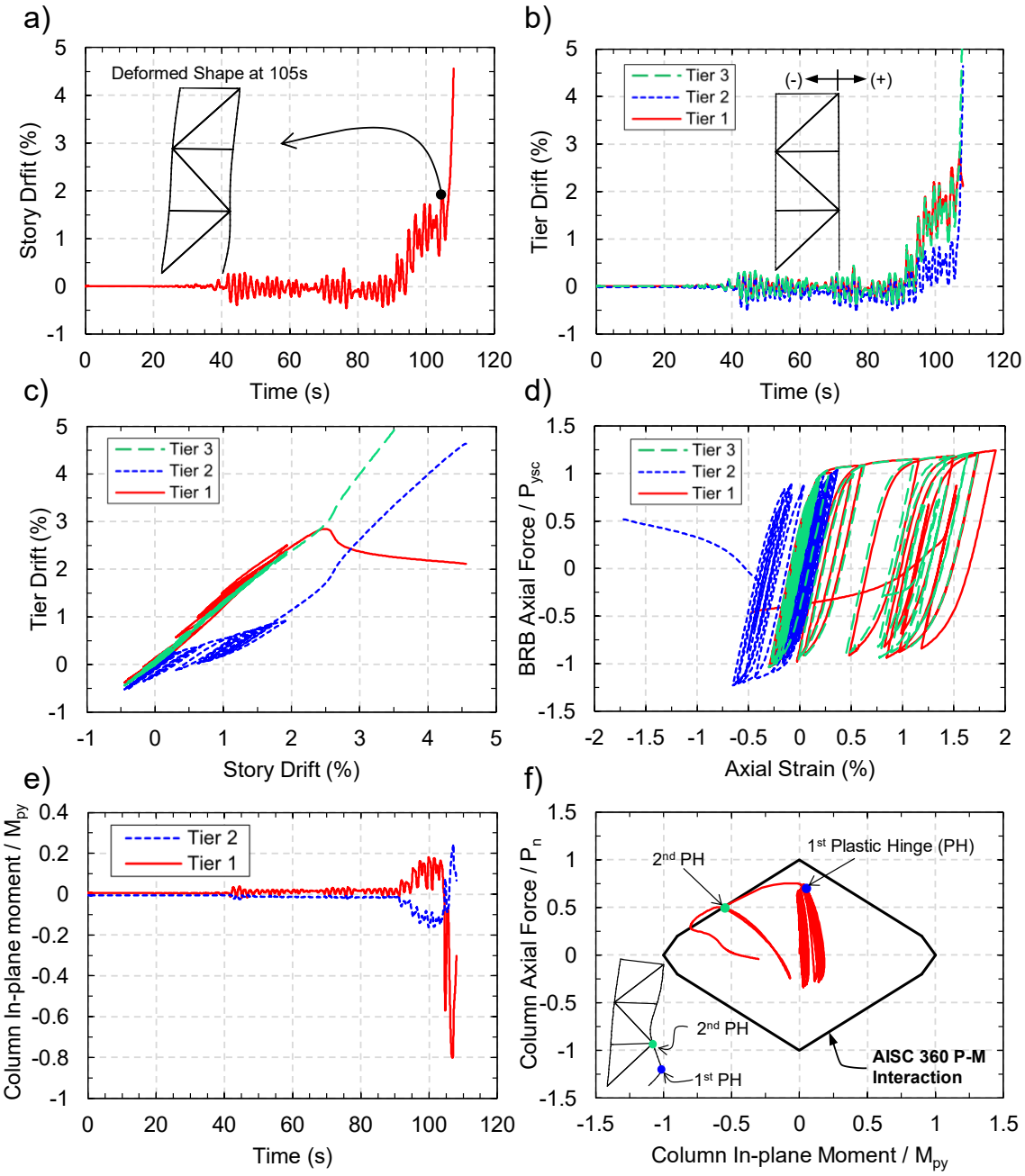

Figure 5.7: Seismic response of three-tiered BRBF under the EW component of the 2011 Tohoku, TAIWA earthquake: a) storey drift history; b) tier drift history; c) tier drift vs. storey drift; d) BRB axial force vs. axial strain; e) column in-plane moment history; f) RHS column P-M interaction at Tier 1 strut level.

5.6.2 Prototype Multi-tiered BRBFs

The parameters affecting the seismic response of the selected multi-tiered BRBFs (Figure 5.3b) were interrogated here using key response parameters, including storey drift, tier drift, BRB force and strain demands, and column force demands. The median and 84th percentile of the peak response parameters obtained from the NLRHA are given in Table 5.4, with the median results representing the average response and the 84th percentile results (in parentheses) illustrating the upper bound response. The median results will be the focus of the discussion in this section.

5.6.3 Frame global response

The peak storey drift, δ_{roof}/h, defined as the ratio of the maximum lateral roof displacement to the storey height, is given in Table 5.4. As shown, the peak storey drift reduces as the frame height increases. No specific trend was found for the drift values of the frames with the same total height. Additionally, Table 5.4 gives the ratio of the storey drift to the design storey drift by ASCE 7 $(\delta_{roof}/h)/\Delta$. Overall, the peak storey drift was well predicted by ASCE 7 for the frames with a total height of 18 m and shorter; however, the variation between the peak storey drift and the design value diverged as the frame height increased with an overestimation in the order of 100% in 30m-tall frames, which could be attributed to the constant deflection amplification factor used for all frames regardless of their total height (Uriz and Mahin 2008; Imanpour et al. 2016b). δ_i/h_i, denoting the peak tier drift, is given in Table 5.4. For all the frames, the median peak tier drifts were less than 2%. Due to the fact that the location of the critical tier or tiers changes for single-diagonal MT-BRBFs as they undergo positive and negative lateral deformation, the median peak tier drifts are fairly close among the tiers for all the frames. Larger tier drifts were observed in frames with Z- and ZS-bracing versus those utilizing S-bracing. Lateral deformation in frames with ZS-bracing tends to concentrate in Tier 1 when the roof displacement is positive, which is the case for the

majority of ground motion records here. To assess drift concentration in a particular tier or tiers along the frame height, the peak tier drift in the critical tier $\delta_{i,c}/h_{i,c}$ and the Drift Concentration Factor (DCF) are provided in Table 5.4. $\delta_{i,c}/h_{i,c}$ is the peak tier drift in the critical tier (the tier or tiers whose BRB yields in tension in each direction of loading) undergoing the greatest tier drift in each loading direction. The DCF is defined as the ratio of the critical tier drift $\delta_{i,c}/h_{i,c}$ to the storey drift δ_{roof}/h. Referring to Table 5.4, the critical tier drift varies between 1.1 and 2.2%. The frames with S-bracing experienced limited drift concentration, DCF ≈ 1.0, which suggests that desirable MT-BRBF response can be achieved by selecting BRBs with identical brace orientations in each loading direction. As opposed to MT-BRBFs with S-bracing, DCF values vary between 1.29 and 1.52 when the Z- or ZS-bracing configuration is used, respectively. Frames with ZS-bracing experience higher drift concentration due to the fact that under positive storey drift they only have one tier yielding in tension (critical tier) whereas frames with Z-bracing have multiple tension tiers and thus more uniformly distribute deformation demands. Generally, the use of a taller first tier (h_1/h_2 = 1.5 vs. h_1/h_2 = 1.0) resulted in a slightly lower DCF, which could be attributed to the fact that stronger BRBs in a taller Tier 1 create relatively higher storey shear resistance when the BRB is in tension (under positive roof displacement) that is closer to the storey shear resistance in the adjacent tier with a BRB in compression, creating a less critical first tier under positive roof displacement, which is the case for the majority of the ground motion records in Table 5.4. Comparing the response of 2022 MT-BRBFs to their 2010 counterparts, 2T-12-1-Z-22 vs. 2T-12-1-Z and 3T-18-1-Z-22 vs. 3T-18-1-Z, a more uniform distribution of frame lateral deformation was achieved, which confirms the effectiveness of the special seismic design provisions in 2022 AISC 341; specifically, no column instability was observed when the frames were redesigned in accordance with 2022 AISC 341. In total, column instability was observed in the first-tier segment

of the right column in 2T-8-1-Z, 2T-12-1-Z, 2T-12-1-Z-Y and 3T-18-1-Z due to the combination of an axial force and large in-plane bending as described earlier for 3T-12-1-Z.

Table 5.4: Statistics of peak frame seismic response parameters from NLRHA.

Parameter	2T-8-1-Z	2T-12-1-Z	2T-12-1-S	2T-12-1.5-Z	2T-12-1-Z-Y	2T-12-1-Z-22	3T-12-1-Z	3T-18-1-S	3T-18-1-Z	3T-18-1-ZS	3T-18-1.5-Z	3T-18-1-Z-22	4T-24-1-Z	6T-24-1-Z	6T-24-1.5-Z	6T-30-1-Z	6T-30-1.5-Z
δ_{roof}/h (%)	1.56	1.31	1.27	1.34	1.28	1.34	1.29	1.21	1.27	1.20	1.33	1.31	1.00	1.01	0.97	0.84	0.84
	(1.95)*	(1.86)	(1.82)	(1.72)	(1.76)	(1.75)	(1.89)	(1.73)	(1.69)	(1.81)	(1.6)	(1.61)	(1.53)	(1.53)	(1.44)	(1.36)	(1.33)
$(\delta_{roof}/h)/\Delta$	1.15	1.05	0.96	0.99	1.03	1.18	0.90	0.86	0.91	0.86	0.97	0.98	0.70	0.61	0.59	0.50	0.52
	(1.44)	(1.49)	(1.38)	(1.28)	(1.41)	(1.54)	(1.32)	(1.24)	(1.21)	(1.3)	(1.17)	(1.21)	(1.07)	(0.93)	(0.87)	(0.81)	(0.83)
$\delta_{i,c}/h_i$ (%)	2.18	1.94	1.30	1.93	2.00	1.56	1.91	1.26	1.72	1.83	1.64	1.55	1.49	1.49	1.44	1.20	1.07
	(3.05)	(2.89)	(1.85)	(2.74)	(2.71)	(2.27)	(2.64)	(1.78)	(2.74)	(2.98)	(2.37)	(2.13)	(2.41)	(2.73)	(2.37)	(2.36)	(2.02)
DCF	1.51	1.50	1.02	1.40	1.50	1.25	1.29	1.04	1.41	1.52	1.29	1.20	1.42	1.54	1.50	1.47	1.37
	(1.67)	(1.65)	(1.03)	(1.8)	(1.73)	(1.34)	(1.74)	(1.07)	(1.63)	(1.72)	(1.58)	(1.42)	(1.69)	(1.77)	(1.72)	(1.7)	(1.51)
δ_6/h_6 (%)	-	-	-	-	-	-	-	-	-	-	-	-	-	1.13	1.06	0.94	0.92
	-	-	-	-	-	-	-	-	-	-	-	-	-	(1.73)	(1.68)	(1.49)	(1.42)
δ_5/h_5 (%)	-	-	-	-	-	-	-	-	-	-	-	-	-	1.12	1.01	0.89	0.88
	-	-	-	-	-	-	-	-	-	-	-	-	-	(1.63)	(1.37)	(1.4)	(1.28)
δ_4/h_4 (%)	-	-	-	-	-	-	-	-	-	-	-	-	1.14	0.98	0.94	0.82	0.85
	-	-	-	-	-	-	-	-	-	-	-	-	(1.69)	(1.45)	(1.26)	(1.15)	(1.26)
δ_3/h_3 (%)	-	-	-	-	-	-	1.31	1.26	1.33	1.12	1.22	1.36	1.01	1.02	0.92	0.80	0.82
	-	-	-	-	-	-	(1.89)	(1.78)	(1.81)	(1.77)	(1.59)	(1.65)	(1.57)	(1.5)	(1.25)	(1.24)	(1.25)
δ_2/h_2 (%)	1.44	1.31	1.30	1.29	1.02	1.23	1.25	1.19	1.12	1.06	1.00	1.12	0.98	0.92	0.92	0.75	0.76
	(2.44)	(2.89)	(1.83)	(2.37)	(1.99)	(1.74)	(2.44)	(1.71)	(2.48)	(1.57)	(1.95)	(1.79)	(1.38)	(1.35)	(1.35)	(1.11)	(1.26)
δ_1/h_1 (%)	1.37	1.30	1.25	1.18	1.51	1.23	1.26	1.16	1.22	1.53	1.29	1.33	1.16	1.15	0.89	0.86	0.85
	(2.65)	(2.19)	(1.82)	(1.92)	(2.38)	(1.8)	(1.81)	(1.68)	(1.78)	(2.3)	(1.86)	(1.68)	(2.12)	(2.24)	(1.74)	(1.66)	(1.63)
$M_{cy\text{-}5}/M_{py}$	-	-	-	-	-	-	-	-	-	-	-	-	-	0.09	0.09	0.08	0.06
	-	-	-	-	-	-	-	-	-	-	-	-	-	(0.17)	(0.15)	(0.13)	(0.1)
$M_{cy\text{-}4}/M_{py}$	-	-	-	-	-	-	-	-	-	-	-	-	-	0.09	0.06	0.06	0.04
	-	-	-	-	-	-	-	-	-	-	-	-	-	(0.17)	(0.11)	(0.14)	(0.06)
$M_{cy\text{-}3}/M_{py}$	-	-	-	-	-	-	-	-	-	-	-	-	0.10	0.09	0.07	0.06	0.04
	-	-	-	-	-	-	-	-	-	-	-	-	(0.14)	(0.16)	(0.11)	(0.14)	(0.07)
$M_{cy\text{-}2}/M_{py}$	-	-	-	-	-	-	0.17	0.01	0.12	0.03	0.10	0.10	0.09	0.08	0.08	0.07	0.04
	-	-	-	-	-	-	(0.27)	(0.02)	(0.22)	(0.04)	(0.19)	(0.14)	(0.13)	(0.15)	(0.12)	(0.14)	(0.07)
$M_{cy\text{-}1}/M_{py}$	0.19	0.13	0.01	0.14	0.14	0.12	0.19	0.02	0.14	0.13	0.14	0.11	0.10	0.12	0.12	0.09	0.08
	(0.25)	(0.25)	(0.02)	(0.22)	(0.2)	(0.2)	(0.31)	(0.02)	(0.26)	(0.2)	(0.21)	(0.19)	(0.19)	(0.25)	(0.2)	(0.18)	(0.14)
P_c/P_n	0.68	0.70	0.77	0.67	0.68	0.22	0.62	0.76	0.70	0.52	0.57	0.34	0.60	0.64	0.61	0.56	0.55
	(0.73)	(0.77)	(0.83)	(0.73)	(0.74)	(0.24)	(0.69)	(0.8)	(0.75)	(0.56)	(0.62)	(0.52)	(0.65)	(0.69)	(0.65)	(0.6)	(0.6)
No. of Column Instability	2	2	0	0	1	0	0	0	2	0	0	0	0	0	0	0	0

*84th percentile results shown in parentheses.

5.6.4 BRB Response

Peak BRB forces and strain demands were computed for the prototype frames at each tier and reported in Table 4.5. For each frame, the peak responses when the BRB is in tension (T) and when it is in compression (C) are given. BRB forces in each tier, P_i, were normalized by the axial yield strength of the steel core, P_{ysc}. Referring to Table 4.5, BRB forces vary between $1.1P_{ysc}$ and $1.2P_{ysc}$ and, in any given loading direction, they are nearly identical when acting in tension and compression. As the height of the frame increases, peak BRB forces tend to decrease mainly because of reduced storey drift, and therefore tier drift, that taller frames experience (see Table 5.5), which mobilize lower post-yield forces in their BRBs. Another interesting observation is that the compressive strength of BRBs in the tier with a compression BRB is somehow bounded by the tensile yielding capacity of the adjacent tier whose BRB yields in tension, affecting the development of the target overstrength in compression BRBs to the extent recorded in the values. This response stems from the nonuniformity of the frame lateral deformation where the tier or tiers with compression-acting BRBs deform less than those with BRBs yielding in tension and attract relatively lower forces.

Peak BRB tensile and compressive strains, ε_{sc}, are given in Table 4.5. Tensile strains are close to anticipated strains from design and vary between 0.54 and 1.04%. Compressive strains, however, vary between -0.32 to -0.56%. Generally, peak compressive strains recorded in the tiers undergoing compressive yielding are nearly half of the peak tensile strains in the tension-acting tiers. For example, tension BRBs in Tiers 1 and 3 of 3T-18-1-Z under positive storey drift reached a peak strain of 0.82 and 0.79%, respectively, while only a peak compressive strain of 0.36% was recorded in the second-tier BRB, which was in compression under positive storey drift. This discrepancy is primarily due to the higher compression post-yield stiffness in steel BRBs resulting in a larger core

elongation in tension tiers compared to core shortening in compression tiers under almost the same storey shear. Overall, BRB strain demands tended to decrease with increasing frame heights. Furthermore, increasing the number of tiers while maintaing the same frame height resulted in lower BRB strain demands due to a more uniform tier drift response achieved by increasing the number of tiers. Lastly, frames consisting of ZS-bracing experienced the highest tensile strain demand in their critical tier.

The comparison between strains in the BRBs of the 2022 designs and those of their 2010 counterparts revealed that the 2022 designs exhibited a lower variation of BRB forces and strains in adjacent tiers, which is likely attributed to the stiffer columns of the 2022 designs. For example, the greatest difference between BRB strains (tensile strain in tension BRBs and compressive strain in compression BRBs) in 3T-18-1-Z is 46% while it reduced to 29% in the respective 2022 design.

Table 5.5: Statistics of peak BRB response parameters from NLRHA.

Parameter	2T-8-1-Z	2T-12-1-Z	2T-12-1-S	2T-12-1.5-Z	2T-12-1-Z-Y	2T-12-1-Z-22	3T-12-1-Z	3T-18-1-S	3T-18-1-Z	3T-18-1-ZS	3T-18-1.5-Z	3T-18-1-Z-22	4T-24-1-Z	6T-24-1-Z	6T-24-1.5-Z	6T-30-1-Z	6T-30-1.5-Z
P_6 / P_{ysc} (T)	-	-	-	-	-	-	-	-	-	-	-	-	-	1.07	1.06	1.05	1.05
	-	-	-	-	-	-	-	-	-	-	-	-	-	(1.13)*	(1.12)	(1.11)	(1.11)
P_6 / P_{ysc} (C)	-	-	-	-	-	-	-	-	-	-	-	-	-	-1.08	-1.08	-1.05	-1.07
	-	-	-	-	-	-	-	-	-	-	-	-	-	(-1.19)	(-1.17)	(-1.16)	(-1.18)
P_5 / P_{ysc} (T)	-	-	-	-	-	-	-	-	-	-	-	-	-	1.05	1.05	1.04	1.04
	-	-	-	-	-	-	-	-	-	-	-	-	-	(1.14)	(1.14)	(1.1)	(1.12)
P_5 / P_{ysc} (C)	-	-	-	-	-	-	-	-	-	-	-	-	-	-1.11	-1.10	-1.07	-1.10
	-	-	-	-	-	-	-	-	-	-	-	-	-	(-1.2)	(-1.2)	(-1.16)	(-1.18)
P_4 / P_{ysc} (T)	-	-	-	-	-	-	-	-	-	-	-	-	1.09	1.06	1.06	1.04	1.04
	-	-	-	-	-	-	-	-	-	-	-	-	(1.14)	(1.12)	(1.11)	(1.08)	(1.11)
P_4 / P_{ysc} (C)	-	-	-	-	-	-	-	-	-	-	-	-	-1.10	-1.09	-1.08	-1.07	-1.09
	-	-	-	-	-	-	-	-	-	-	-	-	(-1.22)	(-1.22)	(-1.17)	(-1.17)	(-1.2)
P_3 / P_{ysc} (T)	-	-	-	-	-	-	1.09	1.14	1.12	1.10	1.12	1.03	1.07	1.04	1.05	1.03	1.04
	-	-	-	-	-	-	(1.27)	(1.22)	(1.22)	(1.2)	(1.23)	(1.13)	(1.18)	(1.14)	(1.14)	(1.1)	(1.11)
P_3 / P_{ysc} (C)	-	-	-	-	-	-	-1.16	-1.12	-1.10	-1.13	-1.12	-1.02	-1.13	-1.11	-1.10	-1.07	-1.09
	-	-	-	-	-	-	(-1.3)	(-1.27)	(-1.2)	(-1.24)	(-1.25)	(-1.14)	(-1.21)	(-1.19)	(-1.18)	(-1.16)	(-1.15)
P_2 / P_{ysc} (T)	1.18	1.15	1.12	1.15	1.10	1.15	1.14	1.13	1.09	1.09	1.09	0.99	1.07	1.06	1.05	1.03	1.04
	(1.34)	(1.28)	(1.26)	(1.28)	(1.23)	(1.27)	(1.29)	(1.21)	(1.17)	(1.18)	(1.18)	(1.08)	(1.12)	(1.11)	(1.1)	(1.08)	(1.1)
P_2 / P_{ysc} (C)	-1.15	-1.10	-1.20	-1.09	-1.05	-1.18	-1.11	-1.12	-1.12	-1.15	-1.16	-1.07	-1.12	-1.10	-1.08	-1.08	-1.10
	(-1.25)	(-1.25)	(-1.37)	(-1.23)	(-1.2)	(-1.33)	(-1.28)	(-1.27)	(-1.22)	(-1.27)	(-1.26)	(-1.17)	(-1.25)	(-1.23)	(-1.18)	(-1.18)	(-1.22)
P_1 / P_{ysc} (T)	1.15	1.11	1.13	1.11	1.06	1.13	1.10	1.13	1.12	1.14	1.13	1.03	1.10	1.06	1.08	1.05	1.06
	(1.27)	(1.28)	(1.27)	(1.26)	(1.21)	(1.28)	(1.28)	(1.22)	(1.22)	(1.25)	(1.24)	(1.13)	(1.21)	(1.17)	(1.17)	(1.13)	(1.16)
P_1 / P_{ysc} (C)	-1.17	-1.15	-1.20	-1.16	-1.09	-1.19	-1.16	-1.12	-1.10	-1.10	-1.12	-1.02	-1.10	-1.09	-1.08	-1.06	-1.07
	(-1.32)	(-1.27)	(-1.37)	(-1.27)	(-1.22)	(-1.31)	(-1.3)	(-1.27)	(-1.2)	(-1.19)	(-1.23)	(-1.14)	(-1.17)	(-1.16)	(-1.15)	(-1.14)	(-1.14)
ε_{sc-6} (T) (%)	-	-	-	-	-	-	-	-	-	-	-	-	-	0.57	0.45	0.44	0.40
	-	-	-	-	-	-	-	-	-	-	-	-	-	(0.95)	(0.88)	(0.85)	(0.8)
ε_{sc-6} (C) (%)	-	-	-	-	-	-	-	-	-	-	-	-	-	-0.33	-0.30	-0.28	-0.30
	-	-	-	-	-	-	-	-	-	-	-	-	-	(-0.49)	(-0.44)	(-0.46)	(-0.47)
ε_{sc-5} (T) (%)	-	-	-	-	-	-	-	-	-	-	-	-	-	0.49	0.38	0.41	0.35
	-	-	-	-	-	-	-	-	-	-	-	-	-	(0.83)	(0.57)	(0.71)	(0.62)
ε_{sc-5} (C) (%)	-	-	-	-	-	-	-	-	-	-	-	-	-	-0.36	-0.32	-0.26	-0.33
	-	-	-	-	-	-	-	-	-	-	-	-	-	(-0.59)	(-0.56)	(-0.46)	(-0.55)
ε_{sc-4} (T) (%)	-	-	-	-	-	-	-	-	-	-	-	-	0.65	0.41	0.37	0.34	0.35
	-	-	-	-	-	-	-	-	-	-	-	-	(1.08)	(0.7)	(0.61)	(0.58)	(0.56)
ε_{sc-4} (C) (%)	-	-	-	-	-	-	-	-	-	-	-	-	-0.34	-0.36	-0.33	-0.31	-0.33
	-	-	-	-	-	-	-	-	-	-	-	-	(-0.63)	(-0.61)	(-0.52)	(-0.55)	(-0.58)
ε_{sc-3} (T) (%)	-	-	-	-	-	-	0.61	0.68	0.79	0.57	0.63	0.75	0.52	0.44	0.37	0.39	0.35
	-	-	-	-	-	-	(1.04)	(1.05)	(1.19)	(1.15)	(0.91)	(1.06)	(0.96)	(0.79)	(0.58)	(0.7)	(0.67)
ε_{sc-3} (C) (%)	-	-	-	-	-	-	-0.35	-0.39	-0.29	-0.39	-0.28	-0.30	-0.35	-0.33	-0.31	-0.26	-0.31
	-	-	-	-	-	-	(-0.75)	(-0.8)	(-0.6)	(-0.65)	(-0.75)	(-0.76)	(-0.61)	(-0.55)	(-0.52)	(-0.44)	(-0.48)
ε_{sc-2} (T) (%)	0.83	0.75	0.59	0.75	0.63	0.66	0.65	0.64	0.54	0.45	0.47	0.43	0.45	0.42	0.39	0.35	0.34
	(1.43)	(1.33)	(0.98)	(1.51)	(1.26)	(1.18)	(1.44)	(0.97)	(1.4)	(0.95)	(1.25)	(1.19)	(0.74)	(0.69)	(0.64)	(0.59)	(0.52)
ε_{sc-2} (C) (%)	-0.33	-0.33	-0.56	-0.33	-0.19	-0.41	-0.31	-0.41	-0.36	-0.47	-0.40	-0.48	-0.41	-0.37	-0.32	-0.32	-0.33
	(-0.51)	(-0.58)	(-1.06)	(-0.58)	(-0.38)	(-0.8)	(-0.55)	(-0.8)	(-0.59)	(-0.74)	(-0.59)	(-0.75)	(-0.74)	(-0.62)	(-0.54)	(-0.55)	(-0.66)
ε_{sc-1} (T) (%)	0.67	0.88	0.61	0.77	1.02	0.74	0.66	0.66	0.82	1.04	0.81	0.77	0.70	0.65	0.57	0.54	0.55
	(1.59)	(1.49)	(1.02)	(1.31)	(1.63)	(1.24)	(1.06)	(1.04)	(1.21)	(1.57)	(1.27)	(1.13)	(1.45)	(1.35)	(1.17)	(1.09)	(1.1)
ε_{sc-1} (C) (%)	-0.34	-0.31	-0.56	-0.35	-0.44	-0.42	-0.36	-0.39	-0.30	-0.22	-0.28	-0.29	-0.29	-0.28	-0.28	-0.21	-0.25
	(-0.64)	(-0.53)	(-1.06)	(-0.68)	(-0.8)	(-0.82)	(-0.75)	(-0.8)	(-0.59)	(-0.47)	(-0.71)	(-0.77)	(-0.45)	(-0.42)	(-0.37)	(-0.37)	(-0.38)

*84^{th} percentile results shown in parentheses.

5.6.5 Column Response

The peak column force demands, including the axial compression force and in-plane flexural bending in the first-tier segment of the RHS column (the critical column for the frame configurations selected here), are given in Table 5.4. The peak column axial force normalized to the column nominal compressive strength P_c/P_n varies between 0.22 and 0.77 for the frames studied. Overall, a descending trend was observed for the column axial force as the frame total height increased. The peak in-plane moment measured at the first-tier strut level was normalized by the weak-axis plastic moment of the column, $M_{cy\text{-}i}/M_{py}$. For the frames with Z- and ZS-bracing, the moment varied between 0.01 to $0.19M_{py}$. Negligible bending was recorded for the frames utilizing S-bracing. The moment demand decreased with an increase in the frame height but increased with an increasing number of tiers while maintaining the same frame height. The reduced moments in taller frames could potentially be associated with relatively flexible columns selected for taller frames with the same number of tiers. Increasing the number of tiers for a certain frame height often increased the number of critical tiers, thus promoting uniform distribution of the frame lateral deformation and lower flexure in the columns. The tier height ratio did not noticeably affect the column moment demand. Nearly identical moments were recorded in the tiers of the frames with Z-bracing, which suggests that the column moment can potentially be related to the adjusted brace strength when a full plastic mechanism is achieved via brace yielding in tension and compression in all the tiers. Frames having the ZS-bracing configuration experienced significantly higher in-plane moment demands in the first tier than in the upper tiers owing to a more pronounced unbalanced brace load between the first and second tiers.

The application of the 2022 design procedure to design MT-BRBFs resulted in significantly lower induced in-plane moment demands than were assumed in design. For instance, for the two-tiered

frame redesigned using the 2022 AISC 341 provisions, 2T-12-1-Z-22, the ratio of the predicted moment obtained in design to the observed median in-plane bending moment demand from the NLRHA was 3.5 (= 202 kN-m / 57 kN-m). Similarly, for the three-tiered frame, 3T-18-1-Z-22, the ratio between the predicted and observed in-plane moment demand was 3.6 (108kN-m / 30kN-m), suggesting that the 2022 AISC seismic provisions for MT-BRBF design may overestimate column in-plane flexural bending demands, potentially resulting in uneconomical designs.

5.7 Recommendations for Enhanced AISC 341 Provisions

The results obtained from the numerical parametric study confirmed that the simultaneous yielding and strain hardening of BRBs to achieve their anticipated adjusted strengths in tension and compression was unlikely in single-diagonal MT-BRBFs when a full plastic mechanism was developed. This is due the tendency for frame lateral deformation to concentrate in the critical tension tier or tiers. Referring to NLRHA results for MT-BRBFs having adjacent BRBs in opposing directions (Table 4.5), the BRB compressive strain ε_{sc} (C) remains approximately half that of the BRB tensile strain ε_{sc} (T) in adjacent tiers (the mean and standard deviation of ε_{sc}(T)/ε_{sc}(C) in adjacent tiers are 2.02 and 0.31, respectively), suggesting that compression BRBs do not achieve their full adjusted strength in compression ($\beta\omega A_{sc}F_y$) mainly due to partial development of the friction adjustment factor, β. This observation was also confirmed through full-scale experimental testing of a two-tiered BRBF with a Z-bracing configuration (Bani 2023). On the basis of the parametric study performed here and in keeping with the simplicity of the 2022 AISC 341 design provisions for multi-tiered BRBFs, the adjusted brace strength in compression used to obtain frame shear, which in turn is used to compute column in-plane flexural bending, is reduced to $\beta'\omega A_{sc}F_y$ where β' is the modified compression strength adjustment factor equal to β' = (β+1)/2. This accounts for the limited compression overstrength observed in single-diagonal, multi-tiered BRBFs

(the mean and standard deviation of P / P_{ysc} (C) when BRBs of adjacent tiers are oriented in opposing directions are 1.1 and 0.05, respectively, or 1.22 and 0.07 using the 84th percentile results). This proposed modification is expected to better represent MT-BRBF response and lead to more realistic column moment demands. In MT-BRBFs where the unbalanced brace loads applied on the columns due to variation in the adjusted brace strengths are equal to zero, a notional load equal to 0.5% of the frame shear obtained from the higher strength adjacent tier should still be used. A similar modification is proposed to adjusted brace strengths used to obtain frame shears between adjacent tiers used to check column flexural stiffness in order to limit tier drift to 2%, provided that the designer opts to use column flexural stiffness for this purpose.

The columns of the three-tiered frame example of Figure 5.4a were redesigned using the proposed adjusted compression brace strength. Figure 5.8a shows the adjusted brace forces used to compute column seismic-induced axial forces and flexural bending. As shown, the updated unbalanced brace loads, which are obtained based on the adjusted tension brace strengths (593 kN) and the adjusted modified compression brace strengths (664 kN), are equal to 27 kN on each column. These forces are imposed on each column at Tiers 1 and 2, producing in-plane flexural bending of M_{uy} = 54 kN-m, as shown in Figure 5.8b. The columns were redesigned to resist the demands induced in their first-tier segment, i.e., the most critical column segment, including the required column axial strength $P_{u,c}$ = 1537 kN and required in-plane flexural strength $M_{uy,c}$ = 54 kN-m. A W410×100 column section was required to resist the applied loads. The tier drift was then verified in the tension tiers to be less than 2% by adding up tier drift components due to roof displacement (= 80 mm) and column bending (= 34mm) as described earlier, which resulted in 1.9% in Tiers 1 and 3. The selected column section (W410×100) was 28% lighter than the one designed using the 2022 AISC 341 provisions (W460×128).

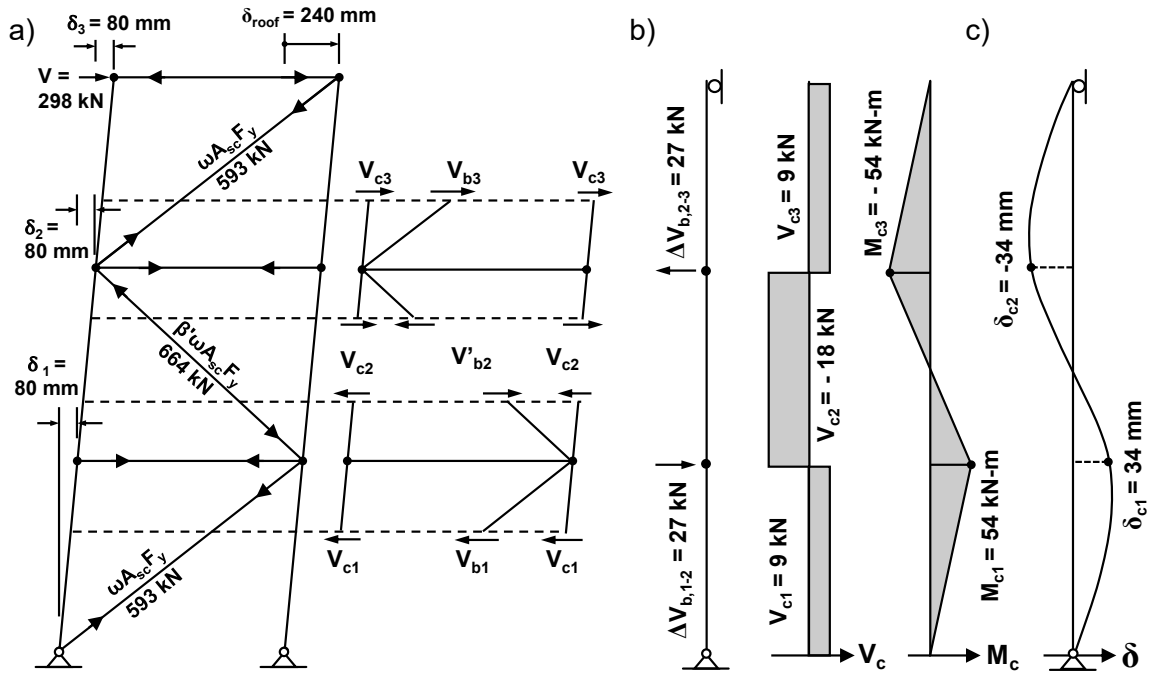

Figure 5.8: Seismic analysis of three-tiered BRBF with W410×100 columns following proposed recommendations: a) Member forces under adjusted tension brace and adjusted modified compression brace forces at positive expected storey drift; b) brace unbalanced loads, column in-plane shear and flexural bending; c) tier deformation due to column bending.

The three-tiered frame example that was redesigned using the proposed recommendations — namely, the adjusted BRB strength in compression — was analyzed under the same set of ground motion accelerations described earlier. Table 5.6 shows the median and 84th percentile (shown in parentheses) values of the seismic response parameters for this frame with the columns meeting the strength requirements and stiffness requirements (W410×100). The peak response parameters from NLRHA are also given in Table 5.6 for the same frame when its columns are designed in accordance with 2010 AISC 341 (W530×101) and 2022 AISC 341 (W460×113 when only strength requirements are considered, and W460×128 when both strength and stiffness requirements are applied). No column instability was observed for the frames designed in accordance with the 2022

AISC 341 method and the proposed design recommendations, while two column buckling cases were observed in the first-tier segment when the frame was designed per 2010 AISC 341. As shown, the peak storey drift was nearly identical in all five frames and was in good agreement with the storey drift predicted by ASCE 7 as indicated by $(\delta_{roof}/h)/\Delta$ values larger than 0.9. A slightly lower drift concentration was recorded for the 2022 AISC design (DCF = 1.20) as opposed to the frame designed using the proposed design method (DCF = 1.30) due to the stiffer W460×128 column section required in the 2022 design compared to the design as per the proposed modification here (with W410×100 columns). The tier drifts in all the frames were mainly distributed between Tiers 1 and 3 (critical tiers when the roof displacement is positive). The median values of the peak tier drift in Tier 1 are lower in the frame designed using the proposed method to meet the drift limit as compared to that designed as per 2022 AISC 341 (e.g., 1.19 vs. 1.33 in Tier 1), but the 84th percentile values are similar in both frames. The median values of tier drifts predicted in Tiers 1 and 2 using the 2022 AISC 341 method are found to be 1.2 and 1.5 times larger than the tier drifts observed using NLRHA, respectively. For the proposed method, the tier drifts predicted in Tiers 1 and 2 are 1.55 and 1.74 times larger. The overestimation in the proposed method is attributed to ground motion variability due to changes in the fundamental period of the frame and the variation of the peak storey drift direction in single-diagonal braced frame configurations. The 84th percentile values of tier drifts and predicted tier drift to the NLRHA drift values for both 2022 AISC 341 design and the frame designed as per the proposed strength adjustment factor here are nearly identical to the predicted tier drifts, confirming the adequacy of the isolated, simply-supported column approach for predicting tier drift in multi-tiered BRBFs.

The comparison of peak column in-plane moment demands between the 2022 AISC 341 strength design (W460×113 columns and M_{uy} = 108 kN-m = 0.4M_{py}) and the frame designed using the

improved method (W410×100 columns) under a reduced moment demand (M_{uy} = 54 kN-m = 0.27M_{py}) show that the moment is almost always overestimated, but with a relatively higher overestimation (3.76–4.11) for the 2022 AISC design and a relatively lower overestimation (2.14 – 2.61) for the improved design proposed here. This overestimation could be attributed to the high unbalanced brace loads assumed in design compared to observed values and the assumption that MT-BRBF columns deform as a simply-supported structure under lateral seismic loads. Furthermore, column in-plane flexural demands are well distributed and nearly equal between Tiers 1 and 2 for both frames. Comparing the frames designed solely for strength and the frames designed to satisfy both the strength and stiffness requirements, similar performance is observed in terms of distribution of lateral deformation between tiers and column in-plane bending. For instance, column in-plane bending moments in the frames designed based on proposed recommendations are only 1.1-1.2% higher than those designed following 2022 AISC 341, for strength design. Overall, the seismic response parameters given in Table 4.6 for both the 2022 and improved design proposed here confirm that the proposed improvement to MT-BRBF design manifests similar seismic performance as the 2022 AISC 341 method while resulting in a more economical frame design with reduced steel tonnage.

Table 5.6: Statistics of peak response parameters for 3T-18-1-Z from NLRHA.

Parameter	2010 AISC 341	2022 AISC 341 (Strength Only)	2022 AISC 341 (Strength & Stiffness)	Proposed Method (Strength & Stiffness)
	W530×101 Columns	W460×113 Columns	W460×128 Columns	W410×100 Columns
δ_{roof} / h (%)	1.27 (1.69)*	1.31 (1.64)	1.31 (1.61)	1.31 (1.73)
$(\delta_{roof}/h) / \Delta$	0.91 (1.21)	0.94 (1.17)	0.98 (1.21)	0.92 (1.24)
δ_{ic} / h_i (%)	1.72 (2.74)	1.56 (2.25)	1.55 (2.13)	1.60 (2.44)
DCF	1.41 (1.63)	1.20 (1.45)	1.20 (1.42)	1.30 (1.58)
δ_3 / h_3 (%)	1.33 (1.81)	1.27 (1.72)	1.36 (1.65)	1.30 (1.88)
$\delta_{3\text{-Predicted}} / \delta_{3\text{-NLRHA}}$	- -	- -	0.97 (0.80)	1.02 (0.71)
δ_2 / h_2 (%)	1.12 (2.48)	1.07 (1.80)	1.12 (1.79)	1.09 (1.77)
$\delta_{2\text{-Predicted}} / \delta_{2\text{-NLRHA}}$	- -	- -	1.50 (0.94)	1.74 (1.07)
δ_1 / h_1 (%)	1.22 (1.78)	1.23 (1.77)	1.33 (1.68)	1.22 (1.81)
$\delta_{1\text{-Predicted}} / \delta_{1\text{-NLRHA}}$	- -	- -	1.20 (1.00)	1.55 (1.05)
$M_{cy\text{-}2} / M_{py}$	0.12 (0.22)	0.11 (0.15)	0.10 (0.14)	0.09 (0.16)
$M_{cy\text{-}2\text{-Predicted}} / M_{py\text{-}2\text{-NLRHA}}$	- -	4.11 (3.01)	3.94 (2.81)	2.61 (1.48)
$M_{cy\text{-}1} / M_{py}$	0.14 (0.26)	0.12 (0.20)	0.11 (0.19)	0.11 (0.18)
$M_{cy\text{-}1\text{-Predicted}} / M_{py\text{-}1\text{-NLRHA}}$	- -	3.76 (2.25)	3.58 (2.07)	2.14 (1.31)
P_r / P_{ny}	0.70 (0.75)	0.38 (0.41)	0.34 (0.37)	0.46 (0.50)
No. of Column Instability	2	0	0	0

5.8 Summary and Conclusions

This paper aimed to assess the seismic response of steel multi-tiered BRBFs designed in accordance with the 2010 and 2022 AISC Seismic Provisions, evaluate the MT-BRBF design provisions implicit in 2022 AISC 341 and propose improvements to these provisions using a numerical parametric study. As part of the parametric study, 16 frames forming part of a single-storey steel building, having different bracing configurations, heights, number of tiers, and relative tier heights, were studied using nonlinear response history analyses. Modifications proposed to enhance the

seismic design of multi-tiered BRBFs in the framework of 2022 AISC Seismic Provisions were demonstrated through a three-tiered BRBF. The proposed improvements were validated using nonlinear response history analyses. The primary findings of this study are as follows:

- In MT-BRBFs with BRBs orientated in opposing directions that are designed in accordance with the 2010 AISC Seismic Provisions, inelastic BRB deformations tend to concentrate in the tier(s) undergoing tensile yielding, i.e., the critical tier(s), which have lower post-yield stiffness and thus exhibit a lower storey shear resistance (on average 1.7% in the critical tier). When BRBs are oriented in the same direction, the lateral frame deformation is almost evenly distributed between tiers.
- In MT-BRBFs with BRBs orientated in opposing directions, asymmetric isotropic and kinematic hardening of BRBs in tension and in compression translates to a slightly higher post-yield stiffness when the BRB undergoes compression, which creates unequal BRB forces between adjacent tension and compression tiers. This response requires columns to contribute to storey shear resistance as their share of lateral stiffness increases while BRBs unevenly lose their initial elastic stiffness. The difference of the storey shear resistances provided by BRBs between any adjacent tiers is compensated by columns through in-plane shear and flexural bending, which combined with a large axial compression force led to column buckling in the first-tier segment in seven cases in frames 2T-8-1-Z, 2T-12-1-Z, 2T-12-1-Z-Y and 3T-18-1-Z.
- Multi-tiered BRBFs designed in accordance with the 2022 AISC Seismic Provisions exhibited an improved seismic response: a more uniform distribution of frame lateral deformation was achieved, and no column instability was observed. However, the 2022

AISC 341 design requirements may overestimate column in-plane flexural demands (e.g., 3.58–3.94 times the observed in-plane bending moment demand for 3T-18-1-Z-22).

- The results of the dynamic analyses confirmed that the simultaneous yielding and strain hardening of BRBs to achieve their anticipated adjusted strengths in tension and compression is unlikely in single-diagonal MT-BRBFs when a full plastic mechanism is developed, because frame lateral deformation tends to concentrate in the critical tension tiers. The BRB compressive strain remains approximately half that of the BRB tensile strain in adjacent tiers (mean and standard deviation of $\varepsilon_{sc}(T)/\varepsilon_{sc}(C)$ are 2.02 and 0.31, respectively) because of the partial development of the strength generated by friction in compression BRBs.
- The 2022 AISC 341 provisions for the design of steel MT-BRBFs was improved by introducing a modified BRB compression strength adjustment factor equal to $\beta' = (\beta+1)/2$ used to calculate column in-plane flexural demands. This improvement results in a more realistic prediction of column seismic demands (2.14 versus 3.76 times the observed moment demand in Tier 1) while achieving an economical column design (W410×100 versus W460×128). No noticeable change was observed in the prediction of tier deformation. The proposed modifications were demonstrated through a three-tiered BRBF example and validated using nonlinear response history analyses.

The current study focused on the in-plane response of steel MT-BRBFs. Future studies should also consider the effect of out-of-plane demands on MT-BRBF columns, specifically out-of-plane demands that may be imposed on the columns by BRB gusset plate connections. The proposed design recommendations should be further refined in the future through examining other BRB configurations not considered here. As an alternative to the current AISC 341 design procedure for

MT-BRBFs, future studies should examine the potential for adapting a displacement-based approach within the framework of the AISC Seismic Provisions by imposing inelastic frame lateral deformation to obtain column seismic demands.

CHAPTER 6 CONCLUSIONS AND RECOMMENDATIONS

6.1 Summary

Steel Multi-Tiered Buckling-Restrained Braced Frames (MT-BRBFs) consisting of multiple Buckling-Restrained Brace (BRB) panels vertically stacked along a storey height are commonly used in tall single-storey buildings or tall stories of multi-storey buildings in moderate-to-high seismic regions of Canada and the United States. When single-diagonal multi-tiered BRBFs are subjected to lateral seismic loads, frame inelastic deformation may distribute unevenly between tiers; tiers with tension-acting BRBs are expected to experience higher lateral deformation compared to the tiers whose BRBs yield in compression due to lower post-yield stiffness of BRBs when yielding in tension. This response can impose flexural bending in the columns, which in the presence of a large axial compression force may compromise the stability of the column. Furthermore, excessive inelastic deformation induced in tension-acting BRBs may cause strains in excess of cumulative plastic capacity of steel BRBs. . However, these concerns had not been verified yet. In particular, there had been no experimental evidence to examine the seismic response of steel multi-tiered BRBF.

The 2019 edition of the Canadian steel design standard, CSA S16-19, does not address the design of MT-BRBFs, leaving engineers without unified design guidelines, which may lead to unsafe or uneconomical design solutions. In the U.S., 2022 Seismic Provisions for Structural Steel Buildings, AISC 341-22, specifies design requirements for MT-BRBFs. These requirements are as follows: 1) intermediate horizontal struts are needed between BRB panels; 2) the columns shall be designed under an axial compression force arising from BRB capacity forces plus an in-plane bending moment due to unbalanced brace loads due to the difference between frame shears from adjusted

brace strengths between adjacent tiers; 3) the columns shall be torsionally braced at every strut-to-column connection; and 4) the lateral deformation of the frame in each tier shall be less than 2% of the tier height when the frame reaches the anticipated design storey drift. However, very limited supporting research was available to verify the adequacy of these design requirements and propose improvements if needed. Therefore, the main objectives of this M.Sc. research project were to comprehend the seismic performance of steel multi-tiered BRBFs using numerical methods and full-scale experimental testing and propose design guidelines in the framework of the Canadian and U.S. standards to improve their seismic response.

The first phase of the project consisted of full-scale experimental testing of a two-tiered BRBF specimen to evaluate the seismic response of such frames and verify the concerns raised. The frame was designed according to AISC 341-10 with no special design requirements and tested using a loading protocol consisting of roof displacement histories obtained from nonlinear response history analyses under a far-field and a near-field ground motion records plus a monotonic push to create storey drift of 4.5%. In the second phase of this project, two stand-alone numerical parametric studies were performed to numerically evaluate the seismic response of a wide range of multi-tiered BRBFs by varying the frame total height, number of tiers, tier height ratio, and BRB orientations. The first set of frames were part of a single-storey building located in Victoria, BC and designed following the Canadian steel design standard, while the second set of multi-tiered BRBFs were designed as the lateral load-resisting system of a single-storey building in Seattle, WA as per AISC Seismic Provisions with and without special seismic provisions for MT-BRBFs following U.S. design practice. On the basis of frame test and numerical parametric studies, an improved design strategy by refining the BRB compression strength adjustment factor was proposed in the framework of AISC 341for U.S. design practice. For the Canadian design practice,

two analysis and design methods– a detailed approach based on the mechanics principles and an alternative (displacement-based) technique with the aid of a structural analysis program – were proposed in the framework of the Canadian steel design standard. The methods were validated using nonlinear response history analyses.

6.2 Conclusions

- A corroborated fibre-based numerical model of multi-tiered BRBFs was developed in the *OpenSees* program and used to conduct numerical parametric studies. The model can accurately capture the inelastic response of the BRBs and columns.
- The results of experimental testing and numerical parametric studies confirmed that in single-diagonal MT-BRBFs (not specifically designed for multi-tier response) with BRBs orientated in opposing directions, frame inelastic deformations tend to concentrate in the tier(s) undergoing tensile yielding as the frame approaches a full plastic mechanism, because tension-acting BRBs exhibit relatively lower post-yield stiffnesses and storey shear resistances than the tier(s) where BRB(s) yield in compression yielding. Non-uniform distribution of frame lateral deformations induces significant in-plane flexural bending demands on the columns.
- The key findings from experimental testing of the two-tiered BRBF specimen are summarized below:
- No column instability occurred during the test, but column yielding was observed at the tier level of the columns at the peak storey drift 3.5% during the displacement histories. Column in-plane flexural demand reached $0.4M_{py}$ at this point.

- At the end of Phase III of loading protocol, the peak storey drift reached 4.5% resulting in an in-plane moment of $0.5M_{py}$ on the columns, which exacerbated flexural yielding in the columns.
- In agreement with the results from the numerical studies, frame inelastic deformation tends to concentrate in the tension tier during the test. For example, the tensile strain of the core in Tier 1 BRB at the peak storey drift under the ground motion-generated displacement histories was 2.8%, which is more than two times the compressive strain of the core in Tier 2 BRB (-1.25%) at the same drift level.
- The BRBs exhibited overall acceptable performance in terms of cumulative ductility capacity (sum of axial deformations in the core) exceeding 200 times the yield displacement, which meets the AISC 341 prequalification testing requirements for steel BBRs.
- The test results also showed that the base of the columns created more like a fixed base condition for column flexure in-plane as it was deformed in double curvature under large moment demands throughout the test.
- Rotational fixity provided by column base connections improved the stability of the bottom tier column and likely prevented potential column instability.
- A computer-aided displacement-based analysis technique was proposed using the test results to analyze MT-BRBF frames for in-plane response, namely column in-plane bending demands and tier deformations.
- The results of the test confirmed the concerns associated with multi-tiered BRBF seismic performance, non-uniform distribution of frame inelastic deformation, significant in-plane

bending demands induced in the columns, and the need for an enhanced design method to improve frame response.

- The numerical studies demonstrated that large in-plane bending moment in the presence of a high axial compression load in multi-tiered BRBF columns resulted in plastic hinge formation in the columns, and in several cases (seven buckling cases in four frames designed to the AISC provisions) column instability, which involved flexural buckling in the plane of the frame. No column instability was observed for the frames designed to the Canadian provisions.
- Column in-plane flexural demands were more pronounced in shorter frames and decreased with increasing frame height. Frames with BRBs oriented in opposing directions in the first two adjacent tiers and in the same direction in the other tiers (ZS-bracing configuration) experienced the most severe concentration of frame lateral deformation and therefore the largest in-plane bending in their columns. For example, column in-plane bending in a three-tiered BRBF with ZS-bracing (3T-18-1-ZS) reached on average 19% of the plastic moment capacity of the column in the frames designed to the Canadian design standard and a median value of 13% (or 84th percentile value of 20%) of the plastic moment capacity in the AISC frames not specifically designed for multi-tier response.
- The results of the numerical analyses and frame test confirmed that the simultaneous yielding and strain hardening of BRBs to achieve their anticipated adjusted strengths in tension and compression is unlikely in single-diagonal MT-BRBFs when a full plastic mechanism is developed because frame lateral deformation tends to concentrate in the critical tension tiers. For single-diagonal BRBFs with opposing BRB orientations, the

compressive strain of the BRB in compression tiers remains approximately half that of BRB tensile strain in adjacent tension tiers.

- A more uniform lateral deformation response was observed in frames where BRBs are oriented in the same direction (S-bracing configuration) resulting in negligible in-plane bending in the columns.
- Numerical studies showed that the empirical storey drifts computed in accordance with 2015 NBC and ASCE 7-10/16 tend to overestimate the storey drift obtained from NLRHA for frames taller than 18 m.
- Multi-tiered BRBFs designed in accordance with 2022 AISC Seismic Provisions exhibited an improved seismic response, namely a more uniform distribution of frame lateral deformation was achieved, and no column instability was observed. However, the 2022 AISC 341 design requirements may overestimate column in-plane flexural demands (e.g., 3.58–3.94 times the observed in-plane flexural bending demand for 3T-18-1-Z-22) leading to potentially uneconomical column designs.
- For the Canadian design practice, two seismic analysis and design methods, a detailed approach and an alternative (displacement-based) method were developed. The two methods are summarized below:
- In the detailed method, column flexural bending is determined as a function of the modified unbalanced BRB shear resistances in adjacent tiers. The frame when a full plastic mechanism is developed is broken down in multiple substructures bounded by on the location of column inflection points located at the tier mid-height. Each substructure is then solved under BRB shear resistances to determine column shear and in-plane moments. The number of substructures is determined based on the location of tension and compression

BRBs in each loading direction. The probable BRB resistance in compression should be calculated using a modified friction adjustment factor equal to $\beta' = (\beta+1) / 2$ to account for the lower deformation demands induced in compression-acting BRBs.

- In the alternative method, column flexural bending is obtained by applying the inelastic frame deformation only to the tiers with BRBs acting in tension. This method is best suited for design with the aid of a structural analysis program.
- BRB strain, which depends on tier drift, should be limited to that corresponding to two times the design storey drift.
- In the detailed method, relative tier deformation in the tiers with BRBs yielding in tension is computed by adding the lateral deformation due to the design storey drift assuming a linear variation over the frame height to the contribution from column bending obtained by isolating a simply-supported column spanning between adjacent (tension and compression) tiers that is subjected to an in-plane transverse load at the strut level within the isolated column with an amplitude of the modified BRB unbalanced load due to the difference between storey shears in the respective adjacent tiers.
- In the displacement-based method, tier drift in the tension tiers is obtained by adding the tier drift due to the elastic storey drift assuming a linear variation over the frame height to the inelastic tier drift obtained by distributing inelastic frame deformation between tension tiers in proportion to height.
- Both loading directions should be examined, and the most critical demands should be used to design the frame.
- The proposed design method in the framework of AISC 341 involves a modified BRB compression strength adjustment factor equal to $\beta' = (\beta+1) / 2$, which should be used to

compute unbalanced brace loads. The same AISC 341 analysis technique involving a simply-supported column isolated from the frame extending between the out-of-plane brace points should be used to determine column moments and tier deformation udner the brace unbalanced loads computed using the proposed modification to the adjusted compression brace strength.

- In-plane flexural stiffness of the BRBF columns was used to control tier drift and in turn BRB strains in the critical tier(s) in the proposed design methods.
- The results of numerical validations indicate that the proposed design methods in Canada and the improved design method in the U.S. result in more realistic estimation of column seismic demands and tier deformations while achieving an economical column design.

6.3 Limitations

The key limitations of this M.Sc. thesis are summarized as follows:

- MT-BRBFs considered in this study were limited to those utilizing single-diagonal bracing configurations with wide-flange column profiles. MT-BRBFs with two BRBs in each tier, e.g., chevron, are deemed to experience less pronounced multi-tier response due to nearly identical tier shear resistance between adjacent tiers, which would significantly reduce the in-plane demands on the BRBF columns.
- Only two-, three-, four- and six-tiered frames part of single-storey buildings were studied.
- Nonlinear response history analyses performed using the numerical model of the BRBF in Chapters 4 and 5 only consider ground motions with positive scaling factors as obtained from ground motion scaling. Both positive and negative scaling factors considered in the dynamic analyses of Chapter 3 confirmed that overall the frame response parameters are not affected noticeably by the sign of the scaling factor.

- The numerical model constructed for the purpose of parametric studies does not explicitly simulate stiffness and strength of brace connections, low cycle fatigue fracture of BRBs, and assumes the column bases are fully pinned.
- Full-scale experimental testing was only conducted for a single two-tiered BRBF utilizing a single-diagonal Z-bracing configuration with equal tier heights part of a single-storey building under displacement histories generated using the nonlinear response history analysis under two ground motion accelerations corresponding to far-field, and near-field earthquake events applied sequentially.
- This research study only studied BRBFs located in high-seismic regions along the west coast of Canada and the U.S.

6.4 Recommendations for Future Studies

Based on the findings of this study, the following recommendations are made for future studies:

- Future studies should consider other bracing configurations possible in multi-tiered BRBFs including, two-bay X, V- and inverted V-bracing and potentially refine the proposed design guidelines.
- The seismic response of multi-tiered BRBFs in multi-storey buildings should also be explored.
- The effect of out-of-plane demands arising from BRB connections on the stability of multi-tiered BRBF columns should be estimated and accounted for in design.
- A more detailed numerical model, considering the potential out-of-plane deformation of BRB connections, should be developed and used to examine the stability response of multi-tiered BRBF columns under in-plane and potential out-of-plane seismic demands.

- The requirement of torsional bracing of the column at the strut-to-column connection level as currently required by AISC 341 should be assessed and relaxed if possible.
- The effect of the flexibility of column base connection on the stability of columns of light BRBF structures, similar to the two-tiered BRBF specimen tested in this study, should be evaluated further using detailed finite element modelling and additional experimental testing. The results should be used to improve seismic design of BRBFs accounting for the flexibility of column base conditions.
- Although more relaxed seismic design requirements are expected in moderate seismic zones, e.g., in eastern Canada and U.S., further calibration of the proposed design guidelines for BRBFs located in moderate seismic regions are necessary in future studies to account for the effect of high-frequency short-duration earthquakes anticipated in those regions.
- The response modification coefficient, R, given in the U.S. ASCE 7 and ductility- and overstrength-related force modification factors, R_d and R_o, specified in the NBC of Canada for special and ductile BRBF systems should be evaluated for BRBFs with multi-tiered configuration using the methodology proposed by FEMA P695 (FEMA 2009) taking into account the respective design parameters and seismic hazard in each country. The response modification coefficient, and ductility- and overstrength-related force modification factors may require adjustments for special and ductile multi-tiered BRBFs in the U.S. and Canada, respectively.
- The influence of the rotational rigidity of the strut-to-column connection on the stability response of multi-tiered BRBF columns should be studied using the detailed finite element analysis method to verify whether or not the additional in-plane bending imposed by semi-

rigid strut-to-column connections due to frame action improve the stability response of such columns.

- Future studies should examine the seismic performance of multi-tiered -BRBFs used in mill buildings with crane supporting structures and those utilized to retrofit existing buildings.

REFERENCES

Aguirre, C., and Palma, I. 2009. Shear lugs for column bases. Proceeding of the 6th International Conference on Behaviour of Steel Structures in Seismic Areas. pp. 247–253.

American Concrete Institute. 2019. ACI 318-19, Building Code Requirements for Structural Concrete. Farmington Hills, MI.

American Institute of Steel Construction. 2005. ANSI/AISC 341-05, Seismic Provisions for Structural Steel Buildings. Chicago, IL.

American Institute of Steel Construction. 2010a. ANSI/AISC 341-10, Seismic Provisions for Structural Steel Buildings. Chicago, IL.

American Institute of Steel Construction. 2010b. ANSI/AISC 360-10, Specifications for Structural Steel Buildings. Chicago, IL.

American Institute of Steel Construction. 2016. ANSI/AISC 341-16, Seismic Provisions for Structural Steel Buildings. Chicago, IL.

American Institute of Steel Construction. 2022. ANSI/AISC 341-22, Seismic Provisions for Structural Steel Buildings. Chicago, IL.

American Institute of Steel Construction. 2017. Steel Construction Manual, 15th ed. Chicago, IL

American Institute of Steel Construction. 2018. Seismic design Manual, 3rd ed. Chicago, IL.

American Society of Civil Engineers. 2010. ASCE/SEI 7-10, Minimum Design Loads for Buildings and Other Structures. Reston, VI.

American Society of Civil Engineers. 2016. ASCE/SEI 7-16, Minimum Design Loads for Buildings and Other Structures. Reston, VI.

American Welding Society. 2016. D1.8/D1.8M:2016, Structural Welding Code - Seismic Supplement. Miami, FL.

Ancheta, T.D., Darragh, R.B., Stewart, J.P., Seyhan, E., Silva, W.J., Brian, A., Chiou, S.J., Wooddell, K.E., Graves, R.W., Kottke, A.R., Boore, D.M., Kishida, T., and Donahue, J.L. 2013. PEER NGA-West2 Database. Berkeley, California.

Ashrafi, A., and Imanpour, A. 2021. Seismic response of steel multi-tiered eccentrically braced frames. Journal of Constructional Steel Research, 181. Elsevier Ltd.

ASTM International. 2008. A36/A36M-08, Standard Specification for Carbon Structural Steel. West Conshohocken, PA.

ASTM International. 2015. A992/A992M-11, Standard Specification for Structural Steel Shapes. West Conshohocken, PA.

ASTM International. 2017a. A572/A572M-12, Standard Specification for High-Strength Low-Alloy Columbium-Vanadium Structural Steel. West Conshohocken, PA.

ASTM International. 2017b. A490-12, Standard Specification for Structural Bolts, Alloy Steel, Heat Treated, 150 ksi Minimum Tensile Strength. West Conshohocken, PA.

ASTM International. 2017c. A193-90a, Standard Specification for Alloy-Steel and Stainless Steel Bolting Materials for High-Temperature Service. West Conshohocken, PA.

ASTM International. 2022. E8/E8M-22, Standard Test Methods for Tension Testing of Metallic Materials. West Conshohocken, PA.

Auger, K., Minouei, Y.B., Elkady, A., and Imanpour, A. 2016. Multi-directional structural component hybrid testing system for the assessment of the seismic response of steel I-shaped columns. Proceedings of the 11th Pacific Structural Steel Conference.

Baker, J.W. 2007. Quantitative classification of near-fault ground motions using wavelet analysis. Bulletin of the Seismological Society of America, 97(5): 1486–1501.

Bani, M. 2023. Seismic performance and design of steel multi-tiered buckling-restrained braced frames. M.Sc. Thesis. University of Alberta, Edmonton, AB.

Bani, M., and Imanpour, A. 2022. Seismic performance of steel multi-tiered buckling-restrained braced frames in Canada. Proceedings of the 10th International Conference on Behaviour of Steel Structures in Seismic Areas. pp. 544–551.

Bani, M., and Imanpour, A. 2023. Dynamic response of multi-tiered buckling-restrained braced frames in high seismic regions of Canada. Proceedings of the 2022 CSCE Annual Conference.

Benzoni, G., and Innamorato, D. 2007. Star Seismic brace tests, Report No. SRMD-2007/05-Rev.2, Dept. of Structural Engineering, University of California, San Diego,. La Jolla, CA.

Black, C.J., Asce, M., Makris, N., and Aiken, I.D. 2004. Component testing, seismic evaluation, and characterization of Buckling-Restrained Braces. Technical Report PEER 2002/08, Pacific Earthquake Engineering Research Center, University of California, Berkeley, CA.

Bruneau, M., Uang, C.-M., and Sabelli, R. 2011. Ductile Design of Steel Structures. In 2nd edition. McGraw-Hill Professional, New York, NY.

Canadian Standards Association. 2009. CSA S16-09, Design of Steel Structures. Mississauga, ON.

Canadian Standards Association. 2019. CSA S16-19, Design of Steel Structures. Mississauga, ON.

Cano, P., and Imanpour, A. 2020. Evaluation of AISC seismic design methods for steel multi-tiered special concentrically braced frames. Engineering Journal, American Institute of Steel Construction, 57(3): 193–214.

Cano, P., Imanpour, A., and Tremblay, R. 2023. Seismic performance of brace middle-connection in steel concentrically braced frames with x-bracing. Proceedings of Eurosteel 2023, Amsterdam, Netherlands.

Clark, P., Aiken, I., Ko, E., Kasai, K., and Kimura, I. 1999. Design procedures for buildings incorporating hysteretic damping devices. Proceedings of the 68th Annual Convention, Santa Barbara, California Structural Engineers Association of California.

Computers and Structures, Inc. (CSI). 2018. SAP2000 V.21.0.0, Structural Analysis Program. Berkeley, CA.

Dalal, S.T. 1969. Some non-conventional cases of column design. Engineering Journal, American Institute of Steel Construction.

Dehghani, M. 2016. Seismic design and qualification of all-steel buckling-restrained braced frames for Canadian applications. Ph.D Thesis. Universite de Montreal, Montreal.

Dehghani, M., and Tremblay, R. 2017. Full-scale experimental assessment of steel-encased buckling restrained braces. Journal of Earthquake Engineering and Structural Dynamics, 47(1): 105-129.

Dehghani, M., Tremblay, R., and Leclerc, M. 2017. Fatigue failure of 350WT steel under large-strain seismic loading at room and subfreezing temperatures. Construction and Building Materials, 145(1): 602–618.

Fahnestock, L.A., Sause, R., and Ricles, J.M. 2007. Seismic response and performance of buckling-restrained braced frames. Journal of Structural Engineering, 133(9): 1195–1204.

Federal Emergency Management Agency. 2009. FEMA P695, Quantification of Building Seismic Performance Factors." Applied Technology Council. Redwood City, CA.

Filippou, F.C., Popov, E.P., and Bertero, V. V. 1983. Effects of bond deterioration on hysteretic behaviourof reinforced concrete joints (UCB/EERC-83/19). Berkeley, CA.

Galambos, T. V., and Ketter, R.L. 1958. Columns under combined bending and thrust. Bethlehem, Pennsylvania.

Helwig, T.A., and Yura, J.A. 1999. Torsional bracing of columns. Journal of Structural Engineering, 125(5): 547–555.

Imanpour, A., Auger, K., and Tremblay, R. 2016a. Seismic design and performance of multi-tiered steel braced frames including the contribution from gravity columns under in-plane seismic demand. Advances in Engineering Software, 101(1): 106–122.

Imanpour, A., and Tremblay, R. 2016. Seismic design and response of steel multi-tiered concentrically braced frames in Canada. Canadian Journal of Civil Engineering, 43(10): 908–919.

Imanpour, A., and Tremblay, R. 2017. Analysis methods for the design of special concentrically braced frames with three or more tiers for in-plane seismic demand. Journal of Structural Engineering, 143(4).

Imanpour, A., Tremblay, R., Davaran, A., Stoakes, C., and Fahnestock, L.A. 2016b. Seismic performance assessment of multitiered steel concentrically braced frames designed in accordance with the 2010 AISC Seismic Provisions. Journal of Structural Engineering, 142(12): 04016135.

Imanpour, A., Tremblay, R., Fahnestock, L.A., and Stoakes, C. 2016c. Analysis and design of two-tiered steel braced frames under in-plane seismic demand. Journal of Structural Engineering, 142(11): 04016115.

Imanpour, A., Tremblay, R., Leclerc, M., Siguier, R., Toutant, G., Balazadeh Minouei, Y., and You, S. 2022. Development and application of multi-axis hybrid simulation for seismic stability of steel braced frames. Engineering Structures, 252.

Iwata, M., and Murai, M. 2006. Buckling-restrained brace using steel mortar planks; performance evaluation as a hysteretic damper. Earthquake Engineering and Structural Dynamics, 35(14): 1807–1826.

Kim, J., and Choi, H. 2004. Behaviour and design of structures with buckling-restrained braces. Engineering Structures, 26(6): 693–706.

Lamarche, C.P., and Tremblay, R. 2011. Seismically induced cyclic buckling of steel columns including residual-stress and strain-rate effects. Journal of Constructional Steel Research, 67(9): 1401–1410.

Li, C.-H., Vidmar, Z., Saxey, B., Reynolds, M., and Uang, C.-M. 2022. A procedure for assessing low-cycle fatigue life of buckling-restrained braces. Journal of Structural Engineering, 148(2). American Society of Civil Engineers (ASCE).

Mazzoni, S., Kishida, T., Contreras, V., Ahdi, S.K., Kwak, D.Y., Bozorgnia, Y., and Stewart, J.P. 2021. NGA-Sub Flatfile: R211022. Dataset.

Mckenna, F., Scott, M.H., and Fenves, G.L. 2010. Nonlinear finite-element analysis software architecture using object composition. Journal of Computing in Civil Engineering, 24(1): 95–107.

Merritt, S., Uang, C.M., and Benzoni, G. 2003a. Subassemblage testing of Star Seismic buckling-restrained braces. La Jolla, CA.

Merritt, S., Uang, C.M., and Benzoni, G. 2003b. Subassemblage testing of CoreBrace buckling-restrained braces. La Jolla, CA.

National Research Council of Canada. 2015a. National Building Code of Canada 2015. Ottawa, ON.

National Research Council of Canada. 2015b. User's Guide – NBC 2015 Structural Commentaries (Part 4 of Division B).

Newell, J., and Uang, C.M. 2006. Cyclic behaviour of steel columns with combined high axial load and drift demand. La Jolla, CA.

Palmer, K.D., Christopulos, A.S., Lehman, D.E., and Roeder, C.W. 2014. Experimental evaluation of cyclically loaded, large-scale, planar and 3-d buckling-restrained braced frames. Journal of Constructional Steel Research, 101: 415–425.

Sabelli, R., Mahin, S., and Chang, C. 2003. Seismic demands on steel braced frame buildings with buckling-restrained braces. Engineering Structures, 25(5): 655–666.

Sabelli, R., and Saxey, B. 2021. Design for local member shear at brace and diagonal-member connections: full-height and chevron gussets. AISC Engineer Journal, 58(1): 45–78.

Sandhu, B.S. 1972. Effective length of columns with intermediate axial load. AISC Engineering Journal, 9(1): 154–156.

Saxey, B. 2022. Personal communication. CoreBrace, West Jordan, UT

Schmidt, B.J., and Bartlett, F.M. 2002. Review of resistance factor for steel: Data collection.

Steven, K., Pedro, A., and Samuel, S. 2012. Earthquake Ground Motion Selection (WA-RD 791.1). Seattle, WA.

Stoakes, C.D., and Fahnestock, L.A. 2016. Strong-axis stability of wide flange steel columns in the presence of weak-axis flexure. Journal of Structural Engineering, 142(5). American Society of Civil Engineers (ASCE).

Sun, M., Fan, F., Sun, B., and Zhi, X. 2016. Study on the effect of ground motion direction on the response of engineering structure. Earthquake Engineering and Engineering Vibration, 15(4): 649–656.

Takeuchi, T., Ozaki, H., Matsui, R., and Sutcu, F. 2014. Out-of-plane stability of buckling-restrained braces including moment transfer capacity. Earthquake Engineering and Structural Dynamics, 43(6): 851–869.

Tremblay, R. 2002. Inelastic seismic response of steel bracing members. In Journal of Constructional Steel Research.

Tremblay, R., Bolduc, P., Neville, R., and DeVall, R. 2006. Seismic testing and performance of buckling-restrained bracing systems. Canadian Journal of Civil Engineering, 33(2): 183–198.

Tremblay, R., Degrange, G., and Blouin, J. 1999. Seismic rehabilitation of a four-storey building with a stiffened bracing system. Proceedings of the 8th Canadian Conference on Earthquake Engineering. pp. 549–554.

Tsai, K.C., and Hsiao, P.C. 2008. Pseudo-dynamic test of a full-scale CFT/BRB frame - Part II: Seismic performance of buckling-restrained braces and connections. Earthquake Engineering and Structural Dynamics, 37(7): 1099–1115.

Uang, C.-M., Nakashima, M., and Tsai, K.-C. 2004. Research and application of buckling-restrained braced frames. Journal of Steel Structures, 4: 301–313.

Uriz, P., and Mahin, S.A. 2008. Toward earthquake-resistant design of concentrically braced steel-frame structures. Berkeley, CA.

U.S. Geological Survey. 2023. Seismic Hazard Model, Maps, and Site-Specific Data.

Wada, A., Connor, J., Kawai, H., Iwata, M., and Watanabe, A. 1992. Damage tolerant structures. Proceedings of the 5th U.S.-Japan Workshop on the Improvement of Structural Design and Construction Practices. pp. 27–39.

Wada, A., and Takeuchi, T. 2017. Buckling-restrained braces and applications. Japan Society of Seismic Isolation.

Watanabe, A., Hitomi, Y., Saeki, E., Wada, A., and Fujimoto, M. 1988. Properties of brace encased in buckling-restraining concrete and steel tube. Proceedings of the 9th World Conference on Earthquake Engineering. pp. 719–724.

Xie, Q. 2005. State of the art of buckling-restrained braces in Asia. Journal of Constructional Steel Research, 61(6): 727–748.

Zaboli, B., Clifton, G.C., and Cowie, K. 2018. BRBF and CBF gusset plates: out-of-plane stability design using a simplified Notional Load Yield Line (NLYL) method. Journal of the Structural Engineering Society of New Zealand, 31(1): 64–76.

Ziemian, R.D. 2010. Guide to stability design criteria for metal structures. In 6th ed.

Zsarnóczay, A. 2013. Experimental and Numerical Investigation of Buckling Restrained Braced Frames for Eurocode Conform Design Procedure Development. Ph.D. Thesis. Budapest University of Technology and Economics.

APPENDIX A SEISMIC PERFORMANCE OF STEEL MULTI-TIERED BUCKLING-RESTRAINED BRACED FRAMES IN CANADA

Abstract: This paper examines the seismic response of steel Multi-Tiered Buckling-Restrained Braced Frames (MT-BRBFs). A two-tiered BRBF part of a tall single-story building is designed per the current Canadian steel design standard seismic provisions. A nonlinear numerical model of the frame is developed, followed by nonlinear static and dynamic analyses to assess its global and local response, including tier drifts, Buckling-Restrained Brace (BRB) forces, and column demands. The results obtained from the analyses indicate that the non-uniform drift response due to the difference between the BRB's strength in com-pression and tension imposes in-plane bending demands on the columns, which in combination with axial compression forces could result in column instability and should be considered in the design of the MT-BRBF columns.

A.1 Introduction

Steel Multi-Tiered Buckling-Restrained Braced Frames (MT-BRBFs) are among the most efficient seismic force-resisting systems used in buildings with tall story heights such as sports facilities, airplane hangars, and industrial buildings. In MT-BRBFs, multiple bracing panels consisting of Buckling-Restrained Braces (BRBs) and horizontal intermediate struts are vertically stacked along the height of the frame be-tween the ground and roof levels. The vertical bracing panels act in series and resist lateral loads as a vertical truss system. An example of such frames is shown in Figure A.1. This framing configuration is often used when employing a single BRB extending the full height of the frame is neither feasible nor economical. The choice of using multiple tiers of BRBs offers several advantages; mainly, due to their enhanced ductility capacity, required BRB core sizes can be reduced significantly, leading to relatively lower capacity-induced design forces

on the connections, beams, and columns. Furthermore, BRBs are permitted by North American design standards to be used in single diagonal configurations, which results in a fewer number of BRBs and connections, making MT-BRBFs highly favorable lateral load-resisting systems.

Figure A.1: Five-tiered BRBFs used in the Seattle Seahawks indoor practice facility in Renton WA (Courtesy of Michael Lawrie).

MT-BRBFs are often placed along the exterior walls of a building. The columns are typically I-shaped sections oriented such that out-of-plane wind loads create strong axis bending on the columns. For bending in the plane of the frame, the columns are typically assumed to be supported at the tier levels by the intermediate horizontal struts. The struts resist the unbalanced forces that develop between tiers and help create a robust load path for the lateral seismic loads.

Although the current Canadian steel design standard, CSA S16-19 [1], does not prohibit the use of steel MT-BRBFs in seismic applications, no seismic design requirements are currently available for such BRBFs in this standard, leaving engineers without comprehensive and unified design guidelines, which may lead to unsafe or uneconomical MT-BRBF designs. The latest edition of the U.S. Seismic Provisions for Structural Steel Buildings, AISC 341-16 [2], specifies design requirements for MT-BRBFs; however, such requirements lack sufficient supporting research.

Over the past decade, there have been extensive numerical studies conducted to examine the seismic response of various conventional multi-tiered concentrically braced frames (MT-CBFs) [3,4], which showed that inelastic lateral deformations under seismic loads do not tend to distribute evenly between braced tiers if the MT-CBF was not designed to special seismic design provisions intended to distribute frame nonlinear response between braced tiers. These studies also confirmed that the non-uniform frame response produces unbalanced brace shear forces, which can induce significant in-plane bending moment in the columns. Such bending moment in the presence of axial compression forces can cause column instability. Furthermore, excessive brace elongation can occur because of uneven brace yielding which may result in brace low-cycle fatigue fracture. Although similar concerns exist in MT-BRBFs, the use of BRBs is expected to provide a more stable seismic response for multi-tiered braced frame structures when compared to their conventional counterparts. The reason being is that BRBs yield in compression as they do in tension with a significant amount of strain hardening, resulting in a potentially more uniform response along the frame height. However, the variation in expected BRB capacities between adjacent tiers may still impose in-plane bending demands on the columns that can compromise column stability.

This paper aims to evaluate the seismic response of steel MT-BRBFs, namely the distribution of inelastic lateral deformations along the frame height, in-plane bending demands on the columns, and column stability. A two-tiered BRBF (2T-BRBF) with equal tier heights and BRBs intersecting at the strut-to-column joint is selected. The frame is then designed per CSA S16-19 seismic provisions. Nonlinear static and dynamic analyses are performed to evaluate the seismic response of the frame.

A.2 MT-BRBF Design

A tall single-story building located in Vancouver, British Columbia, Canada, on site Class C was selected for this study. As shown in Figure A.2a, the plan dimension of the building is 105 m × 60 m with an identical column spacing of 5 m. The roof consists of a steel deck running perpendicular to steel joists supported by long steel trusses spanning between exterior and interior columns. The building is 8 m-tall and has two two-tiered BRBFs along each exterior wall. In this study, one of the BRBFs in the long direction in which the frame height is equally divided between two tiers (Figure A.2b) was selected. The roof dead D, snow S, and live L loads are 1.0 kPa, 1.4 kPa, and 1.0 kPa, respectively. The weight of the exterior cladding is 0.5 kPa. The seismic load was determined according to the National Building Code of Canada, NBCC 2015 [5], using the equivalent static force procedure. The building is of normal importance, I_E = 1.0, and has a seismic weight of 9234 kN. The ductility-related force modification factor, R_d, and the over-strength-related force modification factor, R_o, are 4 and 1.2, respectively. The design fundamental period of the building was taken to be equal to two times the empirical period, i.e., T_a = 2 × 0.2 s = 0.4 s as permitted by NBCC 2015 since the analytical period was calculated to be higher than two times the empirical period. The design spectral response acceleration for the selected site is $S(T_a)$ = 0.82g. The design base shear of the frame including, notional loads, P-Δ effects, and accidental torsion, is equal to 417 kN.

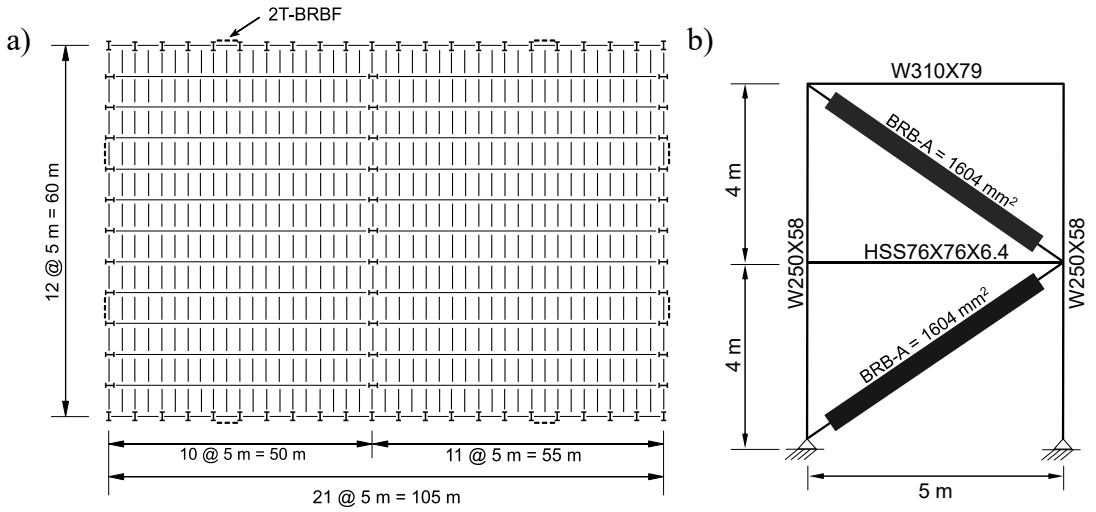

Figure A.2: a) Roof plan of the selected building; b) Elevation of the selected frame.

The frame was designed under the load combination 1.0 D + 1.0 E + 0.5 L as a standard multi-story BRBF in the absence of special seismic design guidelines for MT-BRBFs in the 2019 edition of CSA S16. The BRBs were designed for an axial load of 534 kN. The BRB steel core is assumed to be made from a steel plate conforming to G40.21-350WT with a yield strength, F_y, and expected yield strength, R_yF_y, of 350 MPa and 370 MPa, respectively. A core area, A_{sc}, equal to 1604 mm^2 (2.5 in^2) was then chosen for both tiers to resist the lateral seismic load. The strain hardening adjustment factor, R_{sh}, and the friction adjustment factor, β, were calculated to be 1.35 and 1.28, respectively, using experimental test results of a similar sized BRB [6]. The probable resistances of the BRBs are $A_{sc}R_{sh}R_yF_y$ = 807 kN in tension and $\beta A_{sc}R_{sh}R_yF_y$ = 1033 kN in compression. The rest of the frame was designed to remain elastic following the capacity design principle. The columns and roof beam were selected from wide flange (W-shape) sections conforming to ASTM A992 steel with F_y = 345 MPa. The columns were designed to resist the axial compression load induced by gravity loads in addition to the BRB probable resistances, which resulted in a total axial force of 1346 kN in the bottom tier (Tier 1). A W250×58 section was selected for the columns and

a W310×79 section was selected for the roof beam. An HSS76×76×6.4 section conforming to ASTM A1085 steel F_y = 345 MPa was selected for the intermediate strut. The selected sections for the columns, beam, and strut meet the width-to-thickness ratio limits corresponding to Class 2 sections as specified by CSA S16-19. A stiffness modification factor of 1.33 was calculated and assigned to the BRBs [6]. The design story drift was found to be equal to 1.5% including inelastic effects, i.e., $\Delta R_d R_o / I_E$, where Δ is the story drift under the design seismic load. The design story drift is less than the maximum inter-story drift limit of 2.5% as prescribed by NBCC 2015 for normal buildings.

D.3 MT-BRBF Numerical Model

The numerical model of the 2T-BRBF was created in the *OpenSees* program [7]. Special attention was given to accurately modeling the nonlinear cyclic behavior of the BRBs. For this purpose, a numerical model of a BRB was created using a single-degree-of-freedom (SDOF) corotTruss element and assigned the Steel4 uniaxial material (Figure A.3a). This material was specifically developed for BRBs and is capable of reproducing the isotropic and kinematic hardening responses of steel, plus the asymmetric behavior expected in BRBs [8]. The model was then subjected to an increasing cyclic uniaxial displacement protocol and the Steel4 material parameters were calibrated using previous BRB experimental test data [9]. Since the nonlinear model was limited to the BRB yielding length, the stiffness of the element was modified to account for the added stiffness contributed by the elastic portions of the BRB. The axial force – axial strain of both the numerical BRB element and the BRB test specimen is shown in Figure A.3a. The numerical BRB model was found to well predict the nonlinear cyclic response of the BRB test specimen, including the effects of friction.

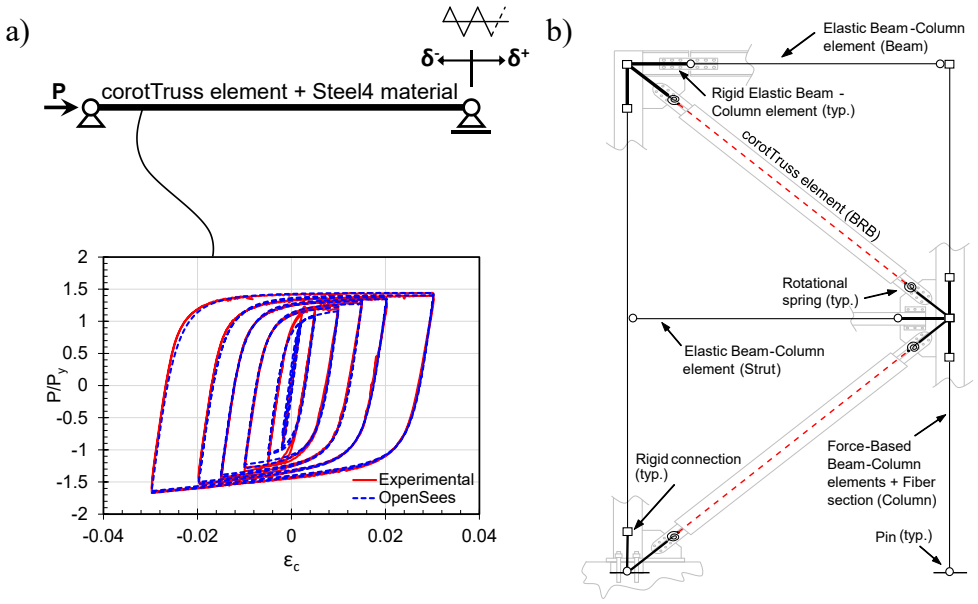

Figure A.3. a) BRB SDOF model and calibrated hysteretic response; b) Fiber-based frame numerical model (leaning column not shown).

The calibrated Steel4 material parameters were used to define the BRBs in the 2T-BRBF numerical model shown in Figure A.3b. At the ends of each BRB, zero-length rotational springs were used to represent the out-of-plane rotational response of the gusset plates. Relatively rigid elastic beam-column elements were used to model the connection regions considering the added stiffness provided by gusset plates. The columns were modeled using multiple nonlinear force-based beam-column elements with fiber discretization of the cross-section. The Steel02 material with isotropic and kinematic hardening was assigned to the columns [10]. Residual stresses and initial out-of-straightness were also assigned to the columns in the plane and out of the plane of the frame. The columns were pinned at the base and laterally braced in the out-of-plane direction at the top of the frame to represent lateral bracing provided by the roof truss. The roof beam and strut were modeled using elastic beam-column elements with pin ends [11]. A corotational transformation technique was used to account for large deformations and geometric nonlinearities. A leaning column was

defined to account for large P-Δ effects due to gravity loads tributary to the frame. For the dynamic analysis, the seismic weight was applied as point loads at the top end of the columns, and the Rayleigh damping method with a mass proportional damping corresponding to 2% of critical was used in the first vibration mode of the frame to reproduce the classical viscous damping matrix.

A.4 Seismic Response Evaluation

A nonlinear static (pushover) analysis was performed following a gravity analysis by gradually increasing the roof lateral displacement of the frame to a target displacement corresponding to a story drift of 6%. The frame was pushed to such a large story drift in order to identify its collapse mechanism. The base shear versus story drift response of the frame is shown in Figure A.4a. As shown, the frame responded in a linear-elastic fashion up to 0.4% story drift; as the BRBs in both tiers started to yield beyond which a significant stiffness degradation was observed. However, due to the inherent strain hardening of BRBs, the base shear continued to increase until approximately 4.8% story drift at which column instability occurred.

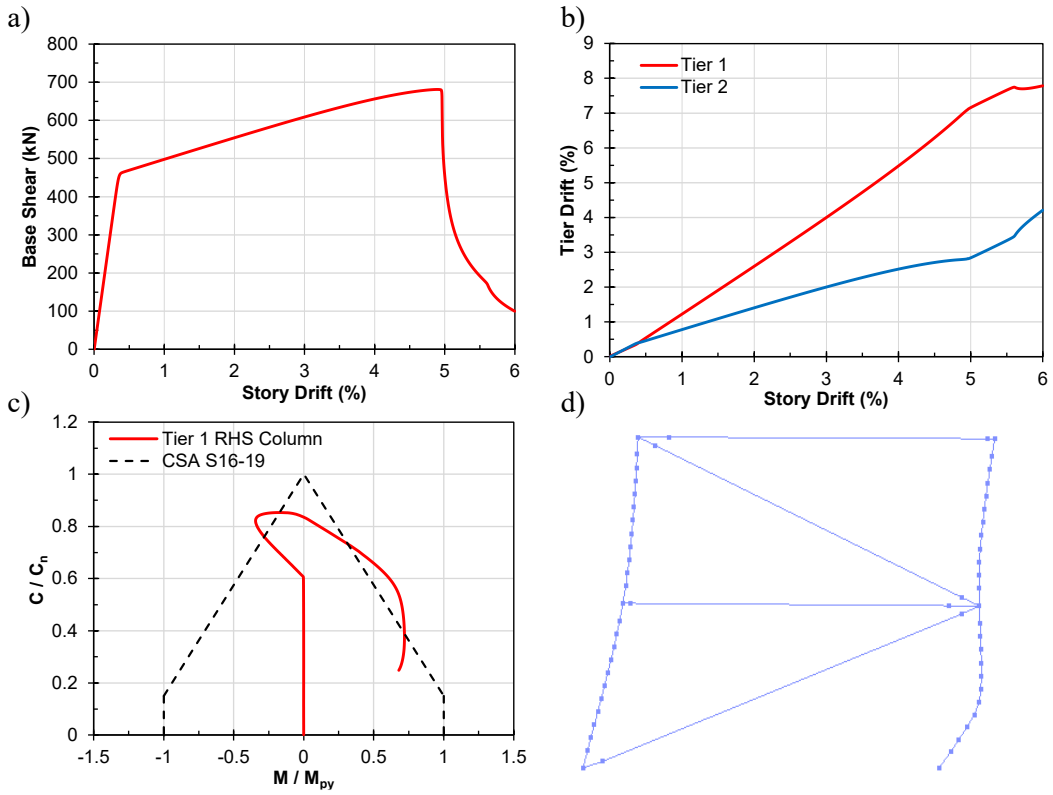

Figure A.4: a) Base shear – story drift response; b) Tier drifts; c) RHS Column P-M Interaction diagram; d) Frame deformed-shape at 4.9% story drift.

As shown in Figure A.4b, tier drifts are nearly identical in the early elastic range until the BRB in Tier 1 yields in tension, and the BRB in Tier 2 yields in compression at a story drift of 0.4%. Beyond this point, the tension-acting BRB in Tier 1 tended to elongate with a lower story shear than that required to shrink the second tier BRB in compression. This response resulted in larger lateral deformations in Tier 1 than those in Tier 2, causing the concentration of the frame drift in Tier 1 (Figure A.4b). Flexural bending was therefore induced in the column due to the difference in BRB story shears when the story drift exceeds 0.4%. The axial force – weak axis moment interaction diagram of the right-hand-side (RHS) column at tier level is plotted in Figure A.4c. When the roof displacement reaches a displacement corresponding to a story drift of 4%, the first flexural plastic hinge formed in the RHS column at approximately mid-height of Tier 1 due to an

in-plane moment of $0.35M_{py}$ where M_{py} is the weak axis plastic moment of the column. By increasing the lateral displacement, the moment at the strut level changed sign, reversing the column's curvature and resulting in the formation of the second flexural plastic hinge shortly after. At this point, the RHS column buckled due to the combined in-plane bending moment and axial force demands amplified by P-Δ. As shown in Figure A.4c, the column demands when the first plastic hinge forms approached the code-specified P-M interaction curve and subsequently exceeded it after column buckling, which was mainly due to material strain hardening while demands redistribute in the member. The frame deformed-shape at 4.9% story drift after the formation of the second plastic hinge is shown in Fig. 4d. The frame response and in particular, column instability observed is in agreement with results obtained from past studies of MT-CBFs [3,4].

Nonlinear time-history analyses were conducted to examine the performance of MT-BRBFs under earthquake ground motions. An ensemble of 33 representative ground motion time histories consisting of crustal, in-slab, and interface subduction events were selected and scaled to the design response spectra of Vancouver site Class C. The seismic response parameters of the frame were computed following the 2015 NBCC Commentary J recommendations [12] by taking the maximum of means over each ground motion suite for the peak response parameters including story drift, in-plane moment demand, and drift ratio. The peak story drift was found to be 1.48%, which is close to that calculated in design. The ratio of the critical tier drift over the story drift was 1.38 resulting in an in-plane moment demand of $0.17M_{py}$.

To better illustrate the seismic response of MT-BRBFs, the histories of story drift, tier drift, and in-plane moment demand under the 2001 Southern Peru - A12P earthquake are presented in Figure A.5. Figure A.5a shows the history of story and tier drifts. As shown, frame lateral displacements

due to inelastic deformation of the BRBs tend to concentrate in Tier 1 (e.g., critical tier) at the first peak of the ground motion (t = 14s) as the frame is pushed to the right creating tension in the first tier BRB. The critical tier then briefly switches to Tier 2 once the story drift becomes negative (t = 16s), resulting in a greater drift demand in Tier 2. Finally, the critical tier changes back to Tier 1 as the frame experiences positive drift for the remainder of the ground motion time. This response induces in-plane bending demands on the columns as shown in Figure A.5b. These column flexural bending demands highly depend on the location of the tension-acting BRB (Figure A.5b) and, in combination with axial forces, must be considered in design.

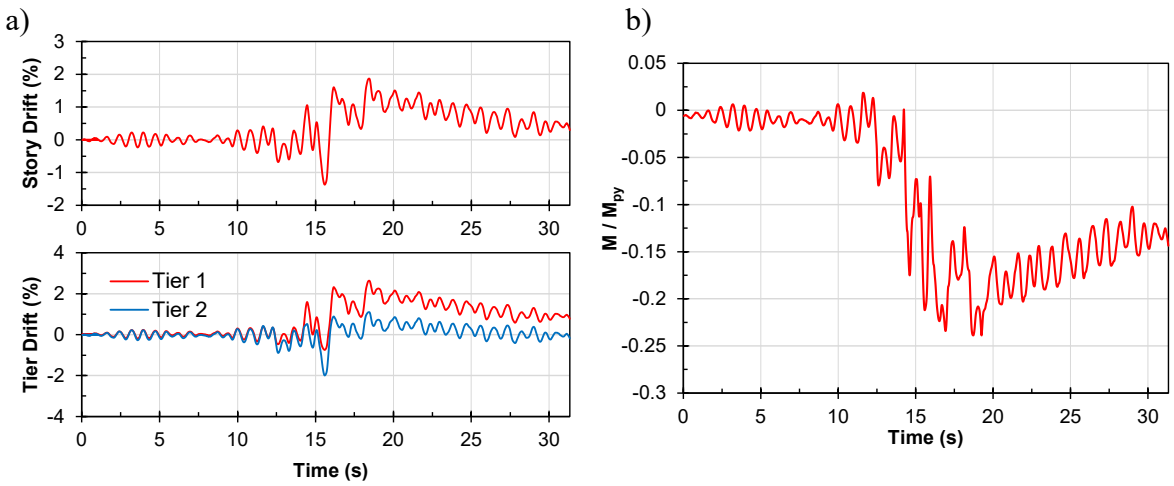

Figure A.5: a) History of story and tier drifts; b) History of RHS column in-plane bending demand.

A.5 Conclusion

This study presented the seismic response of two-tiered BRBFs. The results confirmed that frame lateral deformations are not evenly distributed along the height of the frame but instead concentrate in the tier where the BRB acts in tension. This response produces in-plane bending moments on the BRBF columns, which is not currently considered when designing MT-BRBFs as per CSA S16-19 which can compromise column stability at large story drifts. The results of the nonlinear analyses performed in this paper suggest that MT-BRBF columns should be designed to resist the

combined effects of axial forces and bending moments. Furthermore, the columns should possess sufficient flexural stiffness to promote yielding in the compression BRB to create a more uniform tier drift response.

A.6 References

1. Design of steel structures, CSA S16-19. Canadian Standards Association, Toronto, ON (2019).
2. Seismic provisions for structural steel buildings, AISC 341-10/16. American Institute of Steel Construction, Chicago, IL (2010).
3. Imanpour, A., Tremblay, R., Fahnestock, L. A., Stoakes, C.: Analysis and design of two-tiered steel braced frames under in-plane seismic demand. Journal of Structural Engineering. 142, 04016115 (2016).
4. Imanpour, A., Tremblay, R., Davaran, A., Stoakes, C., Fahnestock, L.A.: Seismic performance assessment of multitiered steel concentrically braced frames designed in accordance with the 2010 AISC Seismic Provisions. Journal of Structural Engineering. 142, 04016135 (2016).
5. National building code of Canada, NBCC 2015. National Research Council Canada, Ottawa, ON (2015).
6. Tremblay, R., Bolduc, P., Neville, R., Devall, R.: Seismic testing and performance of buckling-restrained bracing systems. Canadian Journal of Civil Engineering. 33(1), 183–198 (2006).
7. Pacific Earthquake Engineering Research Center: OpenSees.
8. Zsarnóczay, Á.: Experimental and numerical investigation of buckling restrained braced frames for Eurocode conform design procedure development, (2013).
9. Dehghani, M., Tremblay, R.: Design and full-scale experimental evaluation of a seismically endurant steel buckling-restrained brace system. Earthquake Engineering Structural Dynamics. 47(1), 105–129 (2017).
10. Ashrafi, A., Imanpour, A.: Seismic response of steel multi-tiered eccentrically braced frames. 12th Canadian Conference on Earthquake Engineering. Quebec City (2019).
11. Palmer, K., Roeder, C., Lehman, D.: Connection design recommendations for improved BRBF performance. Engineering Journal. 53, 29-45 (2016).
12. User's guide – NBC 2015 structural commentaries (Part 4 of Division B), NRC-Commentaries. Associate Committee on the National Building Code, Ottawa, ON (2015).

APPENDIX B DYNAMIC RESPONSE OF MULTI-TIERED BUCKLING-RESTRAINED BRACED FRAMES IN HIGH SEISMIC REGIONS OF CANADA

Abstract: This paper aims to examine the seismic response of Multi-Tiered Buckling-Restrained Braced Frames (MT-BRBFs) with a focus on two- and three-tiered frames using the nonlinear dynamic analysis method. The prototype frames are part of a single-storey building located in Victoria, British Columbia, Canada. The frames are designed according to the current Canadian steel design standard and their performance is examined under scaled ground motion accelerations. The results of the numerical simulations indicate that appreciable in-plane moments are imposed on the MT-BRBF columns due to the non-uniform distribution of frame inelastic deformations caused by asymmetric BRB hardening in tension and compression. This moment in combination with high axial compression forces led to yielding of the columns and should be considered in the design of MT-BRBF columns.

B.1 Introduction

Steel Multi-Tiered Braced Frames (MT-BFs) consist of multiple bracing panels (or tiers) stacked vertically along a storey height, i.e., between out-of-plane support locations. MT-BFs are commonly used in North America as lateral load-resisting systems in tall-single storey buildings such as sports facilities, airplane hangars, warehouses, and industrial buildings. These frames are also used in multi-storey buildings with tall storey heights such as convention centres and auditoriums. A multi-tiered configuration is favoured when the use of a single braced panel within a storey height becomes uneconomical or impractical. MT-BF columns are often wide-flange members oriented such that out-of-plane wind loading induces strong axis bending. Intermediate horizontal struts are typically used between tiers to achieve a robust lateral load path under seismic

loading while bracing the columns in the plane of the frame. Although concentrically braced frames (CBFs) are often used in the multi-tiered configuration, the use of high-performance Buckling-Restrained Braces (BRBs) can offer an attractive alternative, particularly in high seismic regions by translating the inherent ductility of steel into system ductility, controlling the response of the structure to severe earthquakes (Watanabe et al. 1988, Uang et al. 2004, Tsai et al 2004, Tremblay et al. 2006). Figure B.1 shows two examples of Multi-Tiered Buckling-Restrained Braced Frames (MT-BRBFs).

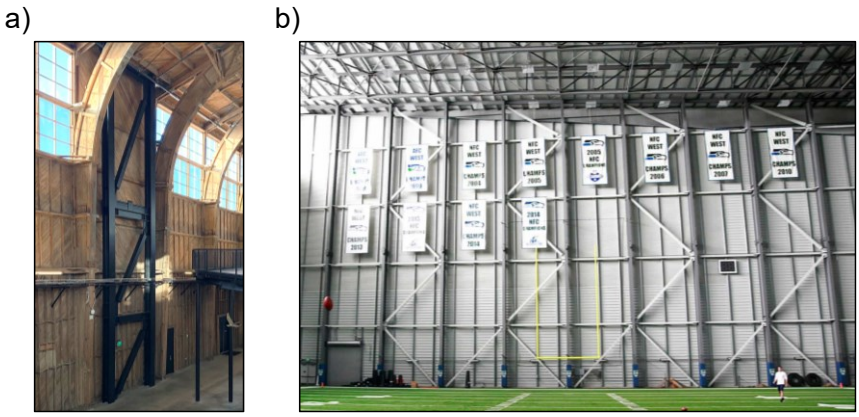

Figure B.1: Multi-Tiered Buckling-Restrained Braced Frames: a) three-tiered BRBF in a retrofit project in Los Angeles, CA (Courtesy of Maren Dougherty); b) five-tiered BRBFs in a sports facility in Renton, WA (Courtesy of Michael Lawrie)

Buckling-Restrained Braces were introduced in the late 1990s in North America as an alternative to conventional steel braces (Clark et al. 1999, Tremblay et al. 1999, Black et al. 2004). Conventional BRBs consist of a steel plate (referred to as the core), encased in a grout- or mortar-filled steel tube. A proprietary un-bonding material is used to decouple the steel core and the grout such that the entire axial load is resisted by the steel core while the grout-filled tube prevents it from buckling, allowing the core to yield in compression. BRBs are designed to concentrate the

inelastic action along the yielding length of the core while the end connection regions remain elastic. Under a major seismic event, the core is expected to yield in tension and compression resulting in a stable hysteretic response. BRBs under cyclic loads are expected to develop compressive forces higher than their respective tensile resistance (in the order of 1.2) due to the frictional forces developed between the core and casing as well as the Poisson's effect. Nevertheless, the nearly-symmetric hysteretic behaviour of BRBs makes them an attractive alternative to their conventional counterparts, which under cyclic loading suffer from significant strength degradation due to global and local buckling or even low-cyclic fatigue fracture (Tremblay 2002).

Design provisions for buckling-restrained braced frames (BRBFs) were introduced in the U.S. in the 2005 edition of the Seismic Provisions for Structural Steel Buildings, AISC 341-05 (AISC 2005) and later in Canada in the 2009 edition of the CSA Steel Design Standard, CSA S16-09 (CSA 2009). Over the past two decades, there has been a significant body of research devoted to the mechanics and behaviour of BRBs, seismic response and design of steel BRBFs, BRB connections, and the development of new and more advanced BRBs. Past analytical and experimental studies confirmed the excellent seismic performance of buckling-restrained braced frames in multi-storey buildings, including higher ductility capacity, better distribution of plasticity over the frame height, and nearly identical storey shear capacity under loading reversal (Sabelli 2003, Kim et al. 2004, Fahnestock et al. 2006). These features make the use of BRBs highly attractive in braced frames in high seismic regions.

Research on MT-BFs over the past decade has mainly focused on Multi-Tiered Concentrically Braced Frames (MT-CBFs) with extensive numerical studies having been conducted to examine the seismic response of low- and highly-ductile MT-CBFs in Canada and the U.S. (Imanpour et al.

2016, Imanpour and Tremblay 2016, Cano and Imanpour 2020). The results of these studies have shown that inelastic lateral deformations under seismic loads tend to concentrate in one of the braced tiers inducing significant in-plane bending in the columns, which in the presence of large axial compression forces can lead to plastic hinging in the columns resulting in column instability. Column buckling was experimentally confirmed using hybrid simulation of a two-tiered CBF designed to the 2010 AISC Seismic Provisions (Imanpour et al. 2022). Furthermore, excessive brace elongation can occur in the tier where brace tensile yielding occurs, which may result in brace low-cyclic fatigue fracture. The results of these past numerical studies resulted in the development of new seismic provisions for steel MT-BFs in Canada and the U.S. (Imanpour et al. 2016, Imanpour and Tremblay 2017). These provisions mainly target the design of the columns of such frames by introducing in-plane and out-of-plane bending moments in addition to the axial compression loads induced by the inelastic response of the braces. Furthermore, a tier drift limit was prescribed to limit the inelastic deformation of braced tiers to the deformation corresponding to brace low-cyclic fatigue fracture. Finally, intermediate struts are required between braced panels to provide a vertical load path after brace yielding and buckling. Although similar performance concerns exist in MT-BRBFs, the use of BRBs is expected to provide a more uniform distribution of inelastic lateral deformations, leading to a more stable seismic response in MT-BRBF structures when compared to their conventional counterparts. The reason being is that BRBs yield in compression as they do in tension with a significant amount of strain hardening, resulting in a potentially more uniform distribution of plasticity along the frame height. However, the variation in expected BRB capacities and post-yield stiffnesses between adjacent tiers can still result in in-plane bending demands on the columns that may compromise column stability. A recent numerical study on a two-tiered BRBF located in Vancouver, BC showed that these moments can reach on

average 17% of the column plastic moment capacity with more severe demands observed under ground motions produced by interface subduction earthquakes, which are one of the major sources of seismic hazard in the west coast of Canada (Bani and Imanpour 2022).

The 2019 edition of CSA S16 (CSA 2019) does not prohibit the use of MT-BRBFs, however, there are no special seismic design requirements currently available, leaving engineers without comprehensive and unified design guidelines, which may lead to unsafe or uneconomical MT-BRBF designs. The latest edition of the U.S. Seismic Provisions for Structural Steel Buildings, AISC 341-16 (AISC 2016) specifies design requirements for MT-BRBFs, which include provisions to design the columns under an axial compression force arising from BRB capacity forces plus an induced in-plane bending moment due to unbalanced forces between BRBs in adjacent tiers. Furthermore, the flexural stiffness of the column must be sufficient to limit the drift in any tier to 2%. When computing the in-plane moment, the MT-BRBF column should be treated as a simply-supported member with a length equal to the distance between points of out-of-plane supports then a set of transverse point loads are applied corresponding to the greater of 1) the summation of frame shears from the adjusted brace strengths between adjacent tiers, and 2) a minimum notional load equal to 0.5% times the frame shear coming from the higher strength adjacent tier. Additionally, the columns should be torsionally braced at every strut-to-column connection location. Very limited research studies were performed to support the provisions prescribed in AISC 341-16 (Imanpour et al. 2016).

To provide insight into the seismic response of steel MT-BRBFs, this paper aims to examine the dynamic response of two- and three-tier steel BRBFs part of a tall single-story building located in a high-seismic region of Canada (Victoria, BC). The frames were first designed per the 2019 Canadian steel design standard. Then a detailed numerical model was developed and was used to

perform nonlinear time history analyses under a set of representative ground motion records. The results of the numerical simulations were finally used to evaluate the response of the frames and confirm the need for special seismic design requirements for MT-BRBFs.

B.2 Frames Studied

A single-storey building representing an indoor sports facility located in Victoria, BC with plan dimensions of 126 m × 70 m was selected in this study. The plan view of the prototype building is shown in Figure B.2a. The building is located on site Class C (dense soil) with a mean shear velocity, V_{s30}, between 360 to 760 m/s. The roof of the building consists of a steel deck supported by 70 m-long steel trusses that span over the full width of the building. The bay width in both principal directions of the building is equal to 7 m. The seismic force resisting system of the building consists of ductile (Type D) steel buckling restrained braced frames (BRBFs). In total, three BRBFs along each exterior wall are used to resist lateral loads. As shown in Figures B.3b and B.3c, two building heights were considered; 12 m for the two-tiered BRBF and 18 m for the three-tiered BRBF. The building height was equally divided between the tiers in both prototype frames. A single diagonal zig-zag bracing configuration was selected for the BRBFs. As shown in Figures B.2b and B.2c, the selected configuration resulted in BRBs in adjacent tiers intersecting at a common joint on the columns. This configuration was selected because it limits the number of connections in the frame and creates a direct lateral load path from the roof to the foundation allowing for smaller strut sizes. Although this configuration can be seen as an efficient solution from a design and construction perspective, it is also expected to create the most critical multi-tier response.

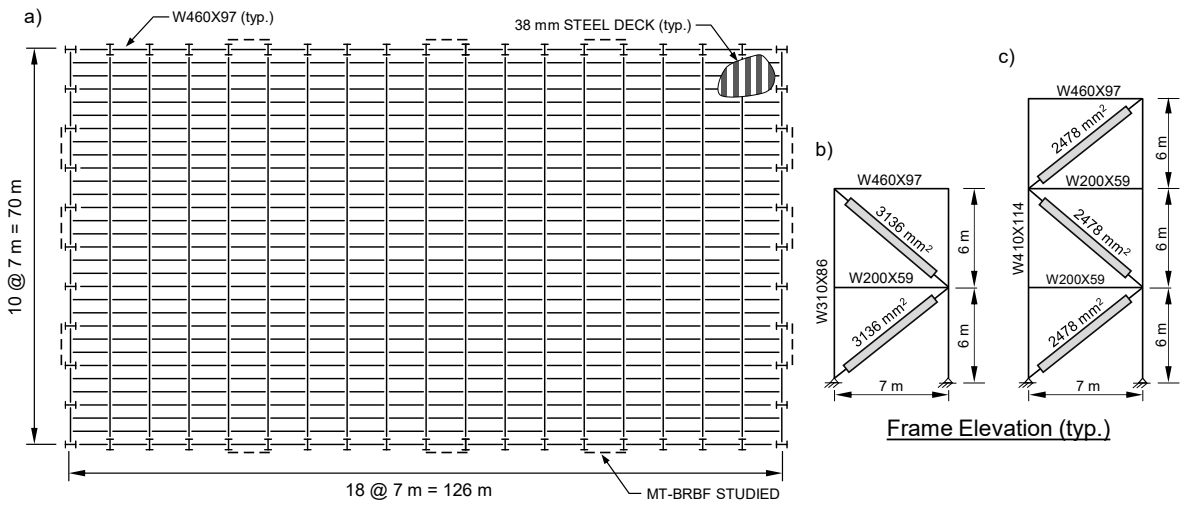

Figure B.2: a) Plan view of the selected building; b) two-tiered BRBF elevation; c) three-tiered BRBF elevation

The roof dead load (D), live load (L), and snow load (S) are equal to 1.2, 1.0, and 1.14 kPa respectively. The exterior cladding consists of insulated metal wall panels with a unit weight of 1.0 kPa. The seismic design base shear was determined using the equivalent static force procedure in the 2015 National Building Code of Canada (NBC) (NRC 2015). The importance factor, I_E, and the higher mode effect factor, M_v, are both equal to 1.0. For BRBFs, the ductility-related force modification factor, R_d, and the over-strength-related force modification factor, R_o, are 4 and 1.2, respectively. As permitted by NBC 2015, the design fundamental period of the building was taken as two times the empirical period ($0.025h$, where h is the height of the building) for both frames. The key seismic design parameters for the frames are summarized in Table B.1.

The 2015 NBC Load Combination 5 ($E+D+0.5L+0.25S$) was used to determine the design forces. The frames were designed as multi-story BRBFs in the absence of special seismic design guidelines for MT-BRBFs in CSA S16-19. The factored column gravity load was found to be 208 kN for both frames. The BRBs were designed using a steel plate conforming to ASTM A36 with an expected

yield strength, R_yF_y, of 290 MPa. The strain hardening adjustment factor, R_{sh}, and the friction adjustment factor, β, of the BRBs were computed as 1.42 and 1.12, using the backbone of the hysteretic response of the BRBs as discussed in Section B.3. The probable resistances of the BRBs are $A_{sc}R_{sh}R_yF_y$ in tension and $\beta A_{sc}R_{sh}R_yF_y$ in compression, where A_{sc} is the steel core area. The roof beam, struts, and columns were sized based on a capacity design approach to resist the probable resistances of the BRBs in addition to gravity loads. Based on the distribution of axial loads along the columns (arising from BRB capacities along the frame height) effective length factors less than unity were used to obtain column in-plane and out-of-plane buckling resistances using an Eigen buckling analysis (Dalal 1969). The columns, struts, and roof beam were selected from wide-flange sections conforming to ASTM A992 steel with a yield strength, F_y, of 345 MPa. The selected sections for the columns, roof beams, and struts satisfy the width-to-thickness ratio limits corresponding to Class 2 sections as specified by CSA S16-19. The selected frame member sizes are shown in Figures B.3b and B.3c for the two-tiered BRBF and three-tiered BRBF respectively. A stiffness modification factor of 1.24 was assigned to all BRBs in both frames to account for the added stiffness provided by the connections and the elastic regions of the BRB when calculating frame lateral deformations. The design story drifts including inelastic effects, $\Delta R_dR_o/I_E$, were found to be lower than the maximum inter-story drift limit of 2.5% as prescribed by 2015 NBC for normal buildings. Lastly, although it did not govern the design of the BRBFs, the lateral wind load was also considered in design.

Table B.1: Design parameters of frames studied.

Design Parameter	Two-tiered BRBF	Three-tiered BRBF
Design fundamental period, T_a, s	0.60	0.90
Analytical period, $T_{analytical}$, s	0.75	1.11
Design spectral acceleration, $S(T_a)$, g	1.07	0.78
Seismic weight per frame, W_{BRBF}, kN	2575	2771
Design base shear per frame*, V_{BRBF}, kN	620	490
Design storey drift, $R_dR_o\Delta_e/I_E$, $\%h_{Storey}$	1.36	1.44

*Including notional loads, accidental torsion, and P-Delta effects.

B.3 Numerical model

A fibre-based numerical model of the prototype frames was developed in the *OpenSees* program (PEER 2021) to examine the dynamic response of MT-BRBFs. Since the selected building is symmetric in plan and torsional effects can be ignored, a two-dimensional BRBF model with six degrees of freedom (DOFs) was used to examine the dynamic behavior of the system. The numerical model of the MT-BRBF is shown in Figure B.3a for the two-tiered frame. The columns are pinned at the base and laterally braced in the out-of-plane direction at the top of the frame to represent lateral bracing provided by the roof truss. Multiple nonlinear force-based beam-column elements with fibre discretization of the cross-section were used to model the columns. The Giuffre-Menegotto-Pinto (Steel02) material model was used to reproduce the nonlinear cyclic response of the columns considering the Bauschinger effect. The Steel02 material parameters were adapted from the calibration performed against cyclic coupon tests of 350W steel (Ashrafi and Imanpour 2019). A Young's modulus, E, of 200 GPa, and Poisson's Ratio, v, of 0.3, was assumed for all frame elements. Residual stresses were assigned to the column elements. To trigger in-plane and out-of-plane buckling, the maximum initial sinusoidal geometric out-of-straightness of the columns was set to 1/1000 times the unbraced length of the member in the plane and out of the plane of the frame. Five integration points were assumed along each element. The roof beams and

struts were modeled using elastic beam-column elements. Relatively rigid elastic elements were used at the ends of the columns, struts, and roof beam to account for the rigidity of the gusset plate connections. A corotational transformation technique was used to account for large deformations and geometric nonlinearities for all elements. An elastic element leaning column carrying the tributary gravity loads of the gravity frames was included in the model to account for P-Delta effects. The seismic masses were lumped at the top end of the columns, and the Rayleigh damping method with a mass proportional damping corresponding to 2% of critical was used in the first vibration mode of the frames to reproduce the classical viscous damping matrix.

The BRBs were modeled using corotTruss elements and assigned the Steel4 uniaxial material. This material model is an expanded definition of the Giuffré-Menegotto-Pinto Model capable of simulating the asymmetric kinematic and isotropic hardening behaviour of BRBs (Zsarnóczay 2013). The Steel4 material parameters were calibrated using experimental results obtained from isolated BRB testing under a quasi-static and dynamic loading protocol (Dehghani and Tremblay 2017) as shown in Figures B.3b and B.3c, respectively. As can be seen, the BRB model is capable of adequately simulating the cyclic inelastic response of BRBs under both loading protocols. A yield strength, F_y, of 290 MPa was assumed for the BRBs, and the Young's modulus was modified by a factor of 1.24 to capture the added stiffness provided by the elastic regions of the BRBs and connections.

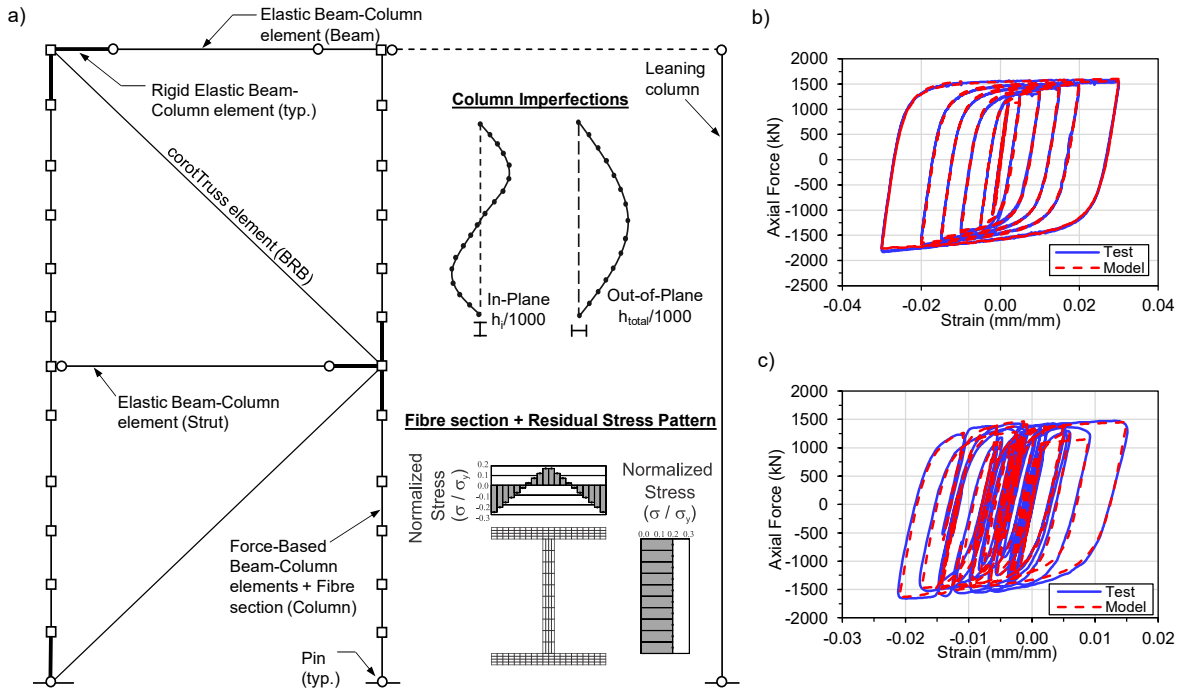

Figure B.3: a) Fibre-based numerical model of a MT-BRBF; b) Steel4 material calibration under a quasi-static loading protocol; c) Steel4 material calibration under a dynamic seismic loading protocol

B.4 Ground Motion Selection

Ground motion records were selected and scaled in accordance with the recommendations outlined in Commentary J of 2015 NBC (NRC-Commentaries 2015). The Uniform Hazard Spectra (UHS) for Victoria at a 2% probability of exceedance in 50 years was split into three seismic scenario-specific period ranges. Three sets of representative ground motions were then selected (one set for each of the potential seismic hazard sources in the west coast of Canada) and scaled within their respective scenario-specific period range. The first set of records consisted of 11 ground motions representing shallow crustal earthquakes dominating the seismic hazard for buildings with short fundamental periods. The second set consisted of 12 records featuring deep subduction in-slab earthquakes, which dominate the intermediate fundamental period range. The third set included 11

records representing large magnitude subduction interface earthquakes, which dominate for longer fundamental periods. The selected ground motion records used in this study are listed in Table B.2.

The *PEER NGA-West2* database was used to select the crustal records (Ancheta et al. 2013) giving priority to the records included in the FEMA P695 far-field record set (FEMA 2009) and the *PEER NGA-Sub* preliminary flatfiles were used for the in-slab and interface records (Mazzoni et al. 2021). Scaling was performed in two steps. First, the individual records in each set were scaled using a factor that minimizes the Mean Squared Error (MSE) between their 5% damped response spectra and the UHS along the scenario-specific period range. Second, all ground motions in a set were collectively scaled using a second scaling factor such that the mean response spectra of all the records in the set does not fall more than 10% below the UHS along the scenario-specific period range. The final selection of records used in this study was based on minimizing the MSE, and avoiding excessively high, i.e., greater than 5, or excessively low, i.e., less than 0.5, scaling factors. Moreover, the records with excessive spectral acceleration peaks greater than 4 g were excluded from the final sets. Figures B.4a to B.4c show the 5% damped response spectra of the scaled ground motion records for crustal, in-slab, and interface events, respectively.

Table B.2: Summary of selected ground motion records

Seismic Source (Database)	Event (Component)	Year	M_w*	R_{rup}** (km)	Station
Crustal (PEER NGA-West2)	Imperial Valley-06 (237)	1979	6.53	15.2	Cerro Prieto
	Victoria (045)	1980	6.33	14.4	Cerro Prieto
	Loma Prieta (000)	1989	6.93	15.2	Capitola
	Landers (LN)	1992	7.28	19.7	Coolwater
	Northridge-01 (090)	1994	6.69	8.7	Arleta - Nordhoff Fire Sta
	Northridge-01 (090)	1994	6.69	10.1	Sun Valley - Roscoe Blvd
	Hector Mine (000)	1999	7.13	11.7	Hector
	Parkfield-02 (090)	2004	6.00	5.2	Vineyard Canyon
	Niigata (EW)	2004	6.63	9.5	NIGH01
	Chuetsu-oki (NS)	2007	6.80	16.1	Yoitamachi Yoita Nagaoka
	L'Aquila (TE)	2009	6.30	6.8	Aterno - Colle Grilli
In-Slab (PEER NGA-Sub)	Olympia (086)	1949	6.70	47.6	OLY0
	Central America-39 (NS)	1982	7.31	60.0	2747
	Central America-38 (NS)	1992	6.51	93.1	2894
	Nisqually (180)	2001	6.80	64.6	WEK
	Nisqually (N)	2001	6.80	65.2	TKCO
	Geiyo (NS)	2001	6.83	43.6	KURE
	Pingtung Doublet-01 (E)	2006	7.02	40.7	KAU082
	Pingtung Doublet-02 (E)	2006	6.94	31.9	KAU082
	South America – 2575090 (EW)	2007	6.74	46.4	MEJILLONE
	Ferndale (360)	2010	6.55	41.2	89509
	Ferndale (360)	2010	6.55	36.2	Loleta
	Ferndale (090)	2010	6.55	32.9	1725
Interface (PEER NGA-Sub)	Michoacan (E)	1985	7.99	18.4	Aeropuerto Zihuatanejo
	Tokachi-oki (EW2)	2003	8.29	85.5	ASYORO-E
	Tokachi-oki (NS)	2003	8.29	92.2	SHIHORO
	Tokachi-oki (EW)	2003	8.29	61.2	47418
	South America – 2844986 (097)	2010	8.81	30.4	CONCEPCIÓN
	South America – 2844986 (T)	2010	8.81	36.5	CONT
	South America – 2844986 (T)	2010	8.81	49.8	HUAL
	Tohoku (NS)	2011	9.12	90.1	41207
	Tohoku (NS)	2011	9.12	86.3	Taiwa
	Tohoku (NS)	2011	9.12	52.6	GN5
	Iquique (E)	2014	8.15	71.4	MNMCX

* Moment magnitude.

** Closest distance to rupture plane.

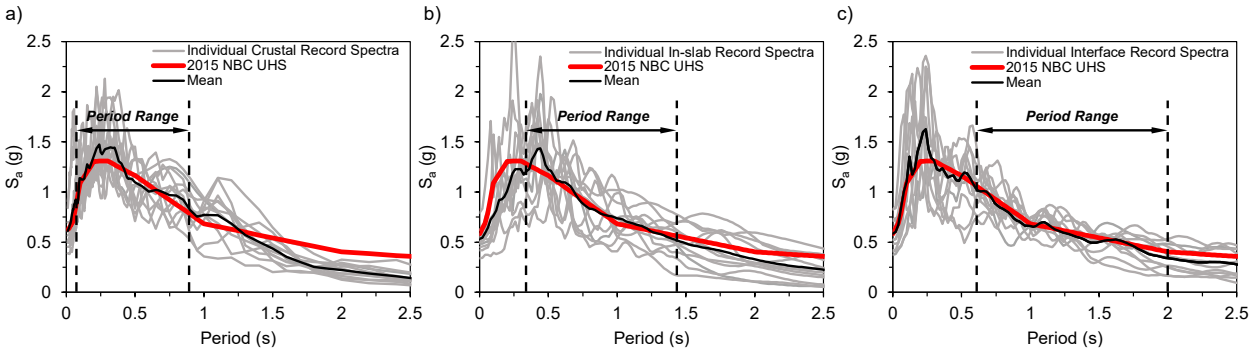

Figure B.4: Response spectra of the selected ground motion records: a) crustal; b) in-slab; c) interface

B.5 Nonlinear Response History Analysis Results

Nonlinear Response History Analysis (NLRHA) was performed under the selected ground motions to evaluate the dynamic response and seismic-induced demands of the prototype MT-BRBFs. The key response parameters including the storey drift, tier drift, drift concentration ratio (DCR), column in-plane bending demand, and BRB strains are examined. The results of the single record case studies for the two- and three-tiered BRBFs are first presented to illustrate the dynamic response of the prototype frames with an emphasis on the response of the columns and BRBs. The statistics of the selected response parameters obtained from the analyses of the prototype frames under the suite of 34 ground motions are then discussed.

B.5.1 Single-Record Case Studies Of MT-BRBF Seismic Response

For the two-tiered BRBF, the results of the dynamic analysis under the 1999 Hector Mine earthquake are presented in Figure B.5. In the plots, the storey drift is computed as the ratio of the roof lateral displacement to the storey height h_{storey} and the tier drift is defined as the ratio of the relative lateral displacement of each tier to its tier height h_{tier}. As shown in Figure B.5a, the selected ground motion resulted in a peak positive storey drift of 1.75% at t = 7s which is 1.3 times the design storey drift. The history of the tier drift is plotted in Figure B.5b. As shown, the drift tended

to concentrate in Tier 1, when the frame is undergoing positive drift inducing tension in the Tier 1 BRB, making it the critical tier. The drift in Tier 1 reaches 2.73% at t = 7 seconds (Figure B.5b), which corresponds to the point where the frame experienced the maximum storey drift (Figure B.5a). A similar response but with a lower storey drift amplitude (-0.65%h_{storey} at t = 5 seconds) occurred in Tier 2 when the frame was pushed to the left inducing tension in the Tier 2 BRB earlier in the ground motion. This uneven distribution of inelastic lateral deformations through the tendency of inelastic demand to concentrate in the tier that undergoes tension is also shown in Figure B.5c. It is important to note that these observations would be different had a different BRB configuration over the frame height been used. Figure B.5d shows the BRB hysteretic response as a function of the normalized BRB force, P_{BRB}/P_y, which is the ratio of the induced axial force in the BRBs to their respective yield strength, versus tier drift. The response seen in Figure B.5d indicates that the Tier 1 BRB deformed significantly more than the Tier 2 BRB in order to carry the same base shear. Due to the asymmetric isotropic and kinematic hardening exhibited in BRBs, the BRB forces in adjacent tiers at a given time after yielding differ, resulting in different horizontal shears contributed by the BRB in each tier. Given that the storey shear in both tiers should remain the same (no inertia forces developed at the strut level), the difference in storey shears is compensated by the columns through their flexural deformations, which induces in-plane bending demands in the columns. The normalized right-hand-side (RHS) column in-plane moment demands, M_y/M_{py}, which is the ratio of the induced moment demand to the weak-axis plastic moment capacity is shown in Figure B.5e. As can be seen, these moment demands are directly related to the difference between tier drifts (Figures B.5b and B.5c). As shown in Figure B.5e, the maximum in-plane moment demand in the RHS column at the strut level reached 0.24M_{py} at t = 7s. The combined effect of the axial forces and induced moment demands in the columns are shown

in the P-M column interaction plot in Figure B.5f. In the interaction plot, C_f/C_n is the ratio of the column axial load to its nominal buckling resistance with positive values indicating compression. In the figure, the failure envelope is defined using the beam-column interaction equation in CSA S16-19. As can be seen, the RHS column is more critical with its P-M interaction approaching the design interaction equation. Although column buckling did not occur under this ground motion, yielding was observed in the flanges of the columns. A plastic hinge formed at the middle of Tier 1, indicating that column buckling would've likely occurred had a second plastic hinge formed at the tier level.

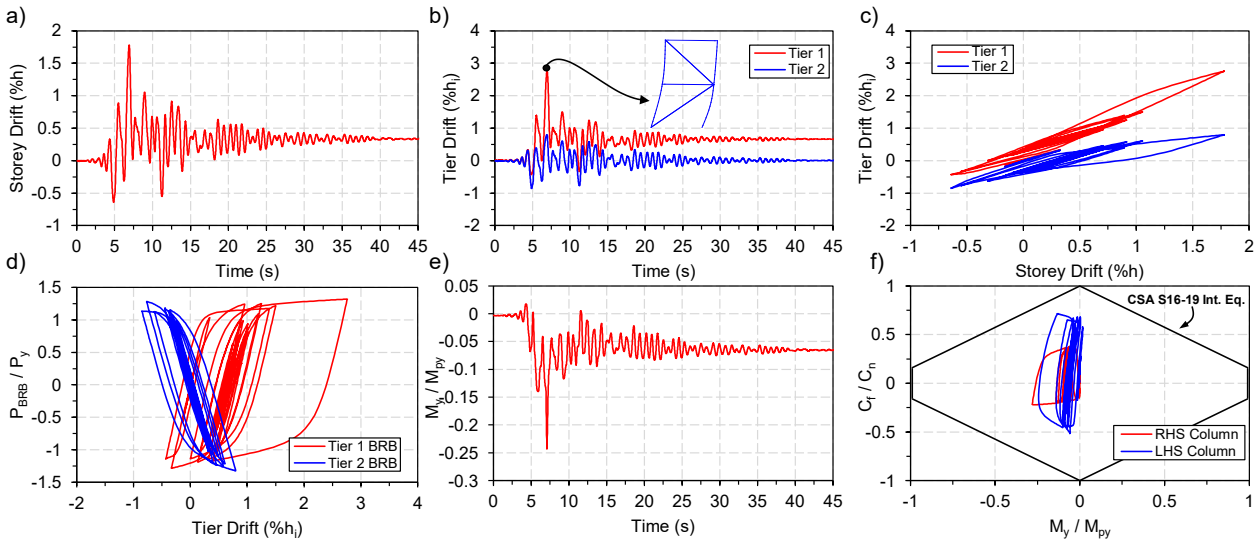

Figure B.5. Response of the two-tiered BRBF under the 1999 Hector Mine earthquake record: a) storey drift history; b) tier drift history; c) tier drift versus storey drift; d) hysteric response of BRBs; e) RHS column in-plane moment demand history; f) column P-M interaction

The response of the three-tiered BRBF under the 2010 Ferndale-Loleta record is presented in Figure B.6. As shown in Figure B.6a, this record features a large drift reversal at $t = 29$ seconds as the frame goes from sustaining a positive storey drift of $0.76\%h_{storey}$ to a peak negative storey drift of $1.31\%h_{storey}$. The observed peak storey drift is close to the anticipated design storey drift. As

shown in Figures B.6b and B.6c, inelastic deformation concentrated in Tier 2 (critical tier) which remains in tension as the frame is pushed to the left at approximately $t = 29$ seconds while Tiers 1 and 3 are both in compression and experienced nearly identical tier drifts and BRB hysteretic behaviours (Figure B.6d). The peak drift in Tier 2 reached 1.77 times the storey drift, indicating significant drift concentration has occurred in Tier 2 under negative storey drift. The observed non-uniform drift response between the tiers induced in-plane bending in the RHS column with a maximum value of $0.31M_{py}$ at the Tier 1 strut level and $0.27M_{py}$ at the Tier 2 strut level as shown in Figure B.6e. These moments are significant and should be considered in design. The column P-M interaction plot shown in Figure B.6f indicates that both columns remain elastic and stable without exceeding the CSA S16-19 beam-column interaction equation in tension and compression.

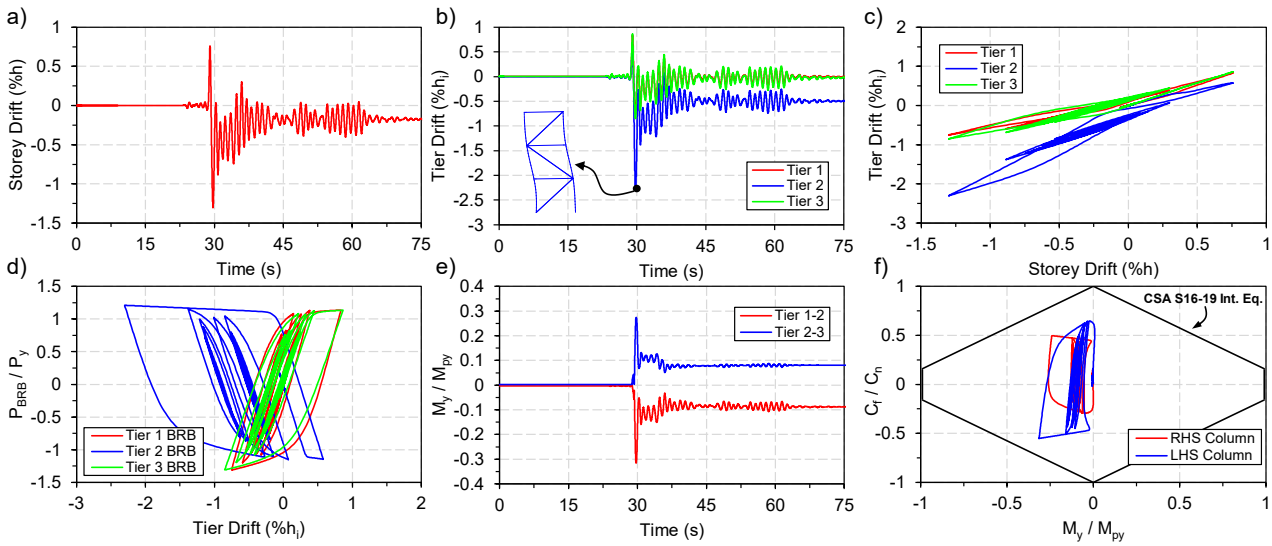

Figure B.6. Response of the three-tiered BRBF under the 2010 Ferndale-Loleta earthquake record. a) storey drift history; b) tier drift history; c) tier drift versus storey drift; d) hysteric response of BRBs; e) RHS column in-plane moment demand history; f) column P-M interaction

B.5.2 Response Statistics

The statistics of the key response parameters including the storey drift, tier drift, drift concentration ratio (DCR), column in-plane bending demand, and BRB strains for the NLRHA are given in Table 3. The mean values presented in the table were computed for each frame by taking the maximum of means over each ground motion hazard scenario set for the peak response parameter following the recommendations by 2015 NBC Commentary J, whereas the median (50^{th} percentile) and 84^{th} percentile values were calculated considering the entire suite of ground motion records analyzed. In this section, only the mean values will be discussed in detail. The median and 84^{th} percentile results are provided to highlight the variability of seismic-induced demands in the prototype frames. For both frames, no column nor frame instability was observed under the selected records. The storey drift in both frames was found to be close to that anticipated in design as indicated by the normalized storey drift values, $\Delta_{roof}/R_dR_o\Delta_{e,}$ which are close to 1.0 for both frames. The critical tier drift in the table represents the drift in the tier which experienced the largest deformation. This value was 1.97% for the two-tiered BRBF and 1.81% for the three-tiered BRBF, which confirms the non-uniform deformation response described in the previous section. The level of non-uniform drift response is indicated by the drift concentration ratio (DCR) which is the ratio of the critical tier drift to the corresponding storey drift, with factors greater than 1.0 indicating a non-uniform distribution of lateral displacements among the tiers. For both frames, some level of drift concentration was observed in all the ground motions studied. Bending demands induced in the RHS columns were measured at the strut levels. The ratios of the induced in-plane bending demands in the columns to the plastic moment capacity, M_y/M_{py}, of the respective column section are presented in Table 3. For the two-tiered BRBF, in-plane bending reached $0.18M_{py}$ in the Tier 1 strut level. Bending moments equal to $0.19M_{py}$ and $0.16M_{py}$ were generated in Tiers 1 and 2 for the

three-tiered BRBF, respectively. These moment demands in the columns are significant and must be accounted for in design. BRB strains were found to be around 1% for all tiers in both frames. These values are well below the strain used in BRB qualification and testing as prescribed in AISC 341-16 Chapter K (AISC 2016), which is around 2% for the prototype frames considered. The comparison of the response parameters among the three seismic hazard sources considered showed that in-slab earthquakes produced the largest demand in the two-tiered BRBF, whereas the long duration interface earthquakes were more critical for the three-tiered BRBF. Lastly, it is worth mentioning that in the prototype frames considered, the BRBs possessed the same yield strength and stiffness in all tiers, an assumption that may not be representative of reality, hence, the presented results represent a lower bound on the seismic demands expected in these systems. That is, a frame with non-uniform BRB properties, such as different yield strengths and stiffnesses in adjacent tiers will likely have more drift concentration and induced bending demands.

Table 3: Statistics of MT-BRBF response parameters

Response Parameter	Two-tiered BRBF			Three-tiered BRBF		
	Mean	Median	84th Percentile	Mean	Median	84th Percentile
Storey Drift (%h_{frame})	1.31	1.17	1.61	1.36	1.21	1.63
$\Delta_{roof}/R_dR_o\Delta_e$	0.96	0.86	1.18	0.95	0.84	1.13
Critical Tier Drift (%h_{tier})	1.97	1.64	2.60	1.81	1.64	2.22
DCR	1.49	1.45	1.63	1.37	1.28	1.61
$M_{in\text{-}plane}/M_{py}$ Tier 3-2	–	–	–	0.16	0.13	0.20
$M_{in\text{-}plane}/M_{py}$ Tier 1-2	0.18	0.14	0.25	0.19	0.16	0.24
ε_{BRB}* (%) Tier 3	–	–	–	0.99	0.74	1.25
ε_{BRB}* (%) Tier 2	1.00	0.69	1.45	0.97	0.86	1.32
ε_{BRB}* (%) Tier 1	1.07	0.93	1.47	1.02	0.72	1.29

* Assuming the yielding length is 65% of the working-point length.

B.6 Conclusions

In this paper, the dynamic response of two- and three-tier buckling-restrained braced frames is presented. The frames are part of a building located in Victoria, BC and are designed according to the current Canadian steel design standard. A detailed numerical model was developed and used to perform nonlinear time history analyses using a suite of ground motions scaled to the building location. The response of the frames was evaluated by examining the results obtained from the numerical analyses. It was found that although not as critical as MT-CBFs, MT-BRBFs are still prone to the concentration of inelastic demand in one or more tiers. For single-diagonal configurations, this concentration happens in the tiers in tension. This non-uniform drift response induced in-plane moment demands on the columns which may lead to frame instability. It was found, that the current method used in predicting BRB strain demands is conservative. Future editions of CSA S16 should require MT-BRBF columns to be designed to resist the combined effects of axial forces and bending moments. Furthermore, the columns should be required to possess sufficient flexural stiffness to promote adequate yielding of the BRBs in all tiers to create a more uniform tier drift response. Future works will look at the behaviour of different frame configurations with non-uniform BRB properties as well as aim to develop comprehensive design guidelines for MT-BRBFs through experimental testing.

B.7 References

AISC. 2005. ANSI/AISC 341-05, Seismic Provisions for Structural Steel Buildings. American Institute of Steel Construction (AISC), Chicago, IL, USA.

AISC. 2016. ANSI/AISC 341-16, Seismic Provisions for Structural Steel Buildings. American Institute of Steel Construction (AISC), Chicago, IL, USA.

Ancheta, T.D., Darragh, R.B., Stewart, J.P., Seyhan, E., Silva, W.J., Chiou, B.S.J., Wooddell, K.E., Graves, R.W., Kottke, A.R., Boore, D.M., Kishida, T., and Donahue, J.L. 2013. PEER NGA-

West2 Database, PEER Report 2013/03, Pacific Earthquake Engineering Research Center (PEER), University of California, Berkeley, CA, USA.

Ashrafi, A., and Imanpour, A. 2019. Seismic Response of Steel Multi-Tiered Eccentrically Braced Frames. *Proceedings of the 12th Canadian Conference on Earthquake Engineering*, Quebec City, QC, CAN.

Bani, M., and Imanpour, A. 2022. Seismic Performance of Steel Multi-Tiered Buckling-Restrained Braced Frames in Canada. *Proceedings of the 10th International Conference on the Behaviour of Steel Structures in Seismic Areas (STESSA)*, Timisoara, Romania. (accepted).

Black, C., Makris, N., and Aiken, I. 2004. Component Testing, Seismic Evaluation and Characterization of Buckling-Restrained Braces. *Journal of Structural Engineering*, **130**(6): 880-894.

Cano, P., and Imanpour, A. 2020. Evaluation of AISC Seismic Design Methods for Steel Multi-Tiered Special Concentrically Braced Frames. *Engineering Journal*, AISC, **57**(3): 193–214.

Clark, P., Aiken, I., Ko, E., Kasai, K. and Kimura, I. 1999. Design Procedures for Buildings Incorporating Hysteretic Damping Devices. *Proceedings of the 68th Annual Convention of the Structural Engineers Association of California*. Santa Barbara, CA, USA, **1**: 355-371.

CSA. 2019. CSA S16-19, Design of Steel Structures, Canadian Standards Association, Mississauga, ON, CAN.

Dalal, S.T. 1969. Some Non-conventional Cases of Column Design. *Engineering Journal*, AISC, **6**(1): 28–39.

Dehghani, M., and Tremblay, R. 2016. Design and Full-Scale Experimental Evaluation of a Seismically Resilient Steel Buckling Restrained Brace System. *Earthquake Engineering and Structural Dynamics,* **47**(1): 105-129.

Fahnestock, L.A. 2006. Analytical and Large-Scale Experimental Studies of Earthquake-Resistant Buckling-Restrained Braced Frame Systems. *PhD Dissertation*, Lehigh University, Bethlehem, PA, USA.

FEMA. 2009. FEMA P695, Quantification of Building Seismic Performance Factors. Federal Emergency Management Agency. Washington, DC, USA.

Imanpour, A., and Tremblay, R. 2016. Seismic Design and Response of Steel Multi-tiered Concentrically Braced Frames in Canada. *Canadian Journal of Civil Engineering*, **43**(10): 908–919.

Imanpour, A., and Tremblay, R. 2017. Analysis Methods for the Design of Special Concentrically Braced Frames with Three or More Tiers for In-Plane Seismic Demand. *Journal of Structural Engineering*, **143**(4): 04016213.

Imanpour, A., Tremblay, R., Davaran, A., Stoakes, C., and Fahnestock, L.A. 2016. Seismic Performance Assessment of Multitiered Steel Concentrically Braced Frames Designed in Accordance with the 2010 AISC Seismic Provisions," *Journal of Structural Engineering*, **142**(12): 04016135.

Imanpour, A., Tremblay, R., Leclerc, M., Siguier, R., Toutant, G., Minouei, Y.B., and You, S. 2022. Development and Application of Multi-Axis Hybrid Simulation for Seismic Stability of Steel Braced Frames. *Engineering Structures*, **252**(2022): 113646.

Kim, J., and Choi, H. 2004. Behavior and Design of Structures with Buckling-Restrained Braces. *Engineering Structures*, **26**(6): 693-706.

Mazzoni, S., Kishida, T., Contreras, V. Ahdi, S.K., Kwak, D.Y., Bozorgnia, Y., and Stewart, J.P. 2021. NGA-Sub Flatfile: R211022. The B. John Garrick Institute for the Risk Sciences. Dataset. https://doi.org/10.34948/N3Z59T

NRC. 2015. National Building Code of Canada. National Research Council of Canada (NRC), Ottawa, ON, CAN.

NRC-Commentaries. 2015. User's Guide – NBC 2015 Structural Commentaries (Part 4 of Division B). Associate Committee on the National Building Code, Ottawa, ON, CAN.

PEER. 2021. Open System for Earthquake Engineering Simulation (OpenSees). Pacific Earthquake Engineering Research Center (PEER), University of California, Berkeley, CA, USA. Available from: http://opensees.berkeley.edu

Sabelli, R., Mahin, S., and Chang, C. 2003. Seismic Demands on Steel Braced Frame Buildings with Buckling-Restrained Braces. *Engineering Structures*, **25**(5): 655-666.

Tremblay, R. 2002. Inelastic Seismic Response of Steel Bracing Members. *Journal of Constructional Steel Research,* **58**(5-8): 665–701.

Tremblay, R., Bolduc, P., Neville, R., and DeVall, R. 2006. Seismic Testing and Performance of Buckling-Restrained Bracing Systems. *Canadian Journal of Civil Engineering*, **33**(2): 183–198.

Tremblay, R., Degrange, G., and Blouin, J. 1999. Seismic Rehabilitation of a Four-Storey Building with a Stiffened Bracing System. *Proceedings of the 8th Canadian Conference on Earthquake Engineering*, Vancouver, BC, CAN.

Tsai, K., Lai, J., Hwang, Y., Lin, S., and Weng, C. 2004. Research and Application of Double-Core Buckling Restrained Braces in Taiwan. *Proceedings of the 13th World Conference on Earthquake Engineering*, Vancouver, BC, CAN. Paper No. 2179.

Uang, C. M., Nakashima, M., and Tsai, K. C. 2004. Research and Application of Buckling-Restrained Braced Frames. *Journal of Steel Structures*, Korean Society of Steel Construction. **4**(4): 301–313.

Watanabe, A., Hitomi, Y., Saeki, E., Wada, A., Fujimoto, M. 1988. Properties of Brace Encased in Buckling-Restraining Concrete and Steel Tube. *Proceedings of the 9th World Conference on Earthquake Engineering*, Tokyo-Kyoto, Japan.

Zsarnóczay, Á. 2013. Experimental and Numerical Investigation of Buckling Restrained Braced Frames for Eurocode Conform Design Procedure Development. *PhD Dissertation*, Budapest University of Technology and Economics, Budapest, Hungary.

APPENDIX C TENSILE COUPON TESTS

To determine the material properties of the BRB core material, three tensile coupon tests were conducted. The coupons were cut from the same steel plate (ASTM A37) used in the test BRB and machined to the required dimensions according to ASTM E8 (see Figure C.1). Figure C.2 shows the tensile coupon dimensions. The test was conducted in a 1.5 MN Instron Universal Testing Machine. Figure C.3 shows the test setup. The test was displacement controlled and the amount of deformation along the 200 mm gage length was controlled by the readings of a clip-on extensometer. The tests were carried out at a constant strain rate of 5.0×10^{-5} mm/mm/s. The engineering stress versus engineering strain curves of the three coupon tests in shown in Figure C.4. The tests were stopped before complete fracture of the coupons to avoid damaging the extensometer. Table C.1 lists the average mechanical properties of the tension coupons.

Figure C.1: Tension coupons.

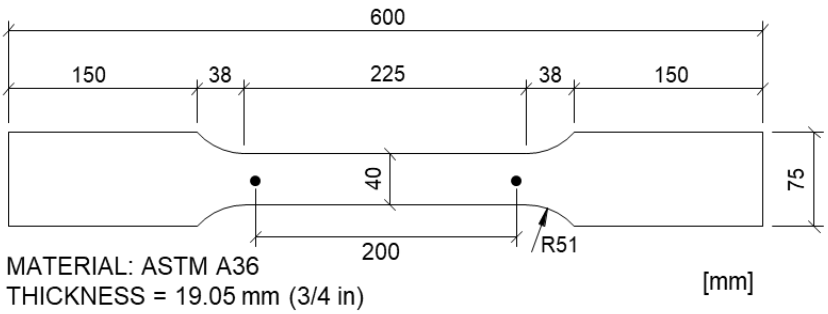

Figure C.2: Geometry of tension coupons.

Figure C.3: Tension coupon in the test machine.

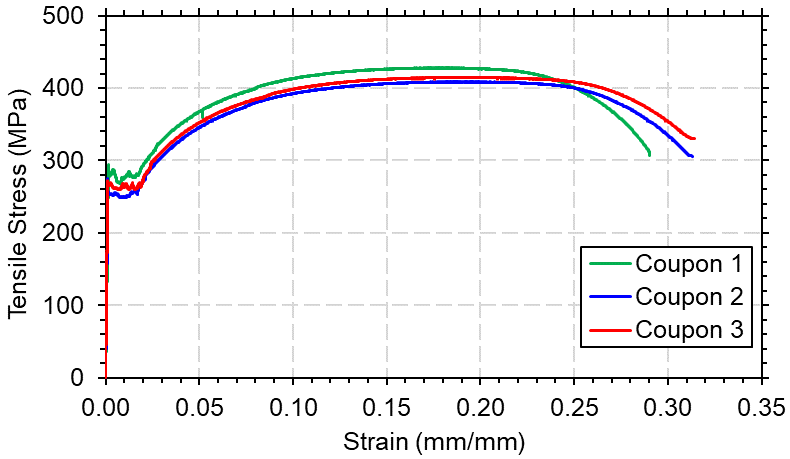

Figure C.4: Stress-Strain curve of coupon specimens.

Table C.1: Average mechanical properties of coupons.

Young's Modulus (GPa)	**Yield Stress (MPa)**	**Upper Yield Stress (MPa)**	**Ultimate Tensile Stress (MPa)**	**Strain at Tensile Ultimate Stress (mm/mm)**
201	268.60	280.45	417.28	0.19

APPENDIX D STUB-COLUMN TEST

To determine the material properties of the W310×67 (ASTM A992) column section used in the two-tiered BRBF test, a stub-column test was carried out. The stub-column specimen is 1-m long and was cut from the same column stock used in the test specimen. The measured dimensions of the stub-column are presented in Table D.1. The test was conducted according to the Structural Stability Research Council Guide (Ziemian, 2010) recommendations using a 12 MN MTS hydraulic press. Figure D.1 shows a picture of the stub-column specimen. The specimen was placed between two thick steel bearing plates at each end. A gypsum bedding was used between the bearing plates and the press crosshead and base to fill in possible gaps and ensure uniform loading. Figure D.1 also shows the instrumentation plan used. Two stick LVDTs, on both flanges, were used to determine the average strains over a 250 mm gage length. On both flanges, six strain gages, at the four corners and column centre line over a gage length of 250 mm at mid-height were added as redundancy and to ensure alignment of loading during testing. Whitewash consisting of hydrated lime was added to the column to held aid in observing the progress of yielding during the test. The press was displacement controlled and the loading was applied at a constant speed rate of 0.01 mm/s. To avoid damaging the LVDTs, the test was stopped when the load decreased to 75% of the predicted yield capacity of the column after local buckling was observed in the flanges and web. The stress-strain curve along with the key material properties are presented in Figure D.2. The Young's modulus was found to be 214 MPa and the tangent modulus at assumed stress of 330 MPa was found to 113 MPa. The difference between the Young's modulus and the tangent modulus reflects the effect of residual stresses on the cross-section. The proportional limit stress, σ_p, was calculated using a strain offset of 1×10^{-5} mm/mm and found to be 290 MPa. The yield strength, σ_y,

was calculated using strain offsets of 0.002 mm/mm and found to be 370 MPa. Figure D.3 shows local buckling of the flanges and web at the end of the test.

Table D.1: Measured specimen properties.

Parameter	Average Measurement
Section Depth, d	308.00 mm
Flange Thickness, t_f	13.66 mm
Web Thickness, t_w	10.77 mm
Flange Width, b_f	206.19 mm
Cross-Sectional Area, A	8597.66 mm^2
Specimen Length, L	1000 mm

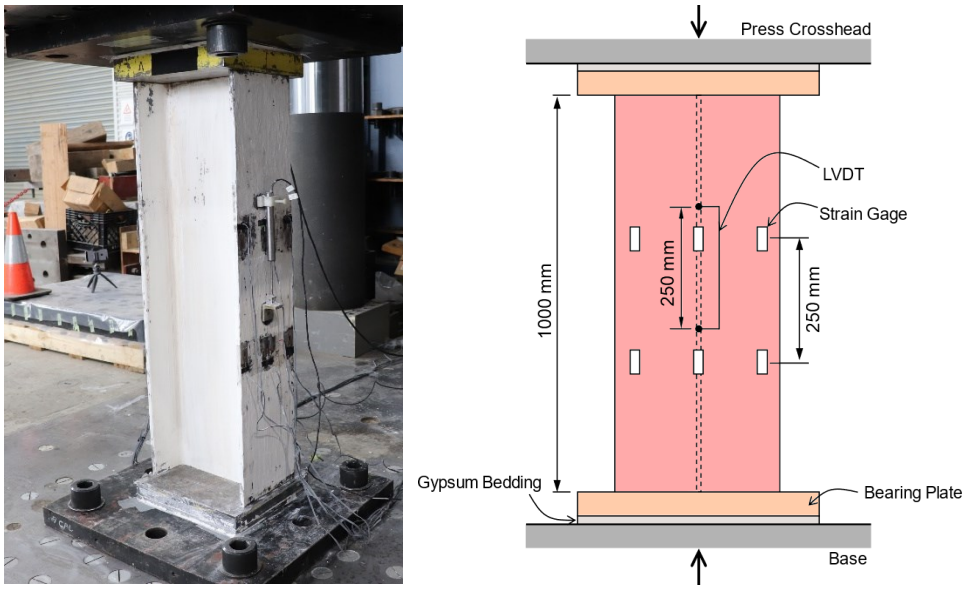

Figure D.1: Stub-Column Setup.

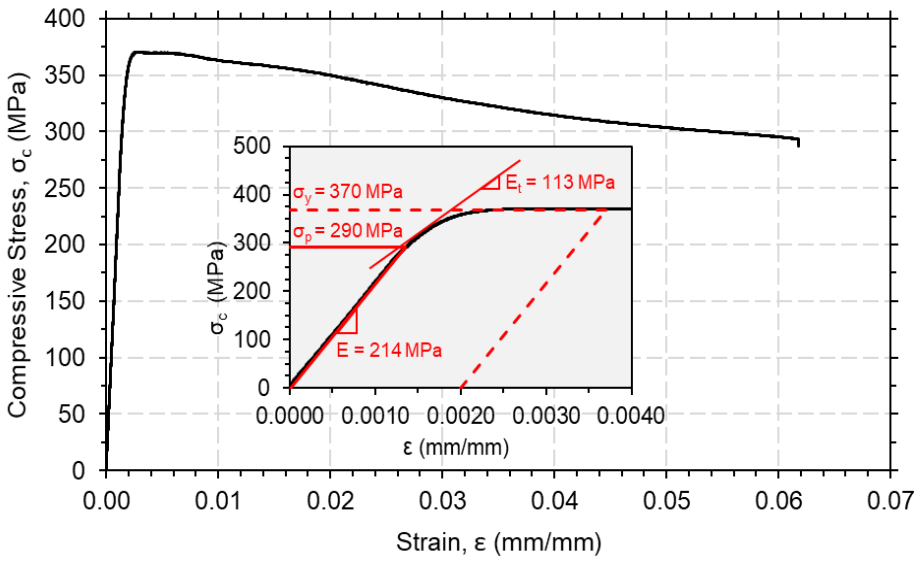

Figure D.2: Stress-strain diagram and key material properties

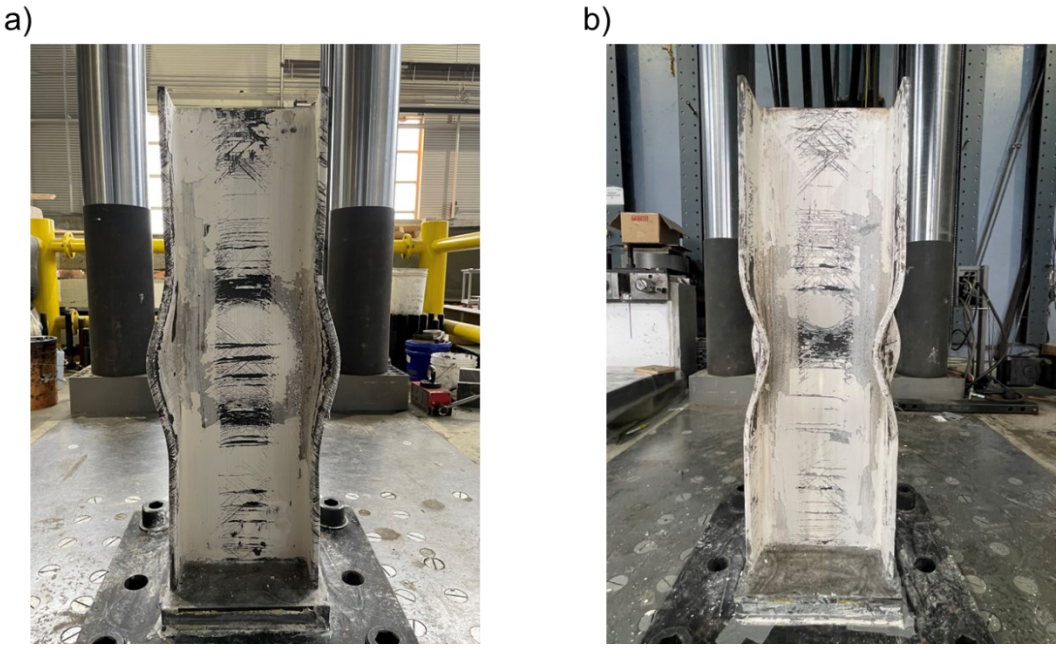

Figure D.3: Stub-Column at the end of test: a) flange and web local-buckling west view; b) flange and web local buckling east view.

APPENDIX E MILL TEST REPORT

EVRAZ | EVRAZ INC. NA
Evraz Oregon Steel 14400 N. Rivergate Blvd., Portland, Oregon 97203

REPORT OF CHEMICAL/PHYSICAL TESTS

CERTIFICATE NO.	DATE	PAGE
1782608	Jun 18, 2021	1

ISO 9001 REGISTERED U.S. PLATE PRODUCER

SOLD TO

SME INDUSTRIES INC [POCATELLO]
5801 WEST WELLS PARK RD
WEST JORDAN, UT 84081
USA

SME INDUSTRIES INC [POCATELLO]
5801 WEST WELLS PARK RD
WEST JORDAN, UT 84081
USA

MILL ORDER NO.	DATE
365363	
CUSTOMER ORDER NO.	
1111-000379	
JOB/REQ. NO.	
SHIPPING NO.	DATE
1782608	06/18/2021
CARRIER	
UNION PACIFIC	
CAR/TRUCK NO.	
TTPX814039	

THIS MATERIAL HAS BEEN MANUFACTURED, TESTED AND FOUND TO MEET THE SPECIFICATIONS AND PURCHASE ORDER REQUIREMENTS
CARBON STRUCTURAL QUALITY PLATE ASTM A36-19/ASME SA36 2019 RESTRICTED YIELD STRENGTH. KILLED. 39 KSI MIN YIELD 46 KSI MAX YIELD.

PHYSICAL PROPERTIES

ITEM NO	DESCRIPTION		HEAT NO.	SLAB	YIELD PSI X 100	TENSILE PSI X 100	% ELONG 8"	% ELONG 2"	% RA	HARDNESS BHN	BEND TEST	IMPACTS
1	0.5000 X 96.000ME X 300.000											
	3 PCS 12252 LBS	+!	RS3910	A607	455	685	31					
					446	680	29					
4	0.7500 X 96.000ME X 300.000											
	4 PCS 24504 LBS	+@	N26292	A24	424	625	32					
					413	625	31					
	3 PCS 18378 LBS	+@	N26319	A25	422	625	30					
					419	625	29					
	10 PCS 55134 LBS TOTALS											

CHEMICAL ANALYSIS

	HEAT NO.	C	Mn	P	S	Si	Cu	Ni	V	Cb	Al	Cr	Mo	Ti	B	N	Ca			CE	McQuaid Ehn Grain Size
+!	RS3910	.18	.34	.012	.002	.20	.39	.10	.000	.001	.042	.10	.02								
+@	N26292	.15	.85	.015	.006	.22	.01	.04	.005		.040	.02								.30	
	N26292:	Cb=<0.005, Mo=<0.005																			
+@	N26319	.14	.84	.015	.006	.20	.01	.04	.002		.046	.02								.29	
	N26319:	Cb=<0.005, Mo=<0.005																			

HEATS INDICATED WITH (!) WERE MELTED & POURED IN CANADA. HEATS INDICATED WITH (@) WERE MELTED & POURED IN RUSSIA.
HEATS INDICATED WITH (+) WERE ROLLED IN THE USA.

I certify the above to be correct as contained in the records of EVRAZ INC. NA By Christopher M Coleman
Quality Supervisor

..... END OF REPORT .....

APPENDIX F TEST SPECIMEN DRAWINGS

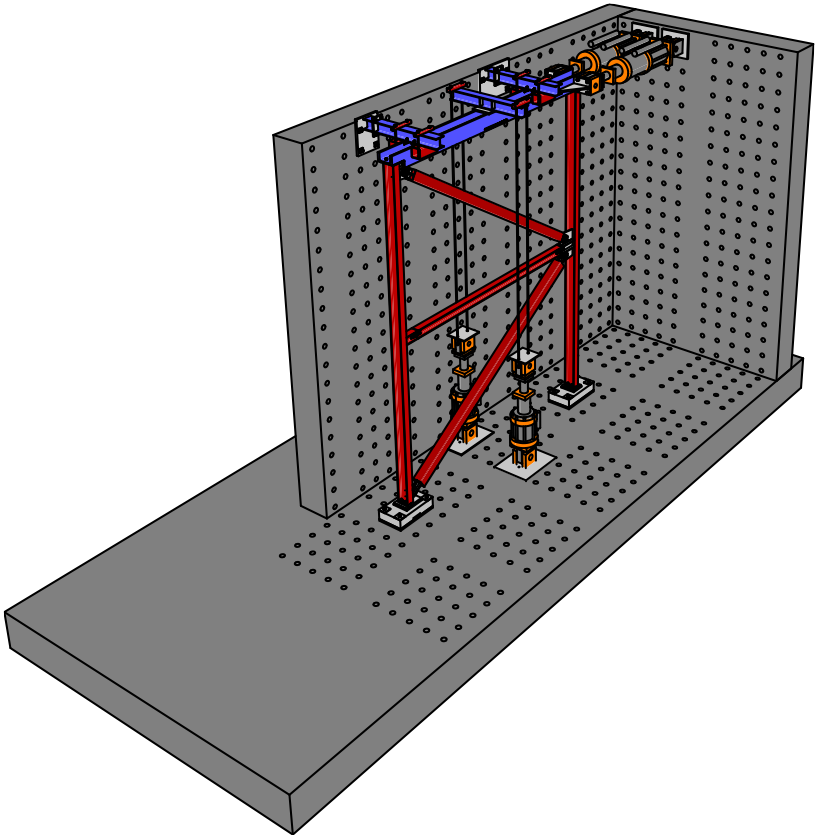

TEST SETUP ISOMETRIC

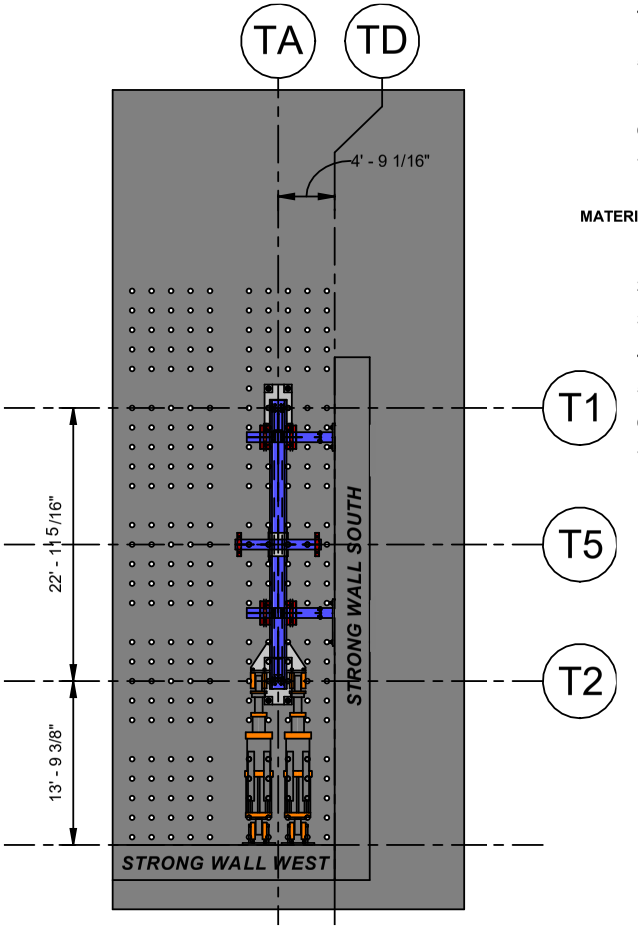

TEST SETUP PLAN

GENERAL NOTES:

1. ALL DIMENSIONS ARE IN FEET AND FRACTIONAL INCHES UNLESS OTHERWISE NOTED.
2. PROVIDE A COPY OF MILL TEST REPORT FOR ALL STRUCTURAL STEEL.
3. BOTH COLUMNS SHOULD BE FABRICATED USING THE SAME HEAT.
4. STRUT AND ROOF BEAM SHOULD BE FABRICATED USING THE SAME HEAT.
5. FOR PLATE SIZES WHERE THE SPECIFIED SIZES ARE UNAVAILABLE THE CLOSEST IMPERIAL PLATE SIZE MAY BE USED.
6. SHOP VERIFY AS NEEDED TO FIT CONNECTIONS.
7. ALL DRAWINGS TO BE PLOTTED ON A3 PAPER.

MATERIALS:

1. COLUMNS: ASTM A992 F_y = 50 ksi (345 MPa)
2. ROOF BEAM: ASTM A992 F_y = 50 ksi (345 MPa)
3. STRUT: ASTM A992 F_y = 50 ksi (345 MPa)
4. PLATES: ASTM A572 F_y = 50 ksi (345 MPa)
5. ELECTRODES: E70XX
6. BOLT HOLE DIA.: 1 1/8"
7. ANCHOR ROD HOLE DIA.: 2 3/8"

LIST OF DRAWINGS:

UNIVERSITY OF ALBERTA | POLYTECHNIQUE MONTRÉAL

CORE BRACE SUPERIOR SEISMIC PERFORMANCE

MT-BRBF TEST FRAME
GENERAL

MB	04/18/2022	S.1

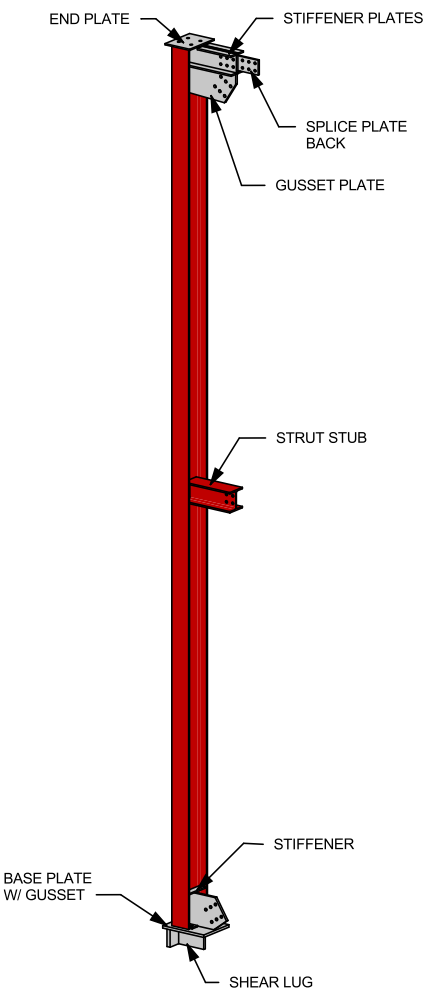

1 LEFT COLUMN

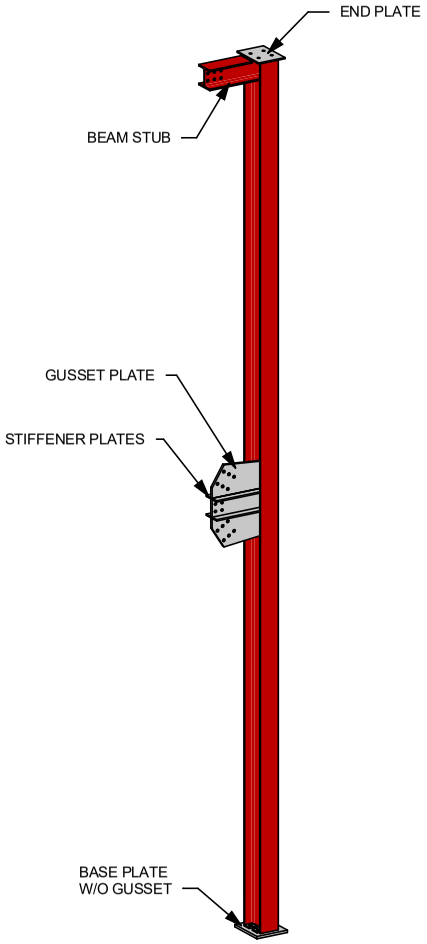

2 RIGHT COLUMN

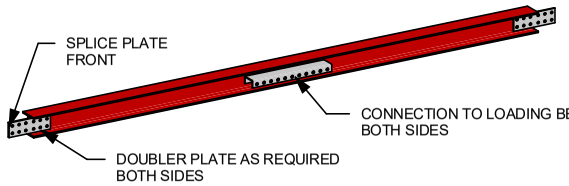

3 ROOF BEAM

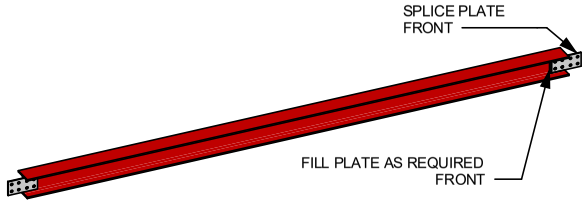

4 STRUT

UNIVERSITY OF ALBERTA | POLYTECHNIQUE MONTRÉAL

CoreBrace SUPERIOR SEISMIC PERFORMANCE

MT-BRBF TEST FRAME
TEST SPECIMENS

MB	04/18/2022	S.2

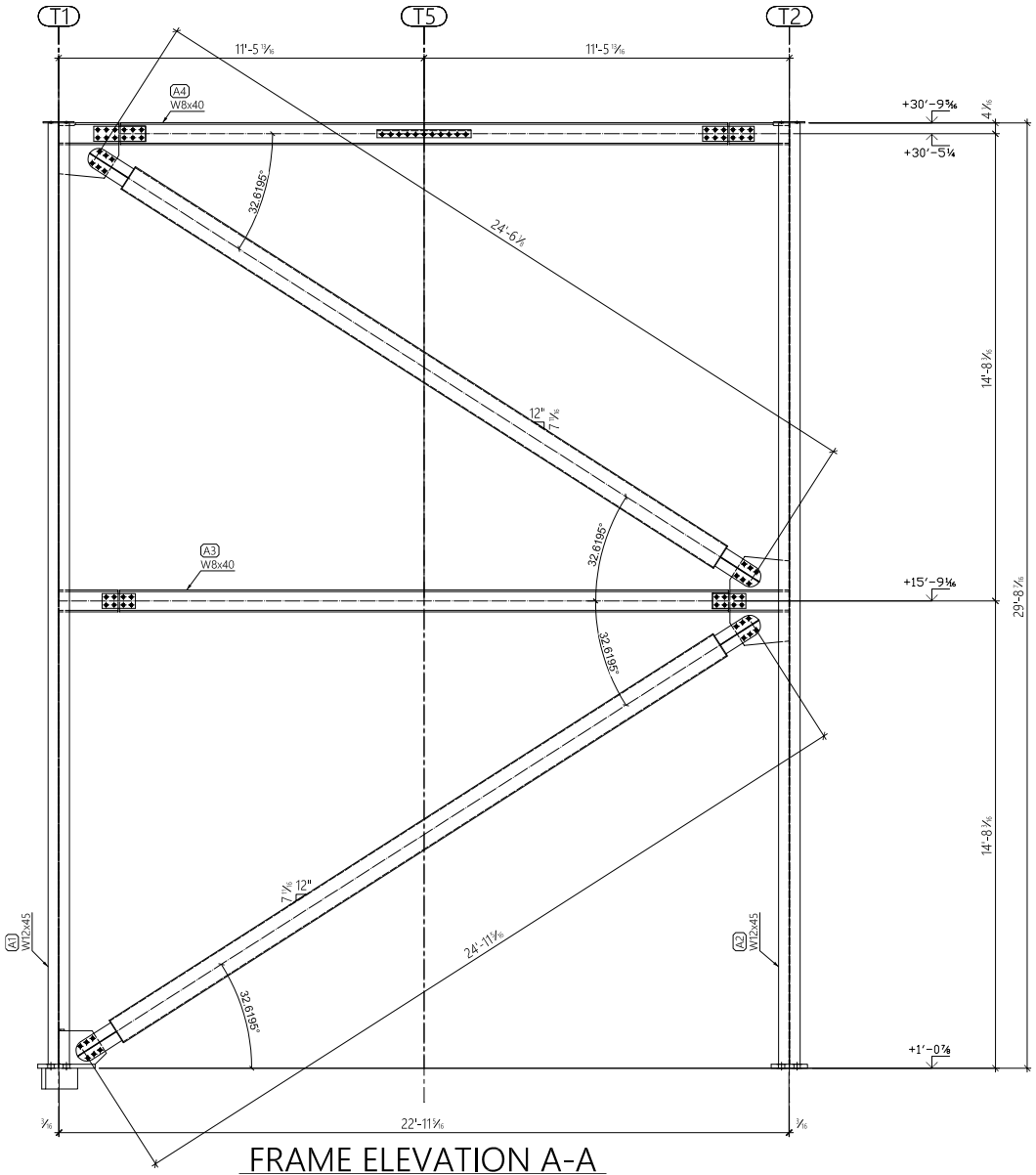

FRAME ELEVATION A-A

UNIVERSITY OF ALBERTA | POLYTECHNIQUE MONTRÉAL

CoreBrace SUPERIOR SEISMIC PERFORMANCE

MT-BRBF TEST FRAME
FRAME ELEVATION

MV	05/10/2022	S.3

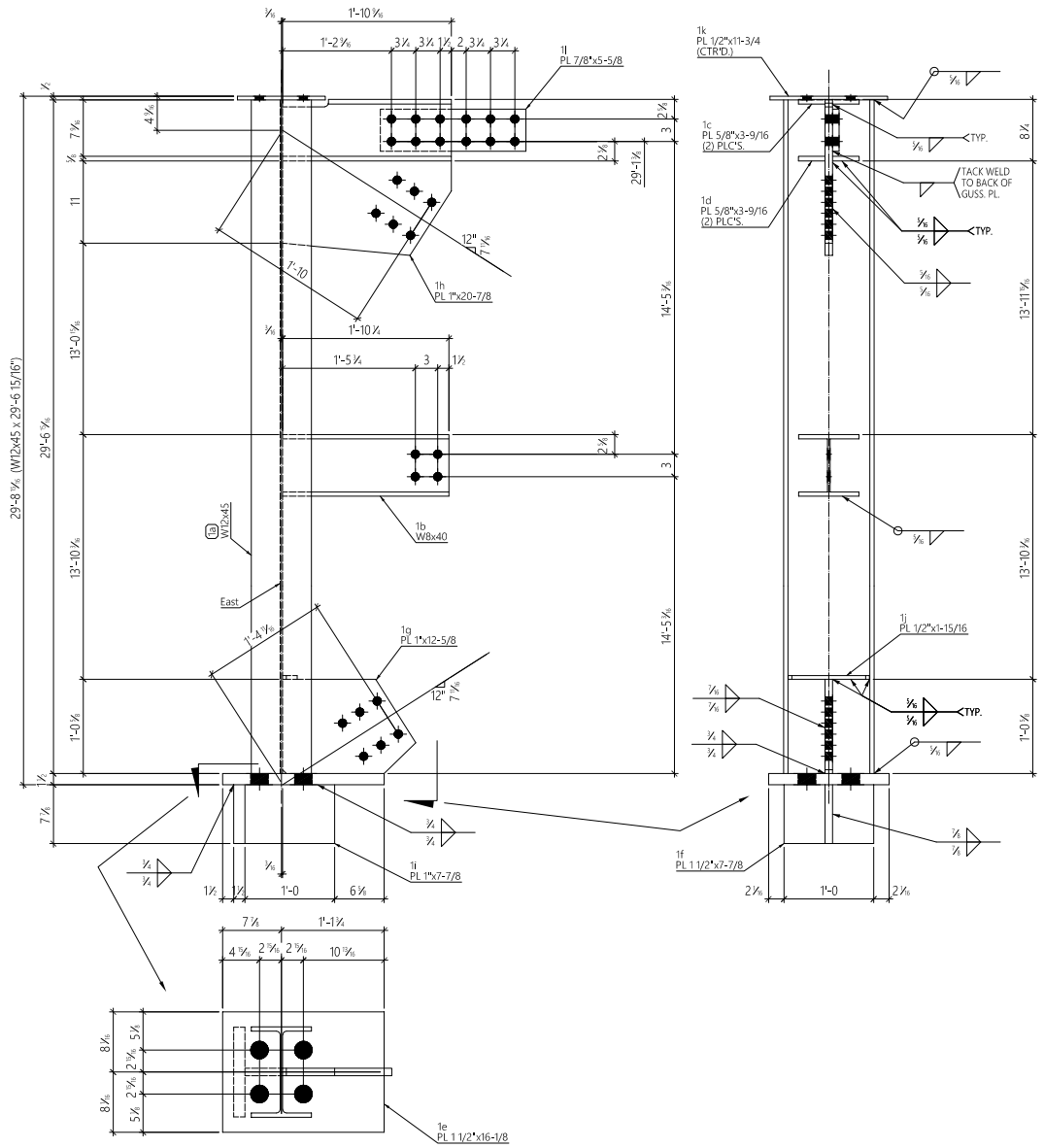

1 - COLUMN - A1

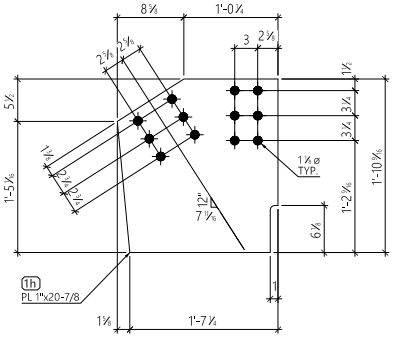

1 - GUSSET PLATE - 1h

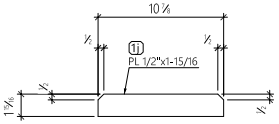

1 - SIFFENER PLATE - 1j

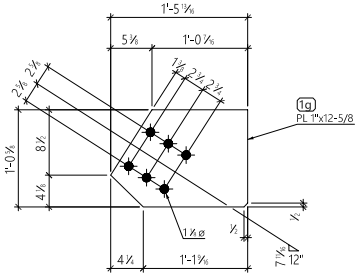

1 - GUSSET PLATE - 1g

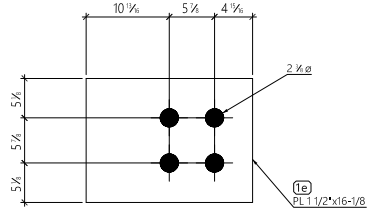

1 - BASE PLATE - 1e

BILL OF MATERIAL						
MARK	QTY	DESCRIPTION	LENGTH	GRADE	REMARKS	SEQ
A1	1	Column				
1a	1	W12x45	29'-6 15/16"	A992		
1b	1	W8x40	1'-10 1/4"	A992		
1c	2	PL 5/8"x3-9/16	1'-4 7/16"	A572		
1d	2	PL 5/8"x3-9/16	1'-10 9/16"	A572		
1e	1	PL 1 1/2"x16-1/8	1'-9 5/8"	A572		
1f	1	PL 1 1/2"x7-7/8	1'-0"	A572		
1g	1	PL 1"x12-5/8	1'-5 13/16"	A572		
1h	1	PL 1"x20-7/8	1'-10 9/16"	A572		
1i	1	PL 1"x7-7/8	1'-0"	A572		
1j	1	PL 1/2"x1-15/16	1'-10 7/8"	A572		
1k	1	PL 1/2"x11-3/4	1'-3 3/4"	A572		
1l	1	PL 7/8"x5-5/8	1'-7 1/2"	A572		

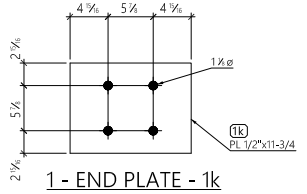

1 - END PLATE - 1k

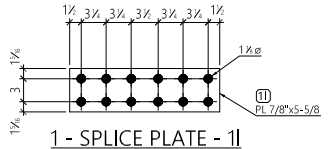

1 - SPLICE PLATE - 1l

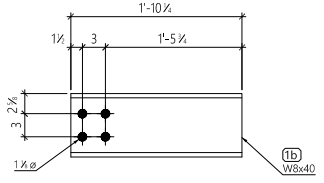

1 - STRUT - 1b

UNIVERSITY OF ALBERTA | POLYTECHNIQUE MONTRÉAL

CoreBrace SUPERIOR SEISMIC PERFORMANCE

MT-BRBF TEST FRAME
WEST COLUMN (A1)

MV	05/10/2022	S.4

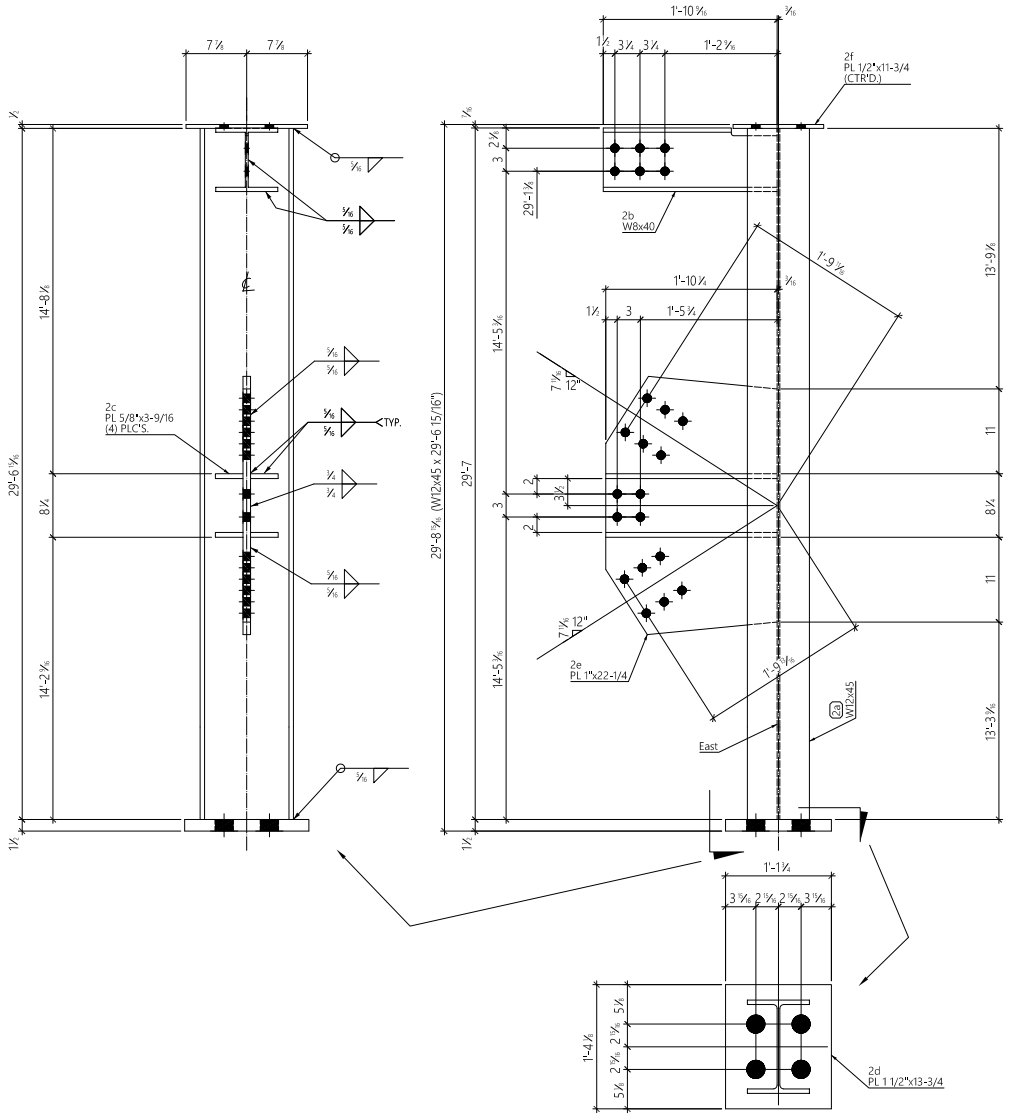

1 - COLUMN - A2

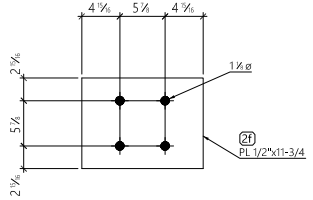

1 - END PLATE - 2f

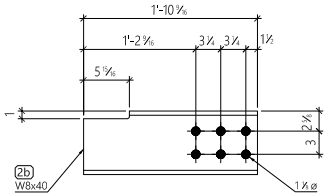

1 - BEAM - 2b

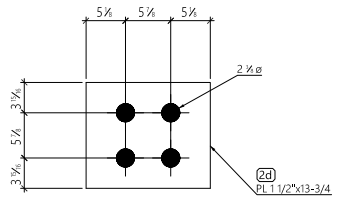

1 - BASE PLATE - 2d

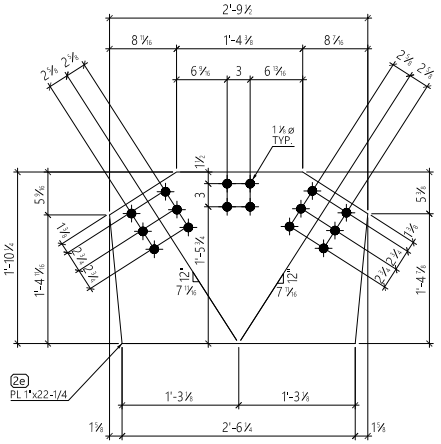

1 - GUSSET PLATE - 2e

BILL OF MATERIAL						
MARK	QTY.	DESCRIPTION	LENGTH	GRADE	REMARKS	SEQ.
A2	1	Column				
2a	1	WT2x45	29'-6 15/16"	A992		
2b	1	W8x40	1'-10 9/16"	A992		
2c	4	PL 5/8"x3-9/16	1'-10 1/4"	A572		
2d	1	PL 1 1/2"x13-3/4	1'-4 1/8"	A572		
2e	1	PL 1"x22-1/4	2'-9 1/2"	A572		
2f	1	PL 1/2"x11-3/4	1'-3 3/4"	A572		

UNIVERSITY OF ALBERTA | POLYTECHNIQUE MONTRÉAL

CoreBrace SUPERIOR SEISMIC PERFORMANCE

MT-BRBF TEST FRAME
EAST COLUMN (A2)

MV	05/10/2022	S.5

BILL OF MATERIAL						
MARK	QTY.	DESCRIPTION	LENGTH	GRADE	REMARKS	SEQ.
A3	1	Strut				
3a	1	W8x40	19'-1 13/16"	A992		
3b	2	PL 1/2"x5-5/8	1'-0 1/2"	A572		
3c	1	PL 5/16"x5-7/8	0'-6 1/16"	A572		

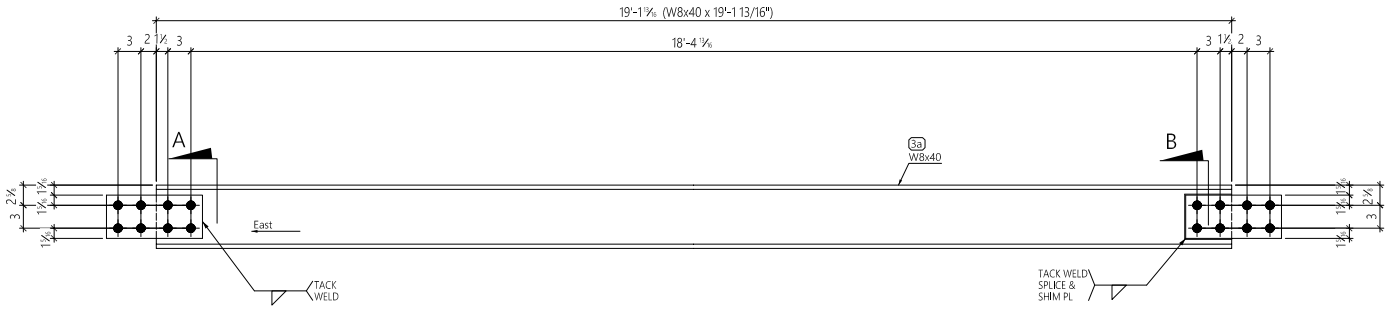

1 - STRUT - A3

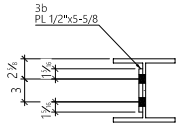

SECTION A

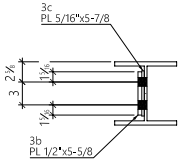

SECTION B

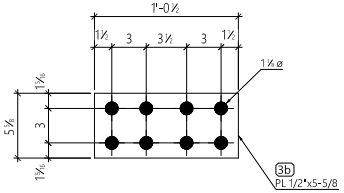

2 - SPLICE PLATE - 3b

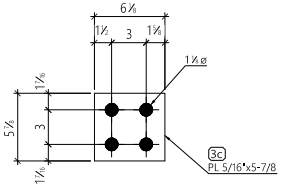

1 - SHIM- 3c

UNIVERSITY OF ALBERTA | POLYTECHNIQUE MONTRÉAL

CoreBrace SUPERIOR SEISMIC PERFORMANCE

MT-BRBF TEST FRAME
STRUT

MV	05/10/2022	S.6

BILL OF MATERIAL						
MARK	QTY.	DESCRIPTION	LENGTH	GRADE	REMARKS	SEQ.
A4	1	Roof Beam				
4a	1	W8x40	19'-1 3/16"	A992		
4b	2	MC6X16.3	2'-11 1/2"	A572		
4c	1	PL 1/2"x5-5/8	1'-7 1/2"	A572		
4d	2	PL 5/16"x5-7/8	1'-6 5/8"	A572		
4e	1	PL 7/8"x5-5/8	1'-7 1/2"	A572		

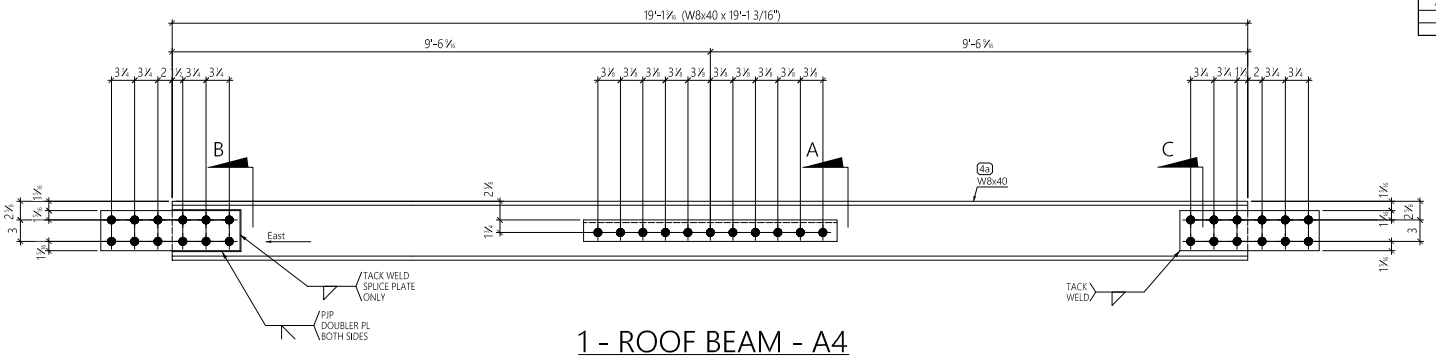

1 - ROOF BEAM - A4

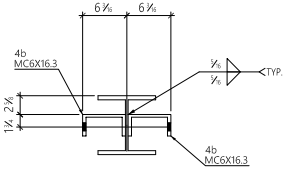

SECTION A

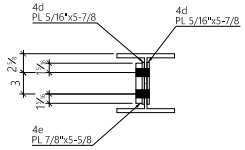

SECTION B

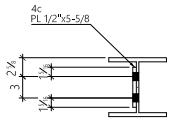

SECTION C

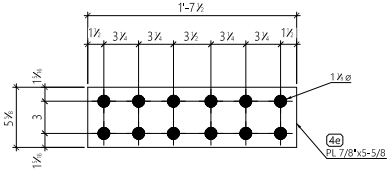

1 - SPLICE PLATE - 4e

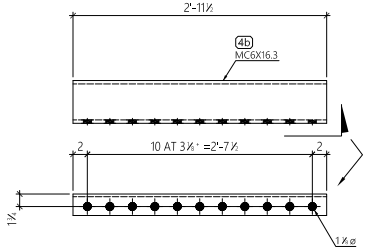

2 - CHANNEL - 4b

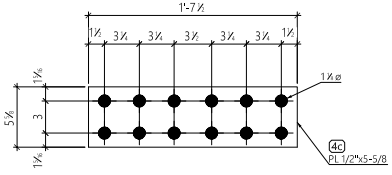

1 - SPLICE PLATE - 4c

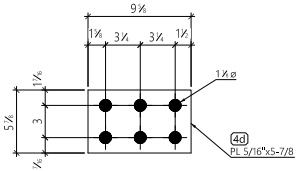

2 - DOUBLER PLATES - 4d

UNIVERSITY OF ALBERTA | POLYTECHNIQUE MONTRÉAL

CoreBrace SUPERIOR SEISMIC PERFORMANCE

MT-BRBF TEST FRAME
ROOF BEAM

MV	05/10/2022	S.7

BILL OF MATERIAL

PIECE MARK	QTY	SIZE DESCRIPTION	LENGTH	REMARK	STEEL GRADE	AML #	SEQ	WEIGHT LB/QTY	PC
4901A	2	BRACE	25 - 5 1/16"						
p0111	2	HSS 10 X 10 X 0.313	22 - 6 1/16"		A500-GR.B			907	
p0211	2	PL 3/4" X 5 3/16"	25 - 5 1/16"	Fysc = 40.89ksi	A36			323.19	
p0310	8	PL 3/4" X 8"	2 - 3 1/2"		A572-GR.50			29.46	
p1510	8	PL 1/4" X 4 3/4"	9 5/8"		ASTM A36 OR ASTM A572 Gr. 50			2.83	
				TOTAL SHIPPING WEIGHT OF BRACE				3359.81	

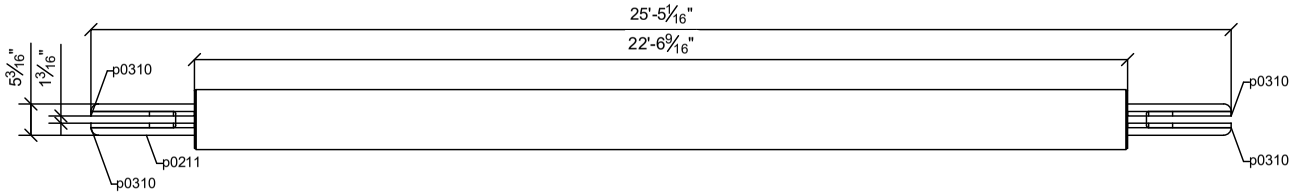

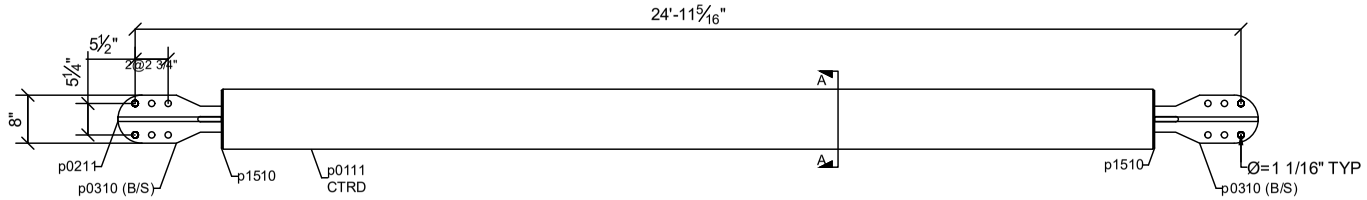

(2)-BRACE MK 4901A

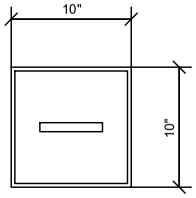

A - A

UNIVERSITY OF ALBERTA | POLYTECHNIQUE MONTRÉAL

CORE BRACE
SUPERIOR SEISMIC PERFORMANCE

MT-BRBF TEST FRAME
TIER 1 BRB (4901A)

BS	05/10/2022	S.8

BILL OF MATERIAL

PIECE MARK	QTY	SIZE DESCRIPTION	LENGTH	REMARK	STEEL GRADE	AML #	SEQ	WEIGHT LB/QTY	PC
4902A	3	BRACE	24' - 11 7/8"						
p0110	3	HSS 10 X 10 X 0.313	22' - 7/8"		A500-GR.B			889.5	
p0210	3	PL 3/4" X 5 3/16"	24' - 11 7/8"	Fysc = 40.88ksi	A36			317.43	
p0310	12	PL 3/4" X 8"	2' - 3 1/2"		A572-GR.50			29.46	
p1510	12	PL 1/4" X 4 3/4"	9 5/8"		ASTM A36 OR ASTM A572 Gr. 50			2.83	
				TOTAL SHIPPING WEIGHT OF BRACE				3236.09	

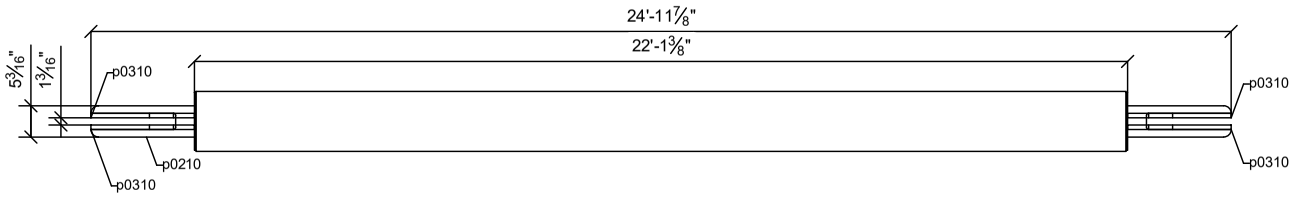

(3)-BRACE MK 4902A

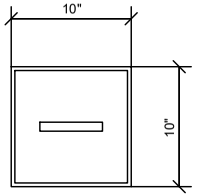

A - A

UNIVERSITY OF ALBERTA | POLYTECHNIQUE MONTRÉAL

CORE BRACE SUPERIOR SEISMIC PERFORMANCE

MT-BRBF TEST FRAME
TIER 2 BRB (4902A)

BS	04/11/2022	S.9

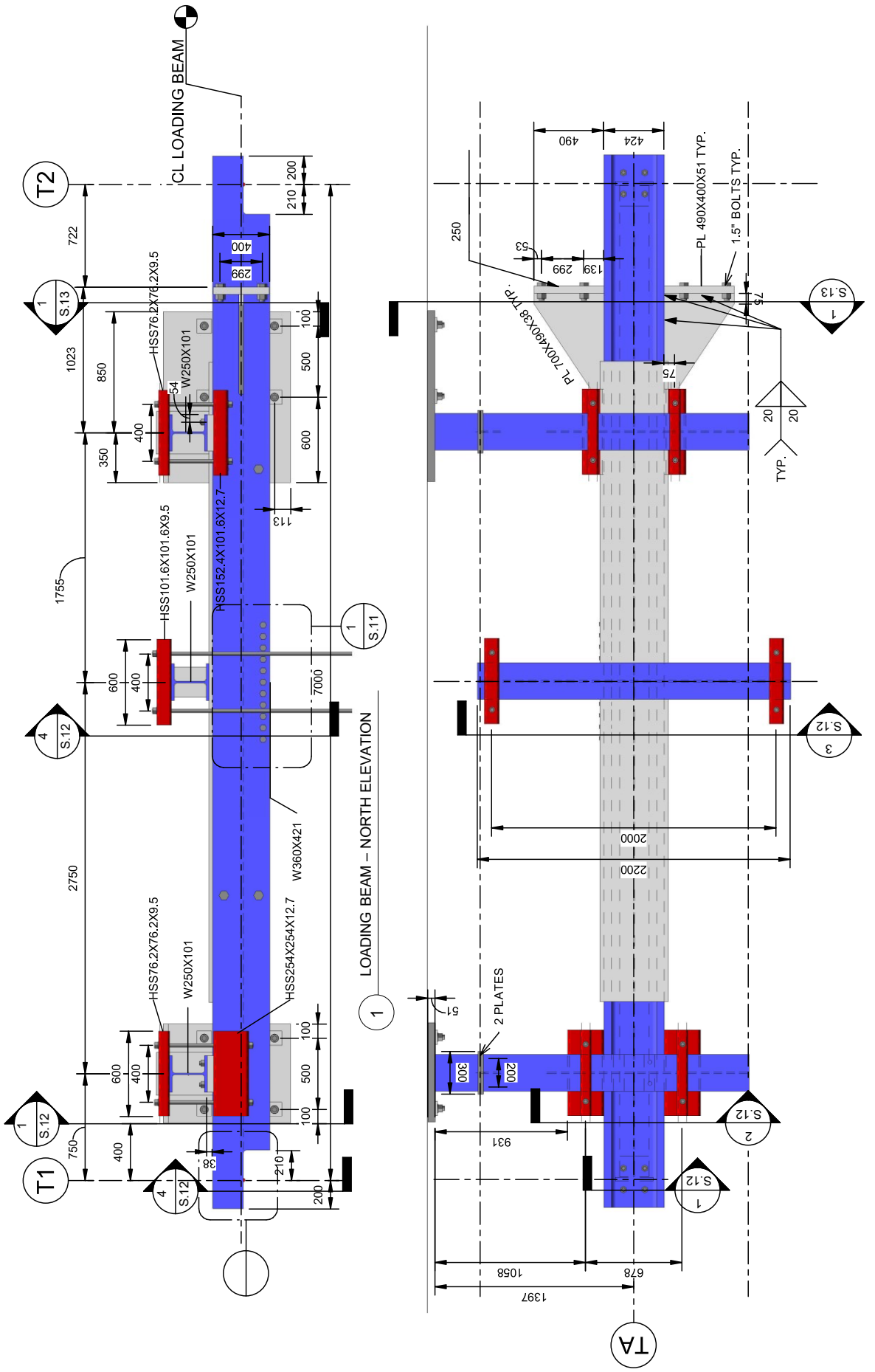

UNIVERSITY OF ALBERTA
POLYTECHNIQUE MONTRÉAL
CoreBrace
SUPERIOR SEISMIC PERFORMANCE

MT-BRBF TEST FRAME
LOADING BEAM DETAILS

PC	04/01/2020	S.10

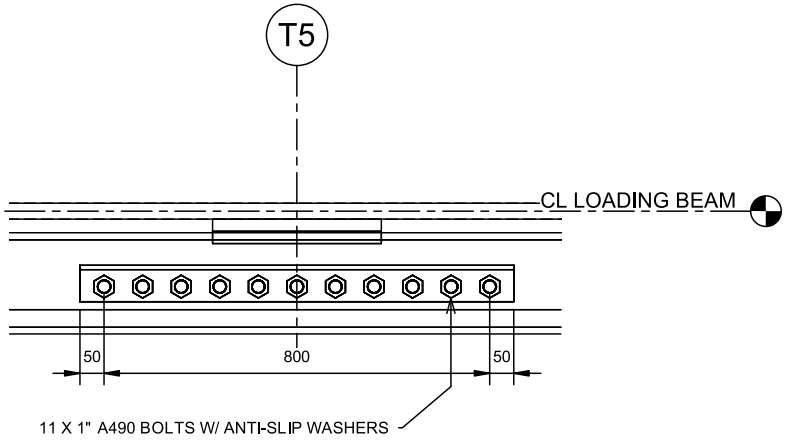

1 LOADING BEAM / ROOF BEAM CONNECTION

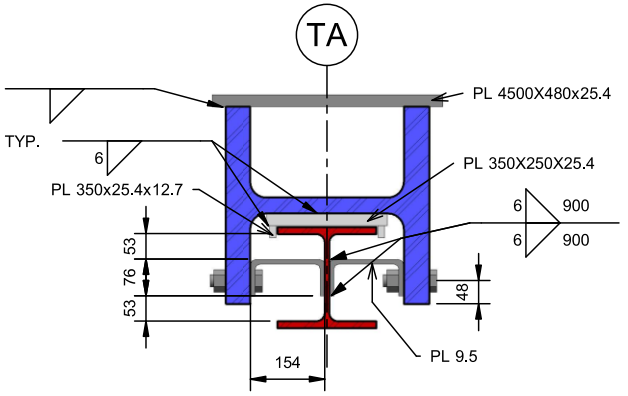

2 LOADING BEAM / ROOF BEAM CONNECTION – SECTION

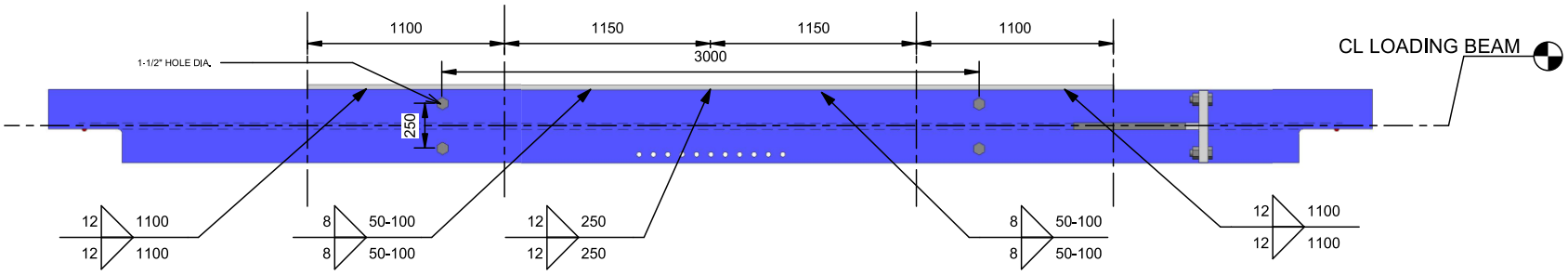

3 LOADING BEAM DETAILS – NORTH ELEVATION

UNIVERSITY OF ALBERTA | POLYTECHNIQUE MONTRÉAL

CORE BRACE SUPERIOR SEISMIC PERFORMANCE

MT-BRBF TEST FRAME
LOADING BEAM DETAILS

PC	04/01/2020	S.11

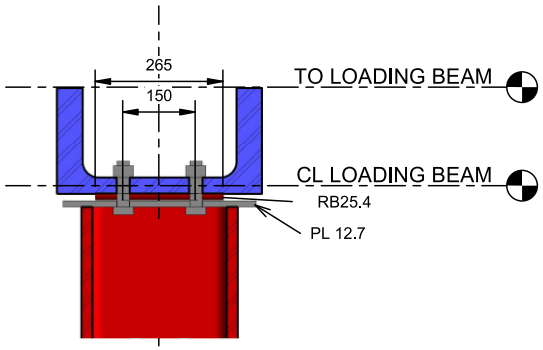

1 LOADING BEAM / COLUMN CONNECTION – SIDE ELEVATION

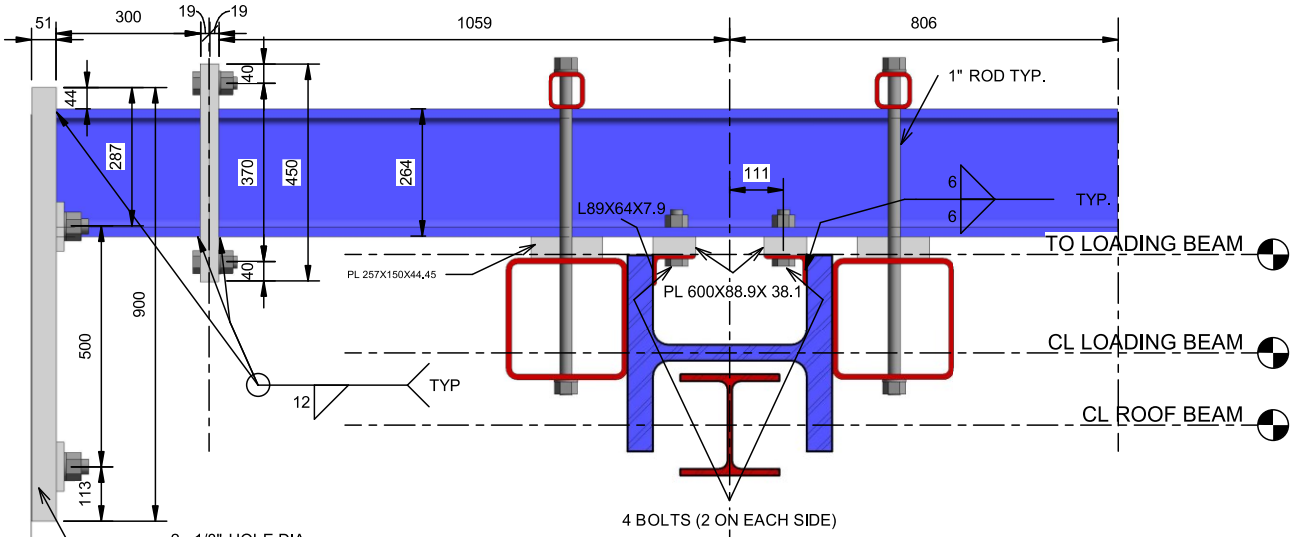

2 LOADING BEAM – LATERAL RESTRAIN (EAST)

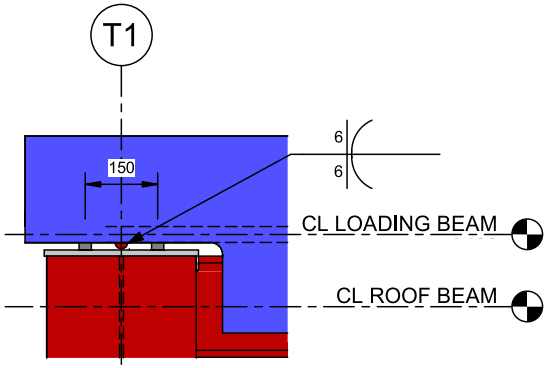

BOLTS BETWEEN COLUMN AND LOANDING BEAM LOOSELY TIGHTEN

1" ROUND BAR CUT IN HALF AND WELDED TO LOADING BEAM

4 LOADING BEAM / COLUMN CONNECTION – FRONT ELEVATION

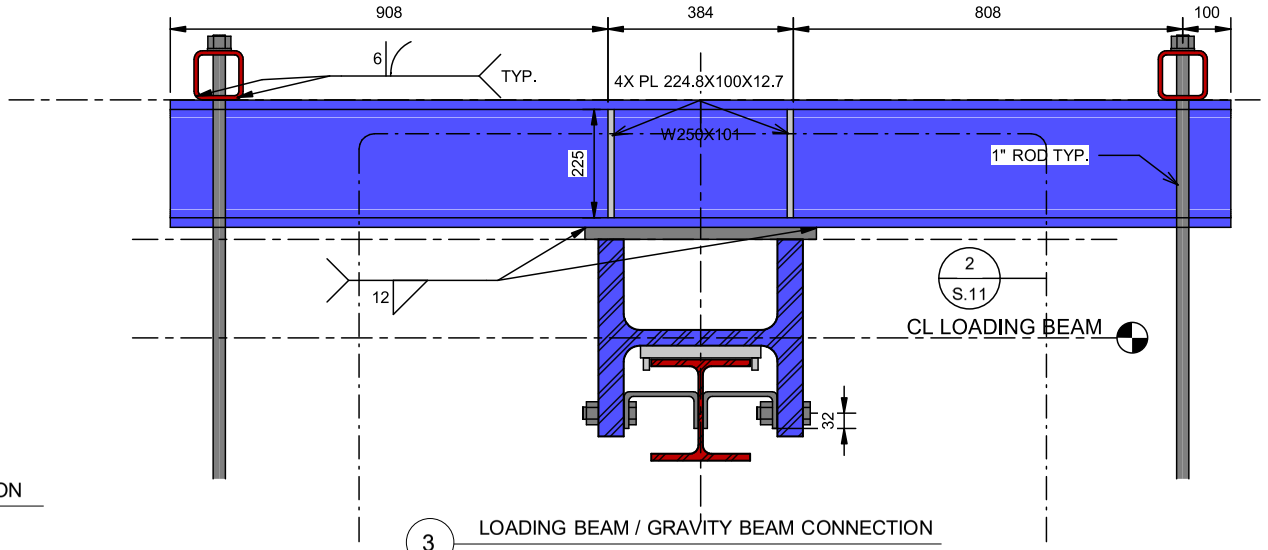

3 LOADING BEAM / GRAVITY BEAM CONNECTION

UNIVERSITY OF ALBERTA | POLYTECHNIQUE MONTRÉAL

CORE BRACE SUPERIOR SEISMIC PERFORMANCE

MT-BRBF TEST FRAME
LOADING BEAM DETAILS

PC	04/01/2020	S.12

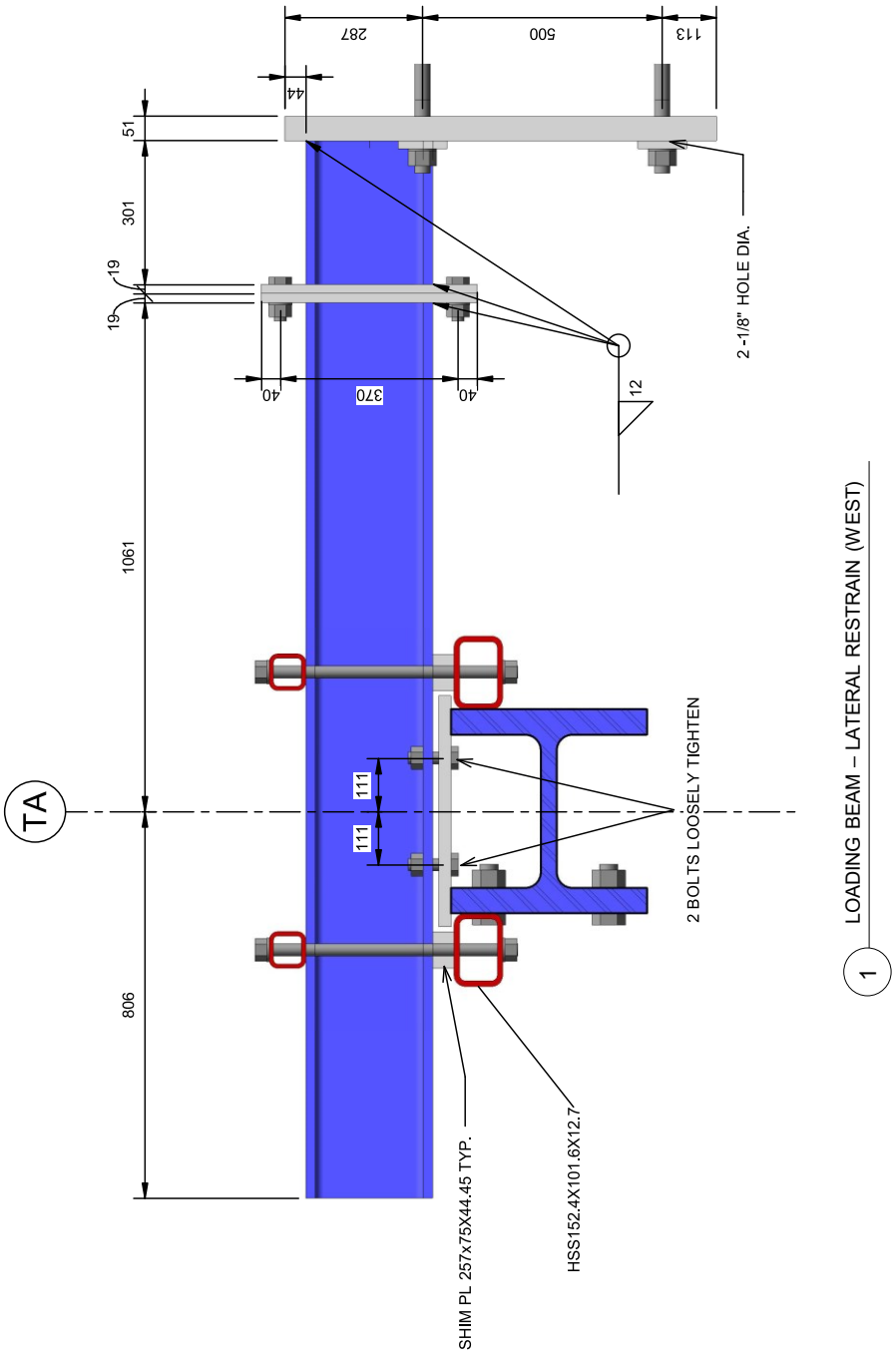

UNIVERSITY OF ALBERTA | POLYTECHNIQUE MONTRÉAL | CoreBrace

MT-BRBF TEST FRAME
LOADING BEAM DETAILS

PC	04/01/2020	S.13

BEAM: ASTM A992 Gr.50
PLATES: ASTM A572 Gr.50
WELDS: E490 XX
BOLTS: N/A
FINISH: TBD

A-A :

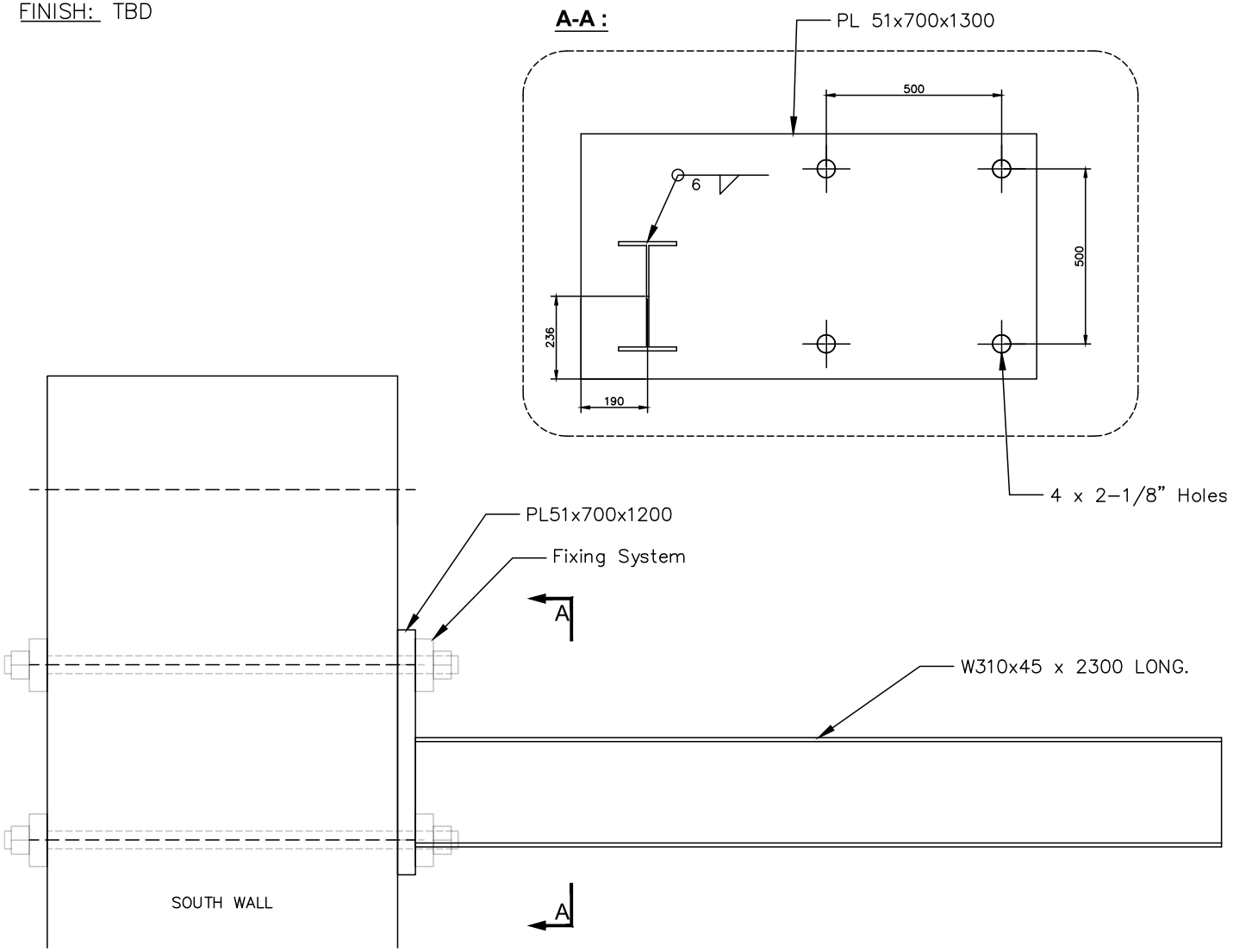

UNIVERSITY OF ALBERTA | POLYTECHNIQUE MONTRÉAL
CoreBrace SUPERIOR SEISMIC PERFORMANCE

MT-BRBF TEST FRAME
ACTUATOR SUPPORT BEAM

CC	07/18/2019	S.14

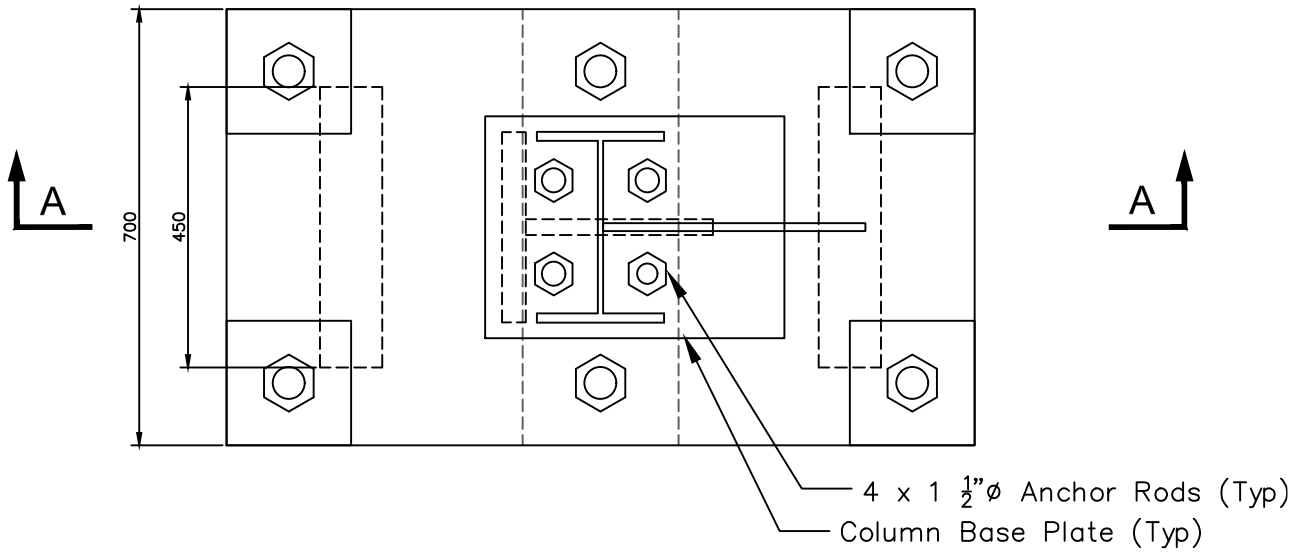

Coupe A-A :

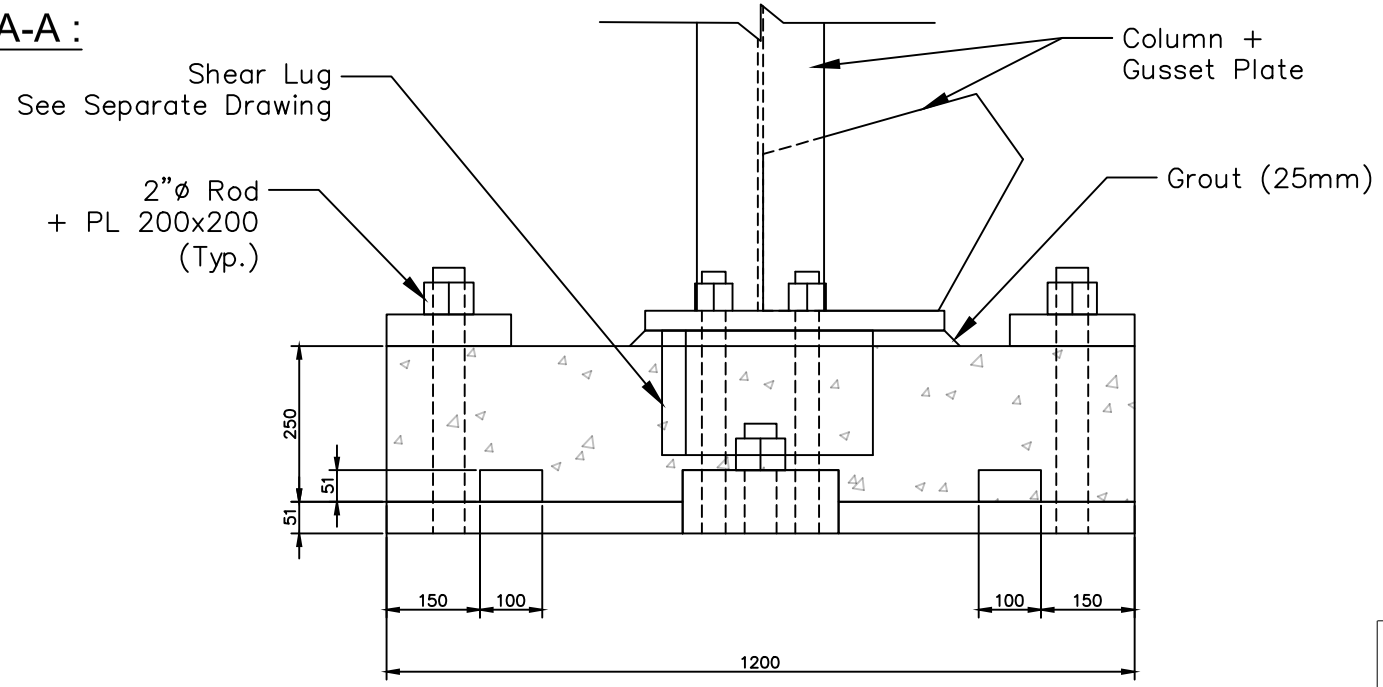

UNIVERSITY OF ALBERTA | POLYTECHNIQUE MONTRÉAL

CoreBrace SUPERIOR SEISMIC PERFORMANCE

MT-BRBF TEST FRAME
FOOTING DETAILS

CC	07/18/2019	S.15

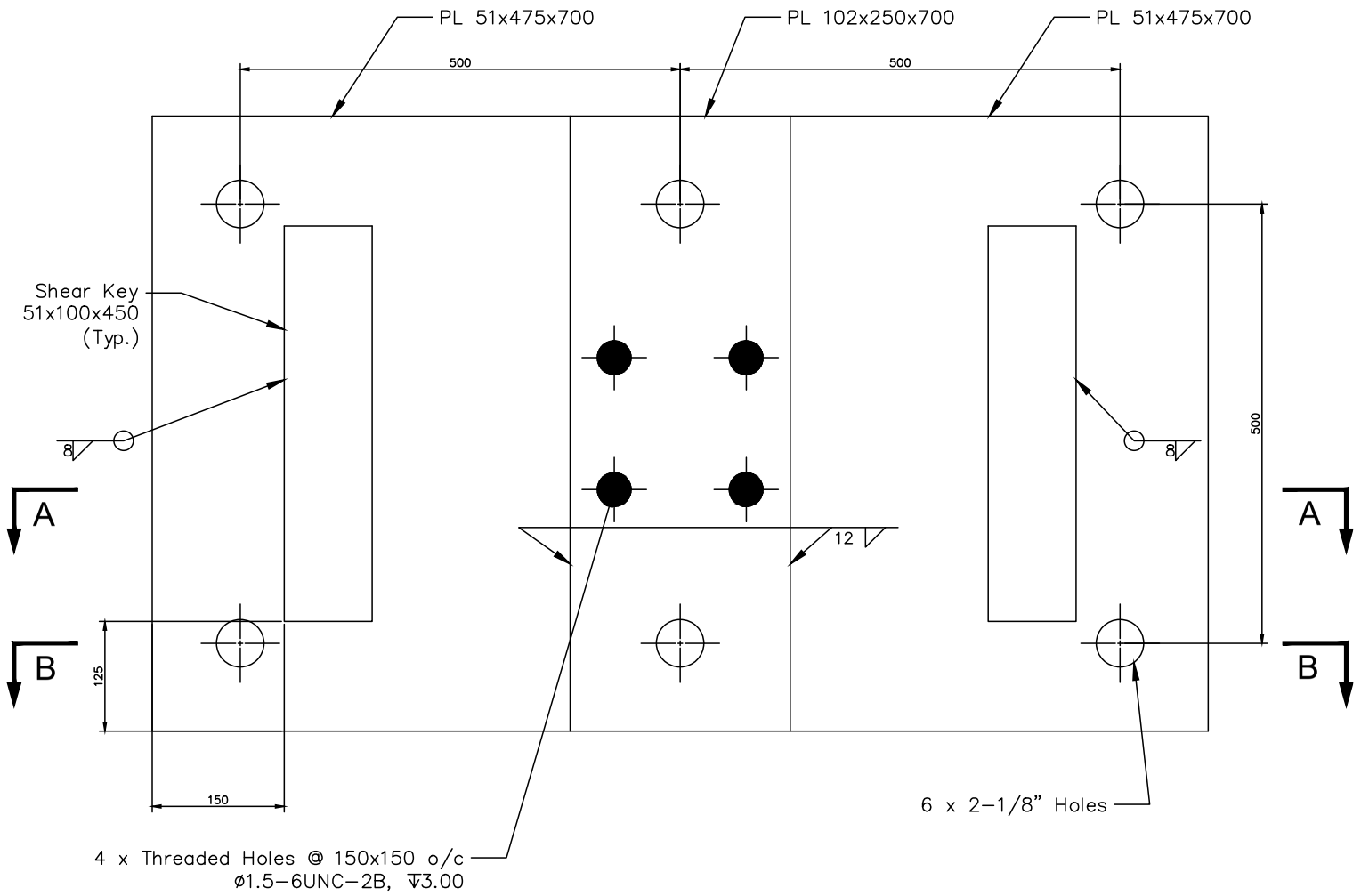

UNIVERSITY OF ALBERTA | POLYTECHNIQUE MONTRÉAL

CORE BRACE SUPERIOR SEISMIC PERFORMANCE

MT-BRBF TEST FRAME
FOOTING PLATE

CC	07/18/2019	S.16

A-A :

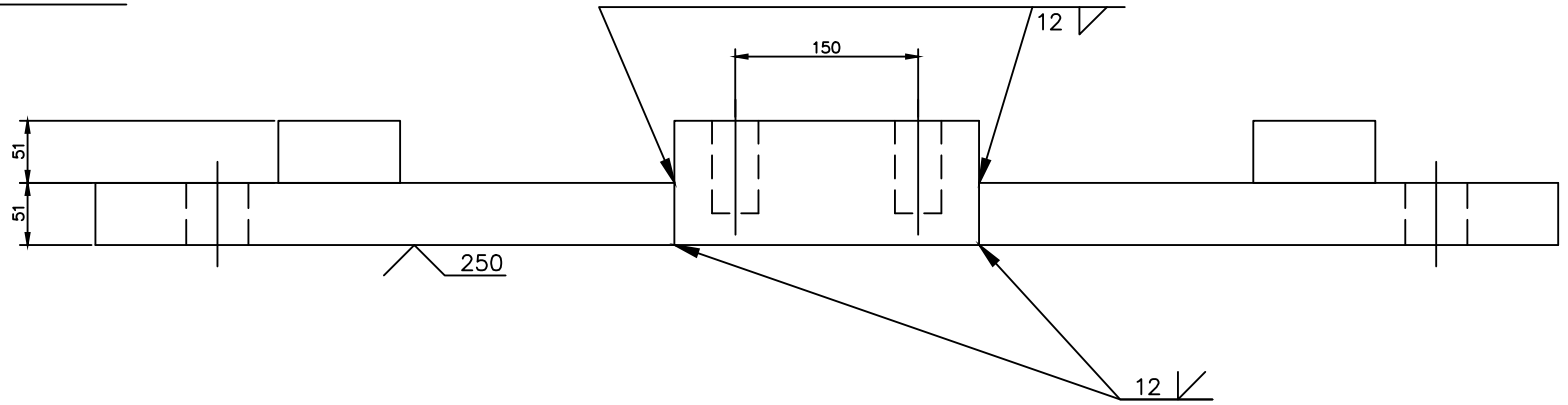

B-B :

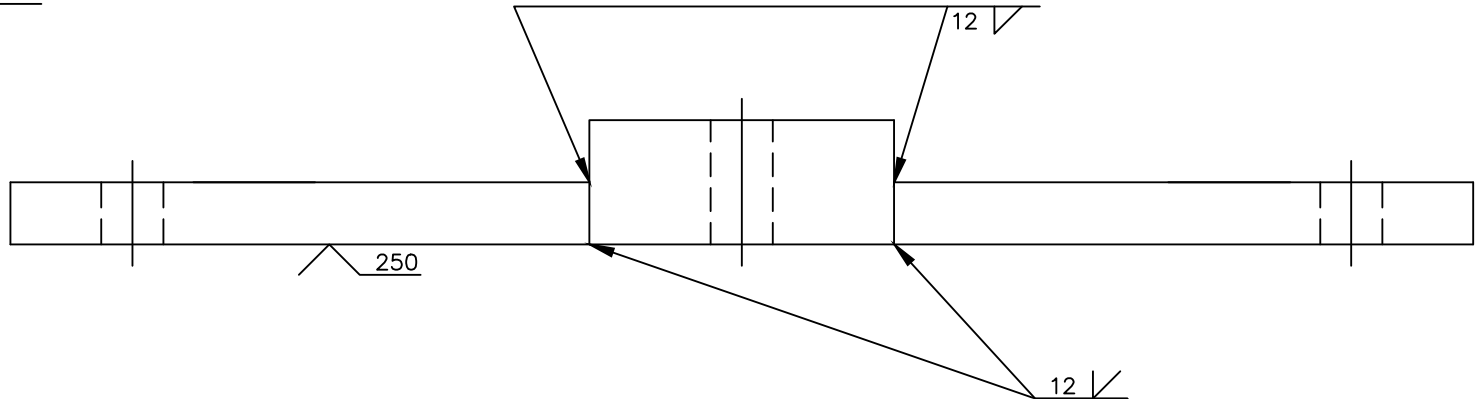

UNIVERSITY OF ALBERTA | POLYTECHNIQUE MONTRÉAL

CoreBrace SUPERIOR SEISMIC PERFORMANCE

MT-BRBF TEST FRAME
FOOTING PLATE SECTIONS

CC	07/18/2019	S.17

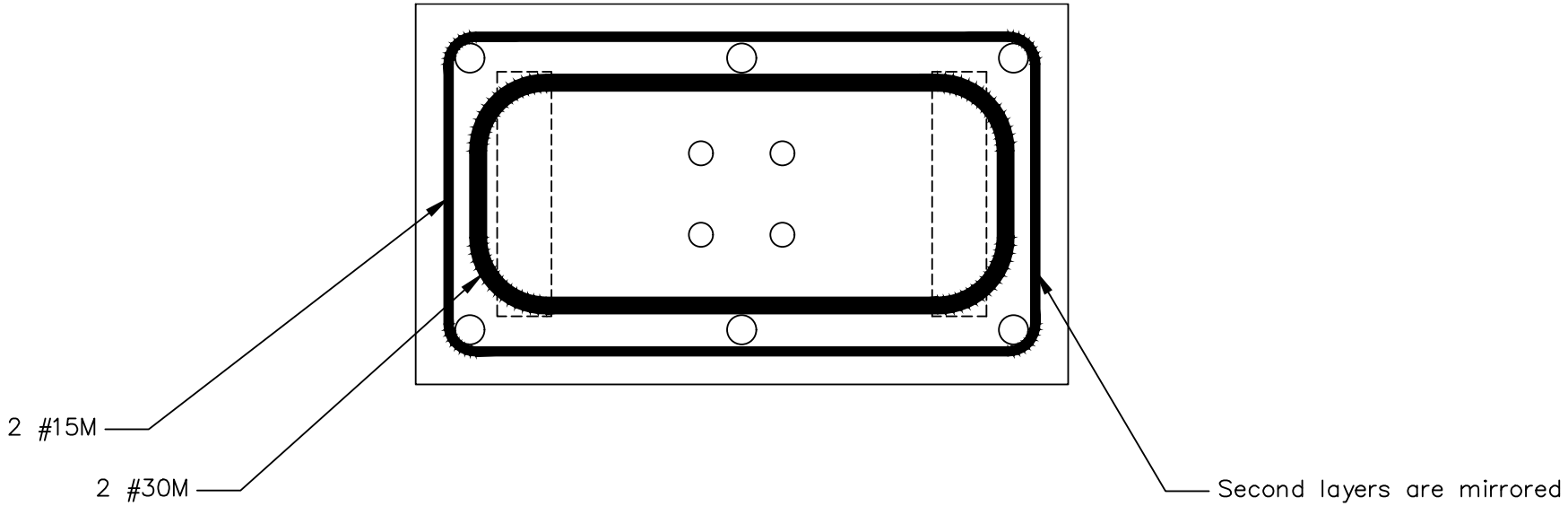

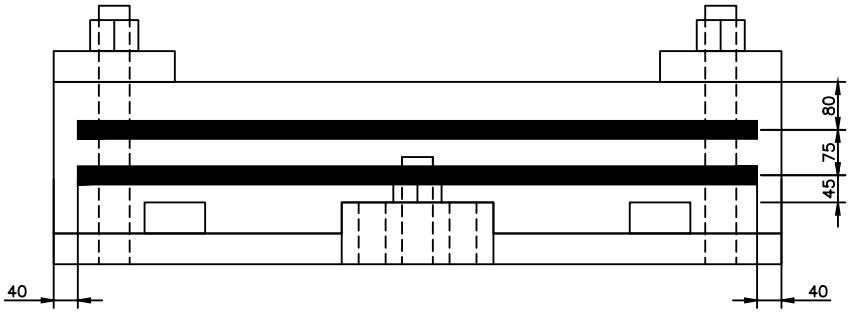

UNIVERSITY OF ALBERTA | POLYTECHNIQUE MONTRÉAL

CoreBrace SUPERIOR SEISMIC PERFORMANCE

MT-BRBF TEST FRAME
FOOTING REINFORCING

CC	07/18/2019	S.18

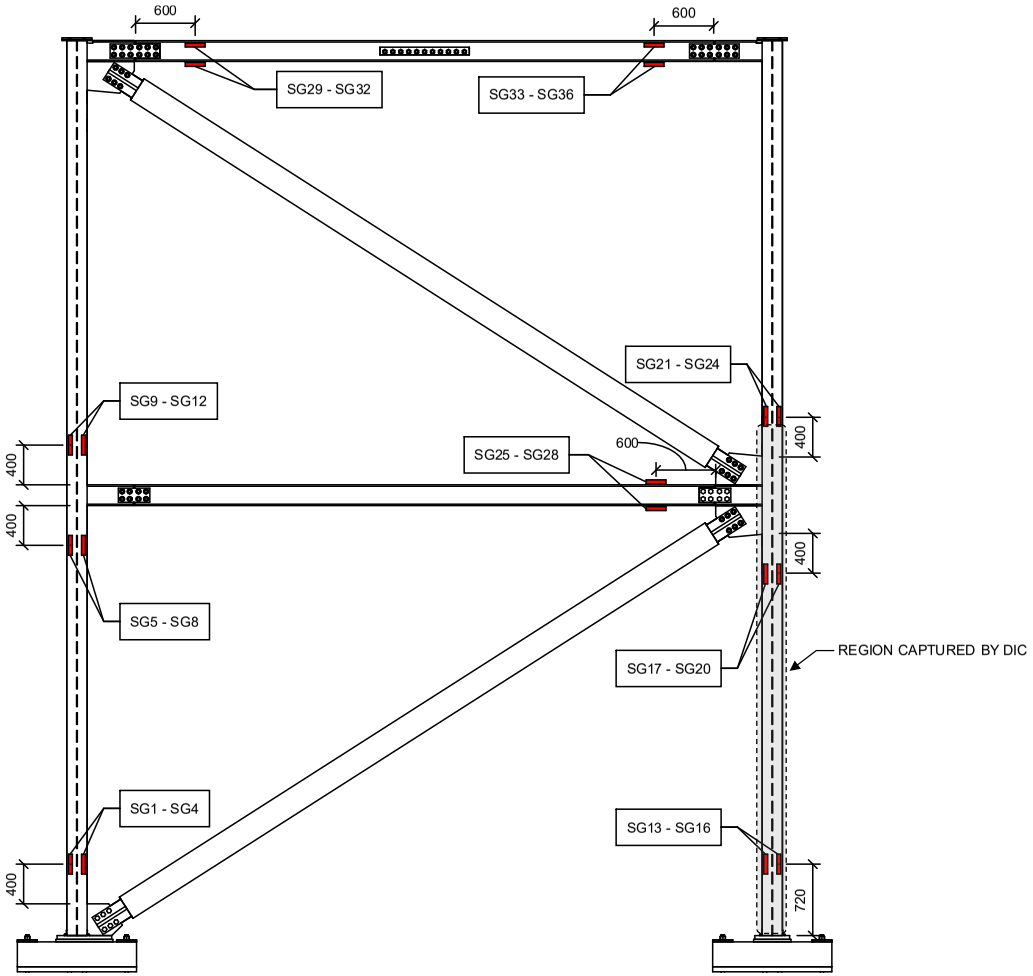

LOCATION OF STRAIN GAGES AND DIC

[mm]

STRAIN GAGE SCHEDULE		
No.	ID	LOCATION
1	SG1	L. COL. BOT. FRONT.
2	SG2	L. COL. BOT. FRONT.
3	SG3	L. COL. BOT. BACK.
4	SG4	L. COL. BOT. BACK.
5	SG5	L. COL. MID-1. FRONT.
6	SG6	L. COL. MID-1. FRONT.
7	SG7	L. COL. MID-1. BACK.
8	SG8	L. COL. MID-1. BACK.
9	SG9	L. COL. MID-2. FRONT.
10	SG10	L. COL. MID-2. FRONT.
11	SG11	L. COL. MID-2. BACK.
12	SG12	L. COL. MID-2. BACK.
13	SG13	R. COL. BOT. FRONT.
14	SG14	R. COL. BOT. FRONT.
15	SG15	R. COL. BOT. BACK.
16	SG16	R. COL. BOT. BACK.
17	SG17	R. COL. MID-T1. FRONT.
18	SG18	R. COL. MID-T1. FRONT.
19	SG19	R. COL. MID-T1. BACK.
20	SG20	R. COL. MID-T1. BACK.
21	SG21	R. COL. MID-T2. FRONT.
22	SG22	R. COL. MID-T2. FRONT.
23	SG23	R. COL. MID-T2. BACK.
24	SG24	R. COL. MID-T2. BACK.

STRAIN GAGE SCHEDULE CONTINUED		
No.	ID	LOCATION
25	SG25	STRUT. TOP.
26	SG26	STRUT. TOP.
27	SG27	STRUT. BOT.
28	SG28	STURT. BOT.
29	SG29	LEFT. BEAM. TOP.
30	SG30	LEFT. BEAM. TOP.
31	SG31	LEFT. BEAM. BOT.
32	SG32	LEFT BEAM. BOT.
33	SG33	RIGHT. BEAM. TOP.
34	SG34	RIGHT. BEAM TOP.
35	SG35	RIGHT. BEAM. BOT
36	SG36	RIGHT. BEAM. BOT

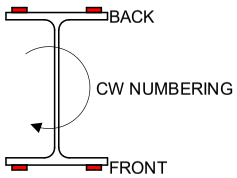

WIDE-FLANGE SECTION

UNIVERSITY OF ALBERTA
POLYTECHNIQUE MONTRÉAL
CORE BRACE SUPERIOR SEISMIC PERFORMANCE

MT-BRBF TEST FRAME
STRAIN GAGES AND DIC

MB	04/11/2022	S.19

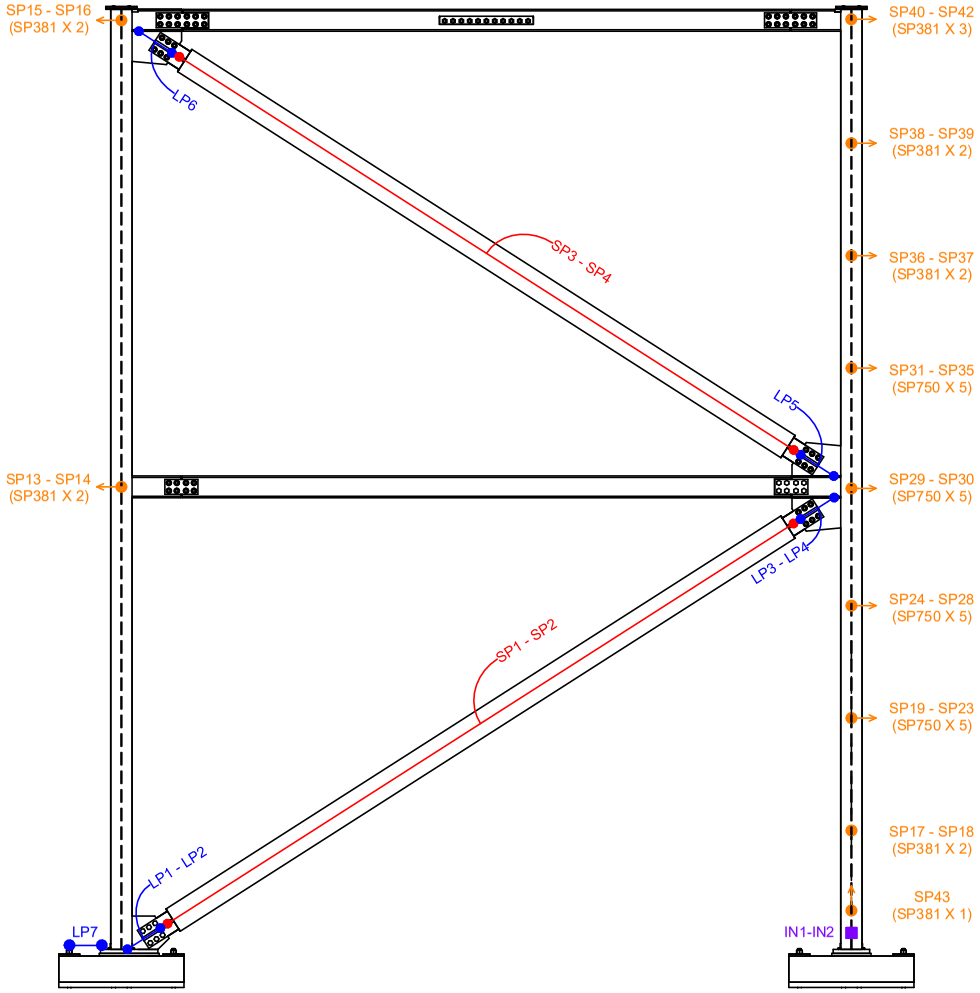

LOCATION OF POTENTIOMETERS, LVDTs AND INCLOMETERS

LEGEND

- BRB POTENTIOMETERS
- CONNECTION LVDTs
- COLUMN POTENTIOMETERS
- COLUMN INCLOMETERS

UNIVERSITY OF ALBERTA | POLYTECHNIQUE MONTRÉAL

CORE BRACE SUPERIOR SEISMIC PERFORMANCE

MT-BRBF TEST FRAME
STRING POTS, LVDTs & INCLOMETERS

MB	04/11/2022	S.20

SPECIFICATIONS

PISTON AREA: 75.60 SQ.IN. [487.7 SQ.CM.]

ROD DIAMETER: 6.00 [152.4]

DYNAMIC STROKE: 30.00 [762.0]

STATIC STROKE: 32.00 [812.8]

FORCE RATING: 220 KIP [1000 KN]
AT 3000 PSI SYSTEM
PRESSURE

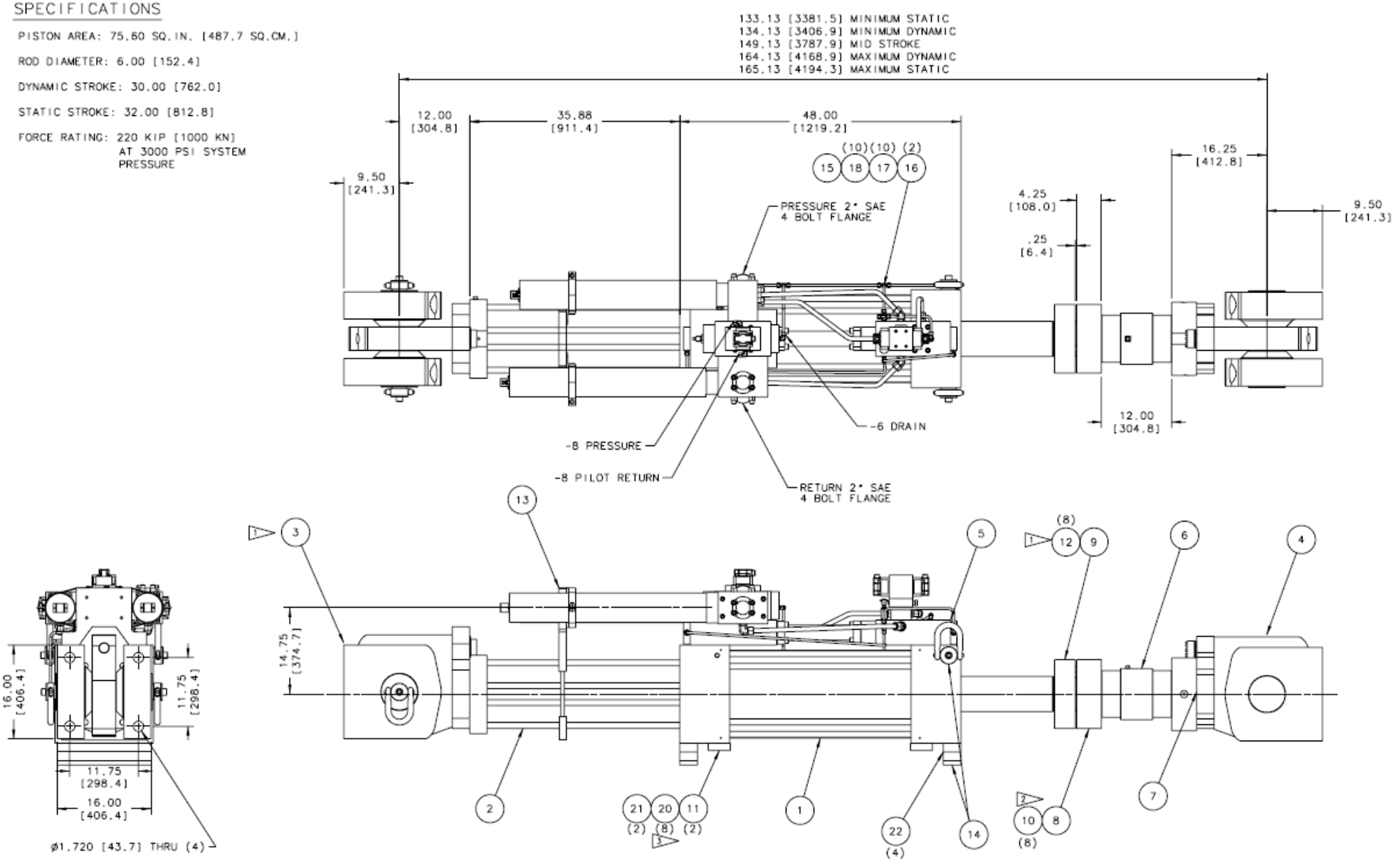

UNIVERSITY OF ALBERTA · POLYTECHNIQUE MONTRÉAL · CoreBrace SUPERIOR SEISMIC PERFORMANCE		
MT-BRBF TEST FRAME MTS 1000 kN ACTUATOR		
MTS	-	S.21